UNIVERSITEIT VAN PRETORIA
UNIVERSITY OF PRETORIA
YUNIBESITHI YA PRETORIA

The dynamics of cut-off lows and their vertical extension to the surface

by

Michael A. Barnes

Supervised by:

Dr. Thando Ndarana

Prof. Willem A. Landman

Submitted in partial fulfilment of the requirements for the degree

DOCTOR OF PHILOSOPHY in METEOROLOGY

in the

Department of the Geography, Geoinformatics and Meteorology

Faculty of Natural and Agricultural Sciences

University of Pretoria

Pretoria, South Africa

July 2021

Declaration

I, Michael Alan Barnes, declare that this dissertation / thesis, which I hereby submit for the degree Doctor of Philosophy in Meteorology at the University of Pretoria, is my own work unless or otherwise explicitly acknowledged by citation of published and unpublished sources and has not previously been submitted by me for a degree at this or any other tertiary institution. Furthermore, I would like to state that, even if the work presented in various chapters of the thesis has been co-authored with my co-supervisors and other colleagues, the conceptualisation and execution of the research was done by me.

Michael A. Barnes (10313029)

Signed: 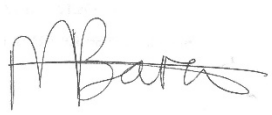

Date: 20 May 2021

Acknowledgements

The author would like to express his appreciation to the following persons and institutions who have contributed towards the success of the research:

- Dr. Thando Ndarana (UP) for his continual support, expertise, and leadership throughout the study. Dr Ndarana's love and passion for dynamic meteorology is boundless and infectious which provided the foundation for the concepts in this work. Without him, this work would simply not have been possible.
- Prof. Willem A. Landman (UP) for co-supervising the work, the many hours of reading and reviews and brilliant ideas that improved the work substantially. His vast academic and scientific expertise, guidance and mentorship were instrumental in the work completed in this thesis.
- Ms. Kate Turner (SAWS) for her operational weather forecasting expertise and co-authorship of one of the journal articles that resulted from this work.
- Dr. Michael Sprenger (ETH Zurich) for providing his potential vorticity inversion code and assistance with compiling and running it. Dr Sprenger also co-authored one of the articles in this thesis giving valuable review, guidance and feedback.
- Dr. Christo Rautenbach (SAWS, NIWA) and Mr. Marc de Vos (SAWS) for their constant encouragement and scientific mentorship. The science and research career opportunities I have been given are largely credit to them, opportunities which were instrumental in my scientific development.
- The South African Weather Service (SAWS) and the SAWS Marine Research Unit for granting me time and space to work on this thesis
- The SAWS Cape Town Weather Office forecasting team circa. 2016-2018 (Mr. Rian Smit, Mr. Henning Grobler, Ms. Stella Nake, Ms. Kate Turner, Ms. Thabisile Ntleko, Mrs. Lebogang Makgati and Ms. Mmathapelo Makgabutlane) for helping shape me into the meteorologist I am today.
- My family for which I owe everything for getting me to this point in my career.
- My fiancé, Amy Wootton, for her continual and unequivocal love and support of everything I do.

Thesis promoters

Dr. Thando Ndarana

Department of Geography, Geoinformatics and Meteorology, University of Pretoria, South Africa

Prof. Willem A. Landman

Department of Geography, Geoinformatics and Meteorology, University of Pretoria, South Africa

Contents

List of Figures

List of Tables

Summary

Cut-off lows (COLs) are closed, upper tropospheric lows that are displaced out of the westerly extratropical jet streak. Although situated in the upper troposphere, these weather systems are often associated with and extend to surface cyclones. An observational study of Cape Storm shows how these COLs develop with respect to Rossby wave breaking (RWB) events and associated intrusions of high-potential vorticity (PV) stratospheric air. Multiple deep intrusions and PV towers are shown to be involved in the development and deepening of the surface cyclone co-incident with the series of COLs. The study of this extreme weather event shows the severe impact that these COL-influenced surface cyclones can have on South Africa. In this case, the Western Cape was battered with heavy rain, damaging strong winds which lead to out-of-control wildfires, large waves and storm surge.

A climatology of the seasonal, temporal and spatial variability of COL surface extensions is undertaken here using ERA-Interim data. Close to 60% of the COLs can be classified as deep (those that extend to the surface) within the southern hemisphere and only 30% classified as shallow (those that only extend to the 500hPa or above). Deep COLs (dCOLs), are most frequent in the autumn months, are longer lasting and found most frequently situated in the high latitudes. PV dynamics also play a role in COL extension. Deep COLs are associated with overturning of PV contours on multiple contours and levels. The depth that PV intrusions reach also seems to be a factor in the development of COL extension. Deeper intrusions are generally associated with deep COLs. However, low level PV-like anomalies that are not in phase with the upper level processes can be an inhibitor for surface cyclonic development. A vertical coupling between the COL and surface cyclones is also identified. It is shown that troughiness develops throughout the atmosphere as the deep COL develops with a closed surface cyclone developing at a similar time to the COL.

PV intrusion depth and its relation to COL extensions are also tested in an idealised setting, utilising the power of PV inversion diagnostics. The idealised experiment confirms the findings of the COL extension climatology that deeper PV intrusions are associated with increased cyclogenetic forcing at the surface. The height of the dynamical tropopause is a factor in COL extensions. Higher tropopauses (such as found in the summer months and in the low latitudes), result in PV intrusions needing to “reach” further to get closer to the surface. The closer to the surface that the intrusion reaches, the more intense the surface cyclogenesis stimulated. This explains the seasonal and latitudinal variability found in the COL extension climatology done within this study.

Finally, we present and develop a conceptual model for COL extension and development from PV perspective. This conceptual model takes classical PV dynamical conceptual models and morphs them

with the findings of this study in the context of southern hemispheric COLs. The conceptual model can be applied in an operational setting thanks to the development of an operational PV dynamics webpage. The web page houses postprocessed PV fields from freely available numerical weather prediction data providing operational meteorologists with a view of COLs and other weather systems from a PV perspective.

Chapter 1: Background and introduction

1.1. Background

1.1.1. Climate of South Africa

South Africa has a unique and varied climate due to its latitudinal position and varied topography. The country is situated in the sub-tropics between the Limpopo river at 22˚S and the southern tip of the African continent at 35˚S (Tyson and Preston-Whyte, 2000). The Southern African climate is varied with respect to longitude. In general, the eastern parts are much wetter than the western parts. This is generally a result of the ocean currents which flow along these respective coastlines. The warm, fast-flowing Agulhas current and warmer Indian Ocean to the east of the country provides moisture rich airmasses to the region. Comparatively, the cold, Benguela current to the west result in drier conditions. The exception to this is the south-western and southern parts of the country due to their extratropical and topographical influences. Tropical weather is largely influenced by the southward positioning of the Inter-Tropical Convergence Zone (ITCZ) during the spring and summer months. An extension of a southward extending trough provides moisture transport from the tropics (D'Abreton and Lindesay, 1993; Taljaard, 1995). Tropical temperature troughs (TTTs), continental tropical lows (CTLs) and Tropical Cyclones (TCs) are all major contributors to the summer rainfall region (van Heerden and Taljaard, 1998). The south-western parts are however influenced mainly by extratropical systems. Winter rains are provided to the region in the form cold frontal bands associated with mid-latitudinal systems generated in the Southern Ocean situated between 40-50˚S (Taljaard, 1995). Surface low pressure cells can also be driven occasionally within the 25-40˚S band and are usually driven by deep cut-off lows (COLs). Synoptic winter weather systems can result in hazardous weather for the region. Strong winds, heavy rains, flooding, high seas, storm surge and snowfalls are all possible with the passage of these systems.

1.1.2. Cut-off lows

A COL is a cold-cored, closed, upper-air low pressure system. These systems develop by becoming displaced equatorward out of the westerly jet in the extra-tropics. COLs can be defined at various pressure levels. Many have defined COLs as being closed circulations at the 500hPa level (i.e. Fuenzalida *et al.*, 2005), whilst others use levels between 200 and 300hPa (Nieto *et al.*, 2005; Singleton and Reason, 2007a; Ndarana and Waugh, 2010; Pinheiro *et al.*, 2019). Whichever the level, the lifecycle of COLs follows a four-stage process (Nieto *et al.*, 2005). An upper level trough develops coincident with a temperature wave situated to the west of the geopotential wave. During this stage, lower tropospheric cold air advection into the centre of the trough results in the amplification of the

geopotential and temperature waves. As the amplitude continues to increase, it starts to detach from the westerly jet. This is the second stage known as the tear-off stage. Eventually, the cold air that has penetrated into the centre of the deep trough gets cut-off from the extratropical air to the south. This third stage is known as the cut-off stage of COL development. In the final stage, the COL dissipates and usually merges again with a trough in the westerly zonal jet. In the tropics, the movement of COLs is however more erratic where COLs can retrograde (move in a westerly direction) or decay with northward trajectory (Favre *et al.*, 2013), not re-merging with the westerly zonal jet.

Various climatologies for COLs have been presented for the SH (Ndarana and Waugh, 2010; Reboita *et al.*, 2010; Pinheiro *et al.*, 2017). These studies followed on from the initial investigation of Fuenzalida *et al.* (2005) who performed the first hemispheric study of COLs at the 500hPa level. Using ERA-40 reanalysis data, Reboita *et al.* (2010) found an average of 348.8 COLs per annum on the 300hPa in the SH. This was far more than the 267.5 COLs and 137.2 COLs respectively at the 200hPa and 500hPa levels. Interestingly, the ERA-40 dataset identified a far greater number of COLs than the NCEP dataset. This corresponds with the lower amount of COLs identified by Ndarana and Waugh (2010) (81 per year). Although there is a discrepancy between the two reanalysis products, climatologies are generally consistent with respect to the regional and seasonal variability of COLs (Reboita *et al.*, 2010).

The variability of COLs within the SH has been well-studied. COLs in general tend to be most concentrated around the continents (Reboita *et al.*, 2010; Muñoz *et al.*, 2020). Studies therefore look at these continental sectors for regional variability. Regionally, the most active area in the SH is the Australia-Pacific region (Reboita *et al.*, 2010; Pinheiro *et al.*, 2017; Muñoz *et al.*, 2020). COLs also have a distinct seasonal variability within the SH. COLs are most frequent during the austral autumn months and are at a minimum during the winter (Pinheiro *et al.*, 2017). This is consistent across all reanalyses products and regions (Reboita *et al.*, 2010; Pinheiro *et al.*, 2017). COLs are generally relatively short-lived. About half of all COLs last less than 2 days, with fewer than 10% lasting more than 4 days (Reboita *et al.*, 2010; Muñoz *et al.*, 2020).

1.2. Cut-off lows over South Africa

COLs are one of the major weather producers over South Africa. In fact, Favre *et al.* (2013) showed that COLs significantly contribute to the South Africa's annual rainfall amounts. This amounts to above 15% of annual rainfall for the majority of the country, besides the north-eastern parts. COL-related rainfall amounts increase to more than 30% over the western central interior of the country. COLs are also responsible for a large amount of severe weather over South Africa including heavy rainfall leading to flooding and flash flooding (e.g. Singleton and Reason, 2006; Taljaard, 1985) as well as heavy snowfalls during the winter months (Stander *et al.*, 2016), Gale force winds and storm surge (e.g.

Rautenbach *et al.*, 2020). COLs can also result in many aviation hazards such as icing, turbulence due to upper-level wind shear and thunderstorm development (Taljaard, 1985). Favre *et al.* (2013) also show that COLs are responsible for over 25% of extreme rainy days along the south and east coasts as well as in the central interior of the country. This increases to up to 50% over the western central interior. Over the Western Cape province, 45% of COLs do not produce any rainfall (Omar and Abiodun, 2020). When they do, they contribute to 11% of the overall rainfall for the province. Over the cape south coast, COLs are present during 16% of the rainfall events (Engelbrecht *et al.*, 2015).

Singleton and Reason (2007b) conducted a climatology for the southern African region using NCEP reanalysis data at a 300hPa level. The results are consistent with the SH climatologies mentioned in Section 1.1.2. As with the SH climatologies, a maximum frequency occurrence of COLs occurs in the southern African region in the austral autumn months. An average of 4 autumnal COLs are present within the southern African region per year with a maximum of 7-8 per year. Spring is the second-most active season with about 2.5 COLs per year. The study also shows that the frequency of COLs is fairly variable from year to year. Within the South African region, COLs are also more prevalent in the south-western parts of the country according to the findings of Singleton and Reason (2007b) receiving more than 35% of the total number of COLs. In the austral Autumn months, COLs also have a tendency to move from the south-west of the country to the south-east with 20% having this behaviour. This would result in these systems affecting the eastern coastline of the South Africa. Although, no significant trends exist for other parts of the country, the north-eastern parts of the country were found to have a tendency towards a greater number of COLs in the late summer and early spring. This is significant since this time of the year is known as a time in which these parts of the country get significant heavy rainfall and severe thunderstorm development.

1.3. The basic mathematical principles of PV theory

There are various tools, diagnostics and methodologies that advance our understanding of the atmosphere and the processes which govern its evolution. One of these tools is *potential vorticity* (PV). PV can be traced back to the early circulation theory of Rossby (1940) who noted that the absolute circulation for a standard mass is constant for adiabatic frictionless flow (Thorpe *et al.*, 2003). This parameter is now referred to as PV. The early work of Rossby (1940) and later of Ertel (1942) derives the non-quasi-geostrophic form of the PV equation. This form of PV is now most commonly referred to as Ertel's PV. Ertel's PV is given by (Lackmann, 2011):

$$EPV = \frac{1}{\rho}\vec{\eta} \cdot \boldsymbol{\nabla}\theta \tag{1}$$

where ρ is the density, $\vec{\eta}$ is the three-dimensional absolute vorticity vector and θ is the potential temperature. Equations (1) describe PV following a parcel of air. Using standard meteorological approximations, PV in equation (1) can also be described in both the isobaric and isentropic coordinate system as:

$$PV = -g\left[\left(f\vec{k} + \vec{\nabla}_p \times \vec{v}\right) \cdot \vec{\nabla}_p\theta\right] \tag{2}$$

and

$$PV = -g\left[\left(f + \vec{k} \cdot \vec{\nabla}_\theta \times \vec{v}\right)/\frac{\partial p}{\partial \theta}\right] \tag{3}$$

respectively (Hoskins *et al.*, 1985), where $\vec{k}$ is the unit vector in the vertical, f is the Coriolis parameter, g is the gravitational constant and $\vec{\nabla}_\theta$ and $\vec{\nabla}_p$ are the three-dimensional gradient operators in the xyp and $xy\theta$ spaces respectively. Potential vorticity can also be described in the quasi-geostrophic framework as is described in various dynamical texts (such as Holton and Hakim (2013)). Quasi-geostrophic PV (QGPV) can be described by:

$$QGPV = \zeta_g + f + f\frac{\partial}{\partial z}\left(\frac{\partial\bar{\theta}}{\partial z}^{-1}\theta\right) \tag{4}$$

where f is the Coriolis parameter, ζ_g the geostrophic relative vorticity and $\bar{\theta}$ is the potential temperature of the reference state.

The initial theoretical work of Rossby (1940) and Ertel (1942) amongst others as well as the early observational work of Palmén (1949), Kleinschmidt (1950) and others lead to the formed the basis of the "Isentropic PV Thinking" methodology of dynamical analysis. Although centuries old, the use of PV however only gained prominence in dynamical analysis due to the work of Hoskins *et al.* (1985). The Isentropic PV thinking is based around the invertibility principle (Hoskins *et al.*, 1985). The invertibility principle states that if PV on each isentropic surface including that of the lower boundary is known, then all other meteorological fields (geopotential height, temperature and horizontal velocity) can be calculated under a suitable balance condition. Vertical velocity can also be calculated using the omega equation, assuming frictional and adiabatic processes are described. Isentropic PV fields can be used to describe the evolution of all other dynamical fields. As a result, isentropic PV has become the standard in analysing dynamical processes including that of COLs. PV dynamical theory through the

power of PV inversions has shown that upper level PV anomalies can stimulated cyclonic rotation around the core of the anomaly (Hoskins *et al.*, 1985).

1.4. COL dynamics

1.4.1. Upper level dynamics of COLs

The dynamics of upper tropospheric cyclonic circulations have been studied in the northern hemisphere since the late 1940s. A first detailed account of COLs was done by Palmén (1949) who showed a case of an upper-level trough deforming and amplifying, with the cold airmass eventually becoming cut off from the polar air to the north. The case study detailed the lowering of the tropopause and how strong upper tropospheric convergence and associated subsidence leads to an increase in relative vorticity and upper level cyclonic development. The development of these systems was also theorised to be sustained by the amount of relative vorticity of the upper level cyclone, with increased cyclonic motion resulting in COLs extending towards the surface (Hsieh, 1949). These studies also showed the extension of isentropic potential vorticity (PV) values well into the mid-levels of the troposphere during these intense COL events. These studies lead to the theory presented by Kleinschmidt (1950) that these high-PV stratospheric intrusions in fact induce the cyclonic circulation of the COL (Bell and Bosart, 1993).

Rossby wave breaking (RWB) is an important process in upper tropospheric dynamics. These events, which involve the irreversible deformation of PV contours (Mcintyre and Palmer, 1983), contribute to processes such as tropospheric-stratospheric exchange and atmospheric blocking. Ndarana and Waugh (2010) theorised that the initial development of COLs are linked to RWB. The study found that the 89% of COLs identified in the SH were associated with RWB with the remainder being associated with equatorward PV intrusions. RWB precede COL events by 2 days and are located within a region of 20˚W of the COL event. RWB events result in stratospheric intrusions of the high-PV anomalies into the upper troposphere. The statically stable air from the lower stratosphere results in an increase in static stability in the region of the COL and RWB. The intrusion leads to the geopotential waves becoming unstable and the development of the upper air trough. A temperature wave also exists to the west of the developing upper level trough. This results in cold air advection into the centre of the trough. As described theoretically by Hoskins *et al.* (1985) and confirmed by reanalysis data by Ndarana and Waugh (2010), these intrusions, together with cold air advection induce cyclonic motion. This leads to a further amplification of the upper level trough which eventually becomes cut-off from the mid-latitude westerlies, becoming a closed circulation.

Recent work by Ndarana *et al.* (2020) has enhanced our understanding of how RWB events facilitate the structure of jet streaks and downstream development that lead to the development of COLs. An eddy kinetic energy centre increase in the midlatitudes, upstream of the COLs development region by the baroclinic conversion of eddy potential energy prior to a COLs development. A split jet streak forms with a small-scale jet streak forming on the northern edge of the COLs development region. The split jet leads to anticyclonic barotropic shear (Nakamura and Plumb, 1994) leading to PV overturning and an anticyclonic RWB (Peters and Waugh, 2003). The strength of the jet streak has been shown to inform the direction and strength of the energy fluxes that influence the development of the COL (Ndarana *et al.*, 2020). A ridge to the south-west of the COL that is developed through the RWB process results in anticyclonically directed supergeostrophic flow which drives the transfer of eddy kinetic energy from the upstream energy centre to the downstream centre and development of the COL.

1.4.2. COLs and cyclogenesis at the surface

COLs are not isolated to the upper troposphere. On occasion these systems can extend throughout the troposphere resulting in the development of a surface cyclone. Several observational studies have shown examples of this (van Delden and Neggers, 2003; Iwabe and Da Rocha, 2009). Surface cyclogenesis has in fact been linked to upper tropospheric and stratospheric processes. Early studies, for example by Reed (1955) showed that stratospheric intrusions can extend into the mid- and lower troposphere as a thin wedge of high-PV air. This results in an amplification of the tropopause waves and eventually tropopause folding. Since then the link between stratospheric intrusions, tropopause folding and surface cyclogenesis has been established. Uccellini *et al.* (1985) investigated one such case in which tropopause folding was observed with an explosive cyclone developing at the surface. In this case high-PV values were found all the way down to the 800hPa level in the hours preceding the cyclone and were deemed to be involved in the resulting development of the explosive surface cyclone.

The development of surface cyclones as a result of high-PV intrusions is also explained by dynamical theory. Stratospheric intrusion PV-induced cyclonic circulation rotation can be induced throughout the troposphere leading to weak cyclonic circulation at the surface (Hoskins *et al.*, 1985). The cyclonic circulation at the surface promotes the poleward advection of warm air ahead of the upper level anomaly. The induced warm surface potential temperature that results, acts like its own PV-like anomaly, stimulating its own cyclonic circulation around it (Hoskins *et al.*, 1985). With time, the induced cyclonic circulation could lead to the formation of a closed surface low-pressure cell.

COLs and associated surface cyclogenesis have foundations in upper tropospheric processes, specifically related to stratospheric intrusions into the upper troposphere. It is well known that some

COLs are restricted to the upper levels of the troposphere, whilst others can induce intense surface cyclones. Some studies have tried to quantify the amount of COLs that were associated with surface cyclones, but these studies are restricted to the European sector of the northern hemisphere. Nieto *et al.* (2005) found that 47% of the COLs in European region were associated with surface cyclones. In the Mediterranean, Porcù *et al.* (2007) found that 43% of the COLs recorded during the study were associated with surface cyclones lasting for at least 12 hours. However, of these cyclones 17% were not vertically correlated to the COL. The study also looked at the depth of COLs. The COL depth refers to the lowest geopotential level that a low-pressure area was found. 60% of the COLs were found to reach the 1000hPa level and 64% reached at least the 850hPa at some point during the lifespan of the COL. A similar quantification experiment has not to this date been done anywhere in the Southern hemisphere. In addition, the differences in the dynamical and PV structures of COLs that extended to the surface against those that do not has never before been studied extensively.

1.5. Research problem

COLs that are associated with surface cyclones can have a large effect on the meteorological and oceanographic conditions in and around South Africa. The factors that result in some COLs extending to associated surface low pressure systems and other COLs remaining shallow, not extending to surface cyclones remains an open question. Various observational studies analysing COLs have been performed for various sectors around the globe. Some of these studies have shown cases where surface lows are present. Few case studies have been performed for the South African region and even fewer based on PV dynamics. One of the few of these studies focussed on ozone exchange as a result of the dynamical mechanisms associated with COLs (Baray *et al.*, 2003). Another study has analysed a cut-off low from an NWP perspective, with the focus on the dynamics that lead to extreme rainfall events (Singleton and Reason, 2007a). No studies over the region have analysed extension mechanisms in an observational analysis in a South African context.

Various COL climatologies and associated identification techniques have been done for the SH in the open literature. The seasonal, temporal and spatial variability of COLs have been well studied in these COL climatologies. However, the key factor of surfaceward extension has remained absent from this work. The number of COLs that extend to the surface and the variability of these extensions remains an open question. Climatologies are a key ingredient to understanding how processes work in the real world. Theoretical knowledge in the form of the quasi-geostrophic framework and PV theory exists for the mechanisms at work during these processes. It is well known that PV anomalies in the upper troposphere can induce cyclonic circulations (Hoskins *et al.*, 1985) and can result in cyclonic circulation at the surface. These theoretical concepts however have not been put to the test in the surfaceward

extension COL problem for the Southern African context. Some detail in these theoretical concepts still remain open questions. The following open questions emerge:

1. Do all COLs have the potential for surfaceward extension?
2. How common are COLs that extend all the way to the surface and are they variable with respect to season, region and latitude?
3. Are COLs surfaceward extensions resulting in surface cyclogenesis dependent on the depth of associated stratospheric intrusions?

1.6. Hypothesis, aims and objectives

Given the research problem stated in Section 1.5, the aim of this research is to describe the processes and mechanisms that result in COLs extending to the surface and resulting in surface cyclones to develop. We hypothesise that deeper stratospheric intrusions of high-PV air result in COLs extending to the surface. We test the hypothesis and investigate the aim by achieving the following research objectives:

1. Perform an observational analysis on a COL associated with surface cyclogenesis in order to identify characteristics and mechanisms that may be at play during surface cyclogenesis.
2. Gain insight into the variability of COLs that are associated with low pressure systems at the surface by creating a COL climatology with respect to COL vertical depth.
3. Explore the mechanisms that may promote or inhibit the surfaceward extension of COLs through use of a climatological COL depth database.
4. Determine the effect that the depth of stratospheric intrusions have on surface cyclogenesis.
5. Create tools for students and operational forecasters to gain an understanding of how the mechanisms of COL extensions work in theory and in practice by means of conceptual models and dynamical postprocessing NWP tools.

1.7. Thesis outline

Chapter 2 is presented in form of journal paper submitted for peer review and publication in *Elsevier's Atmospheric Research*. The paper presents an analysis of a COL and associated surface cyclone, locally referred to as *Cape Storm*. An analysis of the system from its initial development until eventual effect on South Africa are explored from a PV perspective. The meteorological and societal impacts are also presented. Exploring this case study reveals some of the processes that result in the COLs development and the extension to the surface. Chapter 3 is presented in the form of journal paper submitted for peer review and publication in *Springer's Climate Dynamics*. This section provides a climatological review of COLs in relation to their extension to the surface. Using lessons learned from the case study in Chapter 2, the processes that lead to surfaceward extension of COLs from a PV

perspective are also explored in a climatological sense. Chapter 4 is presented in the form of journal paper submitted for peer review and publication in *European Geophysics Union's Weather and Climate Dynamics Discussions*. Chapter 4 explores the PV properties of COLs using the concept of PV inversion. An idealised numerical experiment is conducted as to the effect of stratospheric intrusions, in particular their depth, and their effect on surface cyclogenesis. Finally, Chapter 5 is presented as a more traditional thesis chapter. This chapter explores a conceptual model created for COL extensions in the southern hemisphere, based on the results of previous chapters. A web portal is also created in order to apply the conceptual model operationally by providing PV dynamical numerical weather prediction postprocessing tools and field. We summarise the work and draw conclusions from it in the final Chapter 6. Recommendations for future work are also provided.

This thesis is structured as a collection of journal articles where Chapter 2, 3 and 4 as journal articles, two of which are published and one which is currently under. In order to create a cohesive thesis, the figure and table numbers presented within the thesis may differ from those that are published in the open scientific literature. Chapters 1, 5 and 6 are written in a more traditional thesis format with separate reference lists are provided at the end of each individual chapter.

1.8. References

Baray JL, Baldy S, Diab RD, Cammas JP. 2003. Dynamical study of a tropical cut-off low over South Africa, and its impact on tropospheric ozone. *Atmospheric Environment*, 37(11): 1475–1488. https://doi.org/10.1016/S1352-2310(02)00999-8.

Bell GD, Bosart LF. 1993. A Case Study Diagnosis of the Formation of an Upper-Level Cutoff Cyclonic Circulation over the Eastern United States. *Monthly Weather Review*, 121(6): 1635–1655. https://doi.org/10.1175/1520-0493(1993)121<1635:ACSDOT>2.0.CO;2.

D'Abreton PC, Lindesay JA. 1993. Water Vapour Transport Over Southern Africa. *International Journal of Climatology*, 13: 151–170.

Engelbrecht CJ, Landman WA, Engelbrecht FA, Malherbe J. 2015. A synoptic decomposition of rainfall over the Cape south coast of South Africa. *Climate Dynamics*, 44(9–10): 2589–2607. https://doi.org/10.1007/s00382-014-2230-5.

Ertel H. 1942. Ein neuer hydrodynamischer Wirbelsatz. *Meteorologische Zeitschrift*, 59: 277–281.

Favre A, Hewitson B, Lennard C, Cerezo-Mota R, Tadross M. 2013. Cut-off Lows in the South Africa region and their contribution to precipitation. *Climate Dynamics*, 41(9–10): 2331–2351. https://doi.org/10.1007/s00382-012-1579-6.

Fuenzalida HA, Sánchez R, Garreaud RD. 2005. A climatology of cutoff lows in the Southern Hemisphere. *Journal of Geophysical Research Atmospheres*, 110(18): 1–10. https://doi.org/10.1029/2005JD005934.

Holton JR, Hakim GJ. 2013. *An Introduction to Dynamic Meteorology*. *Academic Press*. Elsevier.

Hoskins BJ, McIntyre ME, Robertson AW. 1985. On the use and significance of isentropic potential vorticity maps. *Quarterly Journal of the Royal Meteorological Society*, 111(470): 877–946. https://doi.org/10.1002/qj.49711147002.

Hsieh Y-P. 1949. AN INVESTIGATION OF A SELECTED COLD VORTEX OVER NORTH AMERICA. *Journal of Meteorology*, 6(6): 401–410. https://doi.org/10.1175/1520-0469(1949)006<0401:AIOASC>2.0.CO;2.

Iwabe CMN, Da Rocha RP. 2009. An event of stratospheric air intrusion and its associated secondary surface cyclogenesis over the South Atlantic Ocean. *Journal of Geophysical Research Atmospheres*, 114(9): 1–15. https://doi.org/10.1029/2008JD011119.

Kleinschmidt E. 1950. Über Aufbau und Entstehung von Zyklonen. *Meteorol. Rdsch.*, 3: 1–6.

Lackmann GM. 2011. *Midlatitude synoptic meteorology: Dynamics, analysis and forecasting*. American Meteorological Society: Boston, MA.

Mcintyre ME, Palmer TN. 1983. Breaking planetary waves in the stratosphere. *Nature*, 305(5935): 593–600. https://doi.org/10.1038/305593a0.

Muñoz C, Schultz D, Vaughan G. 2020. A midlatitude climatology and interannual variability of 200- And 500-hPa cut-off lows. *Journal of Climate*, 33(6): 2201–2222. https://doi.org/10.1175/JCLI-D-19-0497.1.

Nakamura M, Plumb RA. 1994. The Effects of Flow Asymmetry on the Direction of Rossby Wave Breaking. *Journal of the Atmospheric Sciences*, 51(14): 2031–2045. https://doi.org/10.1175/1520-0469(1994)051<2031:TEOFAO>2.0.CO;2.

Ndarana T, Rammopo TS, Bopape M-J, Reason CJC, Chikoore H. 2020. Downstream development during South African cut-off low pressure systems. *Atmospheric Research*. Elsevier B.V., 249(October 2020): 105315. https://doi.org/10.1016/j.atmosres.2020.105315.

Ndarana T, Waugh DW. 2010. The link between cut-off lows and Rossby wave breaking in the Southern Hemisphere. *Quarterly Journal of the Royal Meteorological Society*, 136(649): 869–885. https://doi.org/10.1002/qj.627.

Nieto R, Gimeno L, de la Torre L, Ribera P, Gallego D, García-Herrera R, García JA, Nuñez M, Redaño A, Lorente J. 2005. Climatological Features of Cutoff Low Systems in the Northern Hemisphere. *Journal of Climate*, 18(16): 3085–3103. https://doi.org/10.1175/JCLI3386.1.

Omar SA, Abiodun BJ. 2020. Characteristics of cut-off lows during the 2015–2017 drought in the Western Cape, South Africa. *Atmospheric Research*. Elsevier B.V, 235: 104772. https://doi.org/10.1016/j.atmosres.2019.104772.

Palmén E. 1949. Origin and Structure of High-Level Cyclones South of the: Maximum Westerlies. *Tellus*, 1(1): 22–31. https://doi.org/10.1111/j.2153-3490.1949.tb01925.x.

Peters D, Waugh DW. 2003. Rossby wave breaking in the southern hemisphere wintertime upper troposphere. *Monthly Weather Review*, 131(11): 2623–2634. https://doi.org/10.1175/1520-0493(2003)131<2623:RWBITS>2.0.CO;2.

Pinheiro HR, Hodges KI, Gan MA. 2019. Sensitivity of identifying cut-off lows in the Southern Hemisphere using multiple criteria: implications for numbers, seasonality and intensity. *Climate Dynamics*. Springer Berlin Heidelberg, (0123456789): 1–15. https://doi.org/10.1007/s00382-019-04984-x.

Pinheiro HR, Hodges KI, Gan MA, Ferreira NJ. 2017. A new perspective of the climatological features of upper-level cut-off lows in the Southern Hemisphere. *Climate Dynamics*, 48(1–2): 541–559. https://doi.org/10.1007/s00382-016-3093-8.

Porcù F, Carrassi A, Medaglia CM, Prodi F, Mugnai A. 2007. A study on cut-off low vertical structure and precipitation in the Mediterranean region. *Meteorology and Atmospheric Physics*, 96(1–2): 121–140. https://doi.org/10.1007/s00703-006-0224-5.

Rautenbach, C., Daniels, T., de Vos, M., Barnes, M.A., 2020. A coupled wave, tide and storm surge operational forecasting system for South Africa: validation and physical description. Nat. Hazards. https://doi.org/10.1007/s11069-020-04042-4

Reboita MS, Nieto R, Gimeno L, Da Rocha RP, Ambrizzi T, Garreaud R, Krger LF. 2010. Climatological features of cutoff low systems in the Southern Hemisphere. *Journal of Geophysical Research Atmospheres*, 115(17): 1–15. https://doi.org/10.1029/2009JD013251.

Reed RJ. 1955. A Study of a Characteristic Tpye of Upper-level Frontogenesis. *Journal of Meteorology*, 12(3): 226–237. https://doi.org/10.1175/1520-0469(1955)012<0226:ASOACT>2.0.CO;2.

Rossby C-G. 1940. Planetary flow patterns in the atmosphere. *Quarterly Journal of the Royal*

Meteorological Society (suppl), 68–87.

Singleton, A.T., Reason, C.J.C., 2006. Numerical simulations of a severe rainfall event over the Eastern Cape coast of South Africa: Sensitivity to sea surface temperature and topography. Tellus, Ser. A Dyn. Meteorol. Oceanogr. 58, 355–367. https://doi.org/10.1111/j.1600-0870.2006.00180.x

Singleton AT, Reason CJC. 2007a. A Numerical Model Study of an Intense Cutoff Low Pressure System over South Africa. *Monthly Weather Review*, 135(3): 1128–1150. https://doi.org/10.1175/mwr3311.1.

Singleton AT, Reason CJC. 2007b. Variability in the characteristics of cut-off low pressure systems over subtropical southern Africa. *International Journal of Climatology*, 27(3): 295–310. https://doi.org/10.1002/joc.1399.

Stander, J.H., Dyson, L., Engelbrecht, C.J., 2016. A snow forecasting decision tree for significant snowfall over the interior of South Africa. *South African Journal of Sciencei.* 112, 1–10. https://doi.org/10.17159/sajs.2016/20150221

Taljaard, J.J., 1985. Technical Paper No. 14: *Cut-off lows in the South African region*. Pretoria.

Taljaard JJ. 1995. *Atmospheric Circulation Systems, Synoptic Climatology and Weather Phenomena of South Africa: Part 2*. Pretoria.

Thorpe AJ, Volkert H, Ziemiański MJ. 2003. The Bjerknes' circulation theorem: A historical perspective. *Bulletin of the American Meteorological Society*, 84(4): 471-480+429. https://doi.org/10.1175/BAMS-84-4-471.

Tyson PD, Preston-Whyte RA. 2000. *The weather and climate of southern Africa*. Oxford University Press: Cape Town.

Uccellini LW, Keyser D, Brill KF, Wash CH. 1985. The Presidents' Day cyclone of 18-19 Februarry 1979: influence of upstream trough amplification and associated tropopause folding on rapid cyclogenesis. *Monthly Weather Review*, 962–988.

van Delden A, Neggers R. 2003. A case study of tropopause cyclogenesis. *Meteorological Applications*, 10(2): 187–199. https://doi.org/10.1017/S1350482703002081.

van Heerden J, Taljaard JJ. 1998. Africa and Surrounding Waters. *Meteorology of the Southern Hemisphere*. American Meteorological Society: Boston, MA, 141–174.

Chapter 2: Cape Storm: A dynamical study of a cut-off low and its impact on South Africa

Preface

This chapter consists of one research paper that has been published in Atmospheric Research. The paper went through independent and international peer review. The citation is as follows:

Barnes M.A., Turner K., Ndarana T. and Landman W.A (2021) Cape storm: A dynamical study of a cut-off low and its impact on South Africa, Atmospheric Research, **249**, p. 105290. doi: https://doi.org/10.1016/j.atmosres.2020.105290.

In completion of the first objective of this study, a case study of a cut-off low (COL) extension to a surface low is performed. The case study presented in this paper is of *Cape Storm*, an intense surface low associated with a COL that greatly affected the south-western Cape of South Africa. The analysis of the weather system is performed from a potential vorticity (PV) point of view. The weather system is tracked subjectively to its original development. The intense surface low developed coincident with a COL to the west of South America. Cross-sectional and two-dimensional analyses of PV fields reveal that the development of the system associated with a Rossby-wave breaking (RWB) event and a deep intrusion of high-PV air. Further, two separate COLs and associated RWB events and stratospheric intrusions affected and deepened the associated surface low pressure system. Few dynamical case studies of weather systems over South Africa are available in the scientific literature, with even fewer being performed from a PV perspective. The novelty of this work is increased with the finding that the surface cyclone started developed before the COLs development and many days before its with eventual impact on South Africa.

The enhanced deepening of the surface low had a large impact on the communities of the Western Cape. Strong winds, tremendously high seas, out-of-control wildfires and storm surge lashed the province. These impacts are analysed in this paper from both a societal and meteorological sense. The analysis of meteorological and societal impacts on communities helps to motivate the importance of studying the behaviour of these types of extreme weather systems to the public of South Africa. Few studies have combined dynamical and societal impact analyses of a weather system over South Africa into one package, increasing the novelty of the study.

The paper was co-authored by my two supervisors, Dr. T. Ndarana and Prof. W.A. Landman who supervised, guided and reviewed the work. The work was additionally co-authored by my colleague at the South African Weather Service Miss. K. Turner who assisted in providing valuable on-the-ground and operational insight and collected data, information and images into the impact section of the work. Although the work was co-authored, I conceptualized the work, performed the analysis, wrote, and reviewed the manuscript.

Cape Storm: A dynamical study of a cut-off low and its impact on South Africa

Michael A. Barnes[*1,2], *Kate Turner*[3], *Thando Ndarana*[2] *and Willem A. Landman*[2]

[1] *Marine Research Unit, South African Weather Service, Cape Town, South Africa*

[2] *Department of Geography, Geoinformatics and Meteorology, University of Pretoria, Pretoria, South Africa*

[3] *Forecasting Division, Cape Town Weather Office, South African Weather Service, Cape Town, South Africa*

Abstract

An intense surface low pressure system and associated cut-off low (COL) that affected the south-western Cape of South Africa on 6-7 June 2017 are analysed. The storm, locally named *Cape Storm*, was associated with heavy rains, strong winds, runaway fires, storm surge and extremely large waves. These extreme meteorological conditions resulted in a loss of life and damage to infrastructure in various forms around the province. The societal impacts that occurred have been collected and summarized in this study. Cape Storm was tracked back to its initial development as a COL extension to a surface low pressure system to the south-west of South America. ERA-Interim reanalysis is analysed from a potential vorticity (PV) perspective to assess the factors that influenced the development of this impactful storm. The analysis found that the system was associated with a Rossby wave breaking (RWB) event and an intrusion of high-potential vorticity (PV) from the stratosphere, assisting the development of the surface low pressure system. The COL migrated across the South American continent and made its way across the South Atlantic Ocean. As it migrated towards South Africa, two more COLs associated with RWB events and stratospheric intrusions maintained and deepened the surface low pressure system, increasing its eventual impact on South Africa. The surface cyclone deepening events were both associated with high-PV in both the upper to mid-levels and lower levels of the troposphere. One of these events was associated with a deep, tightly wrapped, cyclonic intrusion of high-PV air into the troposphere and higher PV values in the lower tropospheric, resulting in rapid and intense surface cyclogenesis.

Keywords: Atmospheric dynamics; Explosive cyclogenesis; Stratospheric intrusions; Rossby wave breaking; Weather extremes; Cut-off low; South Africa

2.1. Introduction

On 6 and 7 June 2017, extreme waves, storm surge, heavy rain, wildfires and strong winds lashed the south-western Cape of South Africa. The weather system, named locally in the media as *Cape Storm*, was arguably one of the most intense weather systems that impacted the Cape in recent years owing to the prevailing drought conditions that had plagued the region since 2015 (Mahlalela *et al.*, 2019; Richman and Leslie, 2018). The intensity of the storm was largely attributed to a deep surface low pressure off of the Western Cape coastline resulting in strong Gale force winds and heavy rainfall in the region. This surface low pressure system was also concomitant with a cut-off low (COL) in the upper levels of the troposphere. A COL is a cold-cored, closed, upper-air low pressure system (Palmen and Newton, 1969). These systems develop by becoming displaced equatorward out of the westerly jet in the extra-tropics. South Africa is frequented by multiple COLs every year. In fact, Singleton and Reason (2007) showed that 11 COLs on average affect the southern African region annually. COLs are also more frequent in this region in the transitionary seasons and in particular in the austral autumn months (Favre *et al.*, 2013; Singleton and Reason, 2007a). The southern most parts of the country receive 16% of their total annual rainfall as a result of COLs (Engelbrecht *et al.*, 2015). COLs are also a major contributor to extreme rainfall and flooding over the region, with 20% of all flooding events associated with upper-air cyclones (Singleton and Reason, 2007b).

Many observational studies have looked into the dynamics of observed COL events in various parts of the world (Baray *et al.*, 2003; Bell and Bosart, 1993; van Delden and Neggers, 2003). These studies show that COLs are generally associated with stratospheric intrusions of dry, high-potential vorticity (PV) air advected isentropically and equatorward into the troposphere. Ndarana and Waugh (2010) further linked the process of stratospheric intrusions associated with COL development to the process of Rossby wave breaking (RWB), an irreversible process characterized by negative meridional PV gradients (McIntyre and Palmer, 1985). They found that 89% of COLs identified in the southern hemisphere were linked with RWB. The remaining 11% of COLs were still collocated with high-PV air advected into the troposphere by means of intrusions that exhibit no PV overturning.

A “PV thinking” approach has been a standard in dynamic meteorological analyses since the landmark paper by Hoskins et al (1985). Isentropic PV reasoning is based around the invertibility principle (Hoskins et al, 1985). The invertibility principle states that if PV on each isentropic surface including that of the lower boundary is known, then all other meteorological fields (geopotential height, temperature and horizontal velocity) can be calculated under a suitable balance condition. Vertical velocity can also be calculated using the omega equation, assuming frictional and adiabatic processes are described. Isentropic PV fields can therefore be used to describe the evolution of all other

dynamical fields. As a result, PV and in particular isentropic PV has become the standard in analysing dynamical processes including that of COLs, stratospheric intrusions and associated surface cyclogenesis (e.g. Uccellini *et al.*, 1985; Davis, Grell and Shapiro, 1996; Morgan and Nielsen-Gammon, 1998; van Delden and Neggers, 2003; Iwabe and Da Rocha, 2009). PV theory is also consistent with more traditional frameworks such as the Sutcliffe-Petterssen framework (Brennan *et al*, 2008).

It is well known that COLs, can at times, be associated with significant cyclogenesis at the surface. Kleinschmidt (1950) was the first to emphasize the importance of high-PV air in the development of surface low pressure systems with Eliassen and Kleinschmidt (1957) later linking these high-PV anomalies to the intrusion of stratospheric air into the troposphere. In the Southern hemisphere, high-PV anomalies (comparatively large negative PV values) are associated with cyclonic flow. Hoskins et al (1985) showed how cyclonic circulations initiated by a PV anomaly through a stratospheric intrusion of high-PV air can extend from the upper troposphere towards the surface resulting in cyclonic circulation at the surface.

Several observational studies in both hemispheres have presented COLs with associated surface cyclones (Bell and Bosart, 1993; Singleton and Reason, 2007b, 2006). A study on the President's Day Cyclone of 1979 which affected the United States of America, shows how the presence of an intrusion of dry, high-PV stratospheric air both preceded and was collocated to an explosive surface cyclogenesis event (Uccellini *et al.*, 1985). This intrusion was also associated with dynamical tropopause folding. In this case, the high-PV intrusion extended well into the mid-levels (close to 700hPa). It is currently not known at what depth these intrusions result in surface cyclogenesis. This process was similarly observed by Iwabe and Da Rocha (2009) in the South Atlantic and by Liberato (2014) in the North Atlantic. Iwabe and Da Rocha (2009) also observed that the development of a COL above the surface cyclone resulted in the maintenance of the low-level cyclone and its development. In the Southern African region, few studies of cut-off lows have been done from a PV perspective. One of the few of these studies looked at a tropical COL over the southern African region (Baray *et al.*, 2003). In this COL, the dynamical tropopause dropped to the 500hPa mark (at -1.5PVU). Baray *et al.* (2003) however focused on the effect of these processes on ozone intrusion rather than their link to low-level cyclonic processes and their impact. Another studied a significant rainfall event over the south-western Cape (Singleton and Reason, 2007b). the study was focused on the resulting heavy rainfall where a significant southerly low-level jet, topography and lower tropospheric diabatic heating playing the biggest roles. The Mediterranean has been a region in which upper level tropospheric and stratospheric processes and their links to surface cyclogenesis have been well studied. Porcù *et al.* (2007) showed that 38% of the COLs identified in this region contained well developed cyclonic

structures on the surface, bringing large amounts of precipitation with them. Intense surface cyclogenesis in the region was also found to be linked with RWB induced stratospheric intrusions of high-PV air into the troposphere (Flaounas *et al.*, 2015).

The COL and surface cyclone that affected South Africa on 6-7 June 2017 are analysed from a PV perspective to understand the system and its development. The system is tracked back from its initial development to its eventual impact on South Africa. What mechanisms produced this deep low-pressure system? And how influential were the COL and associated upper level processes in producing and deepening it? Additionally, few scientific studies have focused on the effect that extreme weather events had on the communities that they affect. In this study, we discuss the eventual impact that the weather system had in the Western Cape of South Africa. In Section 2, a brief introduction of the study region is provided followed by a description of the data and methods in Section 3. In Section 4, the COL-surface low pressure system is tracked to its initial point of development. The dynamics of the system throughout its life from a PV perspective are discussed in Section 5. In Section 6, the meteorological impacts are discussed in relation to the impact they had on society. Conclusions are drawn in Section 7.

2.2. The study region

South Africa, at the southern tip of the African continent, is situated in the subtropics. The vast majority of the region receives its rainfall in the summer from convective, tropical weather systems. The Western Cape, a province situated in the south-western parts of the country (Figure 1), however receives mostly winter rainfall by organized, extratropical synoptic systems from the south and west such as cold frontal bands of passing mid-latitude cyclones and COLs. The province boasts a west and south coast with multiple complex embayments, the most notable of which are False Bay and Table Bay situated to the south and north-west of the province's major airport, Cape Town International (marked CT Int. Airport on Figure 1). The province's coastline is framed by the Cape fold mountain ranges (Figure 1). The 1000m rise to the peaks of these ranges play a significant role in increasing rainfall tallies within these areas in onshore flow regimes (Engelbrecht *et al.*, 2015). The plateaued interior of the province is generally drier and semi-arid and also occasionally receives rainfall by convective thunderstorms in the summer. Figure 1 shows the position of the Western Cape within the South African and southern African context. Various automatic weather stations (AWSs) and rain gauges are found within the province and are shown in Figure 1 by black dots.

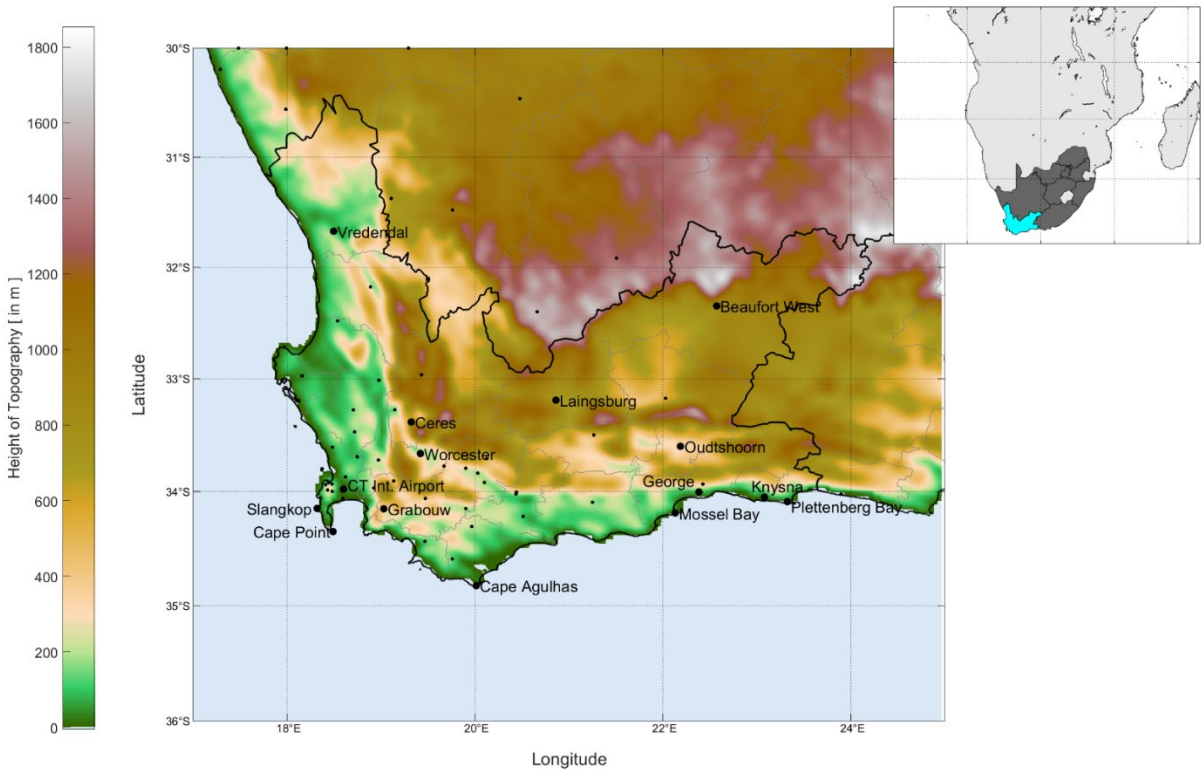

Figure 1: The Western Cape of South Africa. The position of the Western Cape (cyan) within the context of South Africa (dark grey) and southern Africa (light grey) is shown in the inlaid image in the top right corner. Topography (in metres above sea level) is shown by the shaded colours. The various automatic rainfall stations and AWSs available are shown with black dots. Some of the observations specifically mentioned are also labelled.

2.3. Data and methods

The properties of the COL and surface low pressure system that affected the South African coastline on 6-7 June 2017 are analysed by the use of 0.75x0.75-degree ERA-Interim data (Dee *et al.*, 2011). Mapping mean-sea level pressure (MSLP) fields at a contour interval of 1hPa, the surface low pressure system that affected the southern-western Cape of South Africa is located. For the purpose of this study, a surface low pressure system is defined as grid point which contains a local pressure minimum and is encircled by a closed contour on the MSLP field. If more than one neighboring grid-point is encircled by a closed contour, the grid-point with the lowest mean sea level pressure is chosen. The ERA-Interim latitude and longitude of the grid point and its corresponding sea level pressure value are recorded in a database. The surface low pressure is tracked backwards subjectively for each ERA-Interim 6-hourly timestep, recording the latitude, longitude and mean sea level pressure value and adding it to the database, if it existed. A surface low pressure system at a preceding timestep is deemed to be a part of the same surface low pressure system is within 10-degrees (e.g. Flaounas et al., 2014) of the surface low pressure system. If multiple surface low pressure systems are detected, a surface low is chosen based on the trajectory of the overall system. Closed, upper level lows (COLs)

within the vicinity of the surface low are also tracked subjectively. For the purpose of this study, a COL is defined as an upper level (300 and 500hPa) geopotential height minimum enclosed by a geopotential height contour. Closed contours are searched for at a 10gpm contour interval. A COL is deemed to be in the vicinity of a surface low if its centre was found within a 5x5-grid box of the COL (similarly to Porcù et al., (2007)). Similarly to the surface low detection methodology, a COL is deemed to be a part of the same COL-system if it is found within 10-degrees of the preceding timestep and based on the trajectory of the overall COL system.

The dynamical analysis of the system is considered from a PV perspective. Isentropic PV variables are available as part of the ERA-Interim reanalysis suite. The 300K, 315K, 330K and 350K levels are chosen as these are the levels that are closest to the dynamical tropopause from those available in the ERA-Interim suite. Various studies have considered various potential vorticity unit (PVU) contours as the dynamical tropopause (Hoskins, 1991). The dynamical tropopause is determined by looking at how tightly packed the PV contours are through the center of each of the COL systems. From theory, it is well-known that stratospheric intrusions of high-PV air can stimulate cyclonic development in the upper levels and at the surface. The analysis presented examines the PV contour representing the dynamical tropopause using mapped PV contours in both the vertical by means of two-dimensional longitudinal cross-sections as well as in the horizontal on isentropic levels. The analysis takes into the account the depth of the dynamical tropopause in relation to both the upper level and surface pressure systems. This contour representing the dynamical tropopause is analyzed in order to detect overturning as this represents the process of RWB (Ndarana and Waugh, 2011). RWB events are analysed as a key driver of stratospheric intrusions. The identification of overturned isentropic PV contours is a commonly used method for identifying RWB events. An isentropic contour is considered to be overturned if a longitude line intersects the line two or more times (Esler and Haynes, 1999; Ndarana and Waugh, 2011). Maps of PV are analysed on various pressure levels in the region of the COL and surface low pressure system to gain an understanding of the role that the PV fields, specifically relating to stratospheric air intruding into the troposphere has on surface cyclogenesis.

Finally, this study analyses the meteorological and societal impact that Cape Storm has on the south-western Cape of South Africa. Meteorological surface observations from AWSs within the network of the South African Weather Service (SAWS) across the Western Cape province are used. Data is valid between 6 and 8 June 2017. These data are quality controlled in house by the SAWS. For the purpose of this study 10m wind, 2m temperature, surface pressure, rainfall and 2m relative humidity data are used. The temporal resolution of these data is five minutes. Where longer term data is analysed, hourly values are used in the analysis. The impact on society is measured by reports of damages and

losses at various locations. Reports and statements made by the Western Cape government are used with regards to facts and figures of impacts. Media reports quoting government officials (such as in press conferences) are also used but are corroborated by multiple reports where possible.

2.4. Tracking of COLs and the surface low pressure system

The COL and associated surface low pressure system that affected the South African coastline on 6 and 7 June 2017 are tracked backwards in time. The upper level and surface cyclones are tracked using low pressure minima that contained a closed isohypse on the MSLP, 500hPa and 300hPa ERA-Interim geopotential height fields. Tracking is performed in order to investigate the initial development of the system. The first COL (hereafter referred to as COL1) developed on the 300hPa level on 27 May 2017 at 18h00 UTC. The track of this upper low is represented by blue dots on Figure 2. According to Porcù *et al.* (2007), a COL and a surface low pressure system are vertically related if the COL extends down to the surface and is coincident with an independently detected surface low-pressure system. COL1 does in-fact meet this criterion. In addition, the paths of the upper level and surface systems followed similar paths throughout their lifecycles. The surface low pressure system associated with COL1 system preceded the upper level closed circulation by 18 hours and is first visible on the 00h00 UTC field on 27 May 2017. At its initial development, the surface low developed with a central mean sea level pressure in the range of 1011-1013hPa as shown in Figure 3.

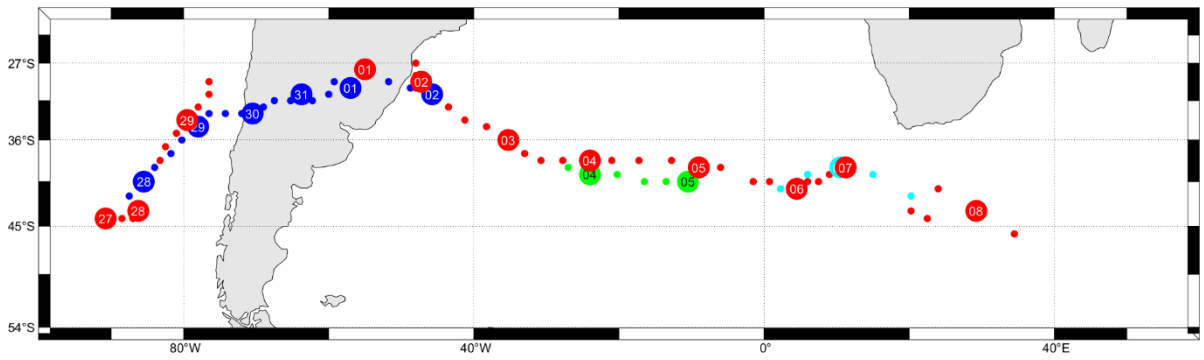

Figure 2: Top panel: Tracks of COLs (COL1 - blue dots; COL2 - green dots; COL3 - cyan dots) and surface low pressure systems (red dots) from initial development on 27 May 2017 until 08 June 2017. Points valid for 00h00 UTC on each day are plotted with enlarged points with a label of the day of the month within each point.

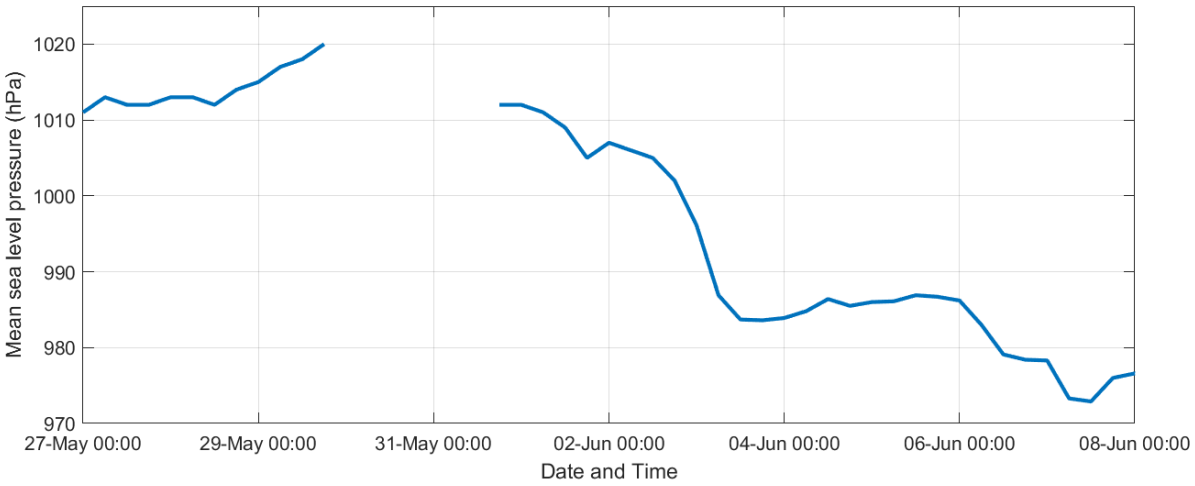

Figure 3: Central mean sea level pressure of the surface low along its track as shown by the red points in Figure 2.

COL1 and the surface low pressure system continued to track northeastwards making landfall over the South American continent during the evening of 29 May 2017. The surface low pressure system could not be detected on the MSLP field as it made its way over the South American continent as can be seen in Figure 2. This is as a result of the significant topography in this area in the form of the Andes mountains. In order to analyse the system as it moves over the Andes mountain, the 600hPa and 700hPa levels are analysed in conjunction with the COL moving above. With a similar method to the tracking of both the COLs and surface low pressure system, tracks of low-pressure systems at both the 600hPa and 700hPa levels were produced. These tracks along with that of COL1 as well as the surface low pressure system are shown in Figure 4. The tracks of the 700hPa and 600hPa lows reveal that the low pressure system is caused to "split off" as it meets the high orography of the Andres, with one track stagnating to the north and another emerging to the east of the Andes and moving with the COL across the South American continent. This is emphasized more so in the 700hPa field (which is closer to the height of the Andes) than the 600hPa field. Figure 5 shows the 700hPa contours and the associated low-pressure systems as they move over the Andes, showing how the systems split into two. The 600hPa geopotential heights shown in Figure 5 show that the overarching low through the mid-levels is still concomitant with the low-pressure system that moves over eastwards over the South American continent. From the movement and timing of the development of these low-pressure cells, it is clear that they have the same driver and therefore for the purpose of this study are considered as part of the same low-pressure system. COL1 weakened as it made its way towards the Atlantic Ocean and by 2 June 2017 06h00 UTC could no longer be detected on the 300hPa and 500hPa geopotential height fields. The surface low pressure system however continued to be maintained. After its exit from South America, the surface system tracked south-eastwards. The surface low pressure system was maintained across the Atlantic Ocean and into Southern Ocean to the south of the African continent. Through the surface low pressure system's track, two further COLs developed. These COLs were both

visible at both the 300hPa and 500hPa levels. The second COL (hereby called COL2, represented in green on Figure 2) developed during 3 June 2017 and was visible at both the 300hPa and 500hPa levels by 18h00 UTC. COL2 weakened during 4 June 2017 and by midnight on 5 June 2017, a closed low was no longer visible. A third COL (COL3, represented in cyan on Figure 2) developed soon after being first visible by midday on 6 June 2017. An analysis was done on all 3 of the COLs identified to determine their vertical relation to the surface low pressure system. A COL and a surface cyclone can be said to be vertically related at a point in time if all levels in the troposphere between the COL and the surface cyclone at a specific contain a local minimum within a 5x5-degree grid of the COL at that time (Porcù *et al.*, 2007). All 3 COLs were found to be vertically related both extending throughout the troposphere down to the surface. In the subsequent sections we look at all 3 COLs from a PV perspective and their direct and indirect effect on the surface low pressure system that eventually affected the South African southwest. The dynamics at play that result in the COLs development are explored and linked to the development, maintenance and deepening of the surface low pressure system. As each of the 3 COLs are vertically related to the surface cyclone, the 3 COLs and the surface low pressure system are considered to be inter-linked and a part of the same larger system. Although each of the COLs had their own development mechanisms, when a new COL developed it became vertically related to the surface low pressure system and re-established as a COL-surface low pressure system.

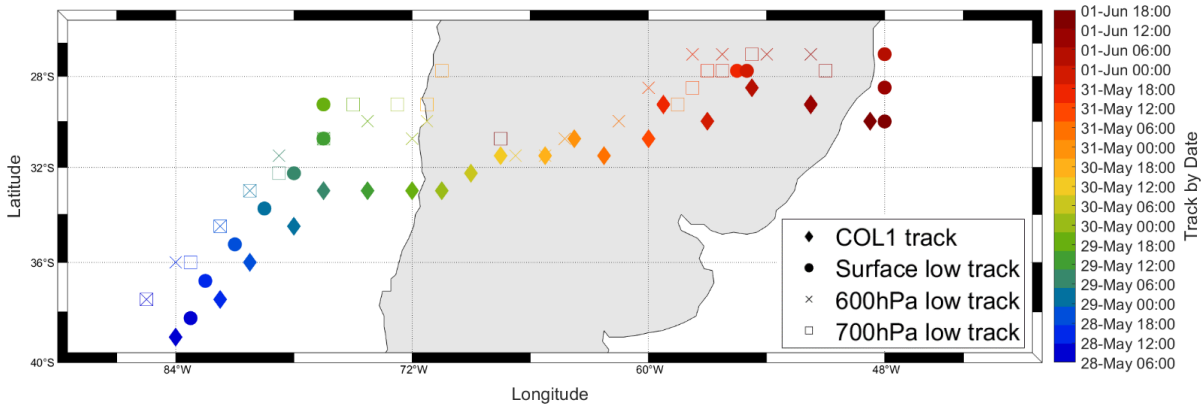

Figure 4: Tracks of the surface low (closed dots), COL (filled diamonds), 700hPa low (open squares) and 600hPa low (crosses) as the system moved over the South American continent

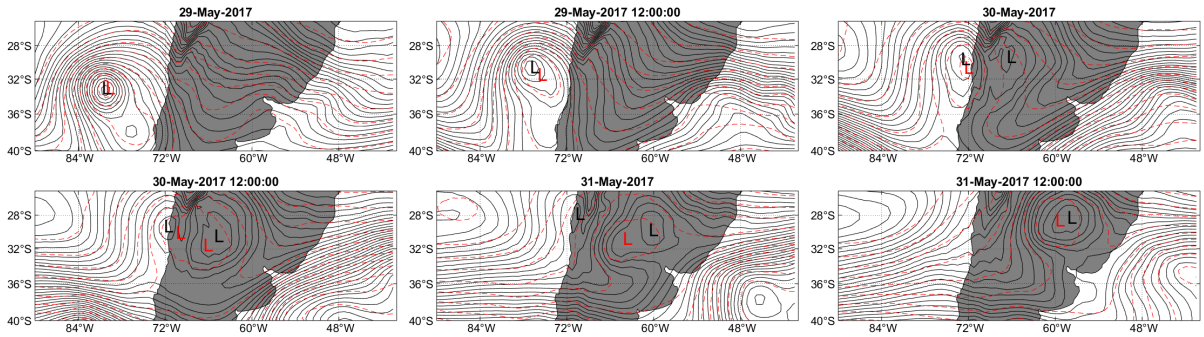

Figure 5: 700hPa (Black) and 600hPa (red dashed) as the surface low pressure system moves over the west coast of South America (29-31 May 2017). The orography of the Andes results in the low splitting in the low levels as shown by the 700hPa contours. The centre of lows are indicated by L's in the corroborating colour.

2.5. Dynamics of the COL-surface low pressure system

2.5.1. Initial development: A South American zone COL

The dynamical tropopause is a line of constant PV separating the highly stratified stratosphere from the weakly stratified tropopause (Morgan and Nielsen-Gammon, 1998). The dynamical tropopause can easily be identified by a sharp gradient increase in PV values with height (Davis and Emanuel, 1991; Morgan and Nielsen-Gammon, 1998). From Figure 6, it is clear that the dynamical tropopause lies in the region of the -1.5 and -2 PVU contours (highlighted by the magenta colours). Figure 6 also shows that the best isentropic level to represent these contours (from available ERA-Interim levels) is the 315K potential temperature level. Figure 7 shows the development of the surface and upper level pressure systems together with the developing dynamical tropopause and PV anomalies. During 26 May 2017 (Figure 7A and D) the -1.5 PVU contour shows signs of equatorward amplification. A positive PV anomaly is present in conjunction with this amplification. The amplification of the isentropic PV contours represents the process of Rossby wave amplification and dynamical tropopause folding. Co-incident with this region a trough in the upper levels begins to develop. This development also occurs at the 500hPa level (not shown). Ahead of this upper tropospheric system, a trough is present on the surface associated with a cold front which extends from the south. The development of low pressure regions in the presence of the tropopause folding is the process as theoretically described by Hoskins et al (1985). When statically stable air descends into the troposphere, it results in the air parcel gaining cyclonic vorticity (Hoskins et al, 1985). This can lead to a cold-cored, closed cyclonic circulation (Iwabe and Da Rocha, 2009). The highly statically stable stratospheric high-PV air invigorates cyclonic motion in the upper air and extends to the surface inducing surface cyclonic motion. This process intensifies throughout 26 and 27 May 2017 as the intrusion reaches towards the surface. Figure 7A-D shows both the low level and upper-level troughs amplifying to the east of the PV anomaly and upper level trough.

The amplification of the -1.5 PVU contour together with the PV anomaly on the same surface suggests there is an intrusion of high-PV air from the stratosphere. The stratospheric-tropospheric exchange is the result of baroclinic instability in the form of Rossby wave amplification. This can be seen in Figure 7C and D by the overturning of the isentropic PV contours. The stratosphere is associated with high static stability and therefore high PV values whereas the opposite is true of the troposphere. This extension from the stratosphere can be seen in Figure 6. Figure 6 shows PV contours extending down from the stratosphere into the mid-levels of the troposphere. The transport of high-PV stratospheric air into the mid-levels (600hPa shown by the -1.5PVU contour) took place. The high-PV intrusion deepens further during 27 May 2017. This does in fact initiate a closed circulation throughout the troposphere. The surface closed low is visible first and develops by midnight on 27 May 2017 in conjunction with an amplifying trough in the mid- and upper-troposphere (Figure 7C). The COL (hereby named *COL1*) develops at both the 300hPa and 500hPa levels soon after the surface low pressure system (Figure 7D).

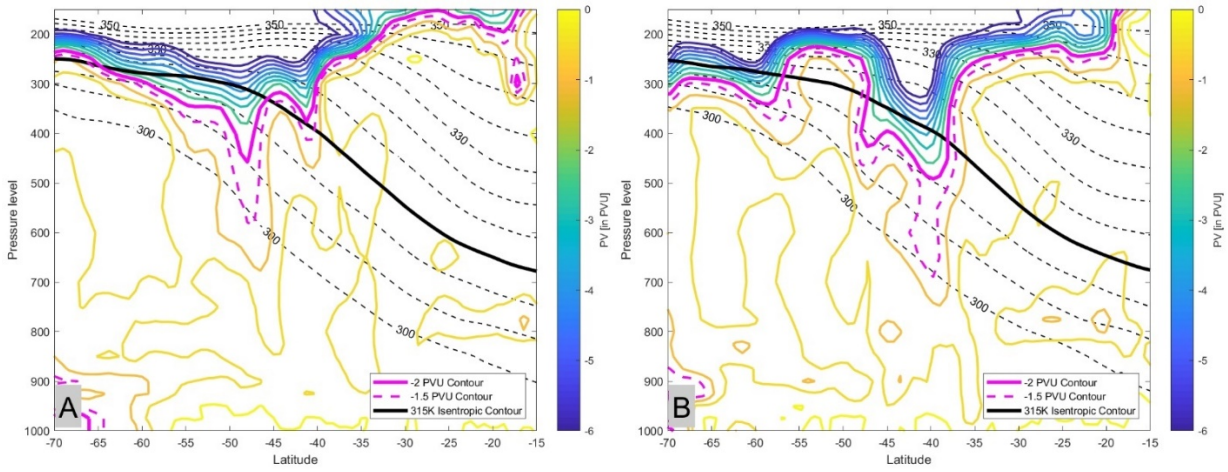

Figure 6: Cross-sections of PV across constant lines of longitude before (A – 26 May 2017 06:00 UTC at 110.25˚W) and during (B – 27 May 2017 18:00 UTC at 88.5˚W) the development of the COL1 and associated surface cyclone. The -2 PVU contour is highlighted as a thicker magenta and the -1.5 PVU contour is highlighted as a thicker dashed magenta line. Zonal mean potential temperature contours are shown by black dotted lines with the 315K line highlighted by a thick, solid black line.

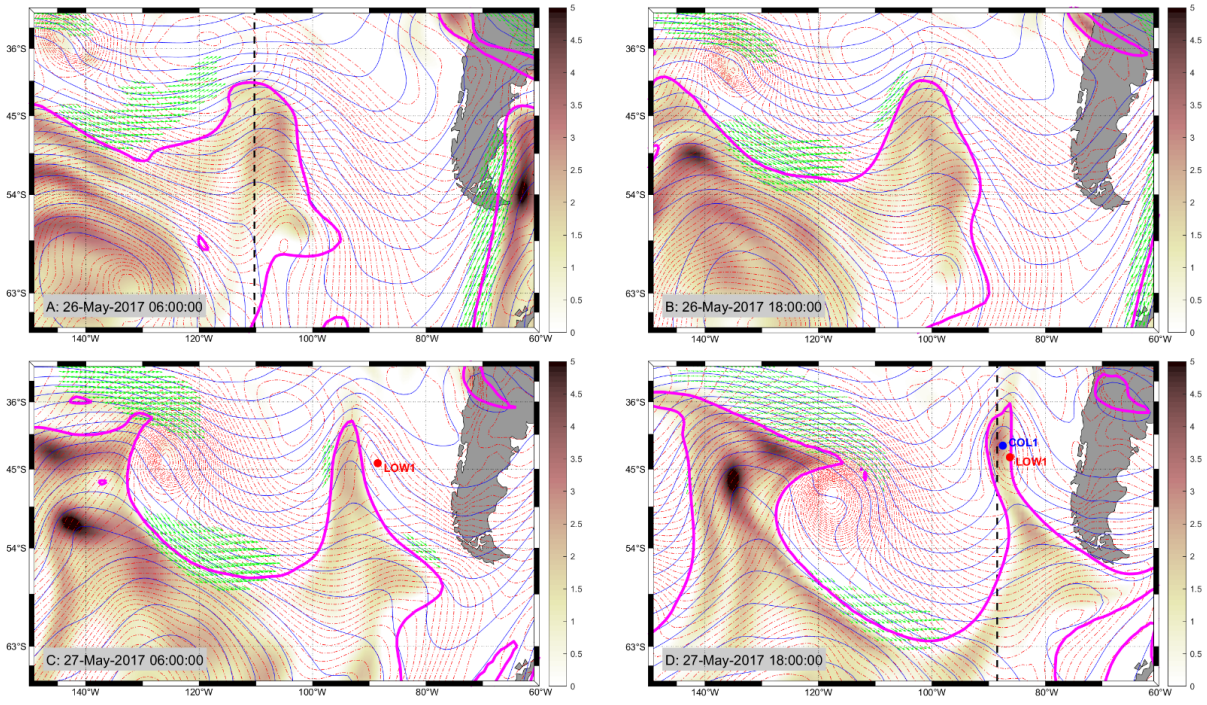

Figure 7: 300hPa (blue lines) and MSLP (red lines) geopotential height contours plotted together with the 1.5 PVU line on the 315K Isentropic surface (thick magenta lines) for the 26 May 2017 (A and B) and 27 May 2017 (C and D) over the Pacific and South American sector. Green arrows represent areas of 300hPa wind speeds over 50m.s^{-1}. Black dotted lines indicate the relevant cross-sections as shown in Figure 6.

2.5.2. Maintenance of the surface low pressure system

For each of the subsequent COL systems, the dynamical tropopause was checked to make sure that the previous stipulation of the dynamical tropopause (-1.5 PVU on the 315K surface) still applied. Figure 8 shows that this still remains true for both COL2 (left panel) and COL3 (right panel).

After COL1 tracked across South America and the surface low pressure system re-emerged within the MSLP field, COL1 decayed and by 06h00 UTC on 2 June 2017 could no longer be detected within the 300hPa and 500hPa geopotential height fields. Another region of high-PV air was being introduced into the region of the surface cyclone by the amplification of a Rossby wave to the south-west of this region (Figure 9A). Over the course of 3 June 2017, complete overturning of the -1.5 PVU contour on the 315K surface occurred indicating a RWB event. The RWB event intensified the amount of high-PV stratospheric air intruding into the upper and mid-troposphere. In a similar process as was described in Section 2.5.1, this allowed for reinvigorated cyclonic motion within the region of surface low pressure system. Figure 8A shows this intrusion down to the 400hPa level. This is not as deep as the previous intrusion associated with COL1. However, Figure 8A shows multiple PV "blobs" throughout the remainder of the troposphere. Often PV structures or "debris" can remain after previous RWB and stratospheric intrusion events (Appenzeller *et al*, 1996). The PV area at the 600hPa level in Figure 8A, is likely a result of the previous RWB event associated with COL1 which showed intrusion down to a

similar level (Figure 6). A significant blob of high-PV air also exists in the low-levels on Figure 8A between the 900 and 800hPa levels. This high-PV is likely the result of diabatic processes. This will be discussed further in Section 2.5.3.

COL2 developed at both the 300hPa level as well as the 500hPa level over the already existing cyclonic circulation at the surface by 3 June 2017. COL2 remained active for approximately 36 hours and by midday on 5 June 2016 was no longer visible on either the 300hPa or 500hPa geopotential height fields. The surface low pressure system maintained its east-south-eastward trajectory as shown in Figure 2. During the course of 5 June 2017, another Rossby wave began to amplify from the south towards the area of the surface low pressure system (Figure 9C). Similarly, to the previous COL, Rossby wave amplification eventually lead to isentropic PV overturning and the subsequent isentropic transport of high-PV air into the upper and mid-levels of the troposphere (Figure 8B). The intrusion of high-PV air from the stratosphere resulted in the formation of COL3 by 6 June 2017 to the south-west of South Africa and further maintenance of the surface low now associated with it.

COL3 was a relatively short-lived COL and decayed throughout the latter half of 7 June 2017. By 8 June 2017, no closed circulation was visible on either the 300hPa or 500hPa geopotential height fields. The surface low pressure system continued to track south-eastwards out of southern African waters and into the Southern Ocean. Although three different COLs were present during the course of the life of the surface cyclone, the role that the upper troposphere played in maintaining and strengthening this surface cyclone is significant. The various COLs and stratospheric intrusions resulted in maintaining the low-pressure system from South American continent. The systems also resulted in the low deepening significantly. A deep, intense low such as the one that eventually affected the South African coastline is unusual for this area. The relatively low pressure of the core and the steep pressure gradient surrounding it resulted in the extreme weather and associated impacts as discussed in Section 6.

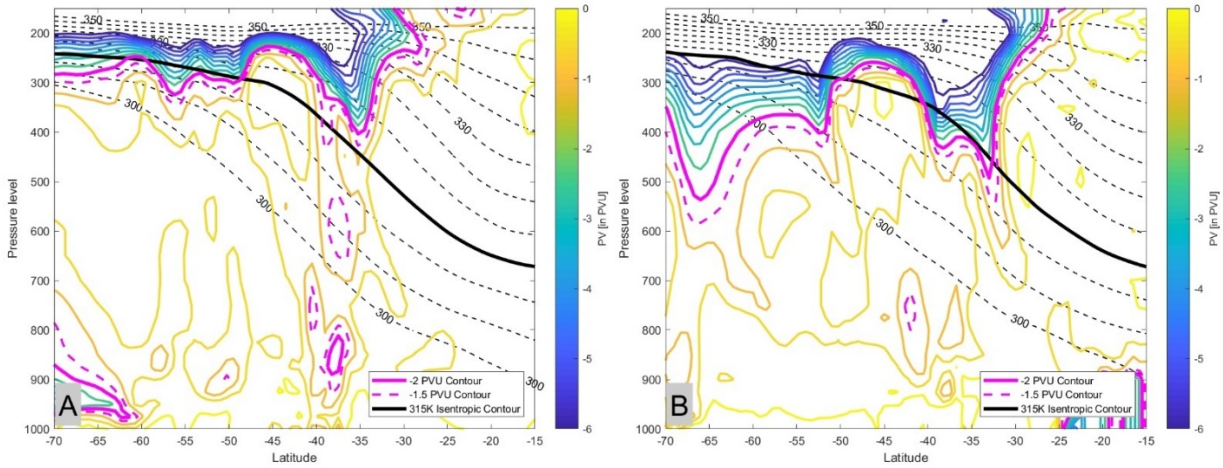

Figure 8: Cross-sections of PV across constant lines of longitude during the development of COL2 (A – 03 June 2017 18:00 UTC at 28.5˚W) and COL3 (B – 07 June 2017 06:00 UTC at 15˚E) and the surface cyclone that tracked from the South American region. The -2 PVU contour is highlighted as a thicker magenta and the -1.5 PVU contour is highlighted as a thicker dashed magenta line. Zonal mean potential temperature contours are shown by black dotted lines with the 315K line highlighted by a thick, solid black line.

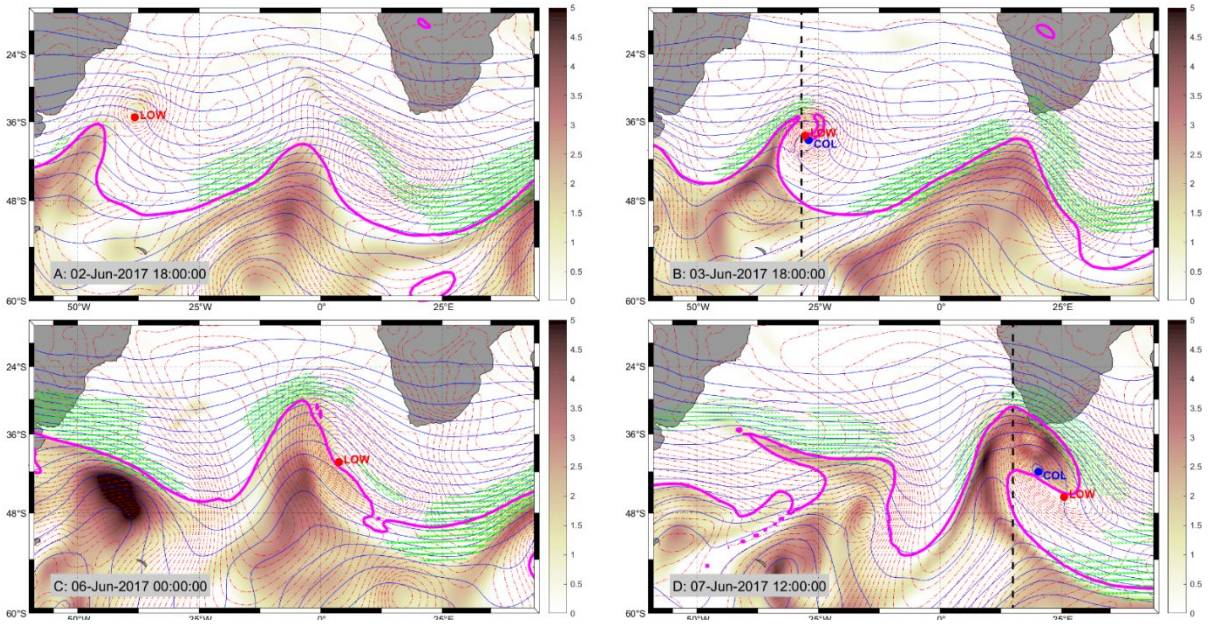

Figure 9: 300hPa (blue lines), 500hPa (black dotted) and MSLP (red lines) geopotential height contours plotted together with the 1.5 PVU line on the 315K Isentropic surface (thick magenta lines) for the COL2 (A and B) and COL3 (C and D). Black dotted lines indicate the relevant cross-sections as shown in Figure 8.

2.5.3. Explosive surface cyclogenesis in relation to upper tropospheric processes

The central mean sea level pressure (MSLP) of the surface low pressure system from the ERA-Interim dataset associated with Cape Storm is shown in Figure 10. If a COL at the 300hPa level was collocated with the surface cyclone at a particular time, a magenta dot is plotted above it. The analysis of the

mean sea level pressure of the surface cyclone reveals the effect that the RWB and COL events had on the low pressure system's development as it travelled over the South Atlantic Ocean towards Africa. The surface cyclone intensified slowly as it moved off of the South American coastline. During 2 June 2017, the surface low pressure system showed some signs of weakening during the decay of COL1. This is seen in Figure 10 by the increase in MSLP towards the end of 1 June 2017. The weakening was however shorted-lived as the low-pressure system started to deepen once again during 2 June 2017. This deepening coincides with the intrusion of stratospheric air into the upper troposphere. The surface cyclone starts to decay once again during 3 June 2017 until the development of the RWB event associated with COL3 as the storm approached the South African coastline. Notably, the 2 different deepening events occurred at different stages of each of the respective COL's life cycles. The deepening associated with COL2 occurred more than a day before the closed circulation could be noted in the upper troposphere. The deepening event associated with COL3 however occurred just hours before the development of COL3. Additionally, the timing of the different decay events also differed between COL2 and COL3. The start of the decay of the surface cyclone coincided with the first appearance of COL2 and decayed throughout COL2's life cycle. The decay of the surface cyclone post COL3 however started during the decay stage of COL3. The differences in the time of decay could be a result of the baroclinicity of the system when each COL developed. When COL2 developed, the system throughout the troposphere was extremely "upright" (as shown in Figure 9B), inhibiting surface development. COL3 on the otherhand still showed significant east-west "lean" with height (as shown in Figure 9D), indicating a baroclinic environment. The differences in deepening and decay of the surface cyclone in relation to each COL shows that both the processes of surface cyclogenesis and COL development "feed off" of the process of isentropic transport of stratospheric air intruding into the troposphere. The development (as shown in Section 2.5.1) or deepening of the surface cyclone is not dependent on a closed circulation in the upper-levels of the troposphere but on the processes that drive it.

Although both the deepening events associated with COL2 and COL3 were significant, the event associated with COL2 was far more rapid and intense. This is particularly evident in the 36 hour period between 2 June 2017 06h00 UTC and 3 June 2017 18h00 UTC. For a cyclogenesis event to be classified an explosive cyclogenesis event or "bomb", the surface pressure must decrease at a rate of $24 \times (\sin(latitude) / \sin 60)$ (Sanders and Gyakum, 1980). Since the low pressure cell centre was situated between 30 and 40˚S a deepening of between 14 and 18hPa is required for the low to be classified as an explosive cyclogenesis event. Calculating 24 hour mean sea level decreases associated with the deepening event with respect to COL2 reveals that the centre of the low deepened at a rate of 18-20hPa per 24 hour during this period. Therefore, the deepening event associated with COL2 can

be classified as an explosive cyclogenesis event. PV-theory can be used to describe this process. Rapid cyclogenesis can result from the interplay between PV anomalies in the upper to mid-troposphere, lower troposphere and near surface (Čampa and Wernli, 2012; Pang and Fu, 2017). The alignment of PV anomalies throughout the troposphere is commonly referred to as a *PV tower*. Figure 10 shows the average of all PV values within a 1.5-by-1.5-degree area of the low pressure cell's centre. From Figure 10 it is clear that the deepening of the low pressure is co-incident with the lowering of mean PV values in the mid- to lower-troposphere. By 3 June 2017, a clearly connected PV tower can be seen throughout the troposphere as shown by the shaded areas on Figure 10. The three, inter-connected PV anomalies generally result from three separate processes. Oceanic surface cyclongenesis however is largely influenced by both the upper and low-level processes compared to that of the surface (Davis *et al*, 1996).

The upper- to mid- level anomaly is the result of a stratospheric intrusion, in this case as a result of RWB. The main difference in the upper-level PV signatures of the two deepening events is the observed structure of the two RWB events. Both the RWB events can be described as cyclonic RWB events. The RWB event associated with COL2 however shows a far "tighter" wrapping cyclonic overturning of the isentropic PV contours than the event associated with COL3. Surface cyclogenesis intensity has been shown to increase when the isentropic PV contours wrap around the western side of the surface cyclone center (Flaounas *et al.*, 2015). Once the isentropic PV streamer has wrapped over the centre of the cyclone, the intensity of cyclogenesis decreased. This decrease in intensity is likely due to increased static stability associated with high PV air from the stratosphere above the surface low pressure system. This stable airmass acts as a "lid" over the surface cyclone preventing further upper level divergence and mid-level vertical motion. In RWB even associated with COL2, this process occurred later due to how narrow the PV-streamer was as seen in Figure 9b. Although stratospheric, high-PV air is a factor which aids in the surface cyclogenesis, the position of this airmass in relation to the developed surface is also crucial to its development as suggested by theory .

The low level anomaly results from diabatic processes such as those associated with preciptation (Brennan *et al*, 2008). This anomaly is clearly stronger during the event associated with COL2 rather than COL3 as shown by the larger PV values in Figure 8. The PV tower associated with COL3 does exist, but is far weaker than for COL2 as shown by Figure 10. This tower is clearly far weaker than the first PV tower event with a lesser PV values shown in the cross-section in Figure 8 and weaker mid-tropospheric PV-values immediately around the surface cyclone as shown in Figure 10. During this event, surface cyclogenesis does exist, but is less rapid than in the preceding deepening event.

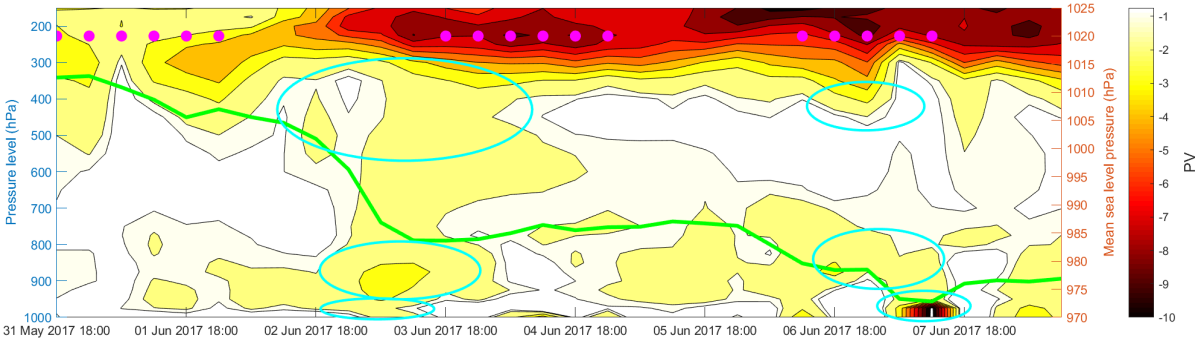

Figure 10: Mean PV within a 1.5x1.5-degree box to the centred on the centroid of the low-pressure cell (yellow-red colour scale) less than -0.75 PVU at each pressure level (left axis). Mean sea level pressure of surface low pressure centres (green line) with values on the right axis. COL centres that existed at 300hPa at each timestep are plotted as magenta dots. PV towers are pointed out by cyan ellipses aligned vertically.

2.6. Meteorological and societal impact of Cape Storm on South Africa

Extreme weather conditions associated with the passage of Cape Storm largely affected the Western and Northern Cape Provinces of the country from the evening of 6 June 2017, peaking in severity on 7 June and abating during 8 June. The general synoptics are of the surface weather system affecting the Western Cape are shown by means of ERA-Interim mean sea level pressure and 10m wind parameters in Figure 11. Although Figure 2 shows the centre of the low-pressure system far south of South Africa, MSLP fields however reveal that this low is bean shaped, with the centre of the low-pressure system extending further north. The northerly extent of this low is situated relatively close to the South African coastline at close to 40˚S. Although other COLs associated with extreme weather along the Cape south coast have been shown to be associated with surface low pressures much closer to the South African coastline (Singleton and Reason, 2007b, 2006), the surface low associated with Cape Storm was proximal to the South African coastline in the context of its depth. The deep surface low-pressure approaches the country from the west on 6 June 2017. The frontal band of the system makes landfall during the night of the 6 June 2017 into the morning of the 7 June 2017 with the deep low-pressure cell passing south of the Western Cape. The main factors contributing to the extreme conditions were the formidable wind strengths; heavy downpours and considerable amounts of rainfall together with the severe wave and surge conditions. Very cold temperatures together with snowfalls were also linked to the system. As a secondary impact, runaway veld fires caused much devastation over a vast area along the Cape South Coast including the towns of Mossel Bay, George, Knysna and Plettenberg Bay (shown on Figure 1) branded by the media as the Knysna Fires.

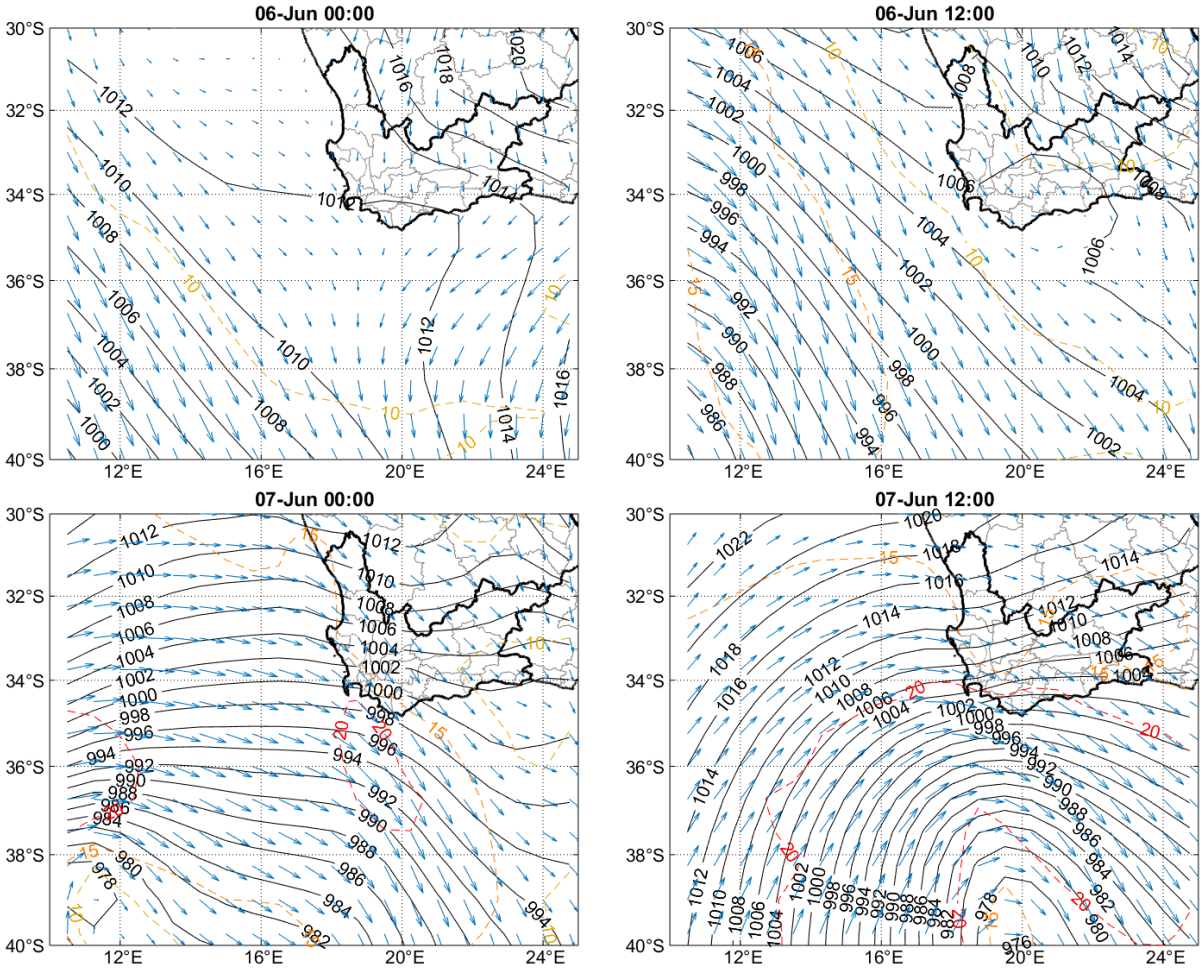

Figure 11: Surface synoptic conditions During 6 and 7 June 2017 around the Western Cape. Mean sea level pressure (black contours) are shown together with 10m surface wind (blue arrows) from the ERA-Interim dataset. Surface wind speeds of over 10m.s^{-1} (yellow), 15m.s^{-1} (orange) and 20m.s^{-1} (red) are also highlighted.

2.6.1. Wind impacts

Westerly to northwesterly winds, generally averaging between 10-15m.s^{-1} were experienced across the majority of the Western Cape and on 7 June. However, it was the wind gust that was the most noteworthy and caused the majority of the wind damage across the province. Wind gusts generally reached 15-25 m.s^{-1} across most of the province. Winds started to increase significantly from the evening of the 6 June as the cold front associated with the surface low pressure system made landfall, particularly in areas along the west and south-west coastal areas as well as the central interior. Strong and gusty winds blew throughout 7 June and continued into the morning of the 8 June. The surface low pressure system resulted in winds sustained over a period close to 30hrs. These exceptionally strong and gusty winds together with the prolonged time period remain uncharacteristic over the Western Cape, especially over the interior of the province. As a result, even infrastructure resilient to strong wind was severely tested. Figure 12 shows the recorded average wind speeds as well as wind gusts over selected towns in the Western Cape from 6-8 June 2017. The highest winds speeds were

recorded along the south-west coast, specifically at Cape Point and Slangkop each reaching maximum wind speeds of 36.2 $m.s^{-1}$ and 25.5 $m.s^{-1}$ respectively. Over the interior, Worcester reached maximum gusts of 34 $m.s^{-1}$, Laingsburg 29.2 $m.s^{-1}$ and Beaufort West 29.9 $m.s^{-1}$ during 7 June 2017. As a result, many trees were uprooted, structural damage to several buildings, houses and vehicles was reported and electrical disruptions from damage to power lines occurred. These incidents were frequent and widespread throughout the province. Some examples of wind damage caused is shown in the appendix (Figure 20-23).

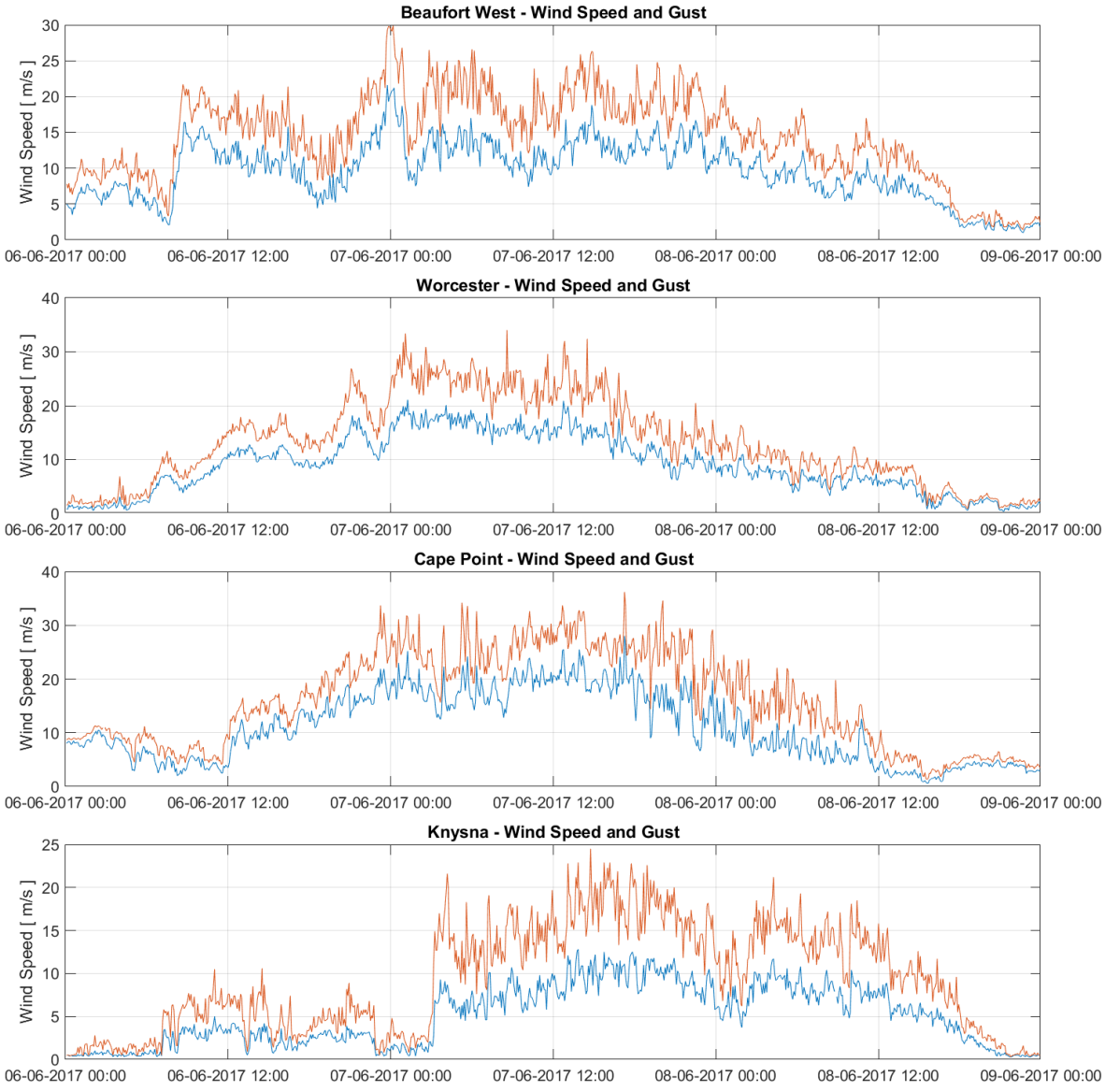

Figure 12: Five-minute wind speed (blue line) and wind gust (orange line) data for selected stations within the Western Cape from 6-8 June 2017.

AWSs along the south coast of the Western Cape measured significantly low humidity values below 20% relative humidity (Table 2) and maximum temperatures spiking above 30˚C (Table 1). It should be noted these conditions are not the norm for this region during the winter months. According to long-

term maximum temperature data for the George weather station, maximum temperatures for June months are 20˚C at this station. The record maximum temperature at the George station during the month of June is 32˚C. The 95th percentile of the maximum temperatures at George is 28 ˚C. June maximum temperatures above 30˚C have only occurred at the station five times (including that of the Cape Storm event) since the record began in 1994. Neighbouring Mossel Bay and Knysna have long-term average maximum temperatures of 19˚C and 22˚C, 95th percentile values of 27˚C and 29˚C and record maximum temperatures of 31˚C and 36˚C respectively. Temperatures peaked above the 95th percentile values at George and Knysna. Hot and dry conditions with offshore wind regimes are typical of so-called berg wind conditions. Berg winds are characterized as a hot, dry wind flowing from the interior plateau down to the coast warming adiabatically through descent (Tyson, 1964). Figure 11 shows general surface flow over the Western Cape. The northerly flow brings warmer, drier air from the interior (1000-1500m above mean sea level) towards the coast (Figure 1). The airmass is further dried and warmed by adiabatic heating effects as it descends, especially as it flows down the Cape fold mountains to the north of the south coast. The northerly flow ahead of the cold front resulted in berg wind conditions along the Cape south coast during 6 June 2017.

Fire danger ratings are algorithms used to identify conditions that are meteorologically ideal for fires to get out of control (Willis *et al.*, 2001). In South Africa, the Lowveld fire danger index (FDI) is currently used for this purpose (Madula, 2013). The Lowveld FDI takes into account relative humidity and temperature together with a wind speed and recent rainfall correction factors to calculate the fire danger. The Lowveld FDI can be expressed by:

$$Lowveld = \left[\left((Temp - 35) - \left(\frac{35-Temp}{30}\right) + \left((100 - RH) * 0.37\right) + 30\right) + 15 + Wind_{Correction}\right] \times Rain_{Correction} \quad (1)$$

Using wind speed (Figure 12), temperature (Table 1) and relative humidity (Table 2) values for the Knysna station, Lowveld FDI values are calculated throughout the day on 6 June 2017. For reference, the wind correction tables which correlate wind speeds are shown in Madula (2013). It should also be noted that the last recorded rainfall at the Knysna station fell 11 days earlier with 2.0mm of rain falling over during 25 and 26 May 2017. Rainfall correction tables shown in Madula (2013) show that this has no effect on the effective Lowveld FDI value and so that rain correction value is set to one. The results of the Lowveld FDI calculation for Knysna are shown in Table 3. Values over 75 correspond to an "extremely dangerous" fire danger rating, the highest fire danger rating in the index. Extremely dangerous FDI values are present throughout the day on 6 June 2017. This shows that conditions within the Knysna area and surrounds were ideal meteorologically for runaway wildfires. An analysis of Enhanced Vegetation Indices (EVI) for the area, also reveal that the vegetation health was worse off than average in the months preceding the fire (Frost *et al.*, 2018). In the context of the drought,

this is an indicator of a lack of recent rainfall and the dry landscape that resulted from the prolonged lack of rainfall. The ideal meteorological conditions along the south coast together with the drought-stricken landscape and winds and wind gusts picking up rapidly overnight on 6 June 2017 into 7 June 2017 (Figure 12), fires set inadvertently in the afternoon on 6 June 2017 fanned and spread through the night. The wildfire reached the outskirts of the town of Knysna during the early in the morning of 7 June 2017, further spreading to affect Plettenberg Bay and Tsitsikama Forest. The fire, spanning at least 100km (Western Cape Government, 2017a) also claimed the lives of 7 people (Western Cape Government, 2017a) and displaced at least 10000 people displaced (Western Cape Government, 2017a). The fire, which spanned a minimum of 100km (Western Cape Government, 2017a), destroyed large areas of land including 1000 houses (Frost *et al.*, 2018). Response teams of 1106 firefighters (Western Cape Government, 2017a) worked tirelessly for 12 days to combat the devastating fires and finally neutralize the threat (DAFF, 2018). Efforts to control the initial blaze on 6 and 7 June were also hampered as water bombing helicopters could not fly due to the strong winds (DAFF, 2018). Smouldering fires and flare ups were controlled for weeks thereafter (DAFF, 2018). Figures 15-17 in the appendix show images taken of the Knysna fires.

Table 1: Recorded hourly (UTC) temperatures for stations along the cape south coast of South Africa on 6 June 2017 and the adjacent interior

Temp (˚C)	0	1	2	3	4	5	6	7	8	9	10	11	12	13	14	15	16	17	18	19	20	21	22	23
Mossel Bay	14.8	14.3	14.5	15.9	15.9	16.9	18.6	22.7	26.6	18.9	19.6	18.1	18.1	17.9	20.8	16.4	15.1	15.4	15.1	14.6	18.7	24.1	23.0	23.8
George	16.6	18.5	17.7	16.2	19.4	20.6	23.1	25.9	27.8	28.7	29.8	30.6	31.2	31.8	19.8	30.7	21.7	13.9	16.7	29.7	15.1	18.0	19.2	25.2
Knysna	11.5	16.2	16.5	17.3	16.3	17.4	23.6	26.6	29.8	30.4	32.3	32.3	34.1	34.2	34.2	31.6	29.8	29.2	29.7	30.2	30.4	21.8	19.4	21.9
Oudtshoorn	9.5	8.9	7.8	7.7	8.2	9.7	9.8	14.9	20.2	28.1	29.2	28.8	31.1	31.9	31.7	30.7	30.0	29.6	29.7	29.9	28.5	27.5	24.3	25.6

Table 2: Recorded hourly relative humidity (%) for stations along the cape south coast of South Africa on 6 June 2017 and the adjacent interior

RH (%)	0	1	2	3	4	5	6	7	8	9	10	11	12	13	14	15	16	17	18	19	20	21	22	23
Mossel Bay	65	66	62	51	50	45	41	36	24	62	64	68	65	66	45	79	89	87	86	88	53	31	32	26
George	48	38	41	46	35	31	26	20	18	17	16	15	14	14	60	17	44	97	71	18	81	55	43	25
Knysna	83	52	47	42	45	38	24	17	14	13	12	13	11	12	12	14	15	16	16	15	15	49	61	41
Oudtshoorn	70	70	73	73	69	65	65	49	32	16	15	15	14	14	15	15	17	17	17	17	18	20	25	25

Table 3: Lowveld FDI values for hourly observational for the Knysna AWS station on 6 June 2017

Lowveld FDI	0	1	2	3	4	5	6	7	8	9	10	11	12	13	14	15	16	17	18	19	20	21	22	23
Knysna	27	58	60	63	61	65	76	92	86	87	90	94	97	102	92	98	96	95	86	86	87	65	58	68

2.6.2. Rain impacts

The south and south-western coastline of the country receive more than 500mm of rain per year (Mahlalela *et al.*, 2019). This increases to 800-1000mm in the mountainous regions in the west and south. The majority of the rainfall was confined to the western parts of the Western Cape where generally between 40-80mm were measured, but up to 130mm was measured in the Grabouw mountains and 100mm in Ceres over the two days (Figure 13). The highest rainfall tallies are located in the western mountain ranges of the Western Cape. This is typical of frontal systems where low-level flow dominates from the west, with orographic lifting enhancing rainfall in these areas. The rainfall tallies associated with this weather system are not unusual for passing COLs and cold frontal bands over the south-western Cape in the context of average annual rainfall totals for these regions. COLs can be associated with much heavier downpours of hundreds of millimetres of rainfall over vast areas that result in flash flooding and other devastating impacts. Examples include the March 2003 COL which resulted in 100-200mm of rainfall over the south coast of the country (Singleton and Reason, 2007b) and the 1968 COL which caused 500mm of rainfall to fall over the Port Elizabeth region, situated about 200km to the east of Plettenberg Bay. However, as the region experienced two of its driest years on record between 2015 and 2017 (Mahlalela *et al.*, 2019), the rainfall received was significant within the context of the prevailing drought conditions. The heavy downpours caused localised flooding within informal settlements, affecting hundreds of dwellings (Western Cape Government, 2017b). Widespread snowfalls fell over the Western and Northern Cape high ground, however did not result in damage or disruption.

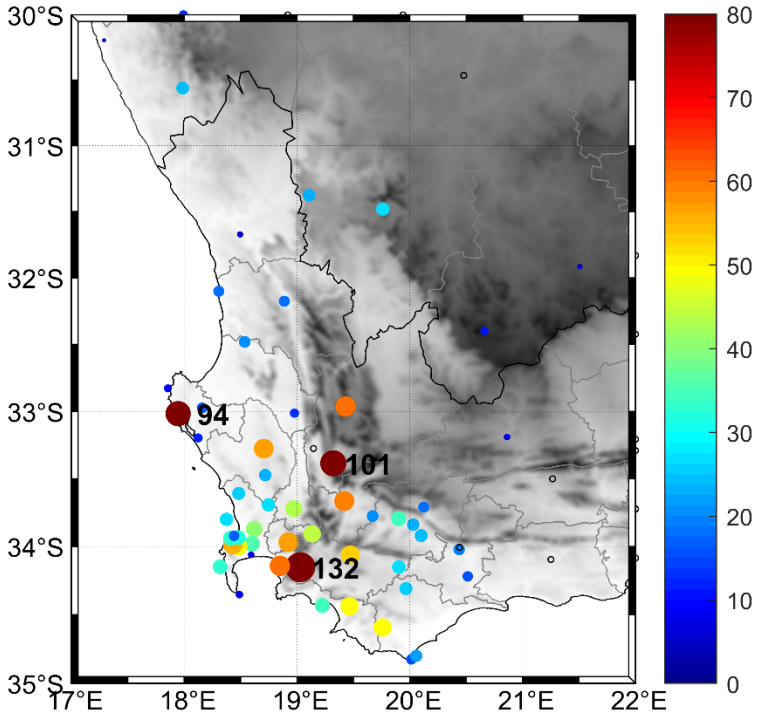

Figure 13: Rainfall totals (in mm) experienced over the Western Cape region of South Africa. Empty circles denote active rainfall stations that did not record any rainfall during 6 and 7 June 2017. Values of large rainfall totals (greater than 80mm) have been plotted together with their respective points.

2.6.3. Oceanographic impacts

The passing of Cape Storm resulted in two main effects along the coastline of the south-western Cape: storm surge and very high seas. A storm surge (sometimes referred to as storm tide) is *the deviation of the sea-surface elevations from the predicted tide, due to storm related atmospheric influences* (Buskey *et al.*, 2015). A storm surge is therefore the water level without the tidal signal. The main atmospheric drivers of storm surges are atmospheric pressure, wind and wave setup.

Rautenbach *et al* (2020) studied the storm surge event during Cape Storm during calibration of an operational storm surge and wave numerical model. The model comprised of a coupled wave and flow model. These were forced by high-resolution (4.4km) winds and atmospheric pressure from a locally run version of the Unified Model (UM) together with WaveWatch III waves and TPXO 8 tidal constituents on the open boundaries of the South African domain. During Cape Storm, water levels around the coastline, but more prominently along the west and south coast, were anomalously high. Water level monitoring stations at Cape Town and Mossel Bay showed storm surge values of 0.4m and 0.7m respectively (Rautenbach *et al.*, 2020). The storm peak in terms of water levels increased throughout 7 June 2017. The increase in water levels were primarily driven by three main atmospheric factors. The central pressure of the surface low pressure system reached a depth of 973hPa according to reanalysis data (Figure 3). As this low was so close to the coastline, relatively low pressure was

experienced around the South African coastline. Pressure reduced to sea level observations at Slangkop and Cape Agulhas recorded low values 998.2hPa and 998hPa respectively. Coastal pressure below 1000hPa occurs infrequently along the subtropical South African coastline. The south and western coastlines are generally affected by passing frontal bands. These frontal bands and the ridging high pressure that generally follows are associated with strong winds and big waves, but extreme pressures of below 1000hPa are rarer. 10 year (2007-2017) hourly AWS pressure data reduced to mean sea level at Slangkop and Cape Agulhas show that pressures of below 1000hPa have only been recorded during 10 and 18 events respectively (1-2 events per year). The low pressure allowed for a general increase in water levels around the coastline.

Wind with a westerly zonal component of over 15-20m.s^{-1} (Figure 11) reaching up to 25-30m.s^{-1} (Figure 12) in places were prevalent to the west of the South African coastline for an extended period of time. These onshore wind regimes caused water to be "piled up" against the coastline of the west and south coast. Using the numerical model, Rautenbach *et al* (2020) found this to be one of the main drivers of surge along the coastline. They showed by neglecting wind in the numerical model, only 45% of the surge peak was described. Strong winds over a large fetch to the west of the country resulted in large waves hitting the Western Cape coastline. The South African south-west coast and to a lesser extent the west coast took the brunt of the extremely high and powerful waves. Wave heights gradually increased to a significant wave height of 12m recorded off of Slangkop along the south-west coastline (Rautenbach *et al.*, 2020) . Massive waves are rare along the South African coastline. Veitch *et al.* (2019) show that 5.4m waves represent that 95th percentile of winter significant wave heights at the same buoy location off of the coast near Slangkop. The wave setup associated with these large waves also played a significant role in the increase of water levels and storm surge in these regions (Rautenbach *et al.*, 2020). Along with the westerly orientation of the waves on 7 June, the large wave climate and anomalously high water levels played a significant role in the severity of the damage that occurred along the coastal strip and beachfront of the south-western Cape. As the storm passed, swells behind the cold front swung round to a southerly component on 8 June and wave heights started to drop to 6-8m. Exposed areas, particularly the Cape Town False Bay and Western Cape south coast, were threatened with the southerly swell component.

As a result of the severe wave and increased water levels conditions, coastal infrastructure was damaged mainly along the Cape Atlantic seaboard of Cape Town. Numerous beachfronts and beach roads were flooded and thrown with foam and sea spray. Several beaches were severely eroded. Bloubergstrand near Cape Town was even closed until further notice as a result of unstable dunes

(Booysen and Daniels, 2017; Le Roux, 2017). Multiple boats and yachts were also damaged. Images of these large waves are shown in the appendix in Figure 17-20.

2.6.4. Summary of societal impacts

Based on the predicted weather conditions presented to provincial government by the SAWS, a decision was made a day before the event to close all the Western Cape schools for 7 June 2017 (Western Cape Government, 2017c). As a result of this drastic measure, the seriousness of the situation was effectively communicated to the public. In essence, this meant that children were home during the severe weather, thus, reducing the risk by reducing the concentration of children in singular areas. Additionally, this created significantly less vehicles on the road making it easier for emergency responders to attend to disasters. In retrospect, the Western Cape Government reported that 135 schools incurred damage across the province (Citizen reporters, 2017; Deklerk, 2017; ENCA, 2017) potentially protecting thousands of children from harm. 41 of these schools underwent significant damage to roofs, whilst others were affected by water damage, fallen trees, damaged fences, etc. (Citizen reporters, 2017; Deklerk, 2017).

The storm did in fact cause significant damage across the Western Cape. Some of the impacts are summarized below:

- Knysna municipality
    - 7 people lost their lives (Western Cape Government, 2017a)
    - 10000 people displaced (Western Cape Government, 2017a)
    - 1000 houses destroyed (Frost *et al.*, 2018)
    - A major highway (N2) closed between George and Plettenberg Bay (Western Cape Government, 2017b)
    - Infrastructure losses worth millions of Rands (DAFF, 2018)
- Transport
    - Thoroughfares such as the Huguenots Tunnel and Chapmans peak closed (Western Cape Government, 2017e)
    - The national railway network (Metrorail) reported major delays (over 60 minutes) and with freight routes train routes Worcester, Malmesbury, Wellington, Muldersvlei suspended (Western Cape Government, 2017e)
- Power outages in areas throughout the province
- 135 schools damaged across the Western Cape (Citizen reporters, 2017; Deklerk, 2017; ENCA, 2017)
- 2000 people displaced in Greater Cape Town, 80 people in Villiersdorp, 100 people in Franschhoek (Western Cape Government, 2017b)

- Flooding in localised areas in Paarl, Bergrivier, Swartland and City of Cape Town (Western Cape Government, 2017e, 2017b)
- Wind damage in the form of blown off roofs, structural damage, power lines blown over in Langeberg, City of Cape Town, Swartland, Bergrivier, Breede Valley, Grabouw, Botriveir, Saldanha Bay (Western Cape Government, 2017e, 2017b)
- Family (4) died from fire caused by lightning in Kraaifontein, 1 person died in Lavender Hill from collapsing building
- Beaufort West airstrip hangar doors blown off also resulted in damage to aircraft (Western Cape Government, 2017e)
- 3m container fell off vessel, Gordon's Bay (NSRI, 2017)
- Pencil rubber duck capsized, Gordon's Bay (NSRI, 2017)

2.7. Summary and Conclusion

In this study we analyse Cape Storm, a COL and associated surface cyclone that affected the south-western Cape of South Africa on 6 and 7 June 2017. The system had large weather-related impacts on the southern and south-western Cape of South Africa. The deep low-pressure system and its tight pressure gradient caused strong winds throughout the region. The resulted in extensive damage to infrastructure and the displacement of vulnerable communities. Dry, hot air in conjunction with the strong winds resulted in out of control wildfires along the Cape south coast, extensive damage to infrastructure worth millions of Rands and the displacement of the thousands of people. Strong winds and large waves together with the low pressure associated with the system also resulted in a storm surge event over the south-western Cape.

Differences in the associated impacts and the regions of the south-western Cape are observed between two previous studies of COLs and associated surface lows (Singleton and Reason, 2007b, 2006). In both of these studies, the surface low associated with the COL was placed just off of South African coastline, with the South Atlantic High ridging in behind the passing low-pressure system. The interplay between the surface low pressure, the South Atlantic high and the COL drove onshore, southerly surface flow and advection of moisture onto the south coast of the Western Cape. These events resulted heavy rainfall along the Cape south coast and Eastern Cape to the east of the Western Cape province. These events were associated with topographical and dynamical uplift. Cape Storm however had a completely different orientation compared to these previously recorded events. The surface low pressure system situated to the south of the country resulted in westerly to northwesterly flow. The depth of the low pressure and the tight pressure gradient resulted in a large fetch of strong surface winds. The westerly flow and associated onshore moisture flux resulted in heavy rainfall over the western parts of the Western Cape, with offshore, berg winds along the Cape south coast. Impacts

associated with Cape Storm were also largely wind-driven compared to the large rainfall impacts associated with that of previous studies. This comparison highlights how crucial the placement of these COLs and associated surface lows are to the eventual impact on the country.

The system was tracked subjectively to its initial development on 27 May 2017 to the west of South America. The system developed as a COL and associated surface low pressure system as a result of a Rossby wave and dynamical tropopause amplification. The system showed continual amplification of the isentropic PV contours which eventually become overturned indicative of a RWB event. This event preceded the development of both the COL and surface cyclone. The RWB event allowed for the intrusion of high-PV air into the mid-levels of the troposphere (700hPa). This event drove both the development of the upper-air driven closed circulation and surface cyclone. Notably, the surface closed surface circulation preceded, if only by hours, the upper level cut-of low. The system made landfall during 30 May 2017 over the South American west coast and exited on the east coast on 2 June 2017. At this stage the COL decayed and was no longer visible in the upper level fields. The surface low pressure system was maintained and deepened over the Atlantic Ocean by the presence of 2 RWB events and associated COLs before it affected the South African coastline.

The severity of the system that eventually impacted the south-western Cape of South Africa was the result of a relatively unique set of circumstances. A surface low that developed to the south-west of South America was further intensified by two other upper-level driven processes. Both the surface cyclone's development to the west of South America as well the deepening of the low-pressure system over the Atlantic Ocean were associated with stratospheric intrusions associated with RWB events. All of the intrusion events also resulted in the development of COLs. However, the timing of the development and decay of the COL and surface cyclone differed between these two deepening events. The differences in timing of the deepening and decay of the surface cyclone compared to that of the COLs emphasizes how the upper and surface-level closed circulations are driven by the dynamical processes surrounding them. Upper-air processes are not the only factors in the development of these extended systems. The analysis of PV showed that PV towers containing low-level high-PV air were present for both of the deepening events preceding the effect of the system on South Africa. The deepening event associated with a stronger presence of PV air in the low-levels resulting in enhanced and rapid deepening and can be classified as an explosive cyclogenesis event.

The study of Cape Storm shows the importance of analyzing the dynamics (PV fields) that drive circulations throughout the troposphere, both on the forecasting desk (Brennan *et al.*, 2008) as well as retroactively. Although the study of COLs and PV-related analyses is relatively advanced throughout the Southern hemisphere, few studies have analysed PV in the South African regional context. In a

previous COL case study (Singleton and Reason, 2007b), it was noted that the lack of routine, high resolution numerical weather prediction hampered accurate forecasting of the meteorological conditions of COLs over the South African region. This is no longer a problem with the SAWS running high resolution forecasts routinely down to 1.5km horizontal resolution. Forecasters have all the variables from these high-resolution NWP products at their disposal in order to diagnose the weather of the day. However, at the time of publication, the SAWS does not analyse systems from a PV perspective in forecast mode. Future work in the region should involve studying different weather systems such as mid-latitude cyclones from a PV perspective and integrating these PV analyses into everyday numerical weather prediction analysis.

2.8. Acknowledgements and author contributions

Michael Barnes under the supervision of Dr Thando Ndarana and Prof Willem A. Landman conceived of all the ideas in this manuscript, did all the analysis and wrote the paper. Kate Turner collected and collated the information and the required data to analyse the meteorological and societal impacts of the system. Working as an operational forecaster in the Western Cape at the time, she also provided significant insights into the impacts that the region experienced during Cape Storm.

2.9. References

Appenzeller, C., Davies, H.C., Norton, W.A., 1996. Fragmentation of stratospheric intrusions. J. Geophys. Res. Atmos. 101, 1435–1456. https://doi.org/10.1029/95JD02674

Baray, J.L., Baldy, S., Diab, R.D., Cammas, J.P., 2003. Dynamical study of a tropical cut-off low over South Africa, and its impact on tropospheric ozone. Atmos. Environ. 37, 1475–1488. https://doi.org/10.1016/S1352-2310(02)00999-8

Bell, G.D., Bosart, L.F., 1993. A Case Study Diagnosis of the Formation of an Upper-Level Cutoff Cyclonic Circulation over the Eastern United States. Mon. Weather Rev. 121, 1635–1655. https://doi.org/10.1175/1520-0493(1993)121<1635:ACSDOT>2.0.CO;2

Booysen, C., Daniels, N., 2017. Big Bay Beach closed after official's dune collapse scare [WWW Document]. IOL. URL https://www.iol.co.za/capetimes/news/big-bay-beach-closed-after-officials-dune-collapse-scare-9650079 (accessed 7.21.20).

Brennan, M.J., Lackmann, G.M., Mahoney, K.M., 2008. Potential vorticity (PV) thinking in operations: The utility of nonconservation. Weather Forecast. 23, 168–182. https://doi.org/10.1175/2007WAF2006044.1

Buskey, E.J., Bundy, M., Ferner, M.C., Porter, D.E., Reay, W.G., Smith, E., Trueblood, D., 2015. System-

Wide Monitoring Program of the National Estuarine Research Reserve System, in: Coastal Ocean Observing Systems. Elsevier, pp. 392–415. https://doi.org/10.1016/B978-0-12-802022-7.00021-3

Čampa, J., Wernli, H., 2012. A PV perspective on the vertical structure of mature midlatitude cyclones in the Northern Hemisphere. J. Atmos. Sci. 69, 725–740. https://doi.org/10.1175/JAS-D-11-050.1

Citizen reporters, 2017. Cape Storm damages 135 schools across Western Cape. Citiz.

DAFF, 2018. The Knysna Fires: 12 Days of Service.

Davis, C.A., Emanuel, K.A., 1991. Potential vorticity diagnostics of cyclogenesis. Mon. Weather Rev. https://doi.org/10.1175/1520-0493(1991)119<1929:PVDOC>2.0.CO;2

Davis, C.A., Grell, E.D., Shapiro, M.A., 1996. The balanced dynamical nature of a rapidly intensifying oceanic cyclone. Mon. Weather Rev. https://doi.org/10.1175/1520-0493(1996)124<0003:TBDNOA>2.0.CO;2

Dee, D.P., Uppala, S.M., Simmons, A.J., Berrisford, P., Poli, P., Kobayashi, S., Andrae, U., Balmaseda, M.A., Balsamo, G., Bauer, P., Bechtold, P., Beljaars, A.C.M., van de Berg, L., Bidlot, J., Bormann, N., Delsol, C., Dragani, R., Fuentes, M., Geer, A.J., Haimberger, L., Healy, S.B., Hersbach, H., Hólm, E. V., Isaksen, L., Kållberg, P., Köhler, M., Matricardi, M., Mcnally, A.P., Monge-Sanz, B.M., Morcrette, J.J., Park, B.K., Peubey, C., de Rosnay, P., Tavolato, C., Thépaut, J.N., Vitart, F., 2011. The ERA-Interim reanalysis: Configuration and performance of the data assimilation system. Q. J. R. Meteorol. Soc. 137, 553–597. https://doi.org/10.1002/qj.828

Deklerk, A., 2017. 135 schools damaged by Western Cape storms [WWW Document]. Times Live. URL https://www.timeslive.co.za/news/south-africa/2017-06-09-135-schools-damaged-by-western-cape-storms/ (accessed 7.20.20).

Eliassen, A., Kleinschmidt, E., 1957. Dynamic Meteorology. pp. 1–154. https://doi.org/10.1007/978-3-642-45881-1_1

ENCA, 2017. Cape Storm damaged 135 schools across province [WWW Document]. www.enca.com. URL https://www.enca.com/south-africa/cape-storm-damaged-135-schools-across-province (accessed 7.20.20).

Engelbrecht, C.J., Landman, W.A., Engelbrecht, F.A., Malherbe, J., 2015. A synoptic decomposition of rainfall over the Cape south coast of South Africa. Clim. Dyn. 44, 2589–2607. https://doi.org/10.1007/s00382-014-2230-5

Esler, J.G., Haynes, P.H., 1999. Baroclinic Wave Breaking and the Internal Variability of the Tropospheric Circulation. J. Atmos. Sci. 56, 4014–4031. https://doi.org/10.1175/1520-0469(1999)056<4014:BWBATI>2.0.CO;2

Favre, A., Hewitson, B., Lennard, C., Cerezo-Mota, R., Tadross, M., 2013. Cut-off Lows in the South Africa region and their contribution to precipitation. Clim. Dyn. 41, 2331–2351. https://doi.org/10.1007/s00382-012-1579-6

Flaounas, E., Kotroni, V., Lagouvardos, K., Flaounas, I., 2014. CycloTRACK (v1.0) – tracking winter extratropical cyclones based on relative vorticity: sensitivity to data filtering and other relevant parameters. Geosci. Model Dev. 7, 1841–1853. https://doi.org/10.5194/gmd-7-1841-2014

Flaounas, E., Raveh-Rubin, S., Wernli, H., Drobinski, P., Bastin, S., 2015. The dynamical structure of intense Mediterranean cyclones. Clim. Dyn. 44, 2411–2427. https://doi.org/10.1007/s00382-014-2330-2

Frost, Pe, Kleyn, L., Van Den Dool, R., Burgess, M., Vhengani, L., Steenkamp, K., Wessels, K., Le Maitre, D., Forsyth, G., Frost, Philip, 2018. The Elandskraal Fire, Knysna: A data driven analysis 73pp.

Hoskins, B.J., 1991. Towards a PV-theta view of the general circulation. Tellus A 43, 27–35. https://doi.org/10.1034/j.1600-0870.1991.t01-3-00005.x

Hoskins, B.J., McIntyre, M.E., Robertson, A.W., 1985. On the use and significance of isentropic potential vorticity maps. Q. J. R. Meteorol. Soc. 111, 877–946. https://doi.org/10.1002/qj.49711147002

Iwabe, C.M.N., Da Rocha, R.P., 2009. An event of stratospheric air intrusion and its associated secondary surface cyclogenesis over the South Atlantic Ocean. J. Geophys. Res. Atmos. 114, 1–15. https://doi.org/10.1029/2008JD011119

Kleinschmidt, E., 1950. Über Aufbau und Entstehung von Zyklonen. Meteorol. Rdsch. 3, 1–6.

Le Roux, I.-M., 2017. Blouberg beach closed to public following dune collapse [WWW Document]. Eyewitness News. URL https://ewn.co.za/2017/06/09/blouberg-beach-closed-to-public (accessed 7.21.20).

Liberato, M.L.R., 2014. The 19 January 2013 windstorm over the North Atlantic: Large-scale dynamics and impacts on Iberia. Weather Clim. Extrem. 5, 16–28. https://doi.org/10.1016/j.wace.2014.06.002

Madula, A.R., 2013. Publication of The Fire Danger Rating System for General Information In Terms Of

Section 9(1) On The National Veld And Forest Fire Act, 1998 (Act No. 101 Of 1998), Government Gazette.

Mahlalela, P.T., Blamey, R.C., Reason, C.J.C., 2019. Mechanisms behind early winter rainfall variability in the southwestern Cape, South Africa, Climate Dynamics. Springer Berlin Heidelberg. https://doi.org/10.1007/s00382-018-4571-y

McIntyre, M.E., Palmer, T.N., 1985. A note on the general concept of wave breaking for Rossby and gravity waves. Pure Appl. Geophys. PAGEOPH 123, 964–975. https://doi.org/10.1007/BF00876984

Morgan, M.C., Nielsen-Gammon, J.W., 1998. Using tropopause maps to diagnose midlatitude weather systems. Mon. Weather Rev. 126, 2555–2579. https://doi.org/10.1175/1520-0493(1998)126<2555:UTMTDM>2.0.CO;2

Ndarana, T., Waugh, D.W., 2011. A Climatology of Rossby Wave Breaking on the Southern Hemisphere Tropopause. J. Atmos. Sci. 68, 798–811. https://doi.org/10.1175/2010JAS3460.1

Ndarana, T., Waugh, D.W., 2010. The link between cut-off lows and Rossby wave breaking in the Southern Hemisphere. Q. J. R. Meteorol. Soc. 136, 869–885. https://doi.org/10.1002/qj.627

NSRI, 2017. Container recovered and father and son rescued from capsized boat Gordon's Bay [WWW Document]. NSRI Newsroom. URL https://www.nsri.org.za/2017/06/container-recovered-and-father-and-son-rescued-from-capsized-boat-gordons-bay/ (accessed 1.13.20).

Palmen, E., Newton, C.., 1969. Atmospheric Circulation Systems. Academic Press, New York.

Pang, H., Fu, G., 2017. Case study of potential vorticity tower in three explosive cyclones over Eastern Asia. J. Atmos. Sci. 74, 1445–1454. https://doi.org/10.1175/JAS-D-15-0330.1

Porcù, F., Carrassi, A., Medaglia, C.M., Prodi, F., Mugnai, A., 2007. A study on cut-off low vertical structure and precipitation in the Mediterranean region. Meteorol. Atmos. Phys. 96, 121–140. https://doi.org/10.1007/s00703-006-0224-5

Rautenbach, C., Daniels, T., de Vos, M., Barnes, M.A., 2020. A coupled wave, tide and storm surge operational forecasting system for South Africa: validation and physical description. Nat. Hazards. https://doi.org/10.1007/s11069-020-04042-4

Richman, M.B., Leslie, L.M., 2018. The 2015-2017 Cape Town Drought: Attribution and Prediction Using Machine Learning. Procedia Comput. Sci. 140, 248–257. https://doi.org/10.1016/j.procs.2018.10.323

Sanders, F., Gyakum, J.R., 1980. Synoptic-Dynamic Climatology of the “Bomb.” Mon. Weather Rev. 108, 1589–1606. https://doi.org/10.1175/1520-0493(1980)108<1589:SDCOT>2.0.CO;2

Singleton, A.T., Reason, C.J.C., 2007a. Variability in the characteristics of cut-off low pressure systems over subtropical southern Africa. Int. J. Climatol. 27, 295–310. https://doi.org/10.1002/joc.1399

Singleton, A.T., Reason, C.J.C., 2007b. A Numerical Model Study of an Intense Cutoff Low Pressure System over South Africa. Mon. Weather Rev. 135, 1128–1150. https://doi.org/10.1175/mwr3311.1

Singleton, A.T., Reason, C.J.C., 2006. Numerical simulations of a severe rainfall event over the Eastern Cape coast of South Africa: Sensitivity to sea surface temperature and topography. Tellus, Ser. A Dyn. Meteorol. Oceanogr. 58, 355–367. https://doi.org/10.1111/j.1600-0870.2006.00180.x

Tyson, P.D., 1964. BERG WINDS OF SOUTH AFRICA. Weather 19, 7–11. https://doi.org/10.1002/j.1477-8696.1964.tb02714.x

Uccellini, L.W., Keyser, D., Brill, K.F., Wash, C.H., 1985. The Presidents’ Day cyclone of 18-19 Februarry 1979: influence of upstream trough amplification and associated tropopause folding on rapid cyclogenesis. Mon. Weather Rev. https://doi.org/10.1175/1520-0493(1985)113<0962:TPDCOF>2.0.CO;2

van Delden, A., Neggers, R., 2003. A case study of tropopause cyclogenesis. Meteorol. Appl. 10, 187–199. https://doi.org/10.1017/S1350482703002081

Veitch, J., Rautenbach, C., Hermes, J., Reason, C., 2019. The Cape Point wave record, extreme events and the role of large-scale modes of climate variability. J. Mar. Syst. 198, 103185. https://doi.org/10.1016/j.jmarsys.2019.103185

Western Cape Government, 2017a. Premier Zille extends gratitude for biggest disaster rescue in SA history [WWW Document]. www.westerncape.gov.za. URL https://www.westerncape.gov.za/news/premier-zille-extends-gratitude-biggest-disaster-rescue-sa-history-0

Western Cape Government, 2017b. Situation Report: Severe Weather Event: 6-8 June 2017 [WWW Document]. www.westerncape.gov.za. URL https://www.westerncape.gov.za/news/situation-report-severe-weather-event-6-–-8-june-2017 (accessed 1.16.20).

Western Cape Government, 2017c. Cabinet Confirms Instruction for One Day Closure of All Schools Tomorrow [WWW Document]. www.westerncape.gov.za. URL

https://www.westerncape.gov.za/news/cabinet-confirms-instruction-one-day-closure-all-schools-tomorrow (accessed 1.16.20).

Western Cape Government, 2017d. PRESS RELEASE: THURSDAY, JUNE 8, 2017 [WWW Document]. www.westerncape.gov.za. URL https://www.westerncape.gov.za/news/press-release-thursday-june-8-2017

Western Cape Government, 2017e. Statement: Severe Weather Situation Report [WWW Document]. www.westerncape.gov.za. URL https://www.westerncape.gov.za/news/statement-severe-weather-situation-report (accessed 1.16.20).

Willis, C., Wilgen, B. Van, Tolhurst, K., Everson, C., D'Abreton, P., Pero, L., Fleming, G., 2001. The Development of a National Fire Danger Rating System for South Africa.

2.10. Appendix

Figure 14: Knysna Fires
Credit: SA Red Cross Air Mercy Services
Available: https://disasters.nasa.gov/south-africa-wildfires-2017

Figure 15: Fires raging near Knysna in the Longmore Forest on 7 June 2017.
Credit: Gallo Images/Die Burger/Werner Hills
Available: https://www.msn.com/en-za/weather/photos/weather-pictures-of-the-month-june-2017/ss-BBDtLOD#image=3

Figure 16: Fire bellowing Kranshoek near Plettenberg Bay June 2017.
Credit: Ewald Stander/Associated Press
Available: https://www.nytimes.com/2017/06/08/world/africa/south-africa-fire-knysna.html

Figure 17: Powerful waves crashing over the Sea Point Promenade, 7 June 2017.
Credit: EPA
Available: https://www.straitstimes.com/multimedia/photos/in-pictures-a-ferocious-storm-pummels-cape-town

Figure 18: Waves crashing over promenade tossing foam on to walkway, 7 June 2017.
Credit: AFP Photo
Available: https://www.msn.com/en-za/weather/photos/weather-pictures-of-the-month-june-2017/ss-BBDtLOD#image=5

Figure 19: Cars drive over flooded roads in Sea Point as waves crash over and throw foam and sea spray far on to beachfront.
Credit: EPA
Available: https://www.straitstimes.com/multimedia/photos/in-pictures-a-ferocious-storm-pummels-cape-town

Figure 20: An electricity pole blown over in Nomzamo, 7 June 2017.
Image: Velani Ludidi
Available: https://www.timeslive.co.za/news/south-africa/2019-06-23-cape-town-storm-pics-informal-settlements-hard-hit-by-high-winds/

Figure 21: Several trees blown over in Cape Town, 7 June 2017.
Credit: Aziz Samaai
Available: https://www.bbc.com/news/world-africa-40185177

Figure 22: The roof blown off house in Nomzamo.
Credit: Velani Ludidi
Available: https://www.timeslive.co.za/news/south-africa/2019-06-23-cape-town-storm-pics-informal-settlements-hard-hit-by-high-winds/

Postface

This chapter analyses the weather system locally named Cape Storm, a COL and surface low pressure system which affected the south-western Cape of South Africa. The analysis is done from a PV perspective, highlighting a PV intrusion in the context of a COL extension to the surface. The observational analysis of a COL extension from a PV perspective completes objective 1 of this study.

Over and above completing the first objective of this study, the work contributes to our understanding of COLs and COL extensions over South Africa. Although various COL case studies have been performed over South Africa and the South Atlantic as mentioned in the above chapter, few look at these systems either from a PV perspective or with respect to their relationship to surface cyclones developing beneath them.

The case study additionally highlights the complexity of surface weather systems that may impact South Africa. Operationally, we think of COLs as developing out of the upper troposphere, slowly extending to the surface and possibility driving the development of a surface cyclone. This case study highlights that this conceptual idea is not always the case. The surface low in question developed far west of South Africa and was developed, maintained and intensified by three separate COLs and associated high-PV stratospheric intrusions.

Finally, the case study combines the study of dynamical processes associated with the weather system's development and maintenance with the local impact that it had on the communities of the south-western Cape of South Africa. The impacts of weather systems are very rarely documented in the scientific literature. Documenting how the processes affect local communities is even more important within the context of South Africa as disaster management-related historical information is at times not readily available. The importance of enhancing our understanding of how these weather systems work and their variability is highlighted by how they can negatively impact the people of South Africa.

The intense weather system explored in this case study highlights the process of COL extensions and how PV dynamics could be a major factor in their development and deepening. The variability of these extensions and the role that PV dynamics plays in a COLs extension to the surface remains an open question. In the next chapter we explore the variability of COL extensions through climatological study of COLs and COL depths, using some of the knowledge gained through the case study in this chapter. Major PV dynamical processes are also analysed from a climatological point of view to gain an understanding of what drives COLs to extend towards the surface.

Chapter 3: Cut-off lows in the Southern Hemisphere and their extension to the surface

Preface

This chapter consists of one research paper that has been published in Climate Dynamics. The paper went through independent and international peer review. The citation is as follows:

Barnes, M.A., Ndarana, T. & Landman, W.A. Cut-off lows in the Southern Hemisphere and their extension to the surface. Clim Dyn (2021). https://doi.org/10.1007/s00382-021-05662-7

The case study of Cape Storm in Chapter 2 shows the influence of the intrusion of high-PV, stratospheric air into the upper troposphere on the development of COLs and the associated surface cyclones. The case study highlights that COLs can directly be associated with surface cyclones. An immediate question that emanates from the study is the variability of these extensions in space and time that occur over the southern hemisphere. Chapter 3 explores the variability and drivers of cut-off low (COL) depth in the southern hemisphere. A novel, 40-year climatology of COLs and their associated depth using ERA-Interim data is created. The COL depth climatology allows for the study of the seasonal, temporal and spatial variability of deep COLs and shallow COLs throughout the southern hemisphere. This answers objective 2 of this thesis.

Another important question emanates from the case study in Chapter 2, namely: what are the mechanisms that either result and promote the extension of COLs to the surface or inhibit its surface extension. Some important clues can be seen in the Chapter 2. One of these relates to effect that the vertical depth has on the COLs vertical extension. Does the depth that a high-PV intrusion reaches effect whether a COL is deep or shallow? We novelly investigate this by means of the COL vertical depth climatology. We additionally note in Chapter 2 that surface cyclones can develop at or near the time of COL development or COLs can develop over pre-existing surface lows. The variability of these differences are explored here. This additionally allows for the exploration of how these different types of COLs evolve in terms of their vertical structure. This evaluation and analysis of these different mechanisms completes objective 3 of this thesis.

The paper was co-authored by my two supervisors, Dr. T. Ndarana and Prof. W.A. Landman who supervised, guided and reviewed the work. Although the work was co-authored, I conceptualized the work, performed the analysis as well as wrote and reviewed the manuscript.

Cut-off lows in the Southern Hemisphere and their extension to the surface

Michael A. Barnes[*1,2], *Thando Ndarana*[2] *and Willem A. Landman*[2]

[1] *Marine Research Unit, South African Weather Service, Cape Town, South Africa*

[2] *Department of Geography, Geoinformatics and Meteorology, University of Pretoria, Pretoria, South Africa*

Abstract

Many cut-off low (COL) climatologies have been done throughout the southern hemisphere. Few have focused on COL vertical depth and their link to surface cyclones that often accompany these systems. Here we extend these climatologies in order to gain an understanding of the spatial, mobility, temporal, and seasonal variability of COL extensions towards the surface. Deep COLs (dCOLs), with extension all the way to the surface, are most frequent in the autumn months, are longer lasting, are more mobile and found most frequently situated in the high latitudes. They are usually collocated with Rossby wave breaking (RWB) on multiple isentropic surfaces. These RWB events drive high potential vorticity air into the upper troposphere. The depths of these intrusions are also shown to be critical to the development of COL extensions with dCOLs associated with deeper intrusions into the mid-troposphere. Upper-level PV features are collocated with warm surface potential temperature anomalies which can play a critical role in surface cyclogenesis. The warm surface potential temperature features, when out of phase with coupled upper tropospheric processes (surface features lagging behind upper level processes), can inhibit surfaceward extension and result in shallow COL (sCOL) development. Composite analysis shows that dCOLs that drive their own surface low development result in the simultaneous amplification of troughs throughout the troposphere, with the surface cyclone developing within a day of the COL.

Keywords: Cut-off low extensions, surface cyclogenesis, potential vorticity, Rossby wave breaking, stratospheric intrusions

3.1. Introduction

Cut-off lows (COLs) are cold-cored, closed, upper-air low pressure systems (Nieto *et al.*, 2005) that develop by becoming displaced equatorward out of the westerly jet in the extra-tropics (Palmén, 1949; Palmen and Newton, 1969). They usually persist for up to 4 days (Singleton and Reason, 2007b), but can on occasion last longer. Over South Africa, COLs contribute significantly to the overall rainfall of the country, especially during the spring and autumn months (Favre *et al.*, 2013). They are also a major contributor of extreme rainfall events particularly over the southern and eastern parts of the country. In fact, COLs contribute to 16% of the total annual rainfall of the cape south coast (Engelbrecht *et al.*, 2015). In addition, deep moist convection taking place within COLs can produce short bursts of extreme rainfall leading to 20% of all flash-flooding events over South Africa (Singleton and Reason, 2007b)

Various southern hemispheric COL climatologies have been completed focussing on COLs on different geopotential levels. Many have defined COLs as closed circulations at the 500hPa level (Fuenzalida *et al.*, 2005), whilst others use levels between 200 and 300hPa (Nieto *et al.*, 2005; Singleton and Reason, 2007a; Ndarana and Waugh, 2010; Pinheiro *et al.*, 2019). Muñoz *et al.*, (2020) compared the climatologies and found that whichever the level COLs are studied, their features remain consistent. There are four stages in the life cycle of COLs (Nieto *et al.*, 2005). First, an upper level trough develops coincident with a temperature wave situated to the west of the geopotential wave. During this stage, lower tropospheric cold air advection into the centre of the trough results in the amplification of the geopotential and temperature waves. As the amplitude continues to increase, it starts to detach from the westerly jet. This is the second stage known as the tear-off stage. Eventually, the cold air that has penetrated the centre of the deep trough gets cut-off equatorward from the extratropics. This third stage is known as the cut-off stage of COL development. In the final stage, the COL dissipates and usually merges again with a trough in the westerly zonal jet. In the tropics, the movement of COLs is however more erratic where COLs can retrograde (move in a westerly direction) or decay with equatorward trajectory (Favre *et al.*, 2013), not re-merging with the westerly zonal jet.

The dynamics of upper tropospheric cyclonic circulations have been studied in the northern hemisphere since the late 1940s. A first detailed account of COLs was done by Palmén (1949) who showed a case of an upper-level trough deforming and amplifying, with the cold airmass becoming cut off from the polar airmass. The case study detailed the lowering of the tropopause and how strong upper tropospheric convergence and associated subsidence leads to an increase in relative vorticity and upper level cyclonic development. The development of these systems was also theorised to be sustained by the amount of relative vorticity of the upper level cyclone, with increased cyclonic motion

resulting in COLs extending towards the surface (Hsieh, 1949). Early studies also showed the extension of isentropic potential vorticity (PV) values well into the mid-levels of the troposphere during these intense COL events. This lead to the theory presented by Kleinschmidt (1950) that these high-PV stratospheric intrusions in fact induce the cyclonic circulation of the COL (Bell and Bosart, 1993). This theory has now formed the basis of the "Isentropic PV Thinking" methodology of dynamical analysis which was later reinvigorated in the landmark paper by Hoskins *et al.* (1985) and has continued to be used in contemporary studies in dynamic meteorology (e.g. Holton and Hakim, 2013; Lackmann, 2011)

Isentropic PV thinking is based around the invertibility principle (Hoskins *et al.*, 1985). The invertibility principle states that if PV on each isentropic surface including that of the lower boundary is known, then all other meteorological fields (geopotential height, temperature and horizontal velocity) can be calculated under a suitable balance condition. Isentropic PV fields can therefore be used to describe the evolution of all other dynamical fields. Since PV is conserved for flow that is adiabatic and frictionless, PV frameworks are extremely useful for studying dynamical processes including that of COLs. COLs are known to be linked with high-PV anomalies (Bell and Bosart, 1993; van Delden and Neggers, 2003; Nieto *et al.*, 2005). High-PV values are negative in the southern hemisphere and positive in the northern hemisphere. These anomalies are the result of intrusions of high-PV stratospheric air transported isentropically and equatorward into the upper troposphere (Hoskins *et al.*, 1985). Theoretical analyses of PV show that positive PV anomalies in the upper troposphere can be viewed from a cross-sectional point of view as surfaceward bends in the dynamical tropopause (Hoskins *et al.*, 1985). The region of higher PV air than that of the air surrounding it results in cyclonic circulation around the high-PV anomaly.

Further, Rossby-wave breaking (RWB) events have also been well established to result in similar high-PV anomalies in the troposphere. RWB, defined as the rapid and irreversible deformation of PV contours (Mcintyre and Palmer, 1983), have been linked with the formation of COLs in many observational studies (e.g Baray *et al.*, 2003). Most recently, a climatological link has been established between COLs and RWB events in the southern hemisphere (Ndarana and Waugh, 2010). 89% of the COLs identified using National Centers for Environmental Protection/National Center for Atmospheric Research (NCEP/NCAR) reanalysis data (Kalnay *et al.*, 1996) were associated with RWB events. The remainder, although not being associated with RWB, were still associated with PV intrusions from the stratosphere. RWB events along lower isentropic surfaces have also been shown to correspond to COLs closer to the surface (500hPa), with RWB on higher surfaces corresponding to COLs nearer the tropopause (Ndarana and Waugh, 2010).

Stratospheric-tropospheric exchanges have also been well linked with cyclogenesis at the surface. An early observational study on the President's Day cyclone of 1979 in the United States of America showed an example of an explosive surface cyclone that was associated with a deep stratospheric event (Uccellini *et al.*, 1985). In this case high-PV values were observed close to the 700hPa level. Similar observational studies have also been conducted in the South Atlantic (Funatsu *et al.*, 2004; Iwabe and Da Rocha, 2009). The focus of observational studies has resulted in the PV-tower theory. PV towers are defined as the vertical alignment of 3 distinct PV anomalies in the upper troposphere, lower troposphere and at the surface (Čampa and Wernli, 2012; Pang and Fu, 2017). These PV anomalies govern the evolution and development of the surface cyclone by resulting in deep cyclonic circulation throughout the troposphere. Čampa and Wernli (2012) have also shown the importance of all three of these anomalies in the maturing and deepening of explosive cyclones. Notably, in weaker cyclones, low-level and surface anomalies are weaker. This suggests the importance of upper level process in the development of closed surface circulations, with low-level and surface anomalies working in unison with upper level processes to evolve the surface circulations.

Although surface cyclogenesis has been studied extensively in a PV framework, the focus of these studies has been on explosive cyclogenesis events. Explosive cyclogenesis events are important due to the large impact they can have on local communities resulting in extreme precipitation events and windstorms (Liberato, 2014; Barnes *et al.*, 2021) as well as large wave and storm surge events (Rautenbach *et al.*, 2020). Few studies have focussed on the development of generic surface lows that are dynamically driven by upper tropospheric processes. Surface lows, even at a low intensity, may result in adverse weather. The climatological variability of southern hemispheric COLs that extend to the surface as opposed to COLs that do not is also an open question. In this study, we extend southern hemisphere COL climatologies to include the extension of these systems to the surface. In conjunction with this database, the number of COLs that are associated with closed surface low pressures are studied. COLs and surface low pressures can also be linked to RWB. RWB is a well-known driver of stratospheric intrusions which in turn can result in cyclonic circulations. RWB-COL linkage statistics are also presented to corroborate the findings of Ndarana and Waugh (2010) with a different reanalysis dataset. PV diagnostics are performed to determine the effect that the depth of stratospheric intrusions has on the development of surface low pressures associated with COLs. Composite analysis of various fields (geopotential height, PV and potential temperature) provide insight into the general behaviour of COLs that extend to the surface and those that do not.

This paper is organised as follows. Section 2 provides a summary of the data used in the analysis. All the algorithms and diagnostic methods are also fully described. The results of the statistical analyses

are presented in Section 3. This section is divided into a general summary of the statistics of COL and COL depth databases with respect to the variability of extensions, a summary of the linkage statistics of the RWB and COLs detected and an analysis of the PV diagnostic and composite analyses. Conclusions are drawn and discussed in Section 4.

3.2. Data and algorithms

3.2.1. Data

In this study, 40 years (1 January 1979 – 1 January 2019) of European Centre for Medium-Range Weather Forecasting (ECWMF) Reanalysis (ERA-Interim) data (Dee *et al.*, 2011) are used. All fields used have a 2.5˚ X 2.5˚ horizontal resolution and a temporal resolution of 6 hours. Although data from the ERA-Interim dataset has a spatial resolution of 0.75˚ X 0.75˚, the lower resolution dataset is used for computational efficiency of the algorithms. A limitation of the use of the course resolution data is that small, sub-synoptic scale or very weak closed circulations may be missed. However since the processes explored in this study such as COLs are of a synoptic scale (600-1200km) and therefore are detectable in the lower resolution data (Fuenzalida *et al.*, 2005; Ndarana and Waugh, 2010; Reboita *et al.*, 2010; Muñoz *et al.*, 2020), this limitation is offset by the major advantage of computational efficiency. A variety of variables on various levels are used throughout the study. Each of these levels and variables are explained as they are used in each algorithm and section.

3.2.2. COL detection algorithm

A database of COLs between 1979 and 2018 is produced from ERA-Interim 2.5-degree data. COLs in this database are defined on the 250hPa geopotential height level at 6-hourly intervals. Although some studies use various levels to define COLs in various COL climatologies (e.g. Fuenzalida *et al.*, 2005; Nieto *et al.*, 2005; Reboita *et al.*, 2010), the 250hPa level is chosen as it represents the vertical position of both the subtropical and mid-latitudinal dynamical tropopauses (Ndarana and Waugh, 2010). This is important as this study aims at linking upper tropospheric processes to the extension of COLs to the surface. The COL detection algorithm used in this study is based on a similar COL detection algorithm used by Ndarana and Waugh (2010) and is a geopotential-based tracking algorithm. Most climatologies use geopotential tracking methodologies for COL climatologies (Muñoz *et al.*, 2020). Other authors use PV frameworks for the detection of COLs (Sprenger *et al.*, 2007). However, a geopotential-based algorithm was chosen here to maintain the COL database's independence from PV since we will later look at their relation to stratospheric intrusions of high-PV. The geopotential framework is quasi-horizontal. This has the disadvantage of not sloping with the dynamical tropopause and thus some COL events may be missed. However, the quasi-horizontal, geopotential framework is

also more readily used by operational users and therefore a geopotential height detection algorithm and subsequent analysis are more beneficial to operational meteorologists. The algorithm to detect COL centres is described in detail below and for ease of reference, a schematic of these steps for COL detection are provided visually in Figure 37 in the Appendix.

Step 1: 250hPa contours at a 1 geopotential meter (gpm) interval are derived at each timestep (6 hours). 1gpm is chosen for computational efficiency of the algorithm but with enough resolution to detect a closed low as soon as it has formed. All contours that are closed (with identical start and end points) are then detected. Finally, the geometric centre of each of these closed contours is obtained and saved into the database as potential COL points.

Step 2: Only COL points between 50˚S and 15˚S are retained in the COL point database. Tropical lows are excluded by excluding lows north of 15˚S. This has been a standard practice in many COL climatologies (e.g. Fuenzalida *et al.*, 2005) eliminating lows anywhere from 10˚S to 20˚S. Lows are excluded below 50˚S to exclude polar lows from the database which are not detached from the polar regions (Muñoz *et al.*, 2020).

Step 3: All high-pressure closed contour centres are then filtered out by applying a geopotential height condition onto each COL point in the database. First, the nearest grid point to the COL point is detected. COL points are filtered out if the nearest grid point to the COL point is lower than six neighbouring of the possible eight grid points by at least 10gpm. This condition has been used in multiple COL climatologies (e.g. Nieto *et al.*, 2005; Porcù *et al.*, 2007).

Step 4: COLs, by definition, need to be fully detached from the westerly wind belt. A zonal wind direction condition is used to apply this condition. A COL point is filtered out of the database if the closest grid point to the COL point and/or the grid point to the south of this grid point has a easterly component. It has been shown that using a single point detection methodology could result in an overestimation of COLs (Pinheiro *et al.*, 2019). This risk is however removed by including a closed contour condition (as performed in Step 1) together with a single point wind condition, as together they imply total cyclonic wind flow.

Step 5: COLs are cold-cored systems and therefore a cold-core condition is applied to the database as has been used in many previous COL climatologies (e.g. Nieto *et al.*, 2005; Reboita *et al.*, 2010). In this study, the cold core condition is applied by detecting 250-500hPa local thickness minima. Thickness fields are used as they provide a better representation of the thermal properties of the layer (Ndarana and Waugh, 2010). A COL point in the database is said to have been associated with a cold core if the thickness of the nearest grid point to the COL point is less than at least five of its eight nearest neighbours. COL points that do not meet this condition are discarded from the database.

Step 6: The database now contains multiple COL points, many of which belong to the same COL, since rings of multiple closed contours would have been identified in Step 1. COL points that share a 10-by-10-degree area are deemed to belong to the same COL. The point within this box with the lowest central

250hPa geopotential height is deemed to be the COL point with the remainder of the COL points filtered out of the database.

Step 7: Randomly sampled, subjective analysis of the COLs identified at the end of Step 6 reveals that COLs are intermittently identified with some timesteps within a COL trajectory missing from the database. This would result in COL trajectories being split into multiple trajectories and an over-estimate of individual COLs in the database. This issue was also previously noted by Porcù *et al.* (2007). Many studies do not have this issue as many use daily averaged data (e.g. Nieto *et al.* 2005; Ndarana and Waugh 2010). This problem was previously solved by filling "gaps" in a COL's trajectory subjectively (Porcù *et al.*, 2007). A COL trajectory was deemed to have a gap if there were no more than two consecutive missing six-hourly detections. In this study, this same technique is applied objectively. A database of simple closed low pressures is gathered using steps 1-3. If a "gap" of no more than 2 timesteps is detected in a COL, the gap is filled with a detected low-pressure centre within a 5x5 degree range of the previous COL centre, if it existed. This step results in grouping COLs points that are part of the same COL system trajectory. Although the size of the 5x5-degree search box in meters is different between the tropics (close to 15˚S) and the extratropics (close to 50˚S), this is deemed to be sufficient since very few COLs travel fast enough such that the COL point will not be contained in the search box at the subsequent timestep (Reboita *et al.*, 2010). Additionally, it has been shown that the zonal mean velocity of COLs is greater towards the poles (Pinheiro *et al.*, 2017) and therefore an increased size search box (in terms of meters) at the poles is in fact appropriate.

Step 8: Finally, a longevity condition is imposed on the COL trajectories in the database. COLs that are not present at 4 consecutive timesteps (24 hours) are removed from the database.

3.2.3. COL vertical structure algorithm

A COL vertical extension study of the Mediterranean is used as a basis for COL vertical structure methodology applied here (Porcù *et al.*, 2007). First, a 5x5 grid-point area is extracted from around the COL grid cell. Low pressure regions at various geopotential height levels are detected. A grid point is considered to be a low-pressure minimum if six or more out of the eight of its neighbouring grid cells are lower than the threshold specified for that particular level. Specified level thresholds are obtained by Porcù *et al.* (2007) who used smoothly decreasing values from 10gpm at 200hPa to 2gpm at 1000hPa. These values represent 30% of the standard deviation of the geopotential height distribution amongst neighbouring grid points. In the event that more than one low pressure minimum is detected for a COL point at a specific timestep, the coordinates of the low-pressure minimum with the lowest geopotential height is chosen and recorded in the low-pressure minimum database for that particular level.

From this detection methodology, a low-pressure minimum database at each level below the COL and time is created throughout the trajectory of the COL. Although each low-pressure minimum was

detected in the region of each COL point, the search is performed independently of the levels above and below it. If a low point was detected at the 300hPa level below a COL point in the COLs trajectory, it is deemed to have a depth of 300hPa. If the COL reached a depth of 300hPa, the search is repeated at the level below. This process is further repeated for all the levels down to the surface at 1000hPa. The COL depth is defined as the minimum depth at which a low is present in the COL point zone throughout the life of the COL.

An independent surface low pressure database is derived to analyse whether a closed and defined surface cyclone is collocated with a detected COL. Surface low pressure minima are detected using a similar procedure to steps 1-3 of the COL detection algorithm as defined in Section 3.2.2. Mean sea level pressure data is used to find closed contours. Closed contours are detected at 1hPa interval. Low pressures are isolated from high pressure closed contours by using the nearest neighbour methodology as before but using a neighbourhood threshold of 2hPa.

3.2.4. Classification of COLs in terms of their depth

For simplicity in analysing the results of COL depths we classify COLs into two groups. D*eep COLs* (dCOLs) refer to COLs which have a depth down to 1000hPa. A s*hallow COL (sCOL)* will refer to a COL with a depth 500hPa of shallower. To determine the relationships between COLs and surface cyclones, we use a method similar to that described by Porcù *et al.* (2007). An independent surface low pressure database is created using mean sea level pressure (MSLP) as described in Section 3.2.3. Similarly to Porcù *et al.* (2007), we define the following classification of COL and surface low relationships:

1. COLs are separated into deep COLs (*dCOLs*) and shallow COLs (*sCOLs*). dCOLs refer to COLs which have a depth down to the surface at 1000hPa (as detected by the algorithm in Section 3.2.3) whilst *sCOLs* will refer to a COL with a depth 500hPa or shallower.
2. dCOLs are separated into COLs that are associated with a surface low (*type 1 dCOLs or d1COLs*) from the independently derived surface low database (as defined in Section 3.2.3) and those that are not (*type 2 dCOLs or d2COLs*). A dCOL is said to be associated with a surface low if the independently detected surface low is found within a 5x5-degree area of the COL point during any time during its trajectory. Since the COLs in this class have already been defined as deep, extending all the way to the surface, the associated low is also vertically related to the COL. This classification differentiates deep-COLs with a distinct surface low-pressure cell at the surface (in which a closed surface low is found on the MSLP surface) from deep-COLs with a weak cyclonic circulation at the surface (in which a low pressure minimum is found at 1000hPa but without closed cyclonic circulation).
3. d1COLs are then separated by their temporal relation to their accompanying surface cyclone. d1COLs are classified into COLs whose surface cyclones formed at or after the first detected point in the COLs life cycle (*type 1a dCOLs or d1aCOLs*) and those formed before the COL developed (*type 1b dCOLs or*

d1bCOLs). This classification aims at determining the number of surface lows that develop as a result of the mechanisms that result in the COLs development versus the number of COLs that move over already pre-existing low-pressure zones or cells. The upper level dynamics associated with the development of a COL can result in the development of closed cyclonic circulation at the surface prior to the closed circulation in the upper levels (associated with the COL) as seen in the case study by Barnes *et al.* (2021). Even though the surface circulation may develop first, it results from the same mechanism that resulted in the COL's development and therefore can still be considered as part of the same system. Therefore, in order to include these processes, surface lows that developed up to 12 hours before the COL are included in type 1a dCOLs (d1aCOLs).

3.2.5. RWB detection algorithm

RWB events are identified using the geometry of their overturned PV features on isentropic surfaces (e.g. Barnes and Hartmann, 2012; Esler and Haynes, 1999; Ndarana and Waugh, 2011). In this study we employ the RWB identification methodology similar to that of Ndarana and Waugh (2011) and Barnes and Hartmann (2012) based on the geometric properties of PV contours. Isentropic PV can be expressed mathematically by:

$$PV = -g(\zeta_\theta + f)\frac{\partial \theta}{\partial p} \quad (1)$$

with ζ_θ the relative vorticity on an isentropic surface, f the Coriolis parameter, θ the potential temperature and p the pressure. The southern (northern) hemispheric stratosphere is associated with larger negative (positive) PV values. The PV contours of -1.5, -2 and -2.5 PVU (PV units, $1\,PVU = 10^{-6}\,K\,m^2\,s^{-1}\,kg^{-1}$) on the 315-, 320-, 330- and 350K isentropic surfaces are used. The dynamical tropopause varies with height both seasonally where it is closer to the surface in winter and latitudinally where it is closer to the surface nearer the poles (Kunz *et al.*, 2011; Ndarana and Waugh, 2011). The choice of the set of isentropic levels considered here are coincident with the dynamical tropopause taking into account the tropopause height variability between different seasons and latitudes (Ndarana and Waugh 2011, their Figure 1) from the available isentropic levels in the ERA-Interim dataset. At each level, contours are found for each of the specified contour intervals. We first eliminate all PV cut-offs and small-scale features by eliminating all contours that have fewer points than the longitude grid (144). Once the large-scale PV contours have been isolated, overturning features of each contour are identified. A contour is considered to be overturned if a longitudinal line intersects the contour two or more times. Overturned contours are detected at a zonal resolution of 1˚. At each longitude where the contour is intersected more than twice, the coordinates of the most northerly and most southerly intersecting coordinates are recorded. Consecutive overturned longitudinal sections are then considered as part of the same RWB event. RWB events are recorded

as closed polygons whose bounds are the upper and lower coordinates recorded by the algorithm. Small-scale RWB events are filtered by only adding RWB events whose overturning area has a span of at least 10˚ to the database. Finally, we filter out areas of the RWB polygons which intersect areas by which $\partial_y PV > 0$. This results in intrusions in which overturning does not take place being removed from the database. Each polygon is recorded with its associated timestep, isentropic level and PV contour interval.

3.2.6. Stratospheric depth algorithm

Stratospheric depth changes associated with intrusions are mapped to correlate with the depth of each COL. The stratosphere is well known to be associated with high-PV air (Holton and Hakim, 2013). Using this fact, stratospheric air can be mapped and differentiated from low-PV tropospheric air. In order to find these intrusions of high-PV air, the algorithm described by Sprenger *et al.* (2003) and later improved by Škerlak *et al.* (2014) is employed. The algorithm makes use of a labelling system differentiating the 5 different airmasses as shown in the schematic in Figure 1 of Škerlak *et al.* (2014). The algorithm is run on ERA-Interim data for the southern hemisphere north of 65˚S using PV values for levels between 50hPa and 1000hPa at a vertical resolution of 50hPa. The stratosphere is initiated at 30hPa with each value given the label 2 indicating that stratospheric air is present. For the purposes of this study, a value of -1.5 PVU is deemed to be the dynamical tropopause. Although -2 PVU is often used to represent the dynamical tropopause, the -1.5 PVU contour is chosen as PV contours closer to the surface are more sensitive and variable in the vertical whilst still being representative of the dynamical tropopause. This allows for a clearer diagnosis of the depth of the intrusion compared to more stratospheric contours. Using a stratospheric PV value of -1.5 PVU, a value is given the label 2 (indicating stratospheric air), if it has a PV value of less than -1.5 PVU and it has a neighbour either horizontally, vertically or diagonally that is also stratospheric air (label 2). If a grid cell has a value of less than -1.5 PVU and it does not have a label 2 neighbour, it is labelled as a label 3 indicating a high-PV stratospheric cut-off or low-level high-PV feature. If the grid cell is greater than -1.5 PVU, it is considered to be tropospheric air and given a label 1. Furthermore, tropospheric cut-offs (grid cells with PV greater than -1.5PVU) that are completely surrounded by stratospheric air are given the label 4. Finally, high-PV values can also be associated with very stable surface layers, especially over the polar regions (Škerlak *et al.*, 2014). These surface-bound high-PV values (high-PV values that are in contact with the surface but not in contact with the stratosphere) are differentiated from stratospheric blobs and are given the label 5.

3.3. Results

3.3.1. COLs and extended COLs in the southern hemisphere

Using the algorithm in Section 3.2.2, a total of 10543 COL trajectories were identified in the southern Hemisphere. This represents an average of about 258 COL events per year. A summary of these events in the form of a density map is shown in Figure 23. The density map of COL points is created by gridding all the COL points in the database into 1˚x 1˚ bins and smoothing the binned data using a 5˚x 5˚ gaussian filter. The densities obtained mirrors COL climatologies in previous studies. High densities are shown to the west of the Andes and the African continents as well as in the Tasman Sea. The effect of topography can be seen with high COL density areas found to the west of mountainous areas such as the Andes, New Zealand Alps and African Plateau promoting upper-level cyclolysis on the leeward side and cyclogenesis on the upstream side of these features (Fuenzalida *et al.*, 2005). Average annual COL numbers found are also in the range of other southern hemisphere climatologies using ERA reanalysis datasets (Reboita *et al.*, 2010; Pinheiro *et al.*, 2017, 2019). It is however a significant rise in COLs found in other studies which uses NCEP/NCAR reanalysis data. On such study is that of Ndarana and Waugh (2010) who found only 81 COLs per year at the 250hPa level. It has however been shown that significant differences can occur between COL climatologies using European Centre for Medium-Range Weather Forecasts Re-Analysis (ERA)-40 and NCEP/NCAR (Reboita *et al.*, 2010). In fact, climatologies over the southern hemisphere using ERA reanalysis can detect up to double the amount of COLs using the same algorithm, depending on the level.

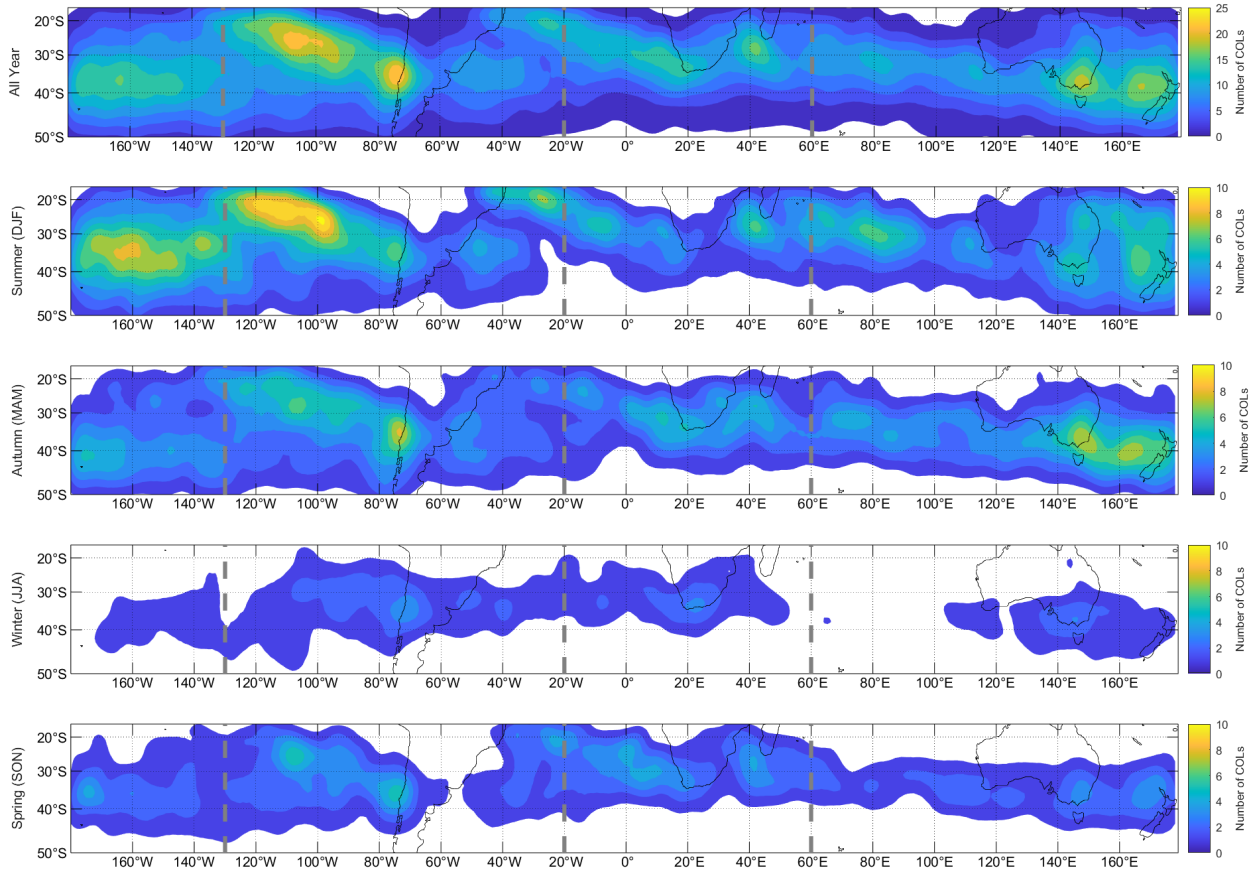

Figure 23: COL densities of all points in the COL database. COL points are gridded into 1˚x 1˚ bins and smoothed using a 5˚x 5˚ gaussian filter. Annual (top panel) and seasonal distributions are provided. Grey dashed lines denote the South American, African and Australia-New Zealand sectors as used throughout this study.

3.3.1.1. A southern hemispheric climatology of extended COLs

The COL depth as defined in Section 3.2.3 is calculated in order to determine the lowest depth that the upper level low pressure system attained during its life cycle. The southern hemispheric COL depths are shown in Figure 24. 57.8% of the COLs in the southern hemispheric database reached the surface (1000hPa level), with only 31.6% and 38.7% reaching the 500hPa and 600hPa levels respectively. This is consistent with the findings of Porcù *et al.* (2007) in the Mediterranean region. Few COLs are very shallow, but generally COLs extend into at least the mid-troposphere (400-600hPa). Interestingly, very few COLs extend down to the 700-925hPa level that do not extend all the way to the surface. This "gap" in the COL depth does differ from the results in the Mediterranean study (Porcù *et al.*, 2007). Although the number of Mediterranean COLs gradually increases to the 500hPa level as is found in the southern hemisphere, the number of COLs extending below the 500hPa level do not decrease sharply in the Mediterranean. Instead the number of Mediterranean COLs reaching the 700-850hPa levels were found to be comparative to the number of COLs extending to the mid-levels. It has been shown that more intense cyclones over the Mediterranean region are generally associated with lesser diabatic-induced low-level PV structures compared to that of the surrounding larger ocean

basins of the northern hemisphere such as the Atlantic and Pacific (Čampa and Wernli, 2012). As the southern hemispheric region studied here is similar to the large oceanic basins, this boost in low-level PV could result in more of the extensions that extend into the low-levels reaching all the way to the surface. In addition, cyclone tracking is a challenge in the Mediterranean region due to the complex topography and stark contrast between the sea and surrounding land (Flaounas *et al.*, 2015). This could indicate that some surface-level low-pressure minima could have been missed in the Mediterranean study enhancing the number of COLs that extend to the low-levels but do not extend to the surface. The results for the COL depth analysis throughout the southern African, Australia-New Zealand and South American sectors as shown in Figure 24 and will be discussed fully in Section 3.3.1.2.

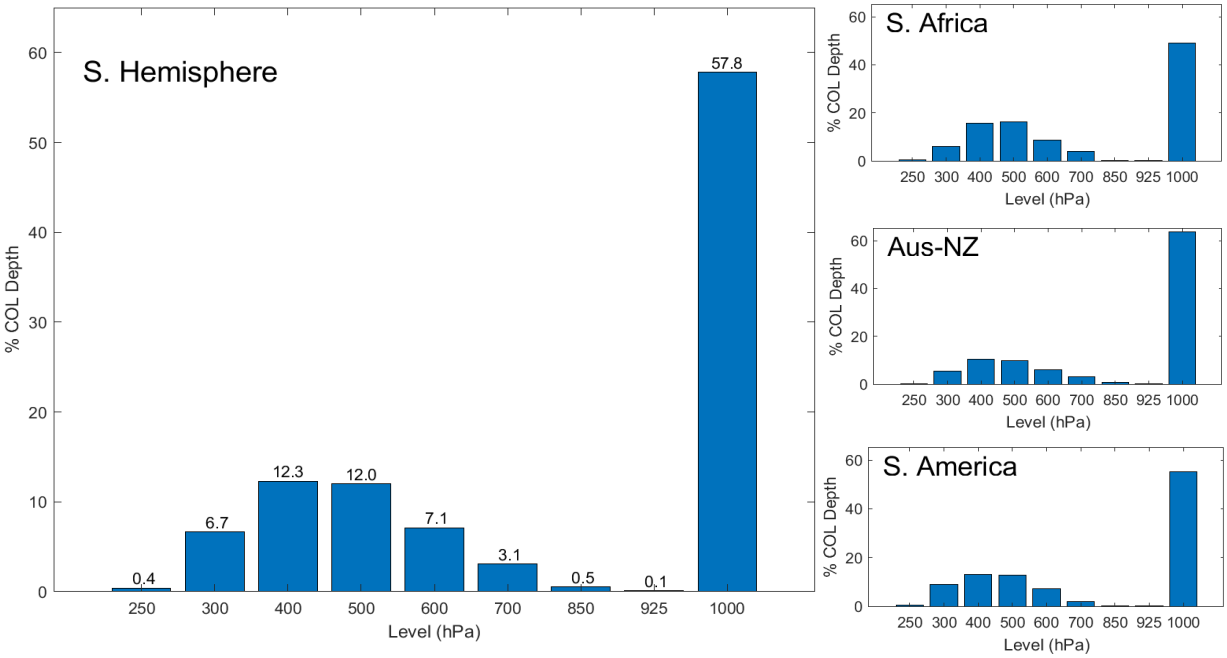

Figure 24: Lowest level in which a low-pressure centre could be detected beneath a detected COL (250hPa). Results for the entire southern hemisphere (left) as well as the southern African, Australia-New Zealand and South American subregions (right) are shown.

COL depths give a sense of the COLs that extend fully to the surface. However, COLs also exist in conjunction with closed surface lows. This was observed to have occurred during various observational studies (Uccellini *et al.*, 1985; Iwabe and Da Rocha, 2009; Barnes *et al.*, 2021). The classification of COL depths in relation to the type of circulation at the surface as defined in Section 2.4, is used to analyse COL extensions. As shown in Figure 24, dCOLs make up 57.8% of the COLs in the southern hemisphere, with sCOLs making up only 31.4%. The classification process found that of the dCOLs, the majority (89.5%) are associated with closed low-pressure circulations at the surface (d1COLs). The remainder of the dCOLs (10.5%) do present with surface low pressure minima (i.e. a surface trough), but have no associated defined, closed cyclonic circulation. Further classifying these d1COLs reveals that a larger proportion of these low-level circulations developed from 12 hours before

the development of the COL. In fact, 53.1% of the d1COLs are classified as type 1a dCOLs (d1aCOLs) with the remainder of the lows developing before initial detection the COL (d1bCOLs). These results show that although the mechanisms that drive COL development can result in the development of surface cyclonic circulations, COLs can also develop in areas where these circulations already exist. The processes that result in the COLs surfaceward extension still influences the low-pressure system at the surface even if it is formed before the COL develops. The upper level processes together with surface level processes can result in a deepening of the surface cyclones. In fact, in the southern hemisphere, 78.4% of the d1bCOLs were associated with a decrease in the 1000hPa geopotential minima identified from the start of the COLs lifecycle. Half of the d1bCOLs showed significant decreases of over 20gpm in the 1000hPa geopotential minima.

3.3.1.2. Spatial variability of extended COLs within the southern hemisphere

The analysis performed in Section 3.1.1. is repeated for specified sectors of the southern hemisphere. The sectors studied are the southern African sector (20˚W to 60˚E), the Australian-New Zealand sector (60˚E to 130˚W) and the South America sector (130˚W to 20˚W). The largest sector, the Australia-New Zealand sector, is the most active COL sector with nearly half of the COLs (5026 COLs, 125 COLs per year) in the database located in this sector. Comparatively the smallest sector, the southern African region is the least active sector with 2290 COLs (57 COLs per year) whilst 3613 COLs (90 COLs per year) are identified in the South American sector. The distribution of COLs between the three sectors is consistent with previous studies (Fuenzalida *et al.*, 2005; Reboita *et al.*, 2010). The variations in the distributions of COLs are likely the result of the variability and preferred position in RWB events (Ndarana and Waugh, 2011) and orographic effects (Fuenzalida *et al.*, 2005). COL depths for the three sectors are shown in Figure 24. The COL depth distributions in each of the three sectors are relatively consistent with results for the entire hemisphere. Very few COLs extend to the low-levels that do not extend fully to the surface. The southern African sector contains the lowest ratio of dCOLs with 49% of the COLs extending all the way to the surface. This region also comprises of more sCOLs than the other two sectors with 38.3% of the COLs extending to only the 500hPa level. Conversely the Australia-New Zealand sector is the most active in terms of dCOL development with 63.6% of the COLs extending to the surface.

Despite the differences in the ratio of sCOLs to dCOLs in each sector, the percentage of dCOLs associated with defined cyclonic surface circulation remains consistent throughout all three sectors. 89-90% of the dCOLs in each sector are classified as d1COLs. The southern African sector stands out in terms of the temporal relationship between the COL and the surface low. This sector comprises of slightly more dCOLs which develop their own surface circulations than the other two sectors. In the

southern African sector, 57.4% of the d1COLs developed surface low pressure cells near or after the development of the COL compared to 52.3% and 51.5% in the Australia-New Zealand and South American sectors respectively. A summary of the results of the classified COLs for both the southern hemisphere and all three of the sectors are given in Table 4.

Table 4: Table of occurrence statistics of all classified COL extensions in both the southern hemisphere and Southern African region

	dCOLs (percentage of total COLs)	sCOLs (percentage of total COLs)	d1COLs (percentage of dCOLs)	d2COLs (percentage of dCOLs)	d1aCOLs (percentage of d1COLs)	d1bCOLs (percentage of d1COLs)
S. Hemisphere	57.8%	31.6%	89.5%	10.5%	53.1%	46.9%
S. Africa	49.0%	38.3%	89.2%	10.1%	57.4%	42.6%
Australia-NZ	63.6%	26.1%	89.1%	10.9%	52.3%	47.7%
S. America	55.2%	35.2%	90.2%	9.8%	51.5%	48.5%

Another notable characteristic difference between dCOLs and sCOLs is the distinct latitudinal discrepancy between the two different types. The distribution of all dCOL and sCOL points in the database with latitude are shown in Figure 25. From the COL point distributions, it is clearly visible that sCOLs are more often found in the subtropics (north of 30˚S), whilst dCOLs are generally found towards the extratropics (south of 30˚S). Of all detected sCOLs within the southern hemisphere, 77.2% of sCOLs contained tracks north of the 30˚S line. Only 22.5% of the dCOLs are found to have crossed the 30˚S latitude line. Conversely, 92.6% of all dCOLs had at least one point south of the 30˚S line. This indicates that the latitude at which COLs develop at or migrate to is an important factor in their extension towards the surface.

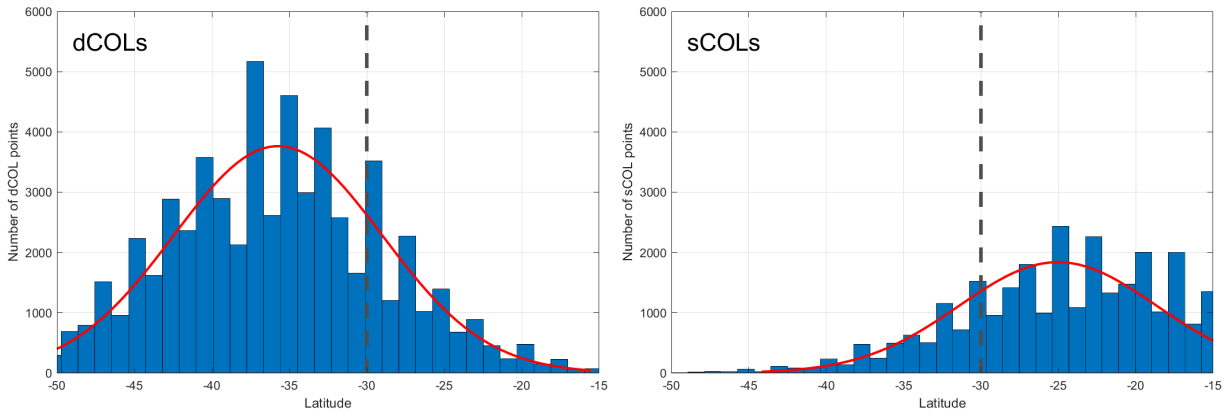

Figure 25: Distribution of all COL points for dCOLs (left) and sCOLs (right) with respect to latitude. Normal distribution curves are also shown by red lines. For ease of reference, the 30°S latitude is highlighted by a grey dashed line.

3.3.1.3. Seasonal variabililty of extended COLs

An important factor to assess in any climatology is the seasonal variability. Seasonal variability has been addressed in previous COL climatologies (Fuenzalida *et al.*, 2005; Reboita *et al.*, 2010; Pinheiro *et al.*, 2017). COLs are subdivided into seasons. The season of the COL is determined by the date on which the COL is initially detected. For example, a COL with a 4-day duration detected on 31 May 2017 will be included as a May or autumn COL even though the COL persisted into June 2017. A monthly analysis is performed, and the results are shown in Figure 26. The data shows that the COLs at 250hPa in the database are most prevalent in the summer (December-January-February) and autumn (March-April-May) months with a peak in the month of March. The frequency of COLs drops throughout winter (June-July-August) with a minimum occurrence in August. This is a very similar trend observed in previous studies of climatologies of COLs on a similar pressure level (Pinheiro *et al.*, 2017). dCOLs seem to approximately follow the trend of the overall COL climatology. The number of dCOLs does however peak slightly later in the year, with a peak percentage of COLs found to be in April. A definite autumnal peak can be seen in the dCOL curve in Figure 26. Table 5 shows that 33.5% of the dCOLs occur in the autumn. This is not the case for sCOLs. sCOLs most often occur during the summer months with a definite peak in January and February. In fact, close to half (49%) of the sCOLs are found in the summer months. A sharp drop in the frequency occurs during autumn with very few sCOLs observed in the winter months. Only 5.2% of all the detected sCOLs are observed during the months of June, July and August.

Table 5 shows the inter-seasonal variability of COLs, dCOLs and sCOLs for the southern African, Australia-New Zealand and South American sectors. The seasonal trend of COLs, dCOLs and sCOLs in each sector remains relatively consistent with the overall seasonal distribution of COLs throughout the southern hemisphere. Both COLs and dCOLs peak towards the late summer and autumn months. sCOLs are most prevalent in the summer months with very few sCOLs present during winter. The South American sector tends to be less variable in terms of dCOLs throughout the seasons than the other sectors. This sector does have the autumnal maximum frequency as in the other two sectors, but the remaining months remain fairly consistent in terms of dCOL frequency. Another small deviation can be seen in the sCOL seasonal distribution in the southern African sector. Although the sector has a large summer maximum like all other sectors, the summer months contain 10% less sCOLs than the other sectors. Additionally, the southern African sector has a greater number of springtime (September-October-November) sCOLs compared to the other sectors and is also the most prone sector to wintertime sCOLs.

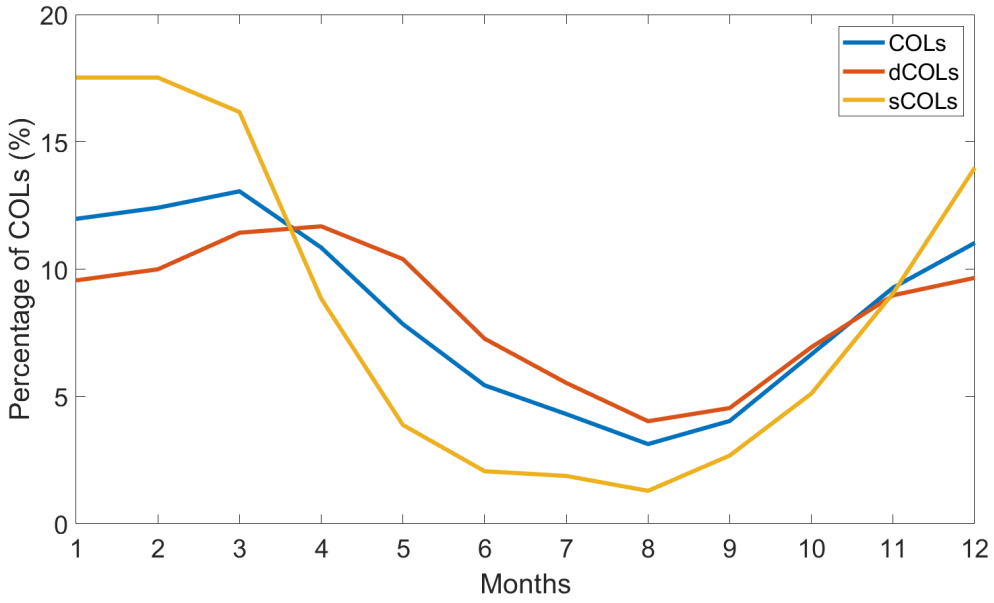

Figure 26: Seasonality of COLs, dCOLs and sCOLs. The percentage of each category that occur in each month are shown.

Table 5: Seasonality of COLs in sectors of the southern hemisphere.

	COLs (%)	dCOLs (%)	sCOLs (%)
Southern Hemisphere			
Summer	**35.4**	29.2	**49**
Autumn	31.7	**33.5**	28.9
Winter	*12.9*	*16.8*	*5.2*
Spring	20	20.5	16.8
Southern Africa			
Summer	29.1	23.6	**40.4**
Autumn	**30.7**	**33.5**	27.4
Winter	14.6	*18.4*	*8.4*
Spring	25.6	24.4	23.7
Australia-New Zealand			
Summer	39.0	**33.8**	**53.1**
Autumn	**32.8**	**33.8**	30.6
Winter	*10.4*	*13.4*	*2.4*
Spring	17.8	19.0	13.8
South America			
Summer	**35**	25.3	**50.7**
Autumn	30.6	**32.9**	27.8
Winter	*14.8*	*20.9*	*5.8*
Spring	19.6	21	15.7

3.3.1.4. Variabililty of extended COL lifetime

The lifetime of COLs has been well studied by various authors in the southern hemisphere (Fuenzalida *et al.*, 2005; Reboita *et al.*, 2010; Pinheiro *et al.*, 2017). These systems are well known to last only a few days. The effect that COL depth has on the temporal variability of these systems is investigated here and the results shown in Figure 27. It should be noted that in this study, COLs are defined to last at least one day (four six-hourly timesteps). The lifespan distribution of COLs in the southern hemisphere as well as the sectors is very similar to what has been observed in various other studies, with the number of COLs lasting more than a day decreasing exponentially. Very few COLs are observed to occur longer than 7 days, although it does infrequently occur. Figure 27 shows that dCOLs tend to last longer than sCOLs. Close to half of the sCOLs observed have a lifetime of between 1 and 2 days in the southern hemisphere. Comparatively, only roughly a third of the dCOLs lasted between 1 and 2 days. For COLs observed to last longer than 2 days, there are a consistently higher frequency of dCOLs compared to sCOLs throughout all sectors of the southern hemisphere until at least 7 days. This is evidence that the depth of COLs could play some role in extending the lifespan of COLs. Results in each of the southern African, Australia-New Zealand and South American sectors are consistent with the temporal distribution of the southern hemisphere with respect to COL depth.

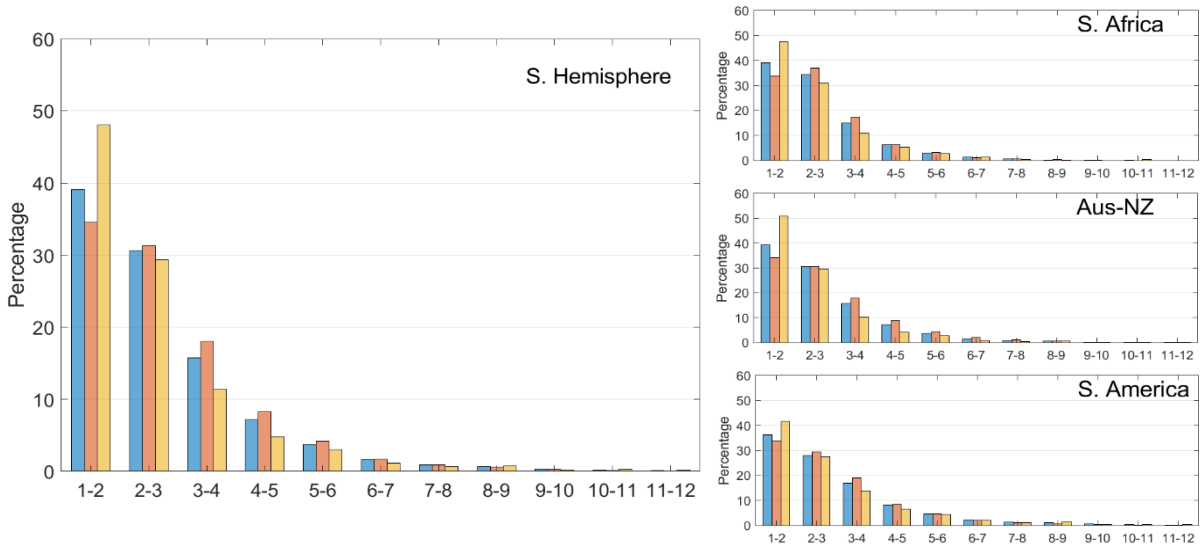

Figure 27: Temporal variability of COLs. The frequency distribution of the lifespan (in days) is given for COLs (blue), dCOLs (red) and sCOLs (yellow). A breakdown for the southern African, Australia-New Zealand and South American sectors are also given (right panel).

3.3.1.5. Mobility of extended COLs

The mobility of COLs has been analysed in previous COL climatologies using various different methodologies. Some studies (e.g. Fuenzalida *et al.* 2005; Reboita *et al.* 2010) have used the distance and time between the start and end points of each COL to determine the velocity whilst others (e.g. Pinheiro *et al.* 2017a) calculate the zonal mean velocity of COLs. The methodologies of Reboita *et al.*

(2010) and Fuenzalida *et al.* (2005) do not take into account that COLs may not move in a straight line. In this study, we update this methodology by calculating the distance between each of the COL points in each COL trajectory to calculate the total distance that the COL has travelled. This provides a more accurate mean velocity for each COL.

Figure 28 shows the distribution of mean speeds for COLs, dCOLs and sCOLs. The maximum frequency of COL mean speeds is between 9-12m/s. This is considerably higher than in previous studies (e.g. Reboita *et al.* 2010). This discrepancy however is due to the methodology used, as in this study we use a more integrated distance (which increases the distance travelled), whilst previous studies use the straight-line distance approach. There is a slight shift in the maximum mean COL velocity between sCOLs and dCOLs. dCOLs (with a maximum frequency in the 9-12m/s category) tend to be slightly faster than sCOLs (with a maximum frequency in the 6-9m/s category). COL mobility is relatively consistent across the three regions with very little variability in the COL mean velocity distribution as can be seen in Figure 28.

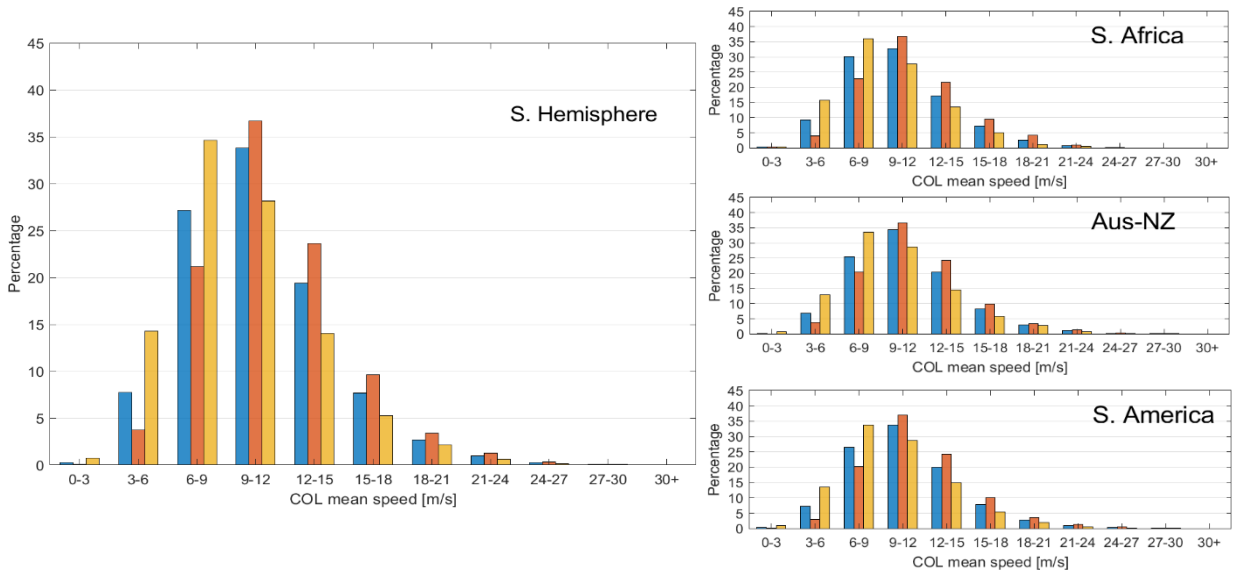

Figure 28: Mobility of extended COLs. The frequency distribution of the mean speed across the entire trajectory of each COL (in m/s) is given for COLs (blue), dCOLs (red) and sCOLs (yellow). A breakdown for the southern African, Australia-New Zealand and South American sectors are also given (right panel).

3.3.2. RWB events and extended COLs

RWB is a known mechanism for inducing stratospheric-tropospheric exchange which may result in COL development (Ndarana and Waugh, 2010). As the mechanism that drives the development of COLs, it is important to investigate whether RWB is linked to vertical extension of COLs. COLs have been climatologically linked to RWB in the southern hemisphere in the study by Ndarana and Waugh (2010). However, this study used NCEP/NCAR reanalysis data whereas we make use of ERA-Interim reanalysis. As explained in Section 3.3.1, COL detection between various versions of ERA and NCEP/NCAR differs

significantly as to the number of COLs detected. For example, Reboita *et al.* (2010) detected 50-75% more COLs using ERA-40 compared to NCEP/NCAR reanalysis data. Due to the large discrepancies between the two reanalysis datasets with respect to COL detection, it is important to confirm that the relationship between COLs and RWB events still hold using the ERA-Interim dataset. A search polygon was created for each COL. The search polygon comprised an area 60˚ to the west, 10˚ to the east and 15˚ north and south of each COLs initial point. RWB occurring during the life of each COL as well as up to 4 days prior to the COLs initial development are considered. If a RWB polygon in the database intersected with the search polygon, the RWB event is said to be associated with the COL. Using this methodology, 99.3% of the COLs in the database throughout the southern hemisphere are collocated with at least one RWB event. Together with the work by Ndarana and Waugh (2010), this reaffirms the climatological link between RWB and COLs.

The COL depth database allows for the exploration of RWB events and their link to the vertical structure of COLs. For the purposes of this study, we define a deep RWB event as an event which occurs on multiple isentropic levels simultaneously. The greater number of levels these events occur on, the deeper the event is said to be. Conversely, shallow RWB occur on fewer of these levels simultaneously. A total of four different isentropic levels (315-, 320-, 330- and 350K) are used in this study. Therefore, the RWB depth is ranked from 0 to 4 where 0 indicates COLs that are associated no RWB event up to 4, which indicates that a COL is affected by RWB events on all 4 isentropic levels. The RWB depth is calculated for both dCOLs and sCOLs and the results are shown in Figure 29. This can also be seen visually in Figure 30 by the composite mean geopotential height and isentropic PV contours of the initial timestep of each dCOL and sCOL. Although a rudimentary approach, the results reveal a very distinct difference in RWB depth between dCOLs and sCOLs. dCOLs are more often associated with RWB events identified on multiple isentropic levels and therefore greater RWB depths than sCOLs. About 90% of all dCOLs were associated with RWB depths of 3 or more. sCOLs are shown to be associated with a variety of RWB depths.

RWB depth is also expressed by the dCOL and sCOL composites in Figure 30. Multiple PV contours on multiple levels are shown to be overturning or already cut-off by the time of the first detected dCOL point. In fact, only the 350K isentropic contours do not overturn situated to the north of the COL. Conversely, the sCOL composite shows very few isentropic PV contours overturning or cut-off surrounding the COL. Interestingly, RWB events in the presence of sCOLs generally occurs on the 350K surface, where dCOLs show no signal of overturning. Figure 29 and Figure 30 show that the intensity or depth of a RWB event could have an impact on the eventual extension of a COL towards the surface, with deeper RWBs on lower isentropic surfaces generally associated with deeper vertical extension.

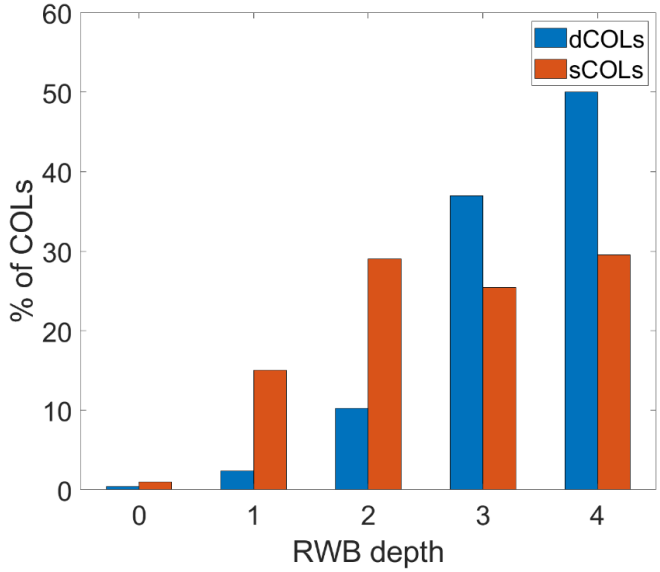

Figure 29: Percentage of dCOLs and sCOLs as a function of RWB depth. RWB depth is defined as the number of isentropic levels (from 315, 320, 330 and 350K) in which an overturned -1.5, -2 or -2.5 PVU contour is found.

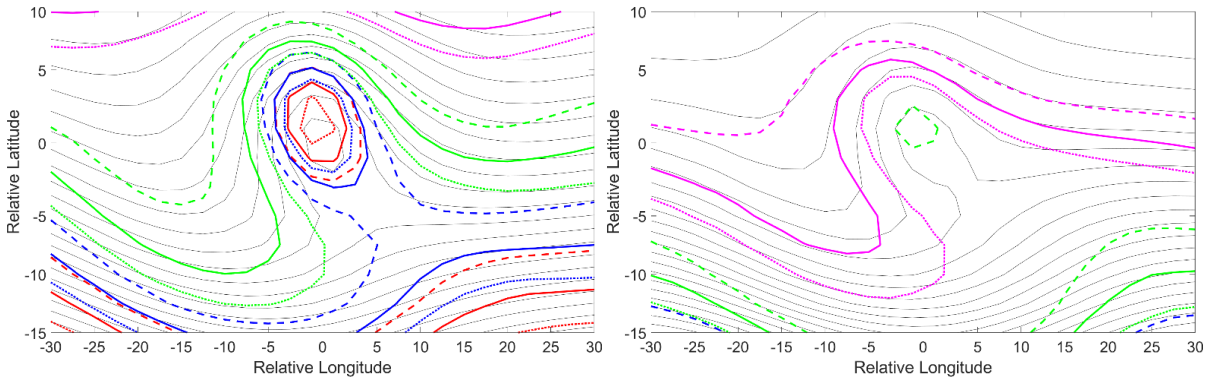

Figure 30: COL and isentropic PV composites for dCOLs (left) and sCOLs (right). The -1.5 (dotted), -2 (solid) and -2.5 (dashed) PVU contours on the 315K (red), 320K (blue), 330K (green) and 350K (magenta) are shown.

3.3.3. Vertical PV profiles in relation to extended COLs

The depth of stratospheric intrusions is compared to the depth of COLs to understand the effect that the depth of an intrusion has on the extension of COLs. First, the stratosphere is mapped and labelled according to the algorithm by Škerlak *et al.* (2014) as mentioned in Section 3.2.6. The lowest level on which stratospheric PV (Label 2, in the algorithm) is then found. The stratospheric intrusion depth related to a COL is determined to be the lowest stratospheric PV value within a 10˚x10˚ grid box of the COL point. The lowest intrusion value is recorded and associated with each COL in the database. The results of the PV depth analysis are shown in Figure 31. Stratospheric intrusion depths are calculated for both dCOLs (Figure 31-A1) and sCOLs (Figure 31-B1). The data shows that dCOLs are generally

associated with stratospheric intrusions of the -1.5 PVU contour to a depth of at least 300hPa. sCOLs on the other hand are generally associated with -1.5 PVU stratospheric intrusions of above 350hPa. This is clear evidence that COLs that are associated with surface lows (dCOLs) are generally associated with stratospheric intrusions that are present closer to the surface. Interestingly, there exists a "middle-world" for the depth of -1.5 PVU stratospheric intrusions between the 300hPa and 350hPa levels in which both sCOLs and dCOLs are both prevalent. Since 300-350hPa depth intrusions are shown to be frequently associated with both sCOLs and dCOLs, it could indicate that there are other processes or mechanisms in the atmosphere which either drive surface cyclonic development or inhibit it beneath these specific COLs.

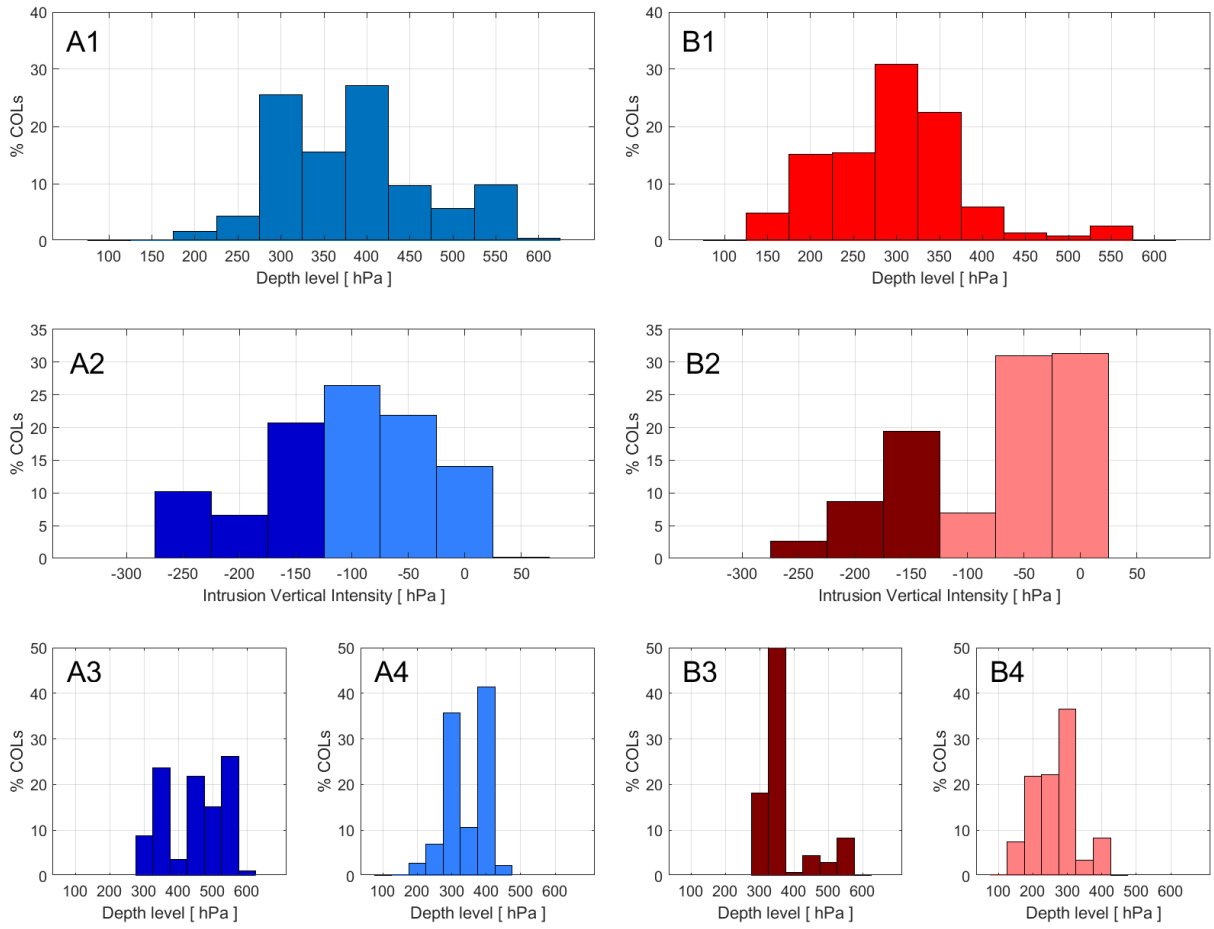

Figure 31: A1: Percentage of stratospheric intrusion depths for all dCOLs. B1: Same as for A1 but for sCOLs. A2: Percentage of stratospheric intrusion vertical intensities (vertical size of the stratospheric intrusion below the climatological tropopause) for all dCOLs. For ease of reference, large vertical intensities are highlighted in dark colours whilst small vertical intensities are highlighted in lighter colours. B2: Same as for B1 but for sCOLs. A3: Percentage of stratospheric intrusion depths for dCOLs with large stratospheric intrusion vertical intensity (less than or equal to -150hPa). B3: Same as for A3 but for sCOLs. A4: Percentage of stratospheric intrusion depths for dCOLs with small stratospheric intrusion vertical intensity (greater than or equal to -100hPa). B4: Same as for A4 but for sCOLs.

As mentioned in Section 3.3.1, dCOLs are generally found in the higher latitudes whilst sCOLs are more often found closer to the tropics. The tropopause is climatologically higher in the tropics and sub-

tropics compared to the extratropics. Naturally this begs the question as to whether the vertical size or intensity of the stratospheric intrusion effects the extension of a COL to the surface or if this is related to the actual depth (or proximity to the surface) that the intrusion reaches. To investigate this, we derive a stratospheric intrusion vertical intensity value for each of the stratospheric intrusions associated with each COL. For the purposes of this study, the stratospheric intrusion vertical intensity is defined as the stratospheric intrusion depth subtracted from the climatological mean dynamical tropopause level. The climatological dynamical tropopause height is calculated based on the average value of PV. The climatological mean PV field is compared to each COL's stratospheric intrusion depth to find the depth of the intrusion relative to the dynamical tropopause. Figure 31 shows the results of the stratospheric intrusion vertical intensity analysis for dCOLs (Figure 31-A2) and sCOLs (Figure 31-B2). In this study, a large vertical intensity is regarded as a stratospheric intrusion is 150hPa below the climatological dynamical tropopause or lower (highlighted in Figure 31 by darker colours) whilst small vertical intensities are considered to be smaller than 150hPa (highlighted in Figure 31 by lighter colours). Figure 31-A2 and B2 show that sCOLs are generally associated with intrusions with a smaller vertical extent than dCOLs. Interestingly however, dCOLs can however be associated with intrusions with smaller vertical extent whilst conversely sCOLs can be associated with intrusions with large vertical extent or intensity.

To investigate the vertical intensity of intrusions with respect to the depth they reach, we separate dCOLs and sCOLs by their vertical intensity or extent and analyse the depths that the associated stratospheric intrusions reach. The analyses are shown in Figure 31-A3, A4, B3 and B4. Larger vertical intrusions associated with dCOLs (Figure 31-A3) are shown to extend further to lower levels extending to at least the so-called intrusion "middle-world" (300-350hPa). Smaller vertical intrusions associated with dCOLs are also shown to extend largely to the "middle-world" levels (Figure 31-A4). Conversely, large vertical intensity intrusions that result in sCOL development generally largely do not extend to lower levels, only extending to the 300-350hPa (or middle-world) levels (Figure 31-B3). This indicates that sCOLs can be associated with vertically larger intrusions of stratospheric air. However, the fact that these intrusions do not extend towards the mid-troposphere results in the COL not extending all the way to the surface. This indicates that the depth that the intrusion reaches (proximity to the surface) is likely more important to COL extension than the vertical intensity or size of the intrusion itself.

These findings also help to explain the latitudinal and seasonal variability of COL extensions. sCOLs are more often found in the lower latitudes. The dynamical tropopause is situated climatologically further away from the surface in the lower latitudes (Kunz *et al.*, 2011). This means that intrusions need to

extend further down from the stratosphere to reach a level in which the system is prone to cyclonic development at the surface (as seen in Figure 31-A3 and A4). The converse is true for the higher latitudes where the lower dynamical tropopause requires only small intrusions to reach a conducive level (as seen in Figure 31-B3 and B4). A similar argument can be made for the seasonal variation of dCOLs and sCOLs. During the summer months the ITCZ moves southwards, raising the dynamical tropopause (Kunz *et al.*, 2011) making it less likely for intrusions to reach a conducive level. This could explain the large amount of sCOL development during the summer months. With the dynamical tropopause lower in the winter months, more dCOLs are prevalent in the winter months compared to sCOLs as shown in Figure 26.

3.3.4. Low level anomalies as extension inhibitors

The results throughout the study show that upper level processes are integral in surface cyclogenesis. These upper level processes are however coupled with low level processes which can also play a role in the development of low-pressure systems. PV theory tells us that upper level PV anomalies also result in mirrored cyclonic motion at the surface (Hoskins *et al.*, 1985). As a result of the north-south surface temperature gradient, the cyclonic motion at the surface will result in warm air temperature advection at the surface ahead of the upper level PV structure. Surface potential temperature (θ) anomalies can act like PV anomalies (Bretherton, 1966). Warm (cold) surface θ anomalies are associated with cyclonic (anticyclonic) flow around them at the surface. Both the low-level θ and upper level PV anomalies feed off one another resulting in either their mutual amplification or decay. For the surface anomaly to be beneficial to the upper level anomaly and development of both cyclones, the system should be baroclinic such that the positive θ anomaly lies to the east relative to the cut-off low and associated upper level PV anomaly. A surface anomaly that is out of phase with the upper level processes could be a factor that results in sCOLs with stratospheric intrusions into the intrusion “middle-world” and deeper intrusions not extending to the surface. To investigate this, we analyse θ anomaly fields at the 1000hPa level around each COL. θ anomalies are calculated using mean θ fields. We first perform a composite analysis of mean surface θ anomalies. Composites are created at the initial detected position of each COL. The evolution of the surface PV anomalies are shown by showing composites for 3 days prior to and 3 days after the initially detected COL point of each COL. The results of this analysis for both dCOLs and sCOLs are shown in Figure 32. The composite of dCOLs clearly shows a warm potential temperature anomaly in phase lying to the east of the COL. This warm anomaly strengthens as the COL develops and weaken once the COL begins to decay after day 1. A stark contrast is seen in the composite surface θ anomaly for sCOLs. An extremely warm anomaly is present to the west and out of phase with the sCOL and upper level PV anomaly. Figure 32 shows that the warm θ anomaly does not strengthen but does move closer to the COL when it

develops, through maturity and decay. The warm anomaly to the west of the COL means that cyclogenesis is out of phase with the upper level processes. As a result, the intense warm θ anomaly to the west of the COL could be an inhibitor to surface cyclonic development.

It is however notable that the entire θ anomaly field for sCOLs is anomalously warm. Therefore, even though there is a large warm θ anomaly out of phase with the COL, the general warm anomaly to the east of the COL axis needs further investigation. An analysis of surface 1000hPa gph fields reveal that the surface field underneath the sCOL is under the influence of a zone of high pressure, advecting warmer tropical air to the west of the COL axis. This explains the large warm θ anomaly as shown in Figure 32 (right panels). An analysis of all the central pressures of all sCOL-associated surface high-pressure cells reveals that the center of the high-pressure cell can however often be located to the east of the COL axis. A composite of all of the eastward-located shows that this surface high extends westwards beneath the COL axis. The anticyclonic flow results in flow from the warmer tropics on both sides of the COL axis and a more intense warm anomaly to the east of the COL axis. As this situation happens frequently, this explains the small warm θ anomaly signals shown to the east of the COL axis in Figure 32. Although these anomalies could induce cyclogenetic forcing in phase with the COL, the strong high-pressure zone persists long enough such that the COL does not extend to a low-pressure zone at the surface.

Another notable difference in the composite of Figure 32 is the cold anomaly θ lying to the west of the dCOL. Conversely, no cold θ anomaly is seen below that of the sCOL. As with the warm θ anomaly of the dCOLs, the cold anomaly strengthens as the COL develops and weaken once the COL begins to decay after day 1. Cold low-level anomalies, associated with anticyclonic flow, have also been linked with RWB resulting in ridging highs over the South African region (Ndarana *et al.*, 2018). Conversely to warm θ anomalies, cold surface θ anomalies are responsible for anticyclonic development. The lack of cold θ anomaly present for sCOLs in Figure 32 shows that dCOL extensions and deep intrusions of stratospheric air could also be critical for the development and ridging of surface highs. Ridging surface highs are an important mechanism for South African rainfall and severe weather (Ndarana *et al.*, 2018).

We now show that the majority of the sCOLs contain a θ anomaly that is out of phase with the upper level processes. In a 10˚x 20˚ latitude-longitude θ anomaly grid box around the initially detected position of the COL, the relative longitudinal position of the maximum value of θ (θmax) to the COL are recorded. Negative relative θmax longitudes indicate that the surface θ anomaly lags behind the upper level processes and is out of phase with the COL (as seen in the composite θ field in Figure 32). If a COL point has a negative relative longitude θmax the COL is marked as a “unconducive surface”

COL. We also consider that the θ grid could contain multiple areas of high anomalous θ values. Therefore, a COL is also marked as an unconducive surface COL if θmax has a positive relative longitude but a high anomalous θ value is found with a negative relative longitude. The converse procedure reveals COL points in which the surface is conducive. In this study a high anomalous θ value is a value that is at least 75% of the θmax value of the θ grid.

The analysis is performed using the first detected position and the last detected position of each sCOL. This choice gives insight into the surface characteristics throughout the lifecycle of the COL as well as any shifts in surface characteristics that may occur during the lifecycle of the COL. The analysis shows that only 12.1% of the sCOLs detected have conducive surface characteristics at the first position of the COL. This rises slightly to 17.2% for the last detected position of each sCOL. The procedure is also performed for dCOLs where positive relative θmax longitudes or high θ values with positive relative longitudes are searched for. 66.1% of dCOLs are marked as conducive surface COLs at the first detected COL position. The amount of dCOLs with conducive surface characteristics however rises to 73.9% by the end of the COLs lifecycle. The low percentage of sCOLs with conducive surface PV characteristics and the high percentage of dCOLs with conducive surface PV characteristics show the importance of the surface PV characteristics being in phase with the upper level processes. If they are not in phase, they can be an inhibiter to COLs extending to the surface. A warm θ anomaly in phase (as shown in Figure 32) can also be a contributor to cyclonic surface development.

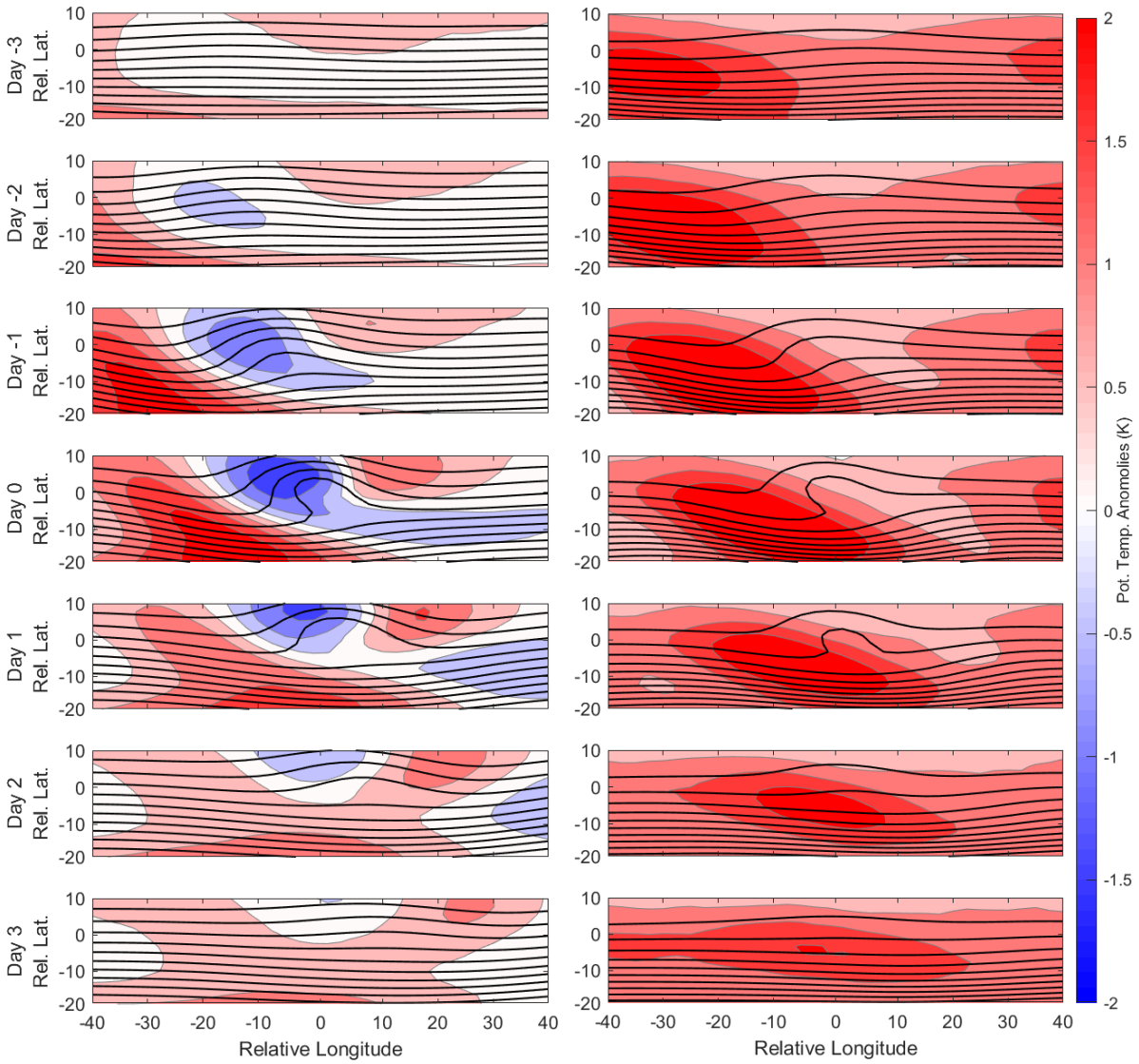

Figure 32: Composite analysis of mean 1000hPa potential temperature anomalies relative to the position of the COLs initial detected position. Composites for dCOLs (left) and sCOLs (right) are shown for 3 days prior and 3 days after the COLs initial detection. Relative latitudes and longitudes are relative to the initial position of the detected COL.

3.3.5. The evolution of COL extensions

Conceptually, we think of COL extensions developing in the upper troposphere and developing and extending towards the surface (Nieto *et al.*, 2005). The temporal aspects of COL vertical extensions are investigated here through composites relative to a COLs initial position. In Section 3.3.1, d1COLs were classified by the relative time a surface low was detected. In this classification d1aCOLs, in which the surface low develops at (within 12 hours) or after the COL are associated with COLs which develop their own surface lows. The temporal evolution of d1aCOLs are therefore studied separately to look at the COLs vertical extension. Composites of latitudinal cross-sections of PV through the initial COL point and composites of geopotential heights at various pressure levels are shown in Figure 33. PV cross-sectional composites of d1aCOLs (top panels of Figure 33) show that the dynamical tropopause

begins to extend towards the surface roughly 2 days before the upper closed low pressure forms. The stratospheric intrusion grows over the next 48 hours to form a tower of increased PV through to the low levels. This is likely a result of the variability of stratospheric intrusion depths that result that can link with low-level diabatic heating PV anomalies.

Geopotential height fields throughout the troposphere reveal that as the PV intrusion extends towards the surface, cyclogenesis starts to occur throughout the troposphere simultaneously. This contradicts our conceptual model of COL extensions whereby the upper level low develops first with subsequent extension and development towards the surface. The composite indicates that a closed surface cyclone develops at the same time as the COL. This suggests that the surface cyclone and each d1aCOL generally develop quasi-simultaneously. An analysis of the time of the first detected surface cyclone compared to the time of the first detected d1aCOL point (as shown in Figure 34) indicates that this is indeed the case. Almost 90% of surface cyclones developed between 12 hours before and 24 hours after the first detected d1aCOL point. Both the COL and the surface cyclone start to degrade after 24-48 hours, with the geopotential composite returning close to the atmospheric state before the COLs development.

The evolution surface pressure system is reminiscent of the θ anomaly evolution as shown in Figure 32. The placement and timing of the surface cyclones development is consistent with the development of the warm θ anomaly. Moreover, the surface high ridging process is clearly seen on the 1000hPa geopotential composites. The anticyclone to the west of the surface cyclone and COL, develops and strengthens throughout the development of the COL and intrusion of the high-PV stratospheric air. This too is consistent with the development of the cold θ anomaly in shown in Figure 32.

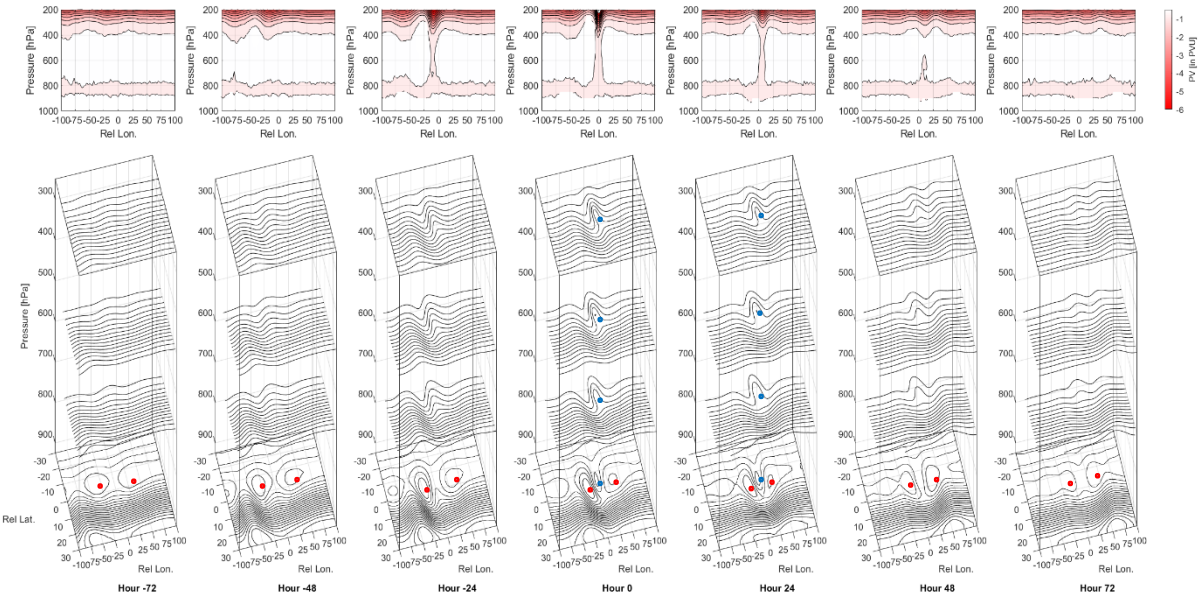

Figure 33: Temporal evolution by means composites of PV (top panel) and geopotential height fields (bottom panel) relative to the initial position of all d1aCOLs with a lifespan of at least 3 days. Composites are provided for between 3 days (72 hours) prior to and 3 days after the initial COL position are provided. PV composites in the top panels are latitudinal cross-sections through the latitude of the first point in each COL trajectory. Geopotential pressure composites at 250hPa, 500hPa, 700hPa and 1000hPa are given in the bottom panels to show the vertical evolution of the pressure systems during d1aCOL development. For ease of reference, relevant high-pressure regions are denoted with red dots whilst low pressure areas are denoted by blue dots.

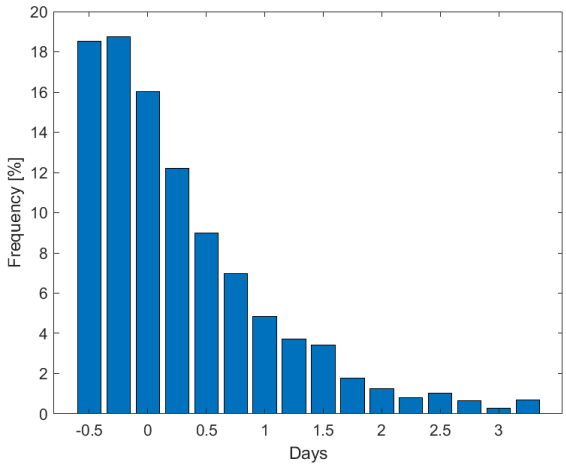

Figure 34: Frequency of time difference (in days) between the first detected surface low pressure and first detected point in each d1aCOL trajectory.

d1bCOLs (dCOLs in which a closed surface cyclone develops more than 12 hours before the COL) are associated with COLs that develop over already existing baroclinic zones or surface lows. The vertical evolution of d1bCOLs is also investigated by means of composite analysis in Figure 35. The cross-sectional PV and stratospheric intrusion evolution are similar to that associated with d1aCOLs (Figure 33). Therefore, the PV mechanisms that drive the d1bCOLs development from the upper troposphere are relatively similar to d1aCOLs. As expected, a surface trough is present beneath the COL at the

surface 72 hours before the COLs development. The surface trough develops into a surface cyclone 24 hours before the development of the COL. A notable difference to the d1aCOL evolution, is increased amplitude of the trough throughout the troposphere at 24 and 48 hours before the COL develops. The enhanced development is likely a result of the enhanced cyclonic development at the surface as this is the only factor changed between d1aCOLs and d1bCOLs. This is consistent with the theoretical concepts explored by Hoskins *et al.* (1985) whereby a surface cyclone can be beneficial to the COLs development and *visa versa* if they are in phase with one another. In addition, the surface cyclone at the surface associated with the d1bCOL persists for longer than with the d1aCOL, with a closed low pressure contour still visible on the surface 2 days after the COLs initial development. This is likely a result of the significant deepening that takes place when a COL develops over an existing surface low pressure system as explained in Section 3.3.1.1 and seen in the case study by Barnes *et al.* (2021) in the south Atlantic.

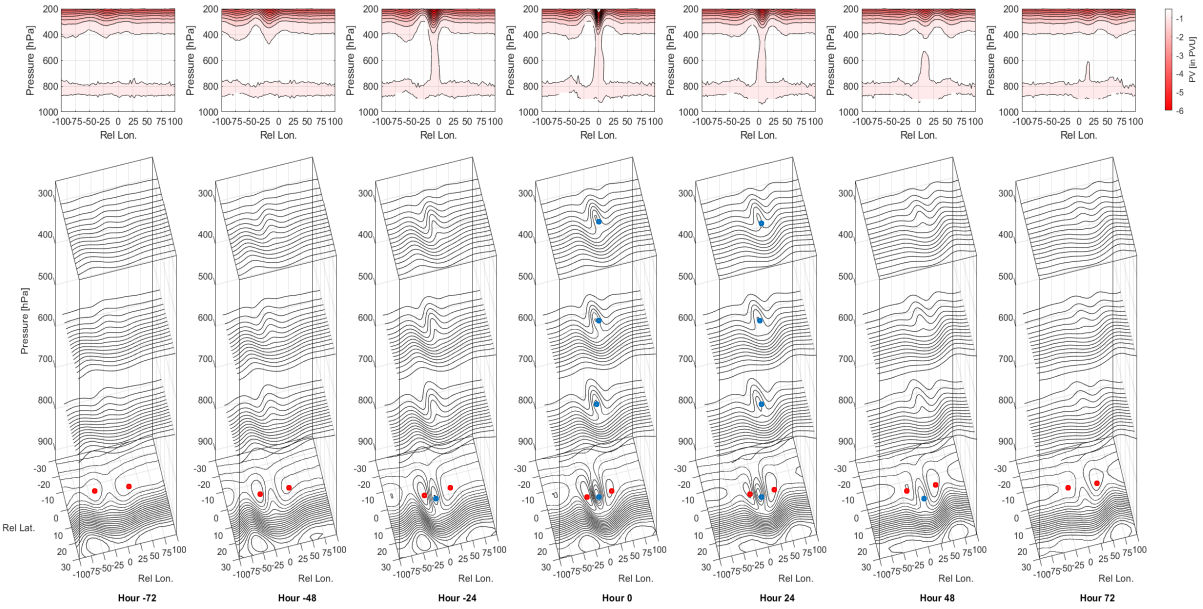

Figure 35: Same as in Figure 33 but for d1bCOLs.

Finally, the vertical evolution associated with sCOLs is analysed. The composites of cross-sectional PV and geopotential heights at various levels, as with d1aCOLs and d1bCOLs, are shown in Figure 36. The cross-sectional PV composites show significant differences to that of the d1COLs. Notably, the dynamical tropopause is situated further from the ground. This is consistent with the associated seasonal and latitudinal variability of sCOLs as previously discussed. Also notably, the PV intrusion is far shallower than that of the d1COLs composites with no enhanced PV in the low to mid-levels and is consistent with the findings shown in Figure 31. The vertical profile of the geopotential height composites also shows large differences to that of the d1COLs in the mid- and low-levels. The 500hPa and 700hPa mean fields start to ridge directly beneath the developing COL. This occurs 48 to 72 hours

before the development of the COL. The mid- to low-level ridge extends to a well-developed high-pressure cell at the surface. As discussed previously, the surface flow feeds back into the circulation above it including the that of COL. Thus, the presence of the well-developed high at the surface could contribute the ridging that is seen in the mid- to low-levels. A surface trough can also be seen to the west of the COL axis. This is coincident with the warm surface θ anomaly zone associated with sCOLs as shown in Figure 32. This trough is out of phase with the COL as previously discussed.

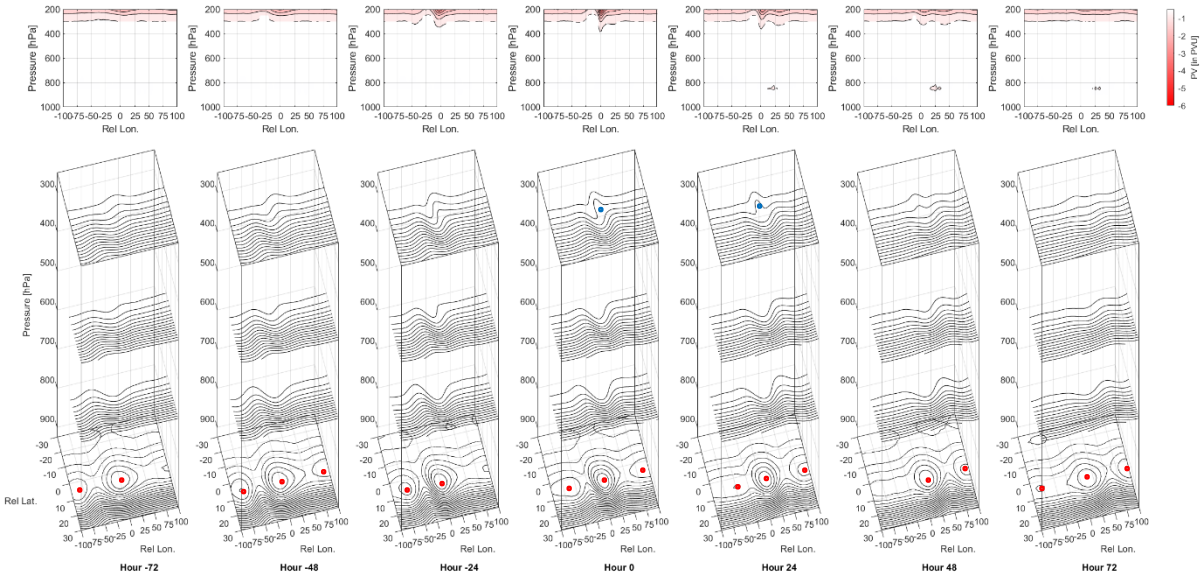

Figure 36: Same as in Figure 33 but for sCOLs.

3.4. Summary and conclusion

In this study, ERA-Interim reanalysis data is analysed to gain an understanding of the processes that result in the extension of COLs to the surface and the development of surface cyclones. To achieve this, a COL climatology is developed. COL climatologies have been extensively done throughout the southern hemisphere at various atmospheric levels for using various methodologies. This study detects COLs at the 250hPa level using an exhaustive detection algorithm taking into account local geopotential minima, closed cyclonic circulation as well as a cold core condition. The resulting COL climatology is on par with other similar climatologies throughout the southern hemisphere using ERA reanalysis datasets. In this study we extend this climatology by calculating the vertical depth of the associated COLs and their relationship to a surface cyclone. The vertical depth analysis reveals that in the southern hemisphere, COLs are generally deep, with nearly 60% of all southern hemisphere COLs extending to the surface (1000hPa). The majority of the remainder of COLs are relatively shallow (up to 500hPa).

The COL vertical extension climatology naturally leads to the classification of COLs in terms of their vertical depth and relationship to a surface cyclone. Deep COLs (dCOLs), COLs which extend vertically to the 1000hPa level, are classified into dCOLs with defined cyclonic circulation (d1COLs) and those without (d2COLs). The majority (~90%) of these dCOLs are associated with defined cyclonic circulations. We further classify d1COLs by the timing of the detection of the closed surface low. d1aCOLs are defined as d1COLs whose surface cyclones are first detected from 12 hours before the development of the COL. The remainder are classified as d1bCOLs. 53.1% of COLs are classified as d1aCOLs in the southern hemisphere. This reveals that COLs do not necessarily always develop closed circulations through their own dynamic development mechanisms. COLs can frequently develop in regions where closed low pressures already exist. Pre-existing surface cyclones provide a baroclinic environment and allows the COL to readily extend to the surface. Although d1bCOLs do not develop their own closed surface circulations, the upper level dynamics still influence the surface cyclones. In fact, over three quarters of the classified d1bCOLs resulted in some form of deepening of associated 1000hPa geopotential minima during the lifecycle of the COL. As a result of this deepening, surface cyclones associated with d1bCOLs generally have a closed circulation for a longer period of time from the COLs initial development than d1aCOLs.

COL extension is also found to be spatially, seasonally, and temporally variable. dCOLs have a high frequency of occurrence in the Australia-New Zealand sector of the southern hemisphere. The southern African sector conversely has a relatively low frequency of dCOLs and the largest frequency of sCOLs. Almost half of the sCOLs identified developed in the summer months, with the peak in frequency in COLs and dCOLs arriving during the autumn months. During the warmer summer months, the meteorological equator shifts southwards resulting in the dynamical tropopause being situated at a higher level in the troposphere. This means that even deep -1.5 PVU stratospheric intrusions do not extend to the mid-troposphere to stimulate surface cyclogenesis. Similar reasoning also explains the vast amount of sCOLs found in or near the subtropics. The southern African region shows the lowest frequency of sCOLs in summer but has the highest frequency of sCOLs. COL depth also seems to play a role in the lifespan of COLs. COLs generally survive for up to 4 days. dCOLs however show a tendency to live longer than sCOLs throughout the southern hemisphere. The lifetime of dCOLs are likely assisted by the surface cyclone which, in phase with the upper level low, can enhance the COL's development.

The mechanisms, from a PV perspective, resulting in the vertical extension of COLs are also explored in this study. COLs are known to be associated with stratospheric intrusions of high-PV air into the troposphere. The mechanism for bringing this stratospheric air into the troposphere through the

development of COLs has been linked to RWB (Ndarana and Waugh, 2010). This link is re-established using ERA-Interim reanalysis showing that most COLs are associated with RWB breaking along the dynamical tropopause. A preliminary analysis undertaken in this study of RWB depth associated with differing COL vertical extension is also performed. It is shown that dCOLs are more likely to be associated with RWB events identified on multiple levels and contours compared to sCOLs. A COL composite analysis reveals that sCOLs are more likely to be associated with RWB on high isentropic levels whilst dCOLs occur on lower isentropic PV contours. This indicates that RWB depth or intensity could be a factor in producing deeper COL vertical depths.

The depth of stratospheric intrusions and their effect on COL depth is analysed by compiling a climatology of stratospheric intrusions throughout the southern hemisphere. This is achieved using a labelling technique defining the stratosphere as a maximum value of PV (-1.5 PVU and -2PVU). The results show that dCOLs are more often associated with deeper stratospheric intrusions compared to sCOLs. There does however exist a "middle world", independent of the PV definition of the stratosphere where both dCOLs and sCOLs can frequently exist. This implies that although upper level PV processes are highly influential, processes in the lower troposphere could influence the depth that a COL reaches. This notion is investigated by means of surface θ anomalies. Positive θ anomalies are known to represent PV-like anomalies at the surface and induce cyclonic circulations. The majority of sCOLs detected are collocated with θ anomalies that lag behind the COL. As the upper and lower processes are out of phase, cyclonic development is hindered throughout the troposphere. The dependence of sCOLs on surface processes reveals the importance of the dynamics of the entire troposphere in the development of these systems. The stratospheric depth analysis also reveals that it is the final depth that is most important in the development of dCOLs rather than the relative depth of the intrusion. Intrusions are required to extend closer to the surface in order to link up with surface processes and further influence surface cyclonic motion.

The proximity of the dynamical tropopause to the surface is likely a major contributor to the development and variability of COL extensions. The dynamical tropopause is situated further from the surface during the summer months and is climatologically higher closer to the tropics. As a result, stratospheric intrusions are required to "reach" further towards the surface in order to produce surface cyclones in summer and in the subtropics. It has been found that even though sCOLs can be associated with vertically larger intrusions of high-PV air, the stratospheric air does not extend very close to the surface as a result of the higher dynamical tropopause height in the summer and sub-tropical latitudes. dCOLs peak in frequency later in autumn (April) than sCOLs (January-February) and the total COLs (March) as the dynamical tropopause is still too high for vertically larger stratospheric

intrusions to have an effect on surface cyclogenesis. Composite PV cross sections also show that sCOLs are generally associated with dynamical tropopauses which are further from the surface than dCOLs.

Importantly, a composite analysis of geopotential heights under d1aCOLs shows that the COLs extension is not a slow, surfaceward extension towards the surface. A trough amplifies throughout the troposphere while the COL develops. The surface cyclone generally becomes closed within a day of when the COL is visible in the upper levels. COL extensions are also associated with ridging at the surface behind the passage of the COL and surface cyclone. This process is also visible in cold surface θ anomalies that lag behind the passage of the dCOL.

3.5. Author contributions and acknowledgements

Michael A. Barnes, under the supervision, review, and guidance of both Dr. Thando Ndarana and Prof. Willem A Landman, conceived of all the ideas in this manuscript. Mr. Barnes performed all the analysis for this work and wrote the manuscript. The authors would also like to thank the three anonymous reviewers whose contributions and suggestions added significantly to this work.

3.6. Appendix A: COL detection algorithm schematics

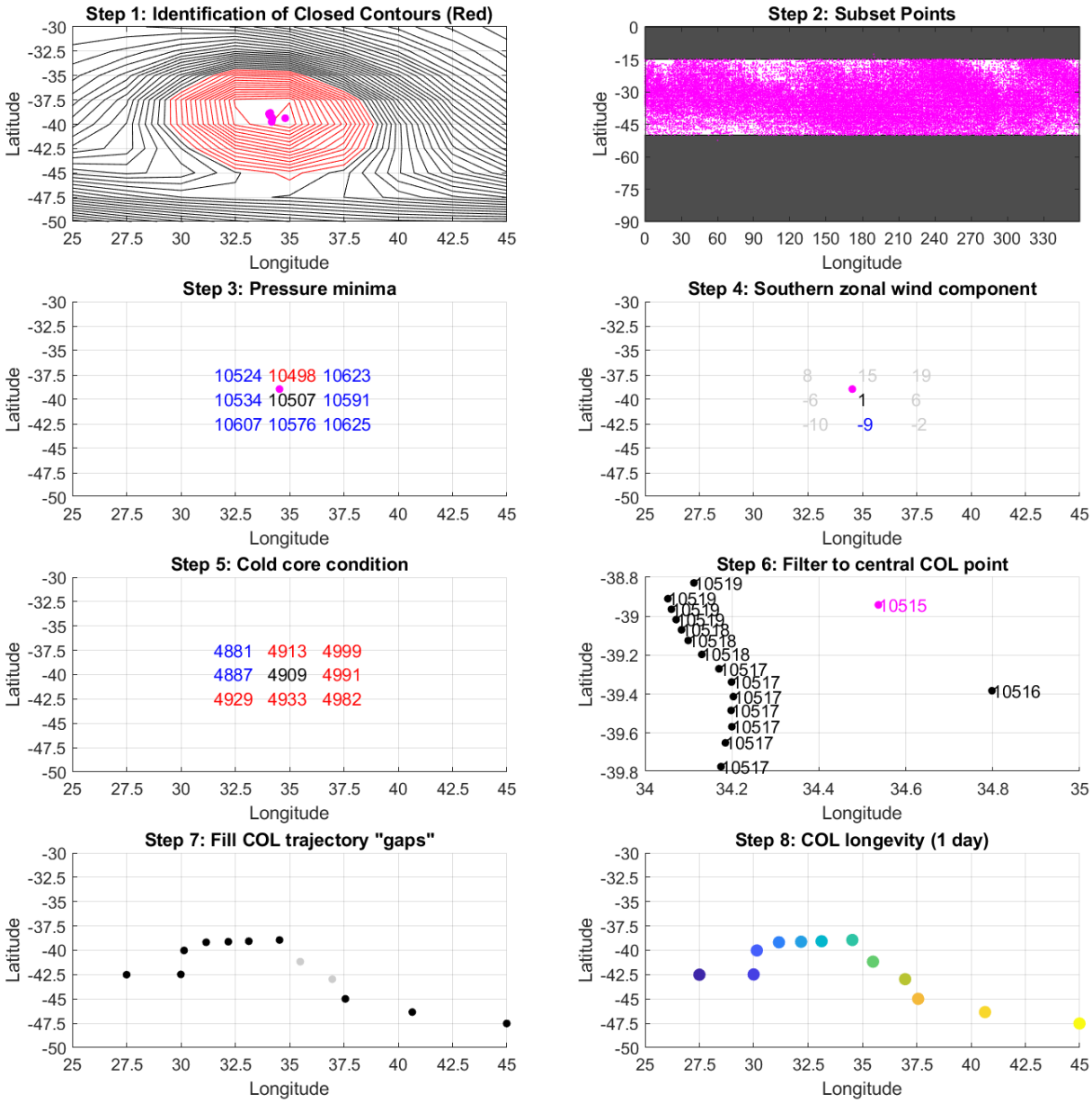

Figure 37: A schematic of the COL detection algorithm as described in Section 3.2.2

3.7. References

Baray JL, Baldy S, Diab RD, Cammas JP. 2003. Dynamical study of a tropical cut-off low over South Africa, and its impact on tropospheric ozone. *Atmospheric Environment*, 37(11): 1475–1488. https://doi.org/10.1016/S1352-2310(02)00999-8.

Barnes EA, Hartmann DL. 2012. Detection of Rossby wave breaking and its response to shifts of the midlatitude jet with climate change. *Journal of Geophysical Research Atmospheres*, 117(9): 1–17. https://doi.org/10.1029/2012JD017469.

Barnes MA, Turner K, Ndarana T, Landman WA. 2021. Cape storm: A dynamical study of a cut-off low and its impact on South Africa. *Atmospheric Research*, 249: 105290. https://doi.org/10.1016/j.atmosres.2020.105290.

Bell GD, Bosart LF. 1993. A Case Study Diagnosis of the Formation of an Upper-Level Cutoff Cyclonic Circulation over the Eastern United States. *Monthly Weather Review*, 121(6): 1635–1655. https://doi.org/10.1175/1520-0493(1993)121<1635:ACSDOT>2.0.CO;2.

Bretherton FP. 1966. Critical layer instability in baroclinic flows. *Quarterly Journal of the Royal Meteorological Society*, 92(393): 325–334. https://doi.org/10.1002/qj.49709239302.

Čampa J, Wernli H. 2012. A PV perspective on the vertical structure of mature midlatitude cyclones in the Northern Hemisphere. *Journal of the Atmospheric Sciences*, 69(2): 725–740. https://doi.org/10.1175/JAS-D-11-050.1.

Dee DP, Uppala SM, Simmons AJ, Berrisford P, Poli P, Kobayashi S, Andrae U, Balmaseda MA, Balsamo G, Bauer P, Bechtold P, Beljaars ACM, van de Berg L, Bidlot J, Bormann N, Delsol C, Dragani R, Fuentes M, Geer AJ, Haimberger L, Healy SB, Hersbach H, Hólm E V., Isaksen L, Kållberg P, Köhler M, Matricardi M, Mcnally AP, Monge-Sanz BM, Morcrette JJ, Park BK, Peubey C, de Rosnay P, Tavolato C, Thépaut JN, Vitart F. 2011. The ERA-Interim reanalysis: Configuration and performance of the data assimilation system. *Quarterly Journal of the Royal Meteorological Society*, 137(656): 553–597. https://doi.org/10.1002/qj.828.

Engelbrecht CJ, Landman WA, Engelbrecht FA, Malherbe J. 2015. A synoptic decomposition of rainfall over the Cape south coast of South Africa. *Climate Dynamics*, 44(9–10): 2589–2607. https://doi.org/10.1007/s00382-014-2230-5.

Esler JG, Haynes PH. 1999. Baroclinic Wave Breaking and the Internal Variability of the Tropospheric Circulation. *Journal of the Atmospheric Sciences*, 56(23): 4014–4031. https://doi.org/10.1175/1520-0469(1999)056<4014:BWBATI>2.0.CO;2.

Favre A, Hewitson B, Lennard C, Cerezo-Mota R, Tadross M. 2013. Cut-off Lows in the South Africa region and their contribution to precipitation. *Climate Dynamics*, 41(9–10): 2331–2351. https://doi.org/10.1007/s00382-012-1579-6.

Flaounas E, Raveh-Rubin S, Wernli H, Drobinski P, Bastin S. 2015. The dynamical structure of intense Mediterranean cyclones. *Climate Dynamics*, 44(9–10): 2411–2427. https://doi.org/10.1007/s00382-014-2330-2.

Fuenzalida HA, Sánchez R, Garreaud RD. 2005. A climatology of cutoff lows in the Southern Hemisphere. *Journal of Geophysical Research Atmospheres*, 110(18): 1–10. https://doi.org/10.1029/2005JD005934.

Funatsu BM, Gan MA, Caetano E. 2004. A case study of orographic cyclogenesis over South America. *Atmosfera*, 17(2): 91–113.

Holton JR, Hakim GJ. 2013. *An Introduction to Dynamic Meteorology*. *Academic Press*. Elsevier.

Hoskins BJ, McIntyre ME, Robertson AW. 1985. On the use and significance of isentropic potential vorticity maps. *Quarterly Journal of the Royal Meteorological Society*, 111(470): 877–946. https://doi.org/10.1002/qj.49711147002.

Hsieh Y-P. 1949. AN INVESTIGATION OF A SELECTED COLD VORTEX OVER NORTH AMERICA. *Journal of Meteorology*, 6(6): 401–410. https://doi.org/10.1175/1520-0469(1949)006<0401:AIOASC>2.0.CO;2.

Iwabe CMN, Da Rocha RP. 2009. An event of stratospheric air intrusion and its associated secondary surface cyclogenesis over the South Atlantic Ocean. *Journal of Geophysical Research Atmospheres*, 114(9): 1–15. https://doi.org/10.1029/2008JD011119.

Kalnay E, Kanamitsu M, Kistler R, Collins W, Deaven D, Gandin L, Iredell M, Saha S, White G, Woollen J, Zhu Y, Leetmaa A, Reynolds R, Chelliah M, Ebisuzaki W, Higgins W, Janowiak J, Mo KC, Ropelewski C, Wang J, Jenne R, Joseph D. 1996. The NCEP/NCAR 40-Year Reanalysis Project. *Bulletin of the American Meteorological Society*, 77(3): 437–471. https://doi.org/10.1175/1520-0477(1996)077<0437:TNYRP>2.0.CO;2.

Kleinschmidt E. 1950. Über Aufbau und Entstehung von Zyklonen. *Meteorol. Rdsch.*, 3: 1–6.

Kunz A, Konopka P, Müller R, Pan LL. 2011. Dynamical tropopause based on isentropic potential vorticity gradients. *Journal of Geophysical Research*, 116(D1): D01110. https://doi.org/10.1029/2010JD014343.

Lackmann GM. 2011. *Midlatitude synoptic meteorology: Dynamics, analysis and forecasting*. American

Meteorological Society: Boston, MA.

Liberato MLR. 2014. The 19 January 2013 windstorm over the North Atlantic: Large-scale dynamics and impacts on Iberia. *Weather and Climate Extremes*. Elsevier, 5(1): 16–28. https://doi.org/10.1016/j.wace.2014.06.002.

Mcintyre ME, Palmer TN. 1983. Breaking planetary waves in the stratosphere. *Nature*, 305(5935): 593–600. https://doi.org/10.1038/305593a0.

Muñoz C, Schultz D, Vaughan G. 2020. A midlatitude climatology and interannual variability of 200- And 500-hPa cut-off lows. *Journal of Climate*, 33(6): 2201–2222. https://doi.org/10.1175/JCLI-D-19-0497.1.

Ndarana T, Bopape MJ, Waugh D, Dyson L. 2018. The influence of the lower stratosphere on ridging atlantic ocean anticyclones over South Africa. *Journal of Climate*, 31(15): 6175–6187. https://doi.org/10.1175/1520-0469(1996)053,3013: IOBSOT.2.0.CO;2.

Ndarana T, Waugh DW. 2010. The link between cut-off lows and Rossby wave breaking in the Southern Hemisphere. *Quarterly Journal of the Royal Meteorological Society*, 136(649): 869–885. https://doi.org/10.1002/qj.627.

Ndarana T, Waugh DW. 2011. A Climatology of Rossby Wave Breaking on the Southern Hemisphere Tropopause. *Journal of the Atmospheric Sciences*, 68(4): 798–811. https://doi.org/10.1175/2010JAS3460.1.

Nieto R, Gimeno L, de la Torre L, Ribera P, Gallego D, García-Herrera R, García JA, Nuñez M, Redaño A, Lorente J. 2005. Climatological Features of Cutoff Low Systems in the Northern Hemisphere. *Journal of Climate*, 18(16): 3085–3103. https://doi.org/10.1175/JCLI3386.1.

Palmén E. 1949. Origin and Structure of High-Level Cyclones South of the: Maximum Westerlies. *Tellus*, 1(1): 22–31. https://doi.org/10.1111/j.2153-3490.1949.tb01925.x.

Palmen E, Newton C. 1969. *Atmospheric Circulation Systems*. Academic Press: New York.

Pang H, Fu G. 2017. Case study of potential vorticity tower in three explosive cyclones over Eastern Asia. *Journal of the Atmospheric Sciences*, 74(5): 1445–1454. https://doi.org/10.1175/JAS-D-15-0330.1.

Pinheiro HR, Hodges KI, Gan MA. 2019. Sensitivity of identifying cut-off lows in the Southern Hemisphere using multiple criteria: implications for numbers, seasonality and intensity. *Climate Dynamics*. Springer Berlin Heidelberg, (0123456789): 1–15. https://doi.org/10.1007/s00382-019-

04984-x.

Pinheiro HR, Hodges KI, Gan MA, Ferreira NJ. 2017. A new perspective of the climatological features of upper-level cut-off lows in the Southern Hemisphere. *Climate Dynamics*, 48(1–2): 541–559. https://doi.org/10.1007/s00382-016-3093-8.

Porcù F, Carrassi A, Medaglia CM, Prodi F, Mugnai A. 2007. A study on cut-off low vertical structure and precipitation in the Mediterranean region. *Meteorology and Atmospheric Physics*, 96(1–2): 121–140. https://doi.org/10.1007/s00703-006-0224-5.

Rautenbach C, Daniels T, de Vos M, Barnes MA. 2020. A coupled wave, tide and storm surge operational forecasting system for South Africa: validation and physical description. *Natural Hazards*. https://doi.org/10.1007/s11069-020-04042-4.

Reboita MS, Nieto R, Gimeno L, Da Rocha RP, Ambrizzi T, Garreaud R, Krger LF. 2010. Climatological features of cutoff low systems in the Southern Hemisphere. *Journal of Geophysical Research Atmospheres*, 115(17): 1–15. https://doi.org/10.1029/2009JD013251.

Singleton AT, Reason CJC. 2007a. A Numerical Model Study of an Intense Cutoff Low Pressure System over South Africa. *Monthly Weather Review*, 135(3): 1128–1150. https://doi.org/10.1175/mwr3311.1.

Singleton AT, Reason CJC. 2007b. Variability in the characteristics of cut-off low pressure systems over subtropical southern Africa. *International Journal of Climatology*, 27(3): 295–310. https://doi.org/10.1002/joc.1399.

Škerlak B, Sprenger M, Wernli H. 2014. A global climatology of stratosphere-troposphere exchange using the ERA-Interim data set from 1979 to 2011. *Atmospheric Chemistry and Physics*, 14(2): 913–937. https://doi.org/10.5194/acp-14-913-2014.

Sprenger M. 2003. Tropopause folds and cross-tropopause exchange: A global investigation based upon ECMWF analyses for the time period March 2000 to February 2001. *Journal of Geophysical Research*, 108(D12): 8518. https://doi.org/10.1029/2002JD002587.

Sprenger M, Wernli H, Bourqui M. 2007. Stratosphere–Troposphere Exchange and Its Relation to Potential Vorticity Streamers and Cutoffs near the Extratropical Tropopause. *Journal of the Atmospheric Sciences*, 64(5): 1587–1602. https://doi.org/10.1175/JAS3911.1.

Uccellini LW, Keyser D, Brill KF, Wash CH. 1985. The Presidents' Day cyclone of 18-19 Februarry 1979: influence of upstream trough amplification and associated tropopause folding on rapid cyclogenesis. *Monthly Weather Review*, 962–988.

van Delden A, Neggers R. 2003. A case study of tropopause cyclogenesis. *Meteorological Applications*, 10(2): 187–199. https://doi.org/10.1017/S1350482703002081.

Postface

This chapter provides a climatological view of COL extensions. COL extensions are classified by means of depth and with respect to their relation to any surface lows that are associated with them. The variability in latitude, region, time and mobility of COL extensions is also investigated. Although the variability of COLs has been well established in the southern hemisphere, the variability of COL extensions has never before been investigated. It is found that deep COLs (that extend all the way to the surface) are most often found closer to the poles, are more mobile, last longer and occur most frequently in autumn. The findings related to the variability of COLs that extend to the surface versus those that do provides valuable and important information to improve our understanding of COL extensions. The investigation into the variability of COL extensions completes the second objective of this study.

Another novel part of this study is the investigation of the effect that the depth of stratospheric intrusions of high-PV air that are associated with the development of COLs has on the vertical extension of COLs. The climatology reveals that deeper intrusions of stratospheric air are generally associated with COLs that extend to surface cyclones. The results show that although both shallow COLs (COLs that only extend to the mid-levels) and deep COLs can be associated with large intrusions, it is the proximity of these intrusions to the surface that affects whether COLs extend to the surface or not. This result is concert with the fact that shallow COLs are generally found in the low latitudes and in summer when the tropopause is situated further from the earth's surface. When the tropopause is situated further away from the surface, intrusions have to "reach" out further in order to extend close enough to the surface to stimulated surface cyclogenesis.

The analysis pf PV intrusion depth reveals that deep and shallow COLs can often exists together in a tropospheric "middle-world". This implies that there may be mechanisms that may inhibit the development of a surface cyclone in situations where intrusions are relatively deep. Warm potential temperature anomalies at the surface are known drivers of surface cyclonic development. However, the result of this chapter show that these warm potential temperature anomalies are out of phase when no extension to the surface occurs. COL extensions can therefore be prevented in these circumstances.

Prior to this work, COLs are conceptually thought to develop in the upper levels and, at times, slowly extend to surface cyclones. The result here, seem to contradict this theory. This was partially seen in the case study in Chapter 2. In the case study one COL and surface cyclone seem to develop simultaneously. Another COL also developed over a pre-existing surface cyclone. A vertical analysis of geopotential composites of COLs that had no pre-existing surface cyclone reveals that troughs develop

throughout the column beneath the developing COL simultaneously. Surface cyclones generally develop within a day of the COLs initial detection. This novelly contributes to re-configure our understanding how COLs extend to the surface.

The analysis of the mechanisms that inhibit and promote the extension of COLs to the surface completes objective 3 of this study. In addition, objective 4 is partially investigated by means of the COL depth analysis in respect to high-PV intrusion depth. The remainder of this objective will be further discussed in the next chapter.

Chapter 4: Stratospheric intrusion depth and its effect on surface cyclogenesis: An idealized PV inversion experiment

Preface

This chapter consists of one research paper that is currently under review in Weather and Climate Dynamics. The citation is as follows:

Barnes, M.A., Ndarana, T., Sprenger, M. & Landman, W.A. Stratospheric intrusion depth and its effect on surface cyclogenesis: An idealized PV inversion experiment. Weather Clim. Dynam. (2021). *Under Review*. http://dx.doi.org/10.5194/wcd-2021-24

In Chapter 3, a climatology of cut-off low (COL) depth is presented. This analysis includes a climatological analysis on how stratospheric depth is related into COL depth and its effect on producing associated surface low pressure systems. The climatology finds that COL depth is climatologically linked to the depth of associated stratospheric intrusions. Climatologies are an important tool in order to gain an understanding of processes in the atmosphere. However, these studies view processes with interference from other processes. Idealised studies allow us to isolate these processes free from interference. In this chapter we study the effect that stratospheric intrusion depth and other characteristics of PV intrusions have on surface cyclogenesis. PV inversion diagnostics are used in idealised numerical experiments in order to drive anomalies into a basic state flow and show the effect it has on surface cyclogenesis. This chapter aims to confirm some of the findings of Chapter 3 regarding stratospheric intrusion depth as laid out in objective 3 and 4.

The paper was co-authored by my two supervisors, Dr. T. Ndarana and Prof. W.A. Landman who supervised, guided and reviewed the work. Dr M. Sprenger provided the numerical framework on which this study was built and provided significant guidance and review of the work. Although the work was co-authored, I conceptualized the work, performed the experiments, undertook the analysis, wrote and reviewed the manuscript.

Stratospheric intrusion depth and its effect on surface cyclogenesis: An idealized PV inversion experiment

Michael A. Barnes[1,2], Thando Ndarana[2], Michael Sprenger[3] and Willem A. Landman[2]

[1] *Marine Research Unit, South African Weather Service, Cape Town, South Africa*

[2] *Department of Geography, Geoinformatics and Meteorology, University of Pretoria, Pretoria, South Africa*

[3] *Institute for Atmospheric and Climate Science, ETH Zurich, Zurich, Switzerland*

Abstract

Stratospheric intrusions of high potential vorticity (PV) air are well-known drivers of cyclonic development throughout the troposphere. PV anomalies have been well studied with respect to their effect on surface cyclogenesis. A gap however exists in the scientific literature describing the effect that stratospheric intrusion depth has on the amount of surface cyclogenetic forcing at the surface. Numerical experiments using PV inversion diagnostics reveal that stratospheric depth is crucial in the amount of cyclogenesis at the surface. In an idealised setting, shallow intrusions (above 300hPa) resulted in a marginal effect on the surface, whilst growing stratospheric depth resulted in enhanced surface pressure anomalies and surface cyclogenetic forcing. The horizontal extent of the intrusion is shown to be more important in developing deeper surface cyclones than the vertical depth of the stratospheric intrusion. The size of vertical intrusion depths is however an important factor determining the surface relative vorticity, with larger intrusions resulting in stronger cyclonic circulations. Deeper stratospheric intrusions also result in intrusions reaching closer to the surface. The proximity of intrusions to the surface is a crucial factor favouring surface cyclogenetic forcing. This factor is however constrained by the height of the dynamical tropopause above the surface.

4.1. Introduction

Potential vorticity (PV) has been well established as a highly useful and important parameter within dynamical meteorology (Hoskins *et al.*, 1985). The usefulness of a PV framework for both operational and academic meteorological analyses is primarily down to two characteristics of PV. The first is the fact PV is conserved for adiabatic and frictionless flow (Hoskins *et al.*, 1985; Holton and Hakim, 2013). The second of these characteristics is the invertibility of PV (Røsting and Kristjánsson, 2012). PV inversion, under suitable balance and boundary conditions, allows for the calculation of other meteorological parameters such as pressure and wind velocity as a result of a distribution of PV (Davis, 1992; Lackmann, 2011). Kleinschmidt (1950) introduced the initial ideas of PV invertibility for specific cases, attributing circulation patterns in the low-levels to an upper-level PV anomaly and introducing the idea of deducing wind, pressure and temperature fields from PV distributions. These ideas became more refined and generalised through the development of quasi-geostrophic theory (Charney and Stern, 1962) which are still continually being developed and improved on today. PV frameworks and invertibility however only started to be a staple of dynamical meteorological analyses after the landmark paper by Hoskins *et al.* (1985).

PV invertibility has allowed for the study of different meteorological phenomena such as cyclogenesis from a PV perspective (Davis and Emanuel, 1991). A key principle in PV analyses is the definition of the dynamical tropopause. Traditionally, the tropopause separates the stratosphere, which is highly stratified, from the troposphere (Kunz *et al.*, 2011). The strict definition from a dynamical or PV perspective is the based on the gradient of isentropic PV contours (Reed, 1955). However, for simplicity, a PV iso-surface is often used. The exact value of PV often differs, however, -1.5 and -2.0 PVU contours (in the southern hemisphere) are most common (Lackmann, 2011). The identification of the dynamical tropopause is crucial in PV analyses. Tropospheric folds can reveal upper-tropospheric fronts and upper-level PV anomalies (Sprenger, 2003). High-PV anomalies of stratospheric air are often introduced into the troposphere by Rossby wave breaking (RWB) (e.g. Thorncroft *et al.* 1993; Ndarana and Waugh 2011; Barnes *et al.* 2021a). PV inversion shows that these high-PV (negative) anomalies can result in the cyclonic flow around the anomaly and cyclogenesis. Basic theory of high-PV anomalies has been discussed by various authors and basic meteorological texts (Hoskins *et al.*, 1985; Lackmann, 2011; Holton and Hakim, 2013) and has led to the basic conceptual model for cyclonic PV anomalies as shown in Figure 38. The conceptual model clearly shows the vast cyclonic motion around the upper-level PV anomaly. This also extends to the surface beneath the upper-level anomaly.

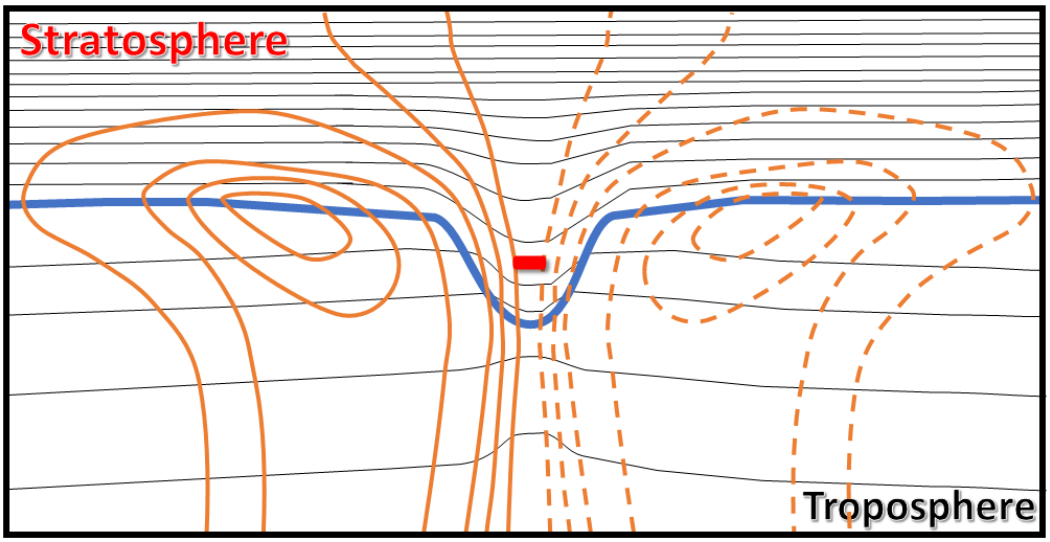

Figure 38: Conceptual model of a cross-section through a high-PV anomaly (negative sign in red) in the southern hemisphere [Adapted from Lackmann (2011)]. Black lines represent isentropes, whilst orange lines represent meridional wind velocities (dotted negative, solid positive). The thin blue line represents the dynamical tropopause (a constant PV contour).

PV inversion is the perfect tool to infer how various PV anomalies affect cyclogenesis throughout the troposphere and stratosphere. PV inversion has been used extensively throughout the scientific literature for this purpose. For example, extratropical cyclogenesis has been studied in the context of how different PV anomalies throughout the troposphere interact to influence cyclogenesis (Huo *et al.*, 1999). Here it was shown through case studies that both the vertical alignment and phase of PV anomalies throughout the troposphere together with interactions between the upper-level anomalies and smaller anomalies within the upper-level mean flow are important to cyclogenesis. PV inversion has also been used to show the effect of upper-level anomalies in a variety of other extratropical (Ahmadi-Givi *et al.*, 2004; Pang and Fu, 2017) and tropical (Moller and Montgomery, 2000; Arakane and Hsu, 2020) settings. Other studies have used PV inversion to diagnose numerical weather prediction (NWP) errors (Brennan and Lackmann, 2005) and the effect on downstream precipitation (Baxter *et al.*, 2011). Few studies have used PV inversion in an idealised setting to study the upper-level and stratospheric intrusion depth's influence on cyclogenesis, especially from a southern hemispheric point of view. A study of stratospheric depths in relation to surface cyclogenesis was performed in relation to cut-off lows by Barnes *et al.* (2021a). This study was done from a climatological point of view in the southern hemisphere. The results show that stratospheric intrusions with a -1.5PVU stratospheric tropopause associated with 250hPa cut-off lows that extend to 300hPa or below, are more likely to result in surface cyclogenesis. This COL extension climatology by Barnes *et al.* (2021a) was based on real-case reanalysis data. This implies that there are other processes such as low-level PV anomalies that influence the amount of cyclogenesis occurring at the surface.

In this study, the effect that the stratospheric intrusion depth has on surface cyclogenetic forcing is studied in an idealised setting. Although the effect that stratospheric intrusions has on surface cyclogenesis is not a new concept (e.g. Hoskins *et al.*, 1985), this study examines the effect that stratospheric depth and intrusion characteristics has on surface cyclogenetic forcing in a highly systematic way. This allows for a correlation between intrusion depths, widths, and intensities with the amount of cyclogenetic forcing at the surface. Additionally, little scientific literature involving stratospheric intrusions depths in idealised settings, has been performed in a southern hemisphere where PV is negative. This study looks at these idealised PV intrusions into the troposphere in a highly systematic way. This study aims to enhance our understanding of the effect PV intrusion depth has on surface cyclogenetic forcing as described in basic theoretical texts (e.g. Hoskins *et al.* 1985). The idealised simulations also confirm and corroborate the findings and hypothesis of the climatology by Barnes *et al.* (2021a) that deeper intrusions are responsible for deeper COLs and surface cyclone development. A collection of numerical experiments using the power of PV inversion is used. Various experiments using variations in the depth and intensity of the simulated intrusion as well as variations in the dynamical tropopause height are performed. This paper is organised as follows. Section 2 introduces the piecewise PV inversion algorithms used for the experiment as well as the various experimental setups for each test. The results of these tests are presented in Section 3. The results are finally discussed holistically and conclusions are drawn in Section 4.

4.2. Methodology

4.2.1. Piecewise PV inversion algorithm

PV invertibility is a mathematical construct. The basic mathematical ideas have been fully described in many textbooks. From Holton and Hakim (2013), quasi-geostrophic PV (q) can be expressed mathematically by:

$$q = \zeta_g + f + f\frac{\partial}{\partial z}\left(\frac{\partial\bar{\theta}^{-1}}{\partial z}\theta\right) \qquad (5)$$

with ζ_g the geostrophic relative vorticity, f the Coriolis parameter ($f < 0$ in the southern hemisphere), θ the potential temperature and $\bar{\theta}$ is the potential temperature of the reference state. The aim of the invertibility principle is to return a variable, say pressure p by integrating (5).

One of the more popular methodologies for solving the equation (5) is the piecewise PV inversion technique. Various variations of this technique are tested and discussed by Davis (1992). It was found that the various techniques to solve the problem in a piecewise approach were found to produce only small differences near the anomalies studied.

In this study, numerical experiments are performed utilising the PV inversion framework of Fehlmann (1997). The set of code provides a diagnostic for reanalysis datasets to diagnose the effect that PV anomalies have on the surrounding meteorological parameters. In this study, however, we use an extension of these algorithms which allows for more idealised experimentation (Fehlmann, 1997; Sprenger, 2007). The set of numerical codes solve the Neumann boundary problem for potential vorticity q and the streamfunction ψ from which the wind components can be derived given by the quasi-geostrophic PV

$$q = \frac{\partial^2 \psi}{\partial x^2} + \frac{\partial^2 \psi}{\partial y^2} + \frac{f^2}{\bar{\rho}} \frac{\partial}{\partial z}\left(\frac{\bar{\rho}}{\bar{N}^2} \cdot \frac{\partial \psi}{\partial z}\right) \tag{6}$$

where $\bar{\rho}$ and $\bar{N}$ denote the density and Brunt-Väsalä for the reference state respectively. The boundary values of potential temperature at the lower and upper boundaries are given by:

$$g \cdot \frac{\theta^*}{\bar{\theta}} = f \cdot \frac{\partial \psi}{\partial z} \tag{7}$$

whilst the lateral boundary condition for the u and v wind components are given by

$$u = \frac{\partial \psi}{\partial y} \; ; v = \frac{\partial \psi}{\partial x} \tag{8}$$

Using various partial differential equations and discretisation techniques as shown in detail by Sprenger (2007) and Fehlmann (1997), the above problem can be solved numerically using a piecewise numerical approach. For details about the numerical aspects of the PV inversion framework, based on successive over-relaxations, see Fehlmann (1997) and Sprenger (2007).

The idealised setup tool of Fehlmann (1997) allows the user to create an idealised basic state. This basic state is based on a user-defined jet stream (height, width, depth and intensity), dynamical tropopause height, static stability (of both the troposphere and stratosphere), latitude and surface baroclinicity. Potential temperature profiles are constructed from the available input by so-called "kink" functions (Fehlmann, 1997). Once defined and setup, a PV anomaly can be defined and introduced into the basic state. The code allows the user to define the intensity of the anomaly, vertical and horizontal dimensions and positions.

4.2.2. Experimental setup

The idealised numerical experimental domain in this study has a zonal dimension of 7500km and a meridional dimension of 5000km with a 25km horizontal resolution. In the vertical, 200 levels are specified with the upper limit at 20000m above ground level (AGL) and the lower limit on the surface. The vertical levels have a resolution of 100m. The PV inversion algorithm allows the user to specify

the surrounding environment for the experiment. In this study, we aim to replicate the conditions of the climatology presented by Barnes *et al.* (2021a), where the dynamical tropopause is considered to be the -1.5 PVU iso-surface. The PV inversion algorithm however considers the tropopause height based on a higher PV contour given a specific height AGL with respect to the static stability parameters. To comply with the convention of the code, the dynamical tropopause is set at a specific height value AGL. The height of the -1.5 PVU iso-surface is calculated from the field after setup. The static stability parameters are then set in such a way that the -1.5 PVU iso-surface can be considered as the clear divide between the stratosphere and the troposphere. This is shown by the meridional PV cross-section of the basic state in Figure 39. In this field, the dynamical tropopause was set to 12500m AGL whilst the resulting -1.5 PVU contour (effective dynamical tropopause) calculated to be at 11285m AGL.

The algorithm also allows for the specification of the jet stream in the upper-levels. The jet was centred around the specified dynamical tropopause with a 4000m stratospheric depth and 6000m tropospheric depth (Figure 40). The westerly jet stream is specified to be zonal with the horizontal centre of the jet in the centre of the domain and a maximum velocity of 35m.s^{-1}. Figure 40 (left) shows the zonal wind speed at the height of the specified dynamical tropopause. The Coriolis force is applied using a constant f-plane approximation. For the entirety of this study, this was deemed to be 42^{o}S. From the above parameters, the algorithm calculates all the basic state meteorological variables. The upper-level pressure field just below the dynamical tropopause and -1.5 PVU contour (at 10000m AGL) that results from the preparation algorithm is shown in Figure 40 (right). No meridional flow exists throughout the basic state domain. Additionally, it is pertinent to point out that the surface field is setup in such a way that no baroclinicity is present. The lack of baroclinicity results in a surface of a constant pressure of 1000hPa and no surface wind flow. The resulting environment from the above and as shown in Figure 39 and Figure 40 is deemed to be the basic state for this study. Except for the specified dynamical tropopause height, this remains unchanged throughout the study.

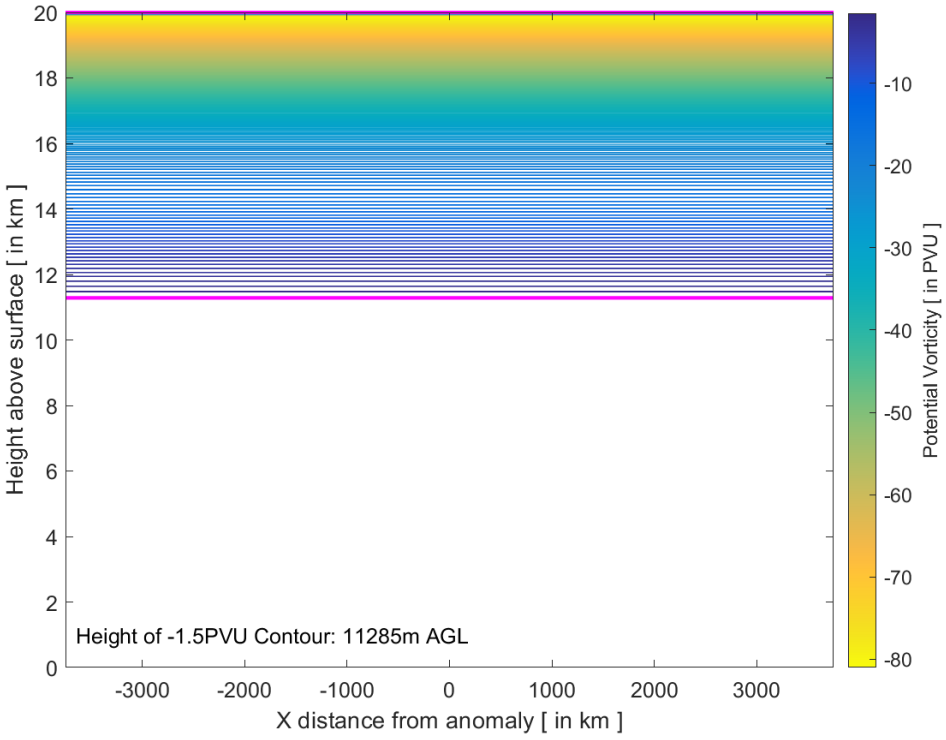

Figure 39: PV zonal cross-section through the centre of the domain. Tropopause was specified at a height of 12500m AGL. The -1.5 PVU contour (highlighted in a thick magenta line) was calculated to be 11285m AGL.

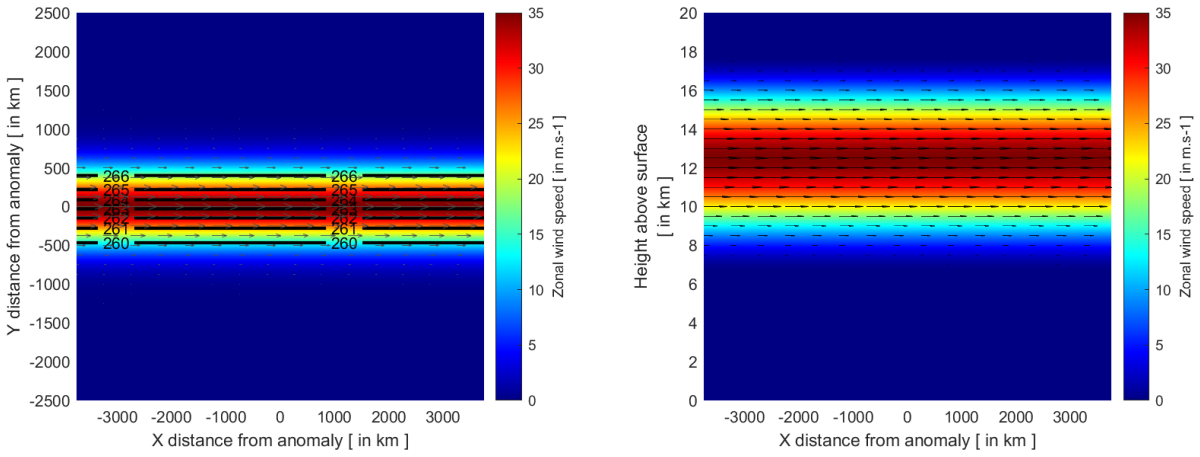

*F*igure 40: The jet stream of the model setup.
Left: The zonal wind speed of the jet stream at the height of given model tropopause (12500m AGL). Pressure contours (in hPa) are overlaid together with zonal wind quivers.
Right: A cross-sectional view of the zonal wind associated with the jet stream through the centre of the domain overlaid with zonal wind quivers.

The study examines how the meteorological fields changed based on a high-PV anomaly which is forced into the domain. The anomaly is a three-dimensional PV anomaly given by:

$$ANO = min\left\{-1.5, -\left(4 \times \left[e^{\frac{-(z-z_{pos})}{z_{size}}}\right] \times \left[e^{\frac{-(y-y_{pos})}{y_{size}}}\right] \times \left[e^{\frac{-(x-x_i)}{x_{size}}}\right]\right)\right\} \qquad (9)$$

where x, y, z are the horizontal and vertical coordinates, $x_{pos}, y_{pos}, z_{pos}$ are the x, y, z coordinates of the centre of the anomaly and $x_{size}, y_{size}, z_{size}$ are the horizontal and vertical radial dimensions of the anomaly. For this study, the anomaly magnitude is set at standard value -1.5 PVU. Equation (9) results in an anomaly with a minimum PV intensity of -1.5 PVU and which increases outward from the central minimum for a distance $x_{size}, y_{size}, z_{size}$. An example of this anomaly is shown in the horizontal and vertical profiles in Figure 41. The anomaly shown in Figure 41 has a $x_{size}, y_{size} = 200km$ resulting in a total maximum width of 400km. The specified $z_{size} = 5000m$ results in a total vertical size of 10000km. This excludes a "halo" of increasing values around the specified anomaly. Applying an anomaly such as shown in Figure 41, results in a lowering of the values in the stratosphere. More importantly, the anomaly results in a tongue of high-PV values emerging below the -1.5 PVU contour.

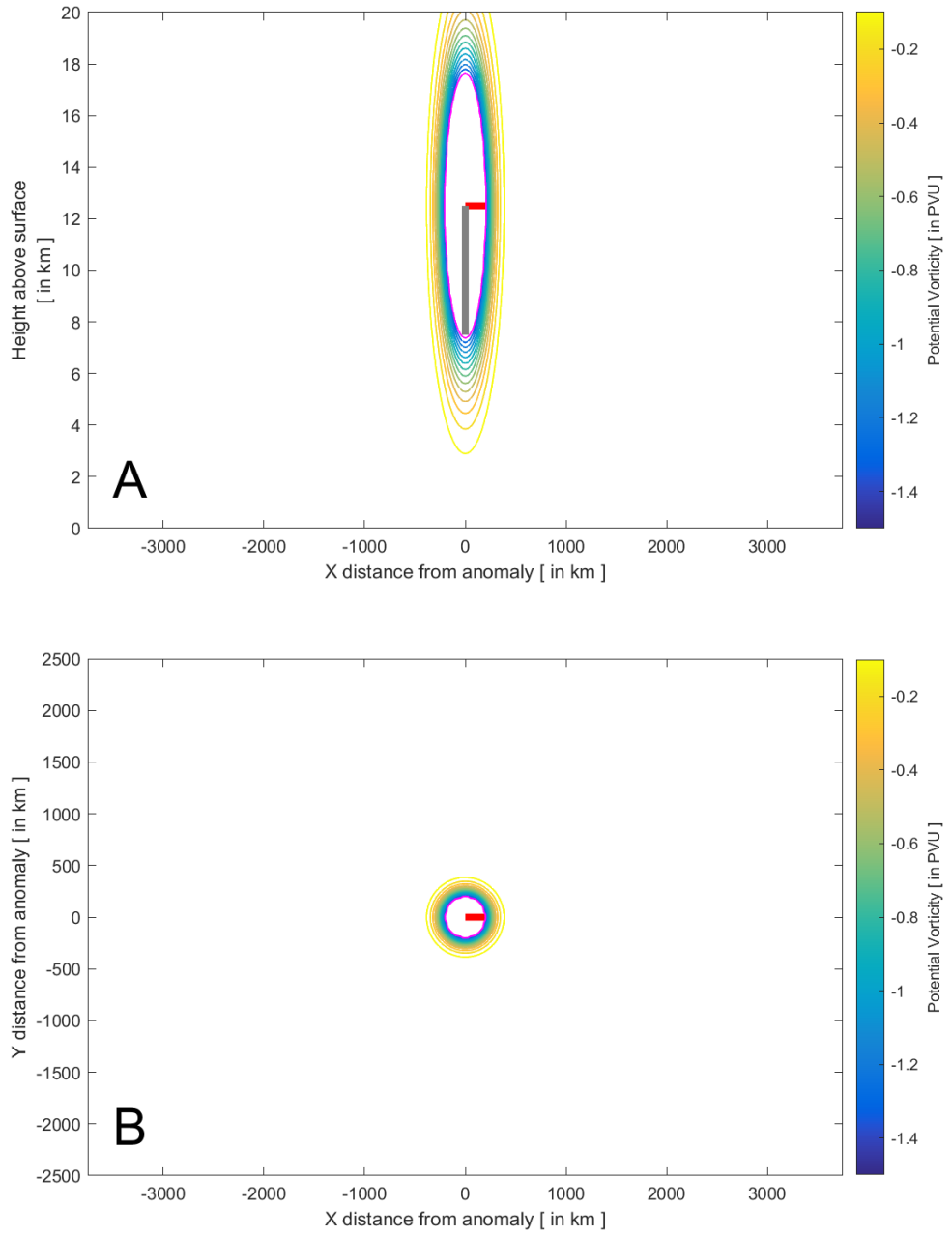

Figure 41: Example of a PV anomaly forced into the idealised domain by means of a longitudinal cross section (A) and a horizontal cross-section (B) through the centre of the anomaly. The anomaly has a maximum horizontal width along the minor axis of 400km and a height of 10000m. This excludes the "halo" of decreasing values to zero around it. The red line is defined as the anomaly radial width (x_{size}, y_{size}), whilst the grey line is defined as the anomaly radial height (z_{size}). The anomaly magnitude (in this case -1.5 PVU) is shown by the magenta contour.

The control experiment (Experiment 0) is used as a reference to gain an understanding of what the algorithm produces and how the PV anomaly affects the meteorological parameters within the domain. Experiment 0 uses the specified values above, namely a dynamical tropopause height of 12500m, an anomaly radial width of 200km and an anomaly radial height of 5000m. The meteorological changes that occur because of the introduction of the anomaly are then analysed, with special focus on surface cyclogenetic forcing as measured by the induced surface relative vorticity and surface pressure changes. This is discussed in the context of basic PV theoretical concepts. Further,

we test the effect of changes to four different parameters with respect to the anomaly and tropopause and their effect on the surface cyclogenetic forcing.

The first (Experiment 1) experiment systemically explores the effect of the depth of stratospheric intrusions on the amount of surface cyclogenetic forcing. The effect that depth of the stratospheric intrusion has on surface cyclogenetic forcing is tested by varying the anomaly radial height. Experiments are performed with anomaly radial height values of lower (2500m) and higher (7500m and 10000m) than the control experiment (Experiment 0, 5000m). Experiment 1 is performed with a constant dynamical tropopause height of 12500m and a constant anomaly radial width of 200km. The varied anomaly radial heights with a constant dynamical tropopause results in tongues of high-PV air extending further towards the surface, as observed in stratospheric intrusions and tropopause fold.

Secondly, the effect that the height of the dynamical tropopause above the surface has on surface cyclogenetic forcing is explored in Experiment 2. The second experiment comprises of three separate model experiments with varying dynamical tropopause heights with constant anomaly radial height of 5000m and a constant anomaly radial width of 200km. Dynamical tropopause heights of 15000m and 10000m are used and the results compared to the control experiment (Experiment 0, 12500m). This experiment gives us an indication of whether the depth of the stratospheric intrusion is more important than the proximity of the intrusion to the surface. This notion was hypothesised in Barnes *et al.* (2021a).

The third set of experiments, Experiment 3, reasserts the notion of stratospheric depth versus proximity to the ground. In Experiment 3, only the anomaly radial width is kept constant at 200km. Both the dynamical tropopause height as well as the anomaly radial height are varied simultaneously such that the eventual height of the intrusion AGL is similar. In this experiment we use dynamical tropopause heights of 15000m and 10000m. Testing anomaly radial heights in 500m intervals, we compare experiments that result in the closest stratospheric intrusion height AGL compared to that of Experiment 0.

Experiment 4 experiments with the magnitude of the intruding anomaly and test how it affects cyclogenetic forcing at the surface. For this experiment, the anomaly description remains the same as in (9). However, all values that are greater than the specified anomaly magnitude are assigned a value equivalent to the anomaly magnitude. A higher (-2 PVU) and lower scenario (-1 PVU) are tested and compared to the control experiment (Experiment 0, -1.5 PVU).

Finally, the effect that the horizontal size of stratospheric intrusions has on surface cyclogenetic forcing is tested by varying the anomaly radial width (Experiment 5). Tests with anomaly radial width

values of 100m, 200m and 400m are performed with a constant dynamical tropopause height of 12500m and a constant anomaly radial height of 5000m. All the above experiments are also provided in the flow chart shown in Figure 42.

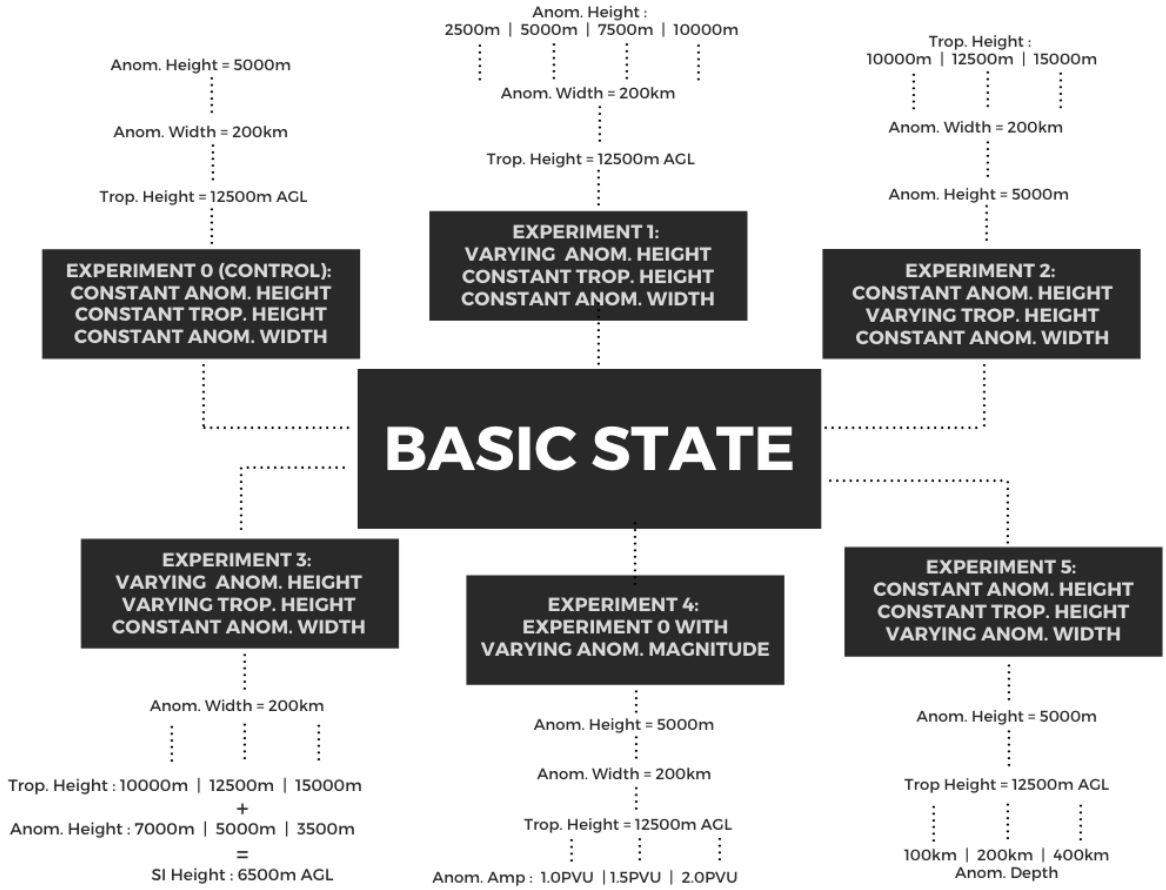

Figure 42: Flow chart of all experiments performed using the PV inversion algorithm. In each experiment, the basic state remains the same with varied dimensions of the PV anomaly, magnitude of the PV anomaly and the height of the dynamical tropopause AGL.

4.2.3. Definition of cyclogenesis to describe cyclogenetic forcing

Cyclone development has long been studied throughout the troposphere. The key to studying these low-pressure systems is the creation of algorithms to track them. Tracking algorithms provide guidance on the parameters that constitute the presence of a surface cyclone. Different tracking algorithms use different parameters for the tracking of different characteristics of surface cyclones (Neu *et al.*, 2013). Surface cyclones have been identified by MSLP minima using various thresholds associated for central depths and pressure gradients (Blender and Schubert, 2000; Nissen *et al.*, 2010). Other algorithms use surface relative vorticity (ζ) as a measure of cyclogenesis (e.g. Flaounas *et al.* 2013, 2014; Hofstätter *et al.* 2016). Relative vorticity thresholds within these studies, although predominantly based in the European region, remain relatively consistent. Relative vorticities in the order of $10^{-5}s^{-1}$ are generally used for this purpose. Flaounas *et al.* (2013) used the requirement of

$10^{-5}s^{-1}$ but with the addition that at least one grid-cell as a part of the event greater than $8 \times 10^{-5}s^{-1}$, which takes into account a threshold found in mature surface cyclones. Others, are more consistent with cyclogenesis requiring a value of around $3 \times 10^{-5}s^{-1}$ (Flaounas *et al.*, 2014; Hofstätter *et al.*, 2016). In this study, we use the threshold of $-3 \times 10^{-5}s^{-1}$ (negative as we are dealing with southern hemispheric values) as the value of cyclogenesis. Cyclogenesis is however a process which implies a temporal aspect. However, this study is performed in a stationary context. Thus the values cyclogenesis definitions are used here as a guide to the extent of cyclogenetic forcing that is supplied by the upper-level PV structure onto the surface. In accordance with the scientific literature (e.g. Flaounas *et al.* 2013, 2014; Hofstätter *et al.* 2016), we stipulate the following definitions:

1. Cyclogenesis: $\zeta \leq -3 \times 10^{-5}s^{-1}$
2. Mature cyclogenesis: $\zeta \leq -8 \times 10^{-5}s^{-1}$
3. Weak cyclogenesis: $\zeta \approx -10^{-5}s^{-1}$, $\zeta > -3 \times 10^{-5}s^{-1}$

Relative vorticity is analysed in conjunction with surface pressure deepening. In this regard, a lowering of the surface pressure and the development of a surface pressure minimum is required. A cyclone can only be said to be developed if the central pressure is enclosed by a closed isohypse at a contour interval of 1hPa. The amount of surface pressure deepening will be analysed and discussed in the context of the type of cyclogenesis (cyclogenetic forcing) identified as defined above. Within the confines of this study, the relative vorticity and surface pressure conditions need to be met for cyclogenesis to have been deemed to have occurred. It should be noted that cyclogenesis in general is a development process and as such has a temporal aspect to it. For the confines of this study, we use these above definitions of when cyclogenesis occurs to describe the type and "strength" of surface cyclogenetic forcing in the static environment of the numerical experiment. If relative vorticity values at the surface fall outside of the definitions above, it is said that cyclogenetic forcing is small or negligible.

4.3. Results

4.3.1. Experiment 0: An idealised stratospheric intrusion and its effect on the domain

A basic, reference experiment is performed to reconstruct the conceptual model of a PV anomaly that extends from the stratosphere. Figure 43 shows a stratospheric intrusion simulated to a depth of 5000m from the dynamical tropopause stipulated at 12500m AGL. The stratospheric intrusion has the standard horizontal radial width of 200km. The -1.5 PVU contour is calculated to be at a height of

11287m AGL (as described in Section 2.2). The stratospheric intrusion extends to a depth of 6594m AGL. Figure 43 also reveals cyclonic motion that is induced around the stratospheric intrusion as is seen in the conceptual model in Figure 38. The cyclonic development is shown in Figure 43 by the positive meridional wind velocities (wind flow "into the page") shown by the solid grey contours to the west of the intrusion and the negative meridional wind velocities (wind flow "out of the page") shown by the dashed grey contours. The upper-level cyclonic development emerges in the upper-level pressure fields as an amplifying trough as shown in Figure 44A. With time, the continued cyclonic development in the upper-levels could result in a closed circulation or COL. This re-emphasises the effect of basic PV theory that shows that cut-off lows are generated from high-PV intrusions of stratospheric air as shown by Hoskins *et al.* (1985). Although strong cyclonic rotation is confined to the area around the intrusion, weak cyclonic rotation is present throughout much of the cross-sectional domain, including the surface. This is shown by the outer-most wind velocity contours in Figure 43.

Figure 44B shows the surface pressure isobars (black contours) together with the surface wind vectors. Before the introduction of the PV anomaly, this field is set at a constant 1000hPa. It is clear that the stratospheric intrusion has resulted in a decrease in the surface pressure and has induced cyclonic rotation around the axis of the stratospheric intrusion, as predicted by theory. A drop of 3hPa in surface pressure is observed as a result of the introduction of the stratospheric intrusion. Moreover, this low-pressure minimum is enclosed by at least one isohypse. Relative vorticities within the centre of the surface circulation are shown by shaded colours in Figure 44B. The lowest relative vorticity observed within the induced surface circulation is $0.9 \times 10^{-5} s^{-1}$, which falls barely outside the thresholds for surface cyclogenesis as defined in Section 2.3. Although by this definition the surface cyclogenetic forcing is very small, this is very close (within $1 \times 10^{-5} s^{-1}$) to the lower limit for weak surface cyclogenetic forcing.

A similar intrusion was observed in the South Atlantic that resulted in a similar decrease in surface pressure and the development of a surface cyclone (Iwabe and Da Rocha, 2009). In that observational study, a similar pressure decrease was seen with the central surface pressure of the surface cyclone decreasing by 4hPa within six hours.

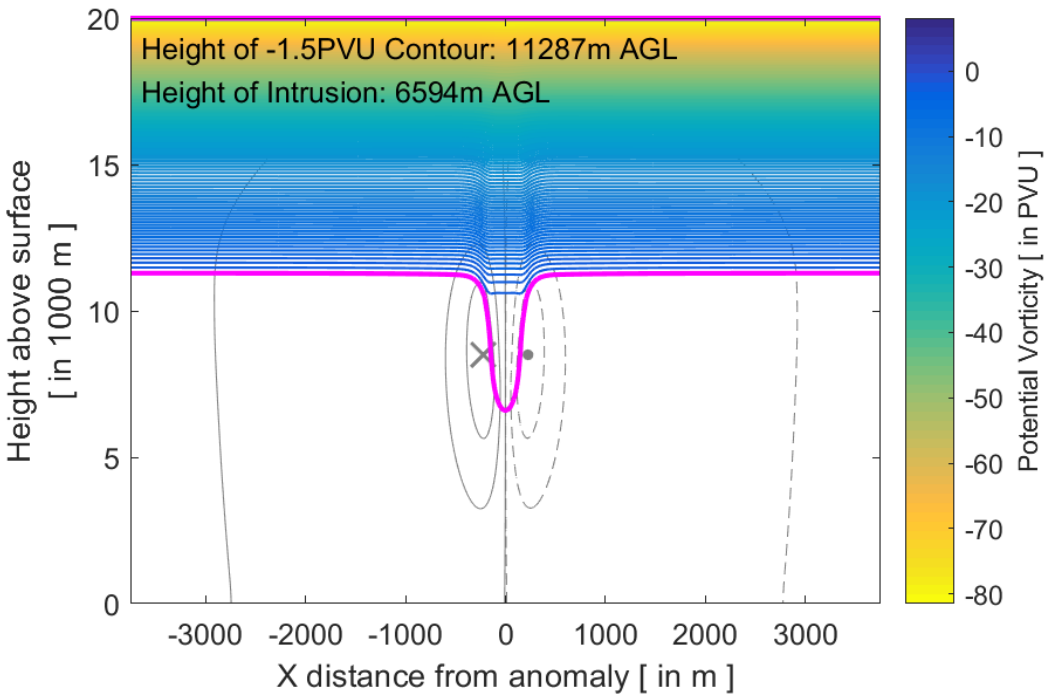

Figure 43: Stratospheric intrusion with a radial width of 200km and depth of 5000m from the dynamical tropopause specified at 12500m AGL. Meridional wind velocities are shown by the grey contours. Solid grey contours and the "X" indicate winds moving into the page, whilst dashed grey contours and the "Dot" indicate winds coming out of the page.

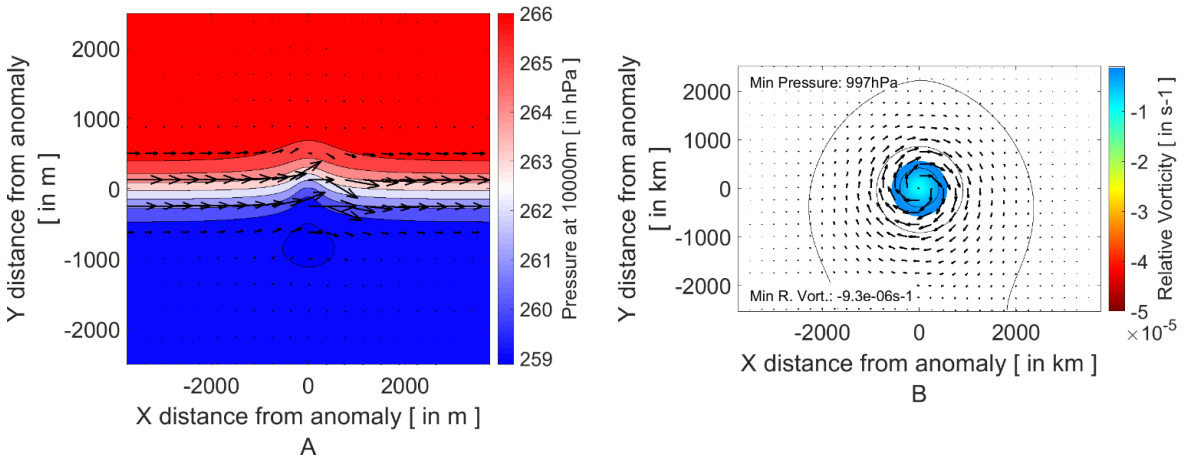

Figure 44: A: Upper-level (10000m AGL, 2500m below the experimentally defined dynamical tropopause) pressure field (shaded) together with wind vectors plotted as black arrows.
B: Surface pressure isobars (black lines) and surface relative vorticity (shaded) together with surface wind vectors plotted as black arrows.

4.3.2. Experiment 1: Varying stratospheric intrusion depth

The effect that the depth of the stratospheric intrusions has on surface cyclogenetic forcing is investigated by systemically varying the anomaly radial depth (as defined in Section 2.2) of Experiment 0. The results of a selection of these varying stratospheric intrusion depth experiments are shown in Figure 45 and a summary of the full set of experiments are shown in Figure 46. Varying stratospheric intrusion depths are all compared to the control experiment as shown in Experiment 4.3.1. For ease

of reference and comparison we show this experiment again in Figure 45-A2 and Figure 45-B2 and is highlighted in green in Figure 46.

Using shallower intrusion depths than in Experiment 0 resulted in limited and weaker cyclonic rotation around the stratospheric intrusion as shown in the shallow intrusion experiment in Figure 45-A1. Maximum meridional wind velocities are in fact almost half of that of Experiment 0 using half the anomaly depth (6m.s^{-1} in Figure 45-A1 and B1 compared to 11m.s^{-1} in Figure 45-A2 and B2). The sphere of influence of the shallower intrusion on the surrounding troposphere is much less than with a standard value of 5000m (Experiment 0, Figure 45-A2 and B2). In comparison, tropospheric intrusions to greater depths resulted in far greater cyclogenetic forcing around the anomaly (as depicted in Figure 45-A3 and Figure 45-A4). Maximum meridional wind velocities of the deeper examples in Figure 45 in fact strengthened to 17m.s^{-1} (Figure 45-A3) and 22m.s^{-1} (Figure 45-A3) using 7500m and 10000m anomaly depths respectively. The enhanced cyclogenetic forcing is also shown in Figure 46 by the increase in the minimum cross-section relative vorticity (dashed lines). This increases almost linearly with a constant increase in PV anomaly depth. The growth in mid-level cyclogenetic forcing is however stunted as it gets closer to the surface. Minimum cross-sectional relative vorticities grow much slower with anomaly depth greater than 8000m. Another important feature seen in these experiments is the location of the maximum mid-tropospheric cyclogenetic forcing. An extended stratospheric intrusion results in the zone of maximum mid-tropospheric cyclogenetic forcing moving closer to the surface.

As expected, shallower intrusions (less than the 5000m used in Experiment 0) result in a much weaker circulation occurring on the surface compared to Experiment 0. MSLP and relative vorticities both increase as the depth of the stratospheric intrusion decreases. Surface pressure decreases below 1hPa according to our definitions of cyclogenetic forcing are deemed to not result in a closed isohypse. Anomaly radial heights of shallower than 3500m did not meet this criterion. An example of the surface pressure anomaly for a shallower intrusion is shown in Figure 45-B2. Notably, no closed isohypse at a contour interval of 1hPa can be seen around the centre of the developing low-pressure minimum. An important factor in our definition of cyclogenetic forcing is the surface relative vorticity. Figure 46 shows that for intrusions shallower than control Experiment 0, our threshold of cyclogenesis of $10^{-5}s^{-1}$ is not met (by a factor of $7x10^{-5}s^{-1}$).

Increasing the depth of the high-PV anomaly also resulted in an increased lowering in the surface pressure and increased rotation at the surface (Figure 46). The centre of the induced surface pressure anomaly decreases exponentially with increasing intrusion depth. The 7500m and 10000m anomaly radial depths (depicted in Figure 45-3 and 4) induce an 8hPa and 12hPa decrease (compared to 3hPa in Experiment 0) in their associated surface pressure respectively. The observational study of Cape

Storm in Barnes *et al.* (2021b) showed a decrease of 6hPa on 7 June 2017 collocated with a stratospheric intrusion to the 550hPa level. The intrusion, similar to that shown in Figure 45-A3, results in a similar surface pressure decrease.

The enhanced cyclonic circulation is also depicted through the increasing relative vorticity present at the surface with increased PV anomaly depth. Intrusions deeper than Experiment 0, result in weak cyclogenetic forcing with intrusions deeper than 6500m meet our cyclogenetic forcing criteria. None of the experiments conducted resulted in instantaneous strong cyclogenetic forcing at the surface. It should be noted that this study does not take any temporal evolution into account as PV inversion is an instantaneous framework. With increased and continual development of the surface cyclone, the surface cyclone may, with time, develop into a mature surface cyclone in which mature cyclogenesis exists at the surface. Additionally, in Experiment 0, an upper-level trough develops coincident with the PV anomaly. With time and continual cyclogenetic forcing in the upper-levels, under the correct conditions, the upper-level trough may develop its own closed, cyclonic circulation (or COL). This echoes the findings of Barnes *et al.* (2021a) who show that, in a climatological sense, deeper intrusions are associated with COLs that extend to the surface. Despite the lack of temporal aspect, within this experimental framework, surface cyclogenetic forcing occurs if the depth surpasses the control experiment depth with an intrusion depth of 5000m (6594m AGL) from the experimental tropopause height of 12500m (11287m -1.5 PVU contour height) AGL.

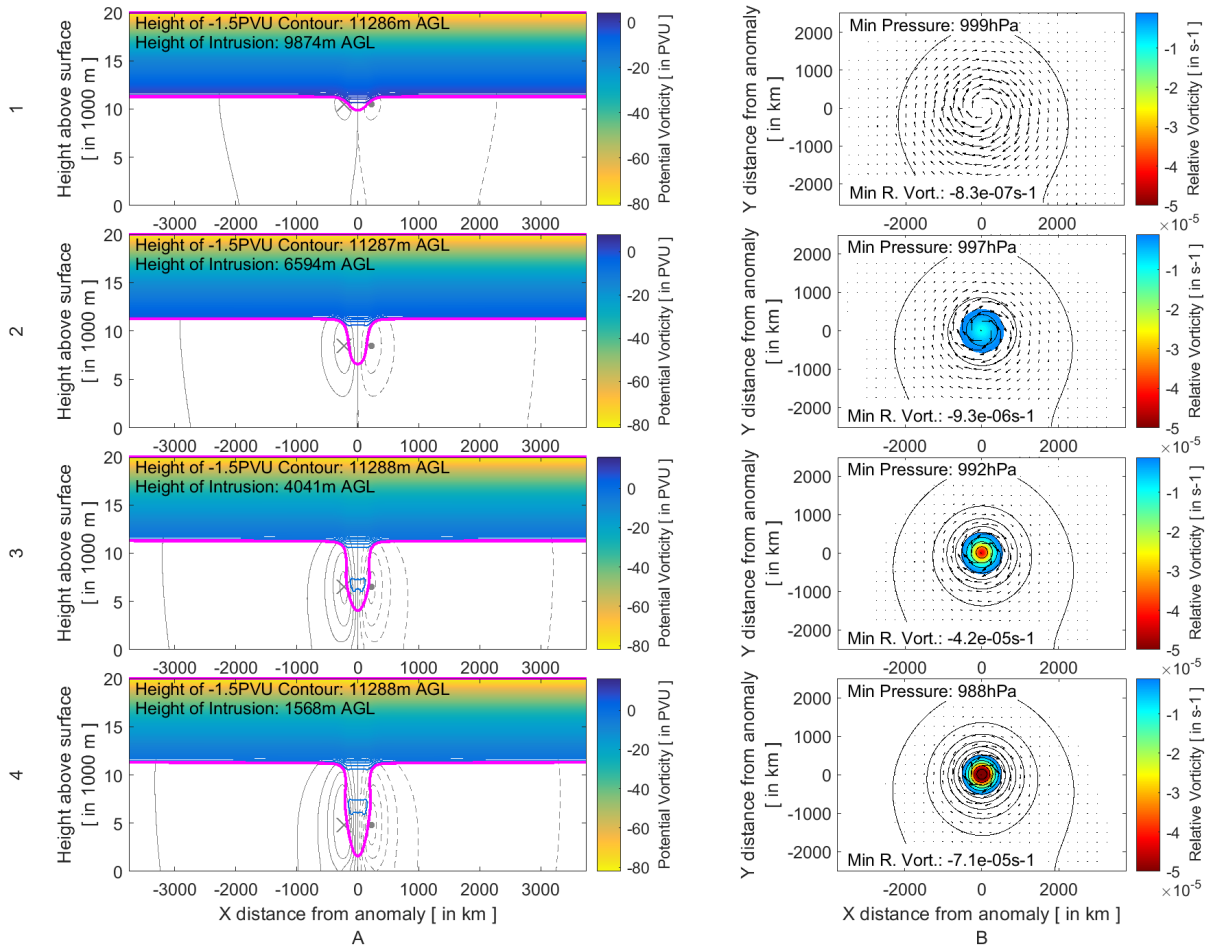

Figure 45: A: Longitudinal PV cross-sections through the centre of the forced anomaly. The -1.5 PVU contour (our definition of the dynamical tropopause for this study) is highlighted in by a thick magenta line. Meridional wind velocities are shown by grey contours. Positive velocities (into the page) are represented by solid contours whilst negative velocities are represented by dashed contours (out of the page).
B: The effect of the intrusion on the surface pressure and relative vorticity are shown in the right panels. Pressure isobars at a 1hPa contour interval are shown by black lines, whilst relative vorticity is shown by the shading.
The panels in rows 1-4 represent different varying stratospheric depths introduced into the domain. For this experiment (Experiment 1), radial anomaly depths given to the system are 2500m (row 1), 5000m (row 2), 7500m (row 3) and 10000m (row 4).

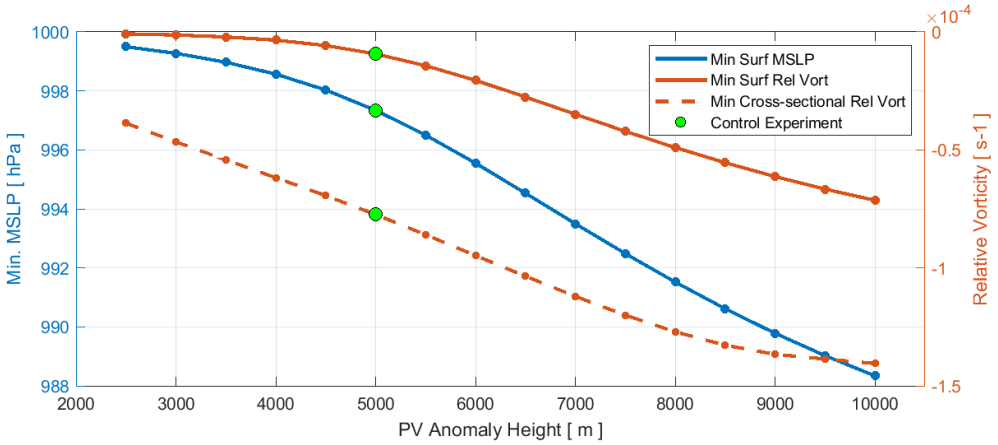

Figure 46: Changes to surface parameters (solid lines) as a function of anomaly height (depth of intrusion). The minimum MSLP (blue) and relative vorticity (orange) on the surface pressure level are recorded and plotted. The cross-sectional minimum relative vorticity as a function of anomaly depth is also shown by the dashed line. The results in Experiment 0 are highlighted in green for convenience.

4.3.3. Experiment 2: Varying tropopause height with constant intrusion depth

The height of the tropopause is variable both spatially and seasonally (Kunz *et al.*, 2011). In the summer months the meteorological equator is situated south of the geographical equator resulting in a raised tropopause, with the converse being true for the winter months. Additionally, the temperature differences between equator and the poles result in the dynamical tropopause being situated closer to the surface in the higher latitudes compared to the lower latitudes (Kunz *et al.*, 2011). Barnes *et al.* (2021a) showed a distinct seasonality and latitudinal discrepancy in the number of COLs that extend to the surface, linking this variability to the height of the tropopause. Lower tropopausal conditions (as found in winter and closer to the poles) tend to produce a greater number of COL extensions in the southern hemisphere than when the tropopause is further from the surface (in the summer months and closer to the equator).

The dependence of tropopausal height on surface cyclogenetic forcing is explored here in a systemic and idealized way by changing the height of the specified tropopause with a constant anomaly radial height of 5000m. The constant anomaly radial height simulates stratospheric intrusions of similar vertical “intensity” in different tropopause height regimes. The standard 12500m tropopause height AGL (as seen in Experiment 0) are depicted by a higher scenario (tropopause height of 15000m) and a lower scenario (tropopause height of 10000m) in Figure 47. A full set of experiments comprising of various higher and lower tropopause scenarios and the resulting amount of cyclogenetic forcing are shown in Figure 48. It should be noted that the tropopause height stipulated and the resulting -1.5 PVU contours (which denotes our definition of the dynamical tropopause) do differ. The actual dynamical tropopause heights (-1.5 PVU contours) for the mid (Experiment 0), high (15000m

tropopause) and low scenarios (10000m tropopause) are situated at 11287m, 13384m and 9172m AGL.

Figure 47A depicts the PV intrusions in the mid, high and low tropopause scenarios. The decreasing height of the dynamical tropopause results in the stratospheric intrusions effectively being in closer proximity to the surface but with no change in the "intensity" of the intrusion. The difference in tropopause height results in different heights of the associated stratospheric intrusion AGL reaching 6594m (Experiment 0), 8776m (higher scenario) and 4332m AGL (lower scenario) respectively. The resulting effects on the surrounding troposphere and surface are shown in Figure 47 and Figure 48.

As with Experiment 1, Figure 47A shows the differences in the induced cyclonic circulation around the PV anomaly in the upper-levels. The increasing dynamical tropopause height, even with a similar vertical PV intrusion intensity or size, has a similar effect on the circulation around the anomaly as seen in Experiment 1. The enhanced mid-tropospheric circulation is readily seen in the decreasing minimum cross-sectional relative vorticities from the highest tropopause to the lowest tropopause scenario (Figure 48). Minimum cross-sectional relative vorticities show a decrease of about $4x10^{-5}s^{-1}$ in the minimum cross-sectional relative vorticity between the high and low tropopause height scenarios. Maximum meridional velocities increase from $9m.s^{-1}$ in the highest tropopause scenario (Figure 47-A1) to $12m.s^{-1}$ in the control (Experiment 0) or intermediate scenario (Figure 47-A2). The lowest tropopause scenario (Figure 47-A3) contains a maximum meridional velocity of $15m.s^{-1}$. The increased rotation from one scenario to the next is not a function of the intensity of the anomaly since the amplitude of the anomaly is kept constant in Experiment 2. With no difference in the PV environment, it follows from (5) that

$$\zeta_g + f = q - f\frac{\partial}{\partial z}\left(\frac{\partial\bar{\theta}}{\partial z}^{-1}\theta\right) \qquad (10)$$

A dynamical tropopause situated closer to the surface is also found on a higher-pressure contour compared to that of the dynamical tropopause situated further away from to the surface. From the high, intermediate and low tropopause scenarios in Figure 47, the dynamical tropopause is situated at around the 110hPa, 175hPa and 260hPa pressure levels respectively. Crucially, the dynamical tropopause coincides with a potential temperature in the range of 330-350K for all three scenarios. These factors result in a more tightly packed potential temperature gradient in the tropopause (high static stability) in the scenario where the dynamical tropopause is closer to the surface compared to the higher tropopause scenario. Therefore, for a PV (q) intrusion of the same intensity, the increased static stability resulting from the lower dynamical tropopause will result in a decrease in the relative vorticity value on the left hand side of (10). Since we are dealing with negative vorticity in and around

the anomaly, the decrease in relative vorticity corresponds to increased rotation around the PV anomaly. The converse argument can of course be made for the scenario in which the tropopause is situated further away from the surface, decreasing static stability and decreasing the cyclonic motion around the anomaly as a result.

Figure 48 shows that the amount of cyclogenetic forcing increases exponentially at the surface with decreased tropopause height. This is seen by both the exponential decrease in pressure and relative vorticity at the surface.

The intermediate scenario (Experiment 0) with an intrusion depth of 6594m resulted in a 3hPa drop in surface pressure. In contrast, with the same vertical intrusion depth, the intrusions from the higher dynamical tropopause (Figure 47-A1 and A2) resulted in a meagre 1hPa decrease in the surface pressure with a closed isohypse. Relative vorticities within the pressure minimum however were small in the order of $-10^{-6}s^{-1}$. The low value of relative vorticity is below the threshold for cyclogenesis as outlined in Section 2.4. Therefore, negligible cyclogenetic forcing resulted beneath the stratospheric intrusion from the high dynamical tropopause. A stark contrast is seen in the scenario from the dynamical tropopause situated closer to the surface (Figure 47-A3 and A3). The lower scenario resulted in a doubling of the pressure decrease at the surface (6hPa) compared to Experiment 0 (3hPa). Additionally, enhanced cyclonic circulation is induced at the surface in the lower scenario. The minimum relative vorticity of $-3x10^{-5}s^{-1}$ within the surface pressure minimum shows that definite cyclogenetic forcing is induced by the PV anomaly situated closer to the surface.

The results of Experiment 2 clearly show that the effective height of the intrusion AGL is a massive factor in the amount of surface cyclogenetic forcing that is induced. With the same intrusion vertical depth, the experiments with lower intrusion height AGL result in more intense lowering of the surface pressure. It should be noted that these tests were also repeated with different vertical depth of intrusions by using different anomaly radial heights of 2500m and 7500m (not shown). The tests show a similar result where intrusions associated with the higher tropopause result in a lesser amount of cyclogenetic forcing than those associated with the lower tropopause.

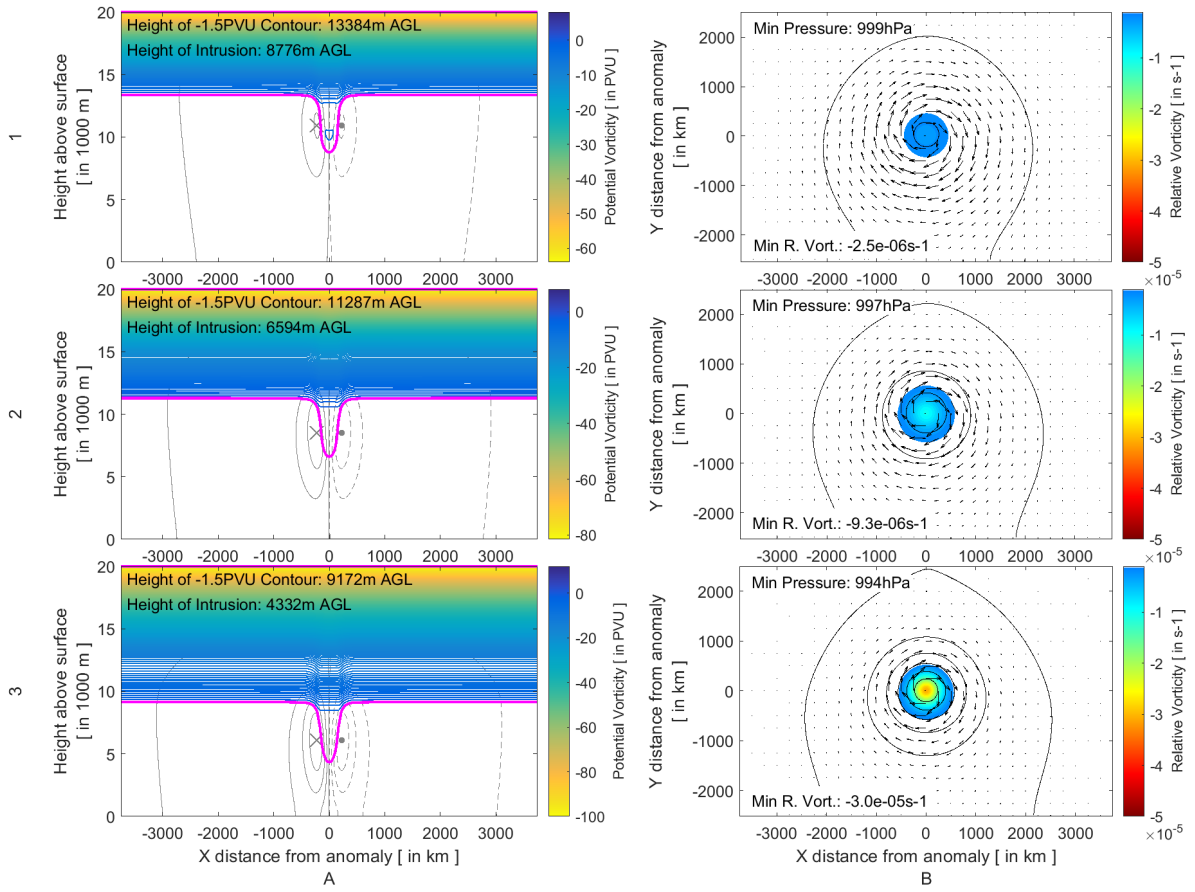

Figure 47: Same as in Figure 45 with the exception that in this case the anomaly radial height is kept constant at 5000m with varying tropopause heights of 15000m (row 1), 12500m (row 2), as in Experiment 0) and 10000m (row 3).

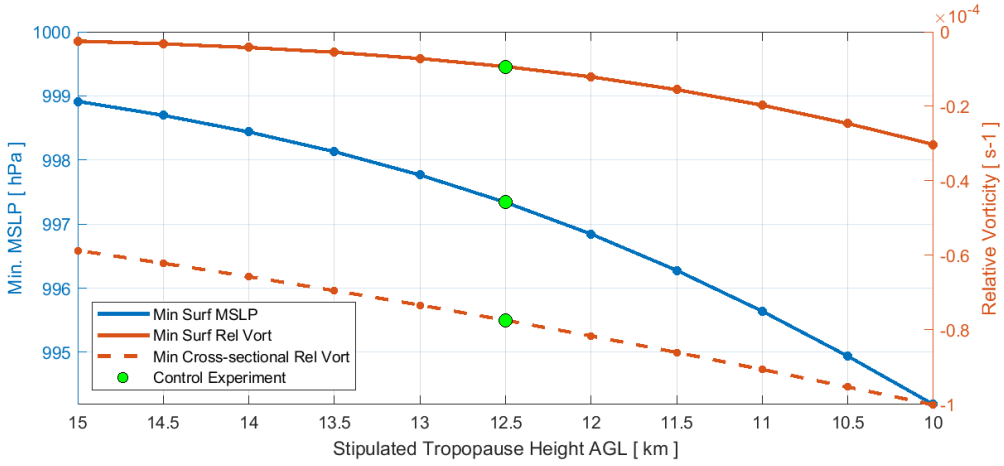

Figure 48: Similar to Figure 46 but for Experiment 2 (varying tropopause height experiments) with tropopause height AGL shown on the x-axis

4.3.4. Experiment 3: Constant intrusion height from varying tropopause height and intrusion depth

The results in Experiments 1 and 2 show that the proximity of stratospheric intrusion to the surface has a larger impact on surface low deepening and surface cyclogenesis than the vertical intensity or

size of the intrusion itself. This was also hypothesized by Barnes *et al.* (2021a) with respect to COL vertical extensions. In order to confirm this concept, anomalies are created such that they extend to a similar height AGL from a varying tropopause height and compared to Experiment 0 (Figure 49-A2 and B2). In this case anomalies with radial heights of 7000m, 5000m and 3500m were introduced into the fields with tropopause heights of 15000m, 12500m and 10000m AGL respectively. The resulting intrusions heights AGL were calculated to be at 6750m, 6594m and 6350m AGL respectively. All three of these intrusions induce cyclonic motion around the anomaly of similar intensity, with maximum meridional wind velocities between 11-12m.s^{-1}. The intrusions also all induce a similar surface level pressure deepening resulting in about a 3hPa surface central pressure drop.

Some small, but noticeable differences can however be seen between the different scenarios in Experiment 3. The larger intrusion emanating from a higher dynamical tropopause (Figure 49-A1), results in a slightly deeper penetration of the high-velocity core around the simulated anomaly compared to lower intensity anomalies in Figure 49-A2 and A3. In Figure 49-A1 the 4m.s^{-1} contour extends to a depth 1000m deeper than in Figure 49-A2 and A3. The effect of this is also noticeable on the surface. Relative vorticities on the surface increase with intrusion vertical intensity from sub-cyclogenesis values in Figure 49-A3 to weak cyclogenesis values in Figure 49-A1. A major difference between these scenarios is the presence of a -2PVU anomaly within the intrusion in Figure 49-A1 that does not appear in Figure 49-A2 or A3. This is an artefact of the basic state setup but could be influencing and enhancing the additional rotation at the surface. The influence of anomaly amplitude will be further investigated in Experiment 4.

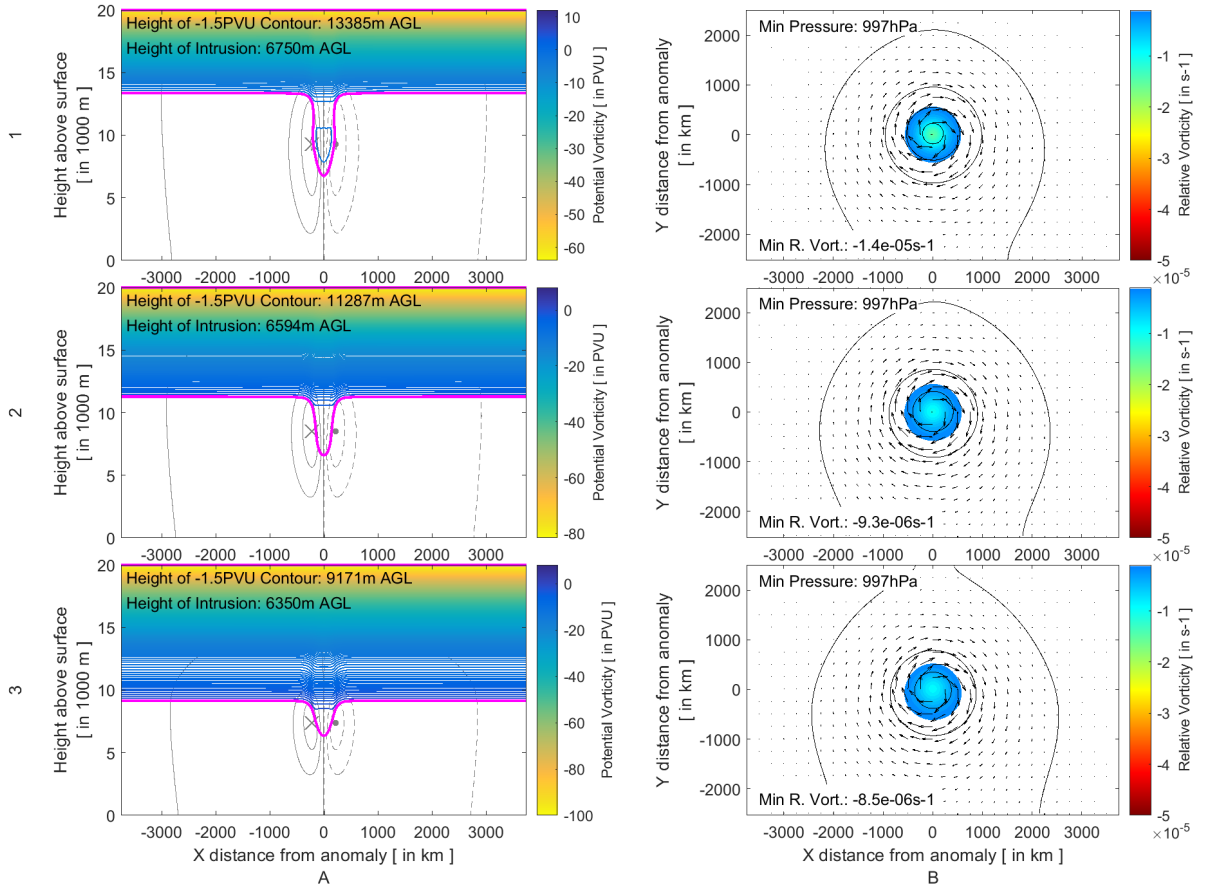

Figure 49: Same as in Figure 45 but with variable anomaly radial heights such that the height of the stratospheric intrusions AGL are similar from varying tropopause heights of 15000m (row 1) and 10000m (row 3). Experiment 0 is given in row 2 for ease of reference.

4.3.5. Experiment 4: Varying anomaly magnitude

Experiment 3 brings forth the question of the magnitude intensity of the stratospheric intrusion with respect to its effect on the cyclonic circulation at all tropospheric levels around the anomaly. Experiment 4 tests this effect by changing the magnitude of the intrusion, i.e. by varying the anomaly amplitude. A lower (-1.0 PVU) and higher (-2.0 PVU) scenario are tested and shown in Figure 50. For ease of reference, the -1.0 PVU contour is also plotted as a dashed magenta line in Figure 50. As our definition of the tropopause continues to be -1.5PVU, the resulting intrusion of the lower scenario is very shallow, but does contain a small anomaly close to the depth of Experiment 0 (Figure 50-A2). Figure 51 shows that the magnitude of the intrusion has some effect on the mid-tropospheric cyclogenetic forcing. Minimum cross-sectional relative vorticity decreases by $3x10^{-5}s^{-1}$ from the low to high anomaly amplitude scenarios, whilst the maximum meridional velocity decreases by $1m.s^{-1}$ around the anomaly. The weaker circulation does result in a slightly lower relative vorticity at the surface (less by only $4x10^{-7}s^{-1}$). Comparable surface pressure lowering still results beneath the anomaly. For the higher magnitude scenario, the opposite is true. A slight strengthening (by similar magnitudes) are seen in both the circulations around the anomaly (increase in maximum meridional

velocity of 1m.s^{-1}) and at the surface (increase in the relative vorticity by 3x10^{-7}s^{-1}). The results of Experiment 4 reaffirm the findings in experiment 3, i.e. that the vertical intensity of the stratospheric intrusion could play a more vital role in affecting surface circulation than the magnitude of the PV intrusion.

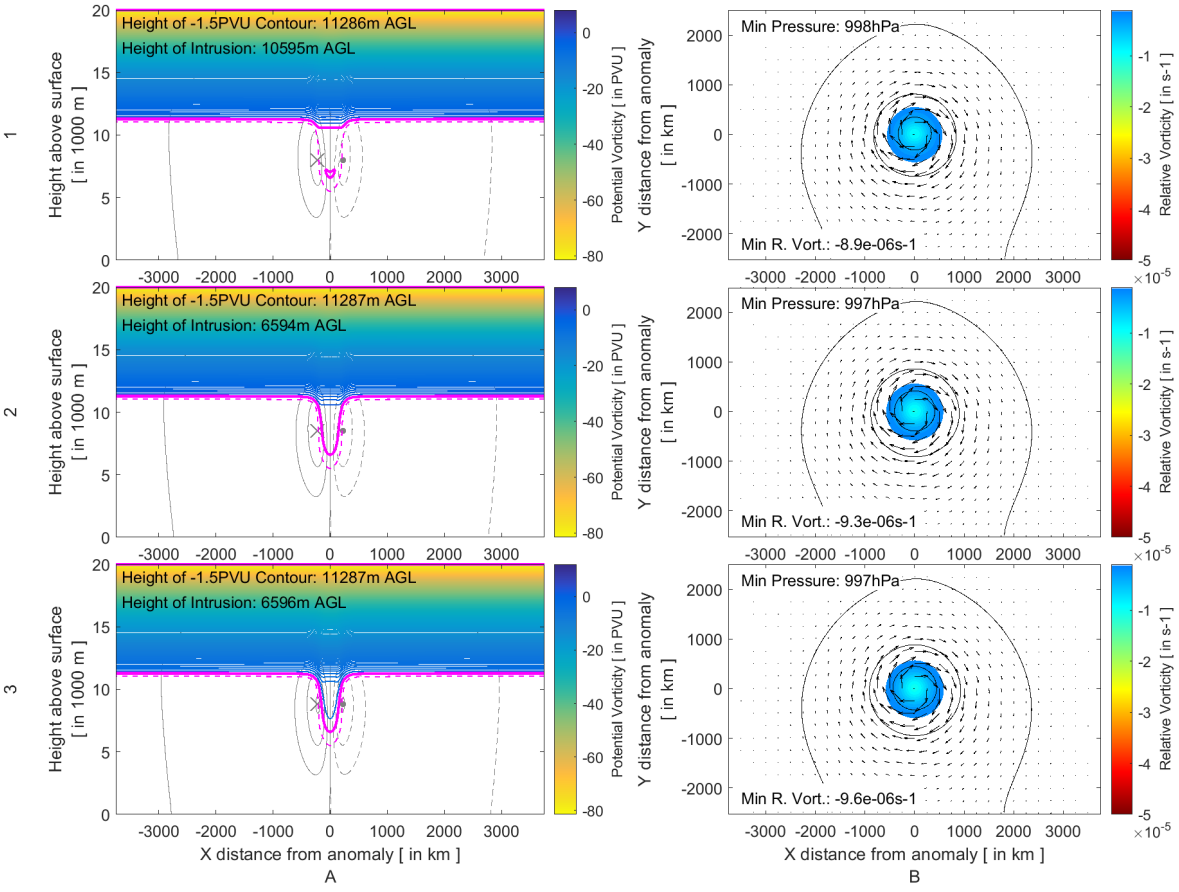

Figure 50: Same as in Experiment 0 with varying anomaly magnitudes of -1.0 PVU (row 1) and -2.0 PVU (row 3). Experiment 0 (with an anomaly magnitude of -1.5 PVU) is shown in row 2. In addition to the -1.5 PVU contour (thick magenta line), the -1.0 PVU contour is also provided for context by a dashed magenta line.

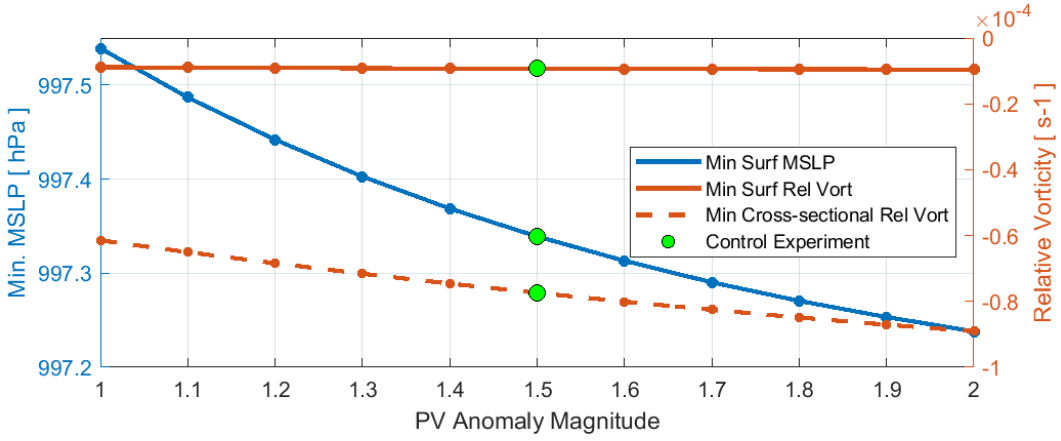

Figure 51: Same as in Figure 46 but for Experiment 4 (varying stratospheric intrusion magnitude experiments)

4.3.6. Experiment 5: Varying anomaly horizontal width

RWB events, which drive stratospheric air into the troposphere, have been classified into 4 distinct categories, namely cyclonic equatorward breaking (LC2), cyclonic poleward breaking (P1), anticyclonic equatorward breaking (LC1) and anticyclonic poleward breaking (P2) (Thorncroft *et al.*, 1993; Peters and Waugh, 1996). These different types of RWB are associated with differing characteristics of the isentropic PV filaments produced and therefore differences in the geometric characteristics of the PV intrusions and the weather patterns they produce. Elongated, thin filaments of stratospheric air are produced by LC1 type breaking events because of the anticyclonic shear on the equator side of the PV structure (Thorncroft *et al.*, 1993). These associated PV filaments eventually roll up and often produce cut-off PV structures. P1 events are also associated with thinner filaments of high-PV air (Peters and Waugh, 1996). Similarly to P2 events respectively, LC2 events are associated with broader high-PV streamers which, under the influence of cyclonic shear, wrapping cyclonically and not resulting in cut-offs (Thorncroft *et al.*, 1993). Recent examples of the different breadth of these streamers can be seen in Barnes *et al.* (2021b) where a thin PV streamer (of ~$1^o \approx 100km$) and broader streamer (of ~$10^o \approx 800km$) affected and deepened a surface cyclone.

The effect that the width of the intrusion has on surface cyclogenesis is tested with a numerical setup similar to that of Figure 41 with varying anomaly radial widths. Selected width experiments are shown in Figure 52 and a summary of the effect of all experiments effect on surface parameters is shown in Figure 53. All stratospheric intrusions were defined such that they reach a similar depth (using a constant 5000m anomaly radial height from the 12500m AGL dynamical tropopause).

Clear differences in the circulation around the anomaly can be seen in Figure 52A and Figure 53. The thinner intrusion (100km width) in Figure 52-A1 results in a much weaker circulation than the standard configuration (Experiment 0, Figure 52-A2) with maximum meridional velocities of 8m.s^{-1} (compared to 11m.s^{-1} in Experiment 0). Conversely, stronger cyclonic circulation is induced around the broader anomaly with a maximum meridional velocity of 15m.s^{-1}. The core of the cyclonic circulation is also augmented by the breadth of the intrusion. The thinner intrusion results in a thinner and shorter jet core around the anomaly, whilst the broader anomaly extends the core both vertically and horizontally, affecting almost the entire cross-sectional domain. The enhanced circulation can also be seen in the minimum cross-sectional relative vorticity associated with different intrusions in Figure 53. The minimum cross-sectional relative vorticity data clearly shows a decrease in the intensity of the mid-level cyclogenetic forcing around the anomaly. The increase in the minimum cross-sectional relative vorticity with increasing width of the anomaly is exponentially increasing from over 1x10^{-4}s^{-2} to 3x10^{-5}s^{-2}.

The width of the intrusion is also important to surface parameters. The thinner intrusion results in a reduction of cyclogenetic forcing with no discernible closed circulation, a much lower central surface pressure (1hPa) and a decrease in the magnitude of relative vorticity (Figure 52-B1). The broader intrusion however enhances cyclogenetic forcing at the surface compared to Experiment 0. Doubling the breadth of the intrusions results in a much deeper surface low pressure (8hPa deeper than Experiment 0). Figure 53 shows that the surface pressure minimum decreases quasi-linearly with increasing PV anomaly width. The differences in the relative vorticity on the surface are however much less significant. Only a slight decrease in the minimum relative vorticity on the surface is discernible between the thin and broad scenarios (Figure 53).

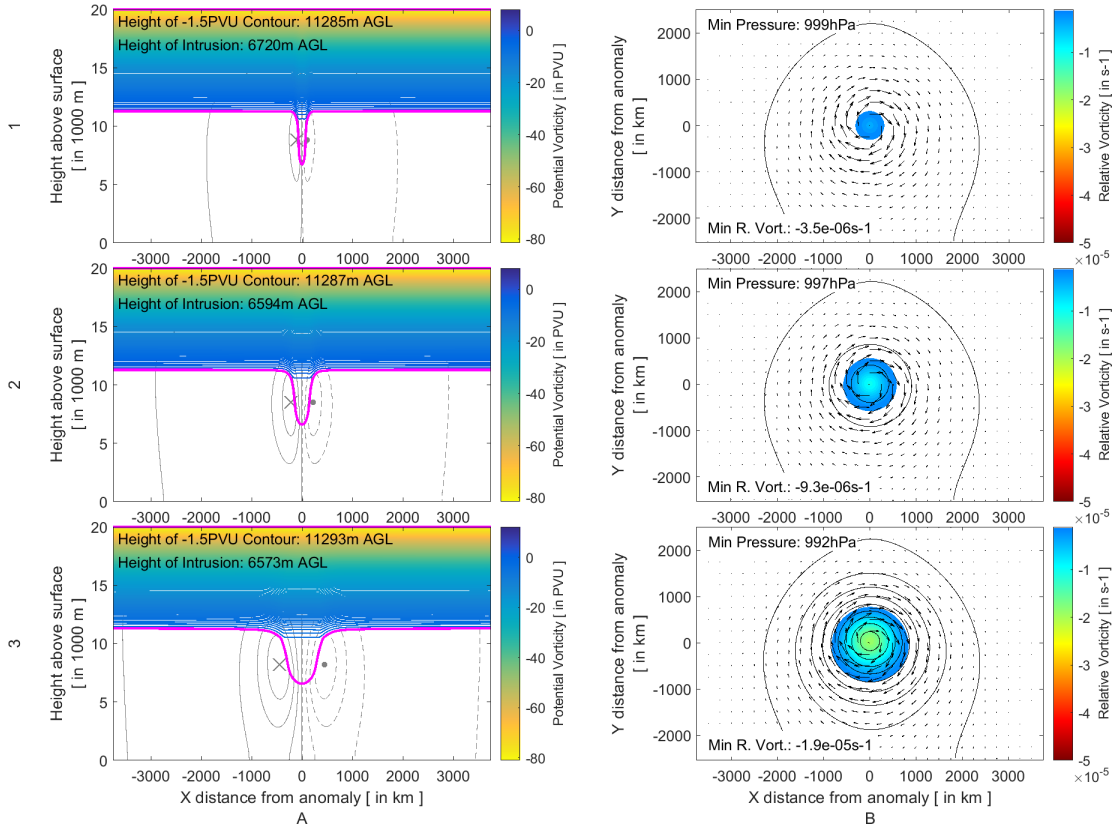

Figure 52: Same as in Figure 45 but with variable anomaly radial widths such that the height of the stratospheric intrusions AGL are similar from a constant dynamical tropopause depth of 12500m. The thinner intrusion is created by an anomaly with a 100km radial width (row 1) whilst the broader intrusion is created by a 400km radial width (row 3). Experiment 0 (200km radial width) is provided in row 2 for convenience and comparison.

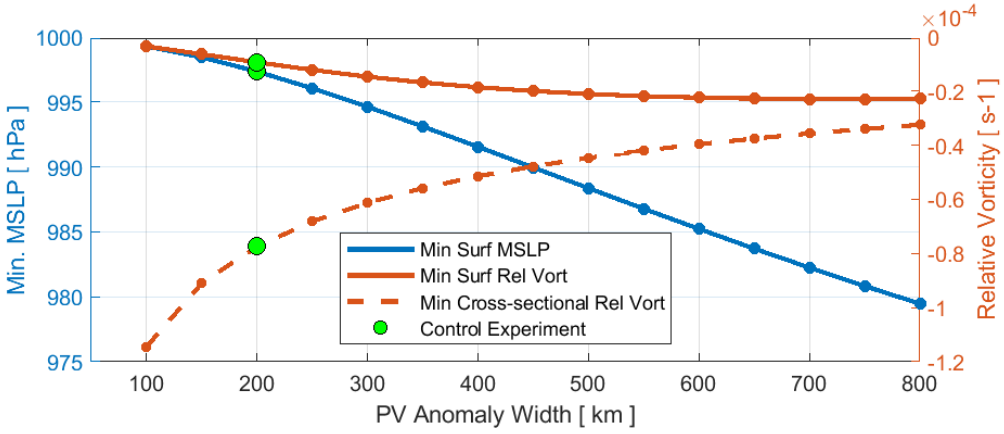

Figure 53: Same as in Figure 46 but for Experiment 5 (varying anomaly radial width experiments)

4.4. Discussion and conclusion

The study by Barnes *et al.* (2021a) showed a climatological link between COL depth and stratospheric intrusion depth. Deep COLs, those associated with surface cyclones, were generally found to be associated with deeper stratospheric intrusions. The climatology Barnes *et al.* (2021a) is performed in the context of the total atmospheric system, where a host of processes at various levels of the atmosphere can affect the development of cyclones at all levels. Therefore, it is pertinent to isolate the link between COLs and the depth of their associated upper-level high-PV anomalies with surface cyclogenetic forcing in an idealised setting. An initial numerical experiment using PV inversion diagnostics (Experiment 0) shows that the numerical model and PV inversion algorithms produce results as we expect from the conceptual model (Figure 38) of a high-PV anomaly in the upper-levels: a core of cyclonic flow is present around the PV anomaly, with general cyclonic motion prevalent, although weak, through the majority of the domain. The longitudinal cross-section and upper-level pressure and wind fields show the development of an amplifying trough. In the real world, the trough with continual amplification could develop into a COL. Cyclonic flow and low-pressure signatures are also observed on the surface. This re-emphasises that upper-level processes are a shared development driver of both the surface cyclone and its associated COL. For Experiment 0, cyclogenetic forcing is very weak or negligible, although relative vorticities indicate that we are on the precipice of surface cyclogenetic forcing being induced. The anomaly does however induce a closed low-pressure on the surface.

Experiment 1 varies the depth of a stratospheric intrusion (i.e. the closest distance of a -1.5 PVU point to the surface). This experiment reveals that the depth that a stratospheric intrusion reaches is an important factor in the amount of surface cyclogenetic forcing induced. Very shallow intrusions resulted in a minimal amount of pressure decrease on the surface, whilst extremely deep intrusions resulted in a pronounced decrease in surface pressure. Surface relative vorticities reveal that surface

cyclogenetic forcing is only initiated for deeper intrusions. Barnes *et al.* (2021a) showed that COLs are more likely to be associated with a surface low if a stratospheric intrusion reaches below the 300hPa level. Using a simple barometric conversion from altitude to pressure with standard sea level pressure and temperature reveals that the stratospheric intrusions shown in Experiment 1 (Figure 45) extend to roughly the 270hPa, 430hPa, 610hPa and 840hPa levels. This corresponds well with the findings of Barnes *et al.* (2021a) with the only intrusion extending to less than the 300hPa, having little effect on the surface. The lower limit for weak cyclogenetic forcing could be deemed to be the control experiment since it is extremely close to the lower limit of cyclogenesis. Therefore, in Experiment 1 cyclogenetic forcing is initiated just past the 430hPa intrusion level. This relative vorticity view of cyclogenetic forcing therefore also corresponds well to the findings of Barnes *et al.* (2021b).

The scenarios in Experiment 1 show how surface cyclogenetic forcing is induced for separate instantaneous intrusions. However, Figure 45, can also be viewed in a temporal sense. An RWB event, results in an intrusion of high-PV air into the stratosphere. The continued amplification of the Rossby wave will result in a continued intrusion of high-PV air into the troposphere. The intrusion will grow and extend towards the surface as shown in Figure 45A. The growth in the intrusion will result in the continued and enhanced development of the surface cyclone and if deep enough, could result in the cyclogenesis.

Barnes *et al.* (2021a) showed that shallow COLs, COLs which only extend into the mid-levels, occur most frequently in the summer months and the lower latitudes. This corresponds to seasons and regions where the dynamical tropopause is furthest away from the surface. This finding together with the finding that shallow COLs are most often associated with shallow intrusions suggest that the height of the stratospheric intrusion is more important than the vertical depth of the intrusion itself. Experiments 2 and 3 show this is indeed the case. Intrusions from high tropopause heights, as would be seen closer to the tropics and in summer, resulted in negligible cyclogenetic forcing at the surface and initiated very little pressure decrease at the surface (Experiment 2). Conversely, lower dynamical tropopauses resulted in surface cyclogenetic forcing and a large surface pressure decrease. Differing intrusion depths to a similar intrusion height AGL were also shown to result in similar pressure deepening (Experiment 3). It was however shown the cyclonic motion at the surface was more enhanced for the larger vertical intrusions compared to the smaller vertical intrusion. The enhanced relative vorticity in the large intrusion suggests that the vertical height of intrusion could play a role in the extreme windstorms (e.g. Liberato 2014). Of course, it should also be noted that anomalies at the surface and in the low-levels can also enhance cyclogenesis when in phase as shown in the example of Cape Storm by Barnes *et al.* (2021b).

A key finding of this study is the relative contribution of each of the different factors tested to surface cyclogenesis. Experiments 1-3 show that it is the depth that the stratospheric intrusion reaches that is the major factor in surface cyclogenesis. Larger intrusions induce greater cyclogenetic forcing in the mid-levels than smaller intrusions. However, if the PV intrusions are situated further away from the surface (from a tropopause further away from the surface), the resulting relative vorticity on the surface is diminished and is comparable to that of a smaller intrusion extending to a similar height AGL from a tropopause height closer to the surface. In terms of surface relative vorticity, wider intrusions are found to have a small, but largely negligible effect, despite the dramatic effect that these differences have in the mid-troposphere. The width of these intrusions do however still have a large effect the surface pressure of beneath them. With constant stratospheric depth (5000m) and constant tropopause height AGL (12500m), a thin filament intrusion with a radius of 100km resulted in a minimal pressure decrease at the surface. Interestingly, the degree of surface pressure was comparable to that of the intrusion of double the width (200km) and half the vertical extent (2500m) as seen in Experiment 1 (Figure 45, top panels).

Conversely, an intrusion with a large area of with radius of 400km resulted in a slightly deeper surface low-pressure comparable to that of the intrusion with half the width and 50% more depth as shown in Experiment 1 (Figure 45, bottom panels). The resulting surface pressure and relative vorticity patterns together provide a picture of the weather systems being forced on the surface. Wider intrusions produce wider, deeper cyclones whilst thinner filaments of PV produce shallower, smaller cyclones.

Conceptually, there is a distinct difference between the surface cyclonic circulations induced by the idealised intrusions presented here and which actually occur in reality. This is explained fully in Hoskins *et al.* (1985) and was touched on in Barnes *et al.* (2021a). Surface lows are generally found to the east of the COL and upper-level PV anomaly axis. In these idealised cases however, the centre of the induced surface cyclonic is directly beneath the PV anomaly. In the real atmosphere, the surface cyclonic motion induced by the upper-level anomaly acts as a mechanism for warm surface temperature advection to the east of the upper-level anomaly. This surface temperature (and therefore potential temperature) anomaly has PV-like properties and can induce its own surface cyclonic circulation. Deeper intrusions will therefore drive more intense warm-air advection to the east of the trough axis, inducing enhanced cyclogenesis. One of the major limitations of this work is the lack of a temporal aspect in the experimental framework. Surface cyclones are not produced instantaneously but grow over time. Additionally, in the real-world atmosphere, upper-level PV anomalies are also influenced by the vertical structure of the air column beneath it. Future work

should include the use of a numerical dynamical core which will have a temporal element and include processes such as upper-level induced surface warm-air temperature advection. This would also improve general analysis of the temporal aspect of intrusions as they grow and decay and the resulting effect on surface cyclogenesis. A dynamical core would also allow for the study of more complex vertical structures such as the inclusion of temperature inversions beneath the PV inversion.

This study analyses idealised stratospheric intrusions in a general sense. Although the climatology of Barnes *et al.* (2021a), looked at PV anomalies with respect to COL development, they are applicable for both intrusions that result in the formation of a closed low as well as those that only ever form an upper-level trough. Regardless, the results clearly confirm the climatological link found by Barnes *et al.* (2021a) that stratospheric intrusion depth is an important contributing factor that results in the extension of a COL to the surface.

4.5. References

Ahmadi-Givi F, Graig GC, Plant RS. 2004. The dynamics of a midlatitude cyclone with very strong latent-heat release. *Quarterly Journal of the Royal Meteorological Society*, 130(596 PART A): 295–323. https://doi.org/10.1256/qj.02.226.

Arakane S, Hsu HH. 2020. A tropical cyclone removal technique based on potential vorticity inversion to better quantify tropical cyclone contribution to the background circulation. *Climate Dynamics*. Springer Berlin Heidelberg, 54(5–6): 3201–3226. https://doi.org/10.1007/s00382-020-05165-x.

Barnes MA, Ndarana T, Landman WA. 2021a. Cut-off lows in the Southern Hemisphere and their extension to the surface. *Climate Dynamics*. https://doi.org/10.1007/s00382-021-05662-7.

Barnes MA, Ndarana T, Landman WA. 2021b. Cut-off lows in the Southern Hemisphere and their extension to the surface. *Climate Dynamics*. https://doi.org/10.1007/s00382-021-05662-7.

Barnes MA, Turner K, Ndarana T, Landman WA. 2021c. Cape storm: A dynamical study of a cut-off low and its impact on South Africa. *Atmospheric Research*, 249: 105290. https://doi.org/10.1016/j.atmosres.2020.105290.

Baxter MA, Schumacher PN, Boustead JM. 2011. The use of potential vorticity inversion to evaluate the effect of precipitation on downstream mesoscale processes. *Quarterly Journal of the Royal Meteorological Society*, 137(654): 179–198. https://doi.org/10.1002/qj.730.

Blender R, Schubert M. 2000. Cyclone tracking in different spatial and temporal resolutions. *Monthly Weather Review*, 128(2): 377–384. https://doi.org/10.1175/1520-0493(2000)128<0377:CTIDSA>2.0.CO;2.

Brennan MJ, Lackmann GM. 2005. The influence of incipient latent heat release on the precipitation distribution of the 24-25 January 2000 U.S. East Coast cyclone. *Monthly Weather Review*, 133(7): 1913–1937. https://doi.org/10.1175/MWR2959.1.

Charney JG, Stern ME. 1962. On the Stability of Internal Baroclinic Jets in a Rotating Atmosphere. *Journal of the Atmospheric Sciences*, 19(2): 159–172. https://doi.org/10.1175/1520-0469(1962)019<0159:OTSOIB>2.0.CO;2.

Davis CA. 1992. Piecewise Potential Vorticity Inversion. *Journal of the Atmospheric Sciences*, 49(16): 1397–1411. https://doi.org/10.1175/1520-0469(1992)049<1397:PPVI>2.0.CO;2.

Davis CA, Emanuel KA. 1991. Potential vorticity diagnostics of cyclogenesis. *Monthly Weather Review*, 1929–1953.

Fehlmann R. 1997. Dynamics of seminal PV elements. Swiss Federal Institute of Technology Zurich.

Flaounas E, Drobinski P, Bastin S. 2013. Dynamical downscaling of IPSL-CM5 CMIP5 historical simulations over the Mediterranean: Benefits on the representation of regional surface winds and cyclogenesis. *Climate Dynamics*, 40(9–10): 2497–2513. https://doi.org/10.1007/s00382-012-1606-7.

Flaounas E, Kotroni V, Lagouvardos K, Flaounas I. 2014. CycloTRACK (v1.0) – tracking winter extratropical cyclones based on relative vorticity: sensitivity to data filtering and other relevant parameters. *Geoscientific Model Development*, 7(4): 1841–1853. https://doi.org/10.5194/gmd-7-1841-2014.

Hofstätter M, Chimani B, Lexer A, Blöschl G. 2016. A new classification scheme of European cyclone tracks with relevance to precipitation. *Water Resources Research*, 52(9): 7086–7104. https://doi.org/10.1002/2016WR019146.

Holton JR, Hakim GJ. 2013. *An Introduction to Dynamic Meteorology*. *Academic Press*. Elsevier.

Hoskins BJ, McIntyre ME, Robertson AW. 1985. On the use and significance of isentropic potential vorticity maps. *Quarterly Journal of the Royal Meteorological Society*, 111(470): 877–946. https://doi.org/10.1002/qj.49711147002.

Huo Z, Zhang DL, Gyakum JR. 1999. Interaction of potential vorticity anomalies in extratropical cyclogenesis. Part I: Static piecewise inversion. *Monthly Weather Review*, 127(11): 2546–2561. https://doi.org/10.1175/1520-0493(1999)1272.0.CO;2.

Iwabe CMN, Da Rocha RP. 2009. An event of stratospheric air intrusion and its associated secondary surface cyclogenesis over the South Atlantic Ocean. *Journal of Geophysical Research Atmospheres*,

114(9): 1–15. https://doi.org/10.1029/2008JD011119.

Kleinschmidt E. 1950. Über Aufbau und Entstehung von Zyklonen. *Meteorol. Rdsch.*, 3: 1–6.

Kunz A, Konopka P, Müller R, Pan LL. 2011. Dynamical tropopause based on isentropic potential vorticity gradients. *Journal of Geophysical Research*, 116(D1): D01110. https://doi.org/10.1029/2010JD014343.

Lackmann GM. 2011. *Midlatitude synoptic meteorology: Dynamics, analysis and forecasting*. American Meteorological Society: Boston, MA.

Liberato MLR. 2014. The 19 January 2013 windstorm over the North Atlantic: Large-scale dynamics and impacts on Iberia. *Weather and Climate Extremes*. Elsevier, 5(1): 16–28. https://doi.org/10.1016/j.wace.2014.06.002.

Moller JD, Montgomery MT. 2000. Tropical cyclone evolution via potential vorticity anomalies in a three-dimensional balance model. *Journal of the Atmospheric Sciences*, 57(20): 3366–3387. https://doi.org/10.1175/1520-0469(2000)057<3366:TCEVPV>2.0.CO;2.

Ndarana T, Waugh DW. 2011. A Climatology of Rossby Wave Breaking on the Southern Hemisphere Tropopause. *Journal of the Atmospheric Sciences*, 68(4): 798–811. https://doi.org/10.1175/2010JAS3460.1.

Neu U, Akperov MG, Bellenbaum N, Benestad R, Blender R, Caballero R, Cocozza A, Dacre HF, Feng Y, Fraedrich K, Grieger J, Gulev S, Hanley J, Hewson T, Inatsu M, Keay K, Kew SF, Kindem I, Leckebusch GC, Liberato MLR, Lionello P, Mokhov II, Pinto JG, Raible CC, Reale M, Rudeva I, Schuster M, Simmonds I, Sinclair M, Sprenger M, Tilinina ND, Trigo IF, Ulbrich S, Ulbrich U, Wang XL, Wernli H. 2013. Imilast: A community effort to intercompare extratropical cyclone detection and tracking algorithms. *Bulletin of the American Meteorological Society*, 94(4): 529–547. https://doi.org/10.1175/BAMS-D-11-00154.1.

Nissen KM, Leckebusch GC, Pinto JG, Renggli D, Ulbrich S, Ulbrich U. 2010. Cyclones causing wind storms in the Mediterranean: Characteristics, trends and links to large-scale patterns. *Natural Hazards and Earth System Science*, 10(7): 1379–1391. https://doi.org/10.5194/nhess-10-1379-2010.

Pang H, Fu G. 2017. Case study of potential vorticity tower in three explosive cyclones over Eastern Asia. *Journal of the Atmospheric Sciences*, 74(5): 1445–1454. https://doi.org/10.1175/JAS-D-15-0330.1.

Peters D, Waugh DW. 1996. Influence of Barotropic Shear on the Poleward Advection of Upper-

Tropospheric Air. *Journal of the Atmospheric Sciences*, 53(21): 3013–3031. https://doi.org/10.1175/1520-0469(1996)053<3013:IOBSOT>2.0.CO;2.

Reed RJ. 1955. A Study of a Characteristic Tpye of Upper-level Frontogenesis. *Journal of Meteorology*, 12(3): 226–237. https://doi.org/10.1175/1520-0469(1955)012<0226:ASOACT>2.0.CO;2.

Røsting B, Kristjánsson JE. 2012. The usefulness of piecewise potential vorticity inversion. *Journal of the Atmospheric Sciences*, 69(3): 934–941. https://doi.org/10.1175/JAS-D-11-0115.1.

Sprenger M. 2003. Tropopause folds and cross-tropopause exchange: A global investigation based upon ECMWF analyses for the time period March 2000 to February 2001. *Journal of Geophysical Research*, 108(D12): 8518. https://doi.org/10.1029/2002JD002587.

Sprenger M. 2007. Numerical piecewise potential vorticity inversion: A user guide for real-case experiments. , 98.

Thorncroft CD, Hoskins BJ, McIntyre ME. 1993. Two paradigms of baroclinic-wave life-cycle. *Q.~J.~R. Meteorol. Soc.*, 119: 17–55. https://doi.org/10.1002/qj.49711950903.

Postface

This chapter studies intrusions of high-PV stratospheric air into the troposphere and examines the results of different characteristics of the intrusions on cyclogenetic forcing. It can be recalled that Chapter 3 showed, from a climatological sense, deep COLs (dCOLs) are generally associated with deeper PV intrusions that extend closer to the surface. To ensure that this is indeed the case, we isolate the effect that the upper-level PV intrusion has on surface cyclogenetic forcing by deploying PV intrusions in an idealised PV framework. Using this framework, we systematically and novelly explore the effect that the stratospheric depth has on surface cyclogenesis.

The results of this work clearly confirm the results of the climatology study in Chapter 3. Larger intrusions are shown here to result in more cyclogenetic forcing throughout the troposphere. A key corroborative finding of the idealised study is that it is the proximity of the PV intrusion to the surface rather than size of the intrusion that results in the greatest amount of surface cyclogenesis, as hypothesised in Chapter 3. This finding also enforces the hypothesis made in Chapter 3 that the seasonal and latitudinal variability of COL extensions is a result of the variability of the height of the dynamical tropopause. A dynamical tropopause that is situated further away from the surface, as occurs during the summer and in the tropics, means that PV intrusions that are to result in surface cyclogenesis must be larger in order to result in surface cyclogenesis and COL extension. Thus, even relatively intense PV intrusions (in terms of vertical size of the PV intrusion) can result in COLs remaining shallow. This explains the high frequency of shallow COLs (sCOLs) found in the low latitudes and during the summer months.

The analysis of the mechanisms that inhibit and promote the extension of COLs to the surface completes objectives 3 and 4 of this study.

Chapter 5: Potential vorticity tools for operational cut-off low analysis

Preface

Chapters 2, 3 and 4 have investigated and discussed the PV dynamics of cut-off low (COL) extensions. This investigation has been done in terms of a case study, COL extension climatology and an idealised numerical investigation. The analyses have led to significant learnings in how PV dynamics affect COLs and the surface low pressure systems that at times develop beneath them. It is however important for the knowledge gained from this work to filter into the knowledge base of both students and operational meteorologists who analyse these weather systems daily. As such, conceptual models of COLs and COL extensions that emanate from this thesis are created. These provide an easy to understand teaching tool as to how COLs develop and extend to the surface from a PV perspective. The conceptual model is presented together with a webpage containing PV dynamical postprocessed NWP fields, allowing for future operational meteorologist and students to see the evolution of PV dynamics as COLs develop. This chapter addresses objective 5 of the overall study.

5.1. Background and introduction

The South African Weather Service (SAWS) is the nationally mandated meteorological service within South Africa. As part of their mandate, the service issues forecasts for the general public as well as for the aviation and marine sectors. This service includes the production of severe weather alerts when extreme weather approaches the country together with other user-specific weather-related products. The severe weather alerts and forecasts are issued by an operational team of meteorologists. Forecast products are produced based on an expert interpretation and analysis of numerical weather prediction (NWP) and observational data including in-situ surface observations, RADAR and satellite imagery.

NWP products and tools have become the life blood of the industry, dominating the weather forecasting process (Benjamin *et al.*, 2019). Globally with the improvement of high-performance computing, NWP predictions have improved dramatically over the past few decades with increasing resolution in both the horizontal and vertical, improved physics amongst others (Bauer *et al.*, 2015). South Africa is no exception. The SAWS currently run an in-house, regional version of the Unified Model (UM) at resolutions down to 4.4km and 1.5km with 72-hour and 48-hour lead times respectively (Stein *et al.*, 2019). The resulting data is used by operational forecasters to assess the forthcoming atmospheric conditions and make predictions. Currently, traditional fields such as geopotential height, pressure, temperature, humidity, velocity amongst others are used. Forecasters are also provided with common indices used globally such as the convective available potential energy (CAPE) and the lifted index (LI) to assist with thunderstorm forecasting together with a variety postprocessed fields such as rainfall totals, snowfall totals and fog and visibility fields.

Currently the SAWS make no use of dynamical postprocessing tools, and in particular potential vorticity (PV) dynamics, within their forecast process. In-house NWP products include no PV fields within the suite of products. PV dynamical theory is taught in university undergraduate and postgraduate coursework. PV dynamics are however never seen in practice in South Africa and therefore the knowledge about these theoretical concepts has diminished over the years within operational personnel. PV analyses have traditionally been used in academia and research (e.g. Hoskins, 1991; Hoskins *et al.*, 1985), but PV diagnostics can be used to enhance the operational forecasting process. One of the initial investigations into operational PV diagnostics showed how the diagnosis of the geometrics of the PV features can help forecasters assess potential model inaccuracies quickly and effectively (Mansfield, 1996). Large scale, synoptic features were shown to be captured by more traditional fields but smaller scale or weak features can be assisted by PV diagnostics. The use of PV for operational forecasting has also been used for identifying latent heat

release within synoptic scale features in order to diagnose surface cyclogenesis and low-level jets (Brennan *et al.*, 2008).

PV dynamical postprocessing also has a place in the academic world. Currently, the University of Pretoria (UP) hosts South Africa's only pure meteorological programme. Meteorological forecasters are required to have the skills outlined in the World Meteorological Organisations Basic Instruction Pack for Meteorologist (BIP-M) (World Meteorological Organization, 2012). Atmospheric dynamics and NWP form a part of the skills required for a BIP-M compliant meteorologist. Although UP's meteorology degree does offer students both dynamics and NWP courses, the amount of time spent on taking the dynamical meteorological ideas learned in theory into the more practical domain of NWP has lacked behind. UP meteorology students who go onto become meteorological forecasters and scientists at the SAWS therefore have limited understanding of how dynamical processes such as PV dynamics work and affect processes in a real-time setting. Allowing meteorology students at UP access to dynamical postprocessed NWP forecasts in real-time would enhance their understanding of these processes. This enhanced knowledge of dynamical processes will ultimately filter into an improved understanding of PV dynamics in an operational setting at the SAWS.

In this chapter, we provide a conceptual model for PV evolution with respect to cut-off lows (COLs) based on the basic theory provided by Hoskins *et al.* (1985) and other basic theoretical texts (e.g. Holton and Hakim, 2013; Lackmann, 2011) together with findings presented in this study. The conceptual model is presented in Section 5.2. This especially is pertinent since many theoretical texts are written with respect to the northern hemisphere where PV has positive values rather than negative values. The conceptual model is followed by the presentation of a PV diagnostic webpage in Section 5.3, which supplies dynamically postprocessed NWP data operationally. The webpage aims to be a springboard to dynamical postprocessed NWP in South Africa for operational personnel and meteorology students alike.

5.2. PV conceptual models

5.2.1. Current PV theoretical conceptual models

A variety of basic dynamical meteorology texts show the conceptual model of a PV anomaly resulting from a stratospheric intrusion and its effect on the cyclonic circulation around the centre of the PV anomaly. An example of this conceptual model by Lackmann (2011) is shown in Chapter 4. The majority of these idealised models emanate from that presented by Hoskins *et al.* (1985). The simplest of these models is shown in Figure 54 and is not dissimilar from the results shown in Chapter 4. Figure 54 shows the effect of a stratospheric intrusion of high-PV air on cyclonic rotation.

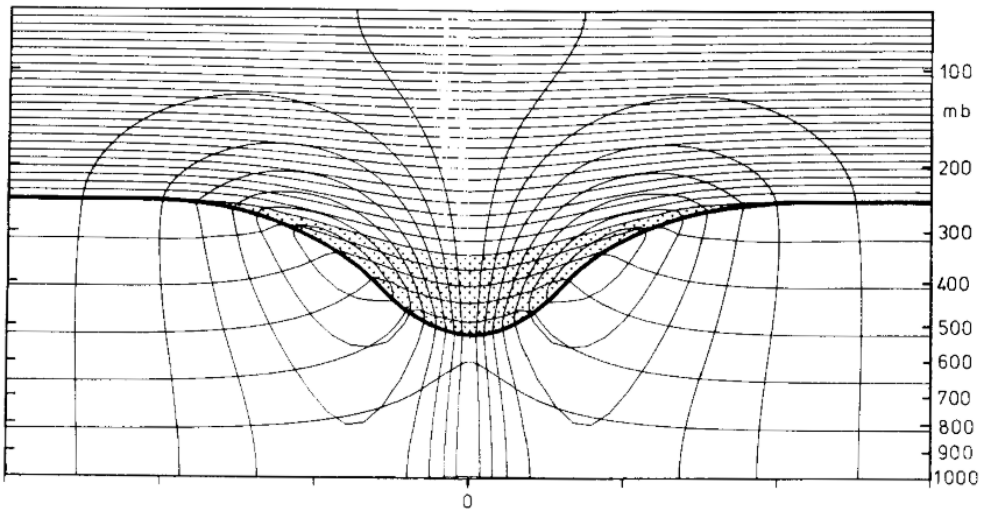

Figure 54: Conceptual model of a positive PV anomaly (dotted) presented in Hoskins et al. (1985) resulting in cyclonic motion (concentric lines) around the stratospheric intrusion represented by a bulge in the dynamical tropopause (thick black contour).

Low-level anomalies are also dealt with by Hoskins *et al.* (1985), where it is shown that a similar process can occur for low-level PV-like anomalies in the potential temperature field, as discussed in Chapter 3. Surface warm potential temperature anomalies can act like PV anomalies stimulating cyclonic rotation in the same manner as high-PV anomalies. Similarly to Figure 54, the warm potential temperature anomaly at 0 on the x-axis of Figure 55 is shown to induce cyclonic motion around this point. This cyclonic rotation also extends into the upper levels.

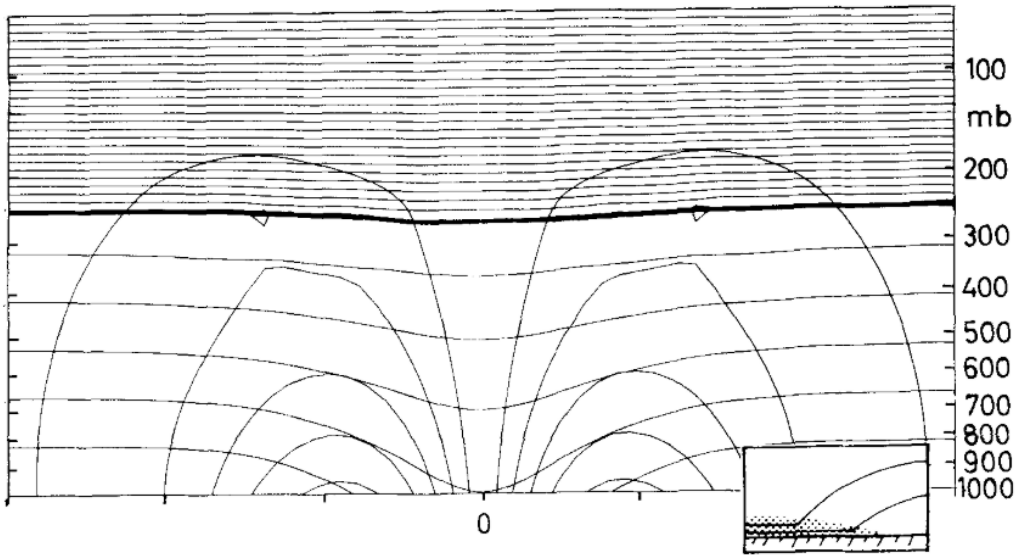

Figure 55: Conceptual model of a warm potential temperature anomaly at 0 on the x-axis presented in Hoskins et al. (1985) resulting in cyclonic motion (concentric lines) leading to a slight bulge in the dynamical tropopause above it.

Importantly however, the upper level (Figure 54) and low-level (Figure 55) anomalies interact with one another as is suggested in Chapter 3. This process is depicted in Figure 56. As Figure 56a suggests, and has been shown in Figure 54 and Chapter 4, the upper level anomaly leads to cyclonic motion

around the anomaly as well as on the surface below it. The surface cyclonic flow however results in warm air advection at the surface to the east of the anomaly axis, leading to a warm potential temperature anomaly at the surface as depicted in Figure 56b. The warm potential temperature anomaly however induces its own circulation at the surface as well as some weak cyclonic rotation in the upper levels. This leads to the surface cyclonic circulation tending to lie ahead (eastward) of the upper level closed circulation (COL). Similarly, the extension of the cyclonic circulation induced by the surface anomaly extends towards the upper levels and enhances cyclonic motion in the upper levels. While the two circulations remain in phase, they both promote the mutual amplification of one another.

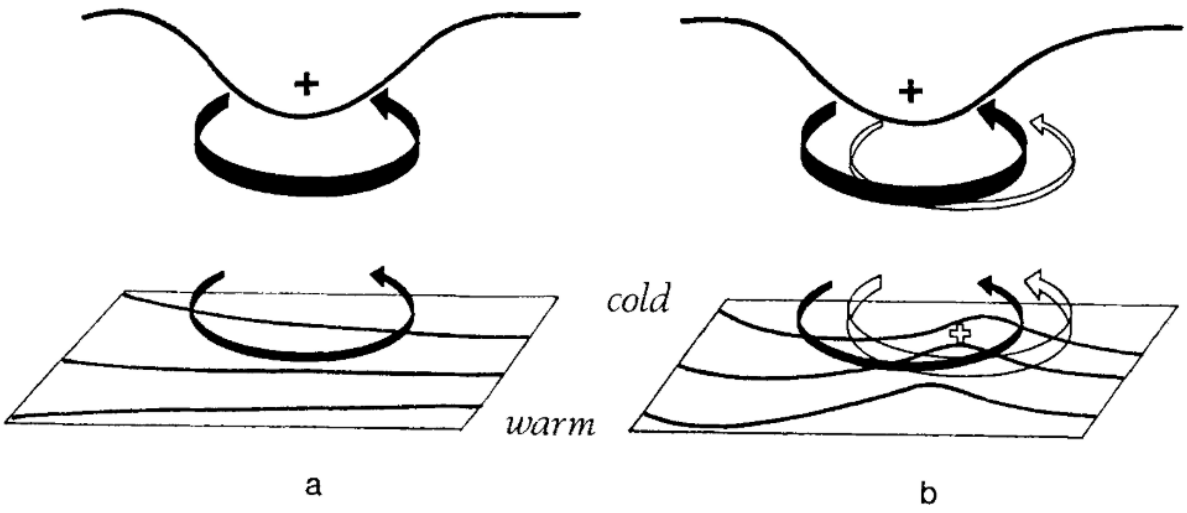

Figure 56: Conceptual model by Hoskins et al. (1985) depicting the interaction between low-level and upper level PV anomalies resulting in their mutual amplification.

5.2.2. New southern hemispheric conceptual PV model of COL extensions

A new conceptual model is developed based on PV dynamical conceptual models in theoretical texts such as shown in Section 5.2.1 as well as the findings throughout Chapter 2, 3 and 4. The new conceptual model provides an ideological idea of how COLs extend to the surface to both operational personnel and students. Section 5.2.2.1 provides the idealised basic state before any perturbations or intrusions (also called “Stage 0”). In stage 1 (Section 5.2.2.2), a small perturbation introduced into the basic state flow results in baroclinic instability resulting in an amplification of the upper level isentropic PV field. In the two-dimensional PV field, this can be seen as a small surfaceward extension of the dynamical tropopause. The stratospheric intrusion stimulates cyclonic motion around the anomaly as shown in the Section 5.2.1 and Chapter 4, with negligible effect on the surface. The perturbation in the isentropic PV field grows further, extending deeper towards the surface and resulting in an intensification of cyclonic motion throughout the troposphere. This is depicted in Section 5.2.2.3. The

resulting cyclonic flow on the surface results in warm air temperature advection to the east of the PV anomaly, causing a warm potential temperature anomaly to develop at the surface. As shown in the Figure 55, the warm potential temperature anomaly stimulates its own cyclonic circulation resulting in the beginning of the development of a surface low to the east of the amplifying trough of both isentropic PV and pressure in the upper levels. Similarly, the cold air advection that occurs on the western side of the anomaly results in anticyclonic motion and a pressure rise. Continual amplification and baroclinic instability can lead to exponential growth of the amplitude of the trough and the eventual overturning isentropic PV contours. Overturning is a sign of Rossby wave breaking (RWB). RWB results in the continual intrusion of high-PV stratospheric air into the troposphere. The intrusion of stratospheric air extends deeper into the troposphere. As shown in Chapter 3 and 4, deeper intrusions of stratospheric air result in enhanced cyclonic development around the PV anomaly and enhanced surface cyclonic motion. The enhanced cyclonic motion eventually yields closed low pressure cells in both the upper levels and surface as seen in Section 5.2.2.4. Finally, diabatic heating processes can lead to the development of a low-level PV anomaly. The anomalies at the surface together with those in the upper and lower levels results in the formation of a so-called “PV tower”. PV towers, as discussed int the Chapter 2, have been shown to result in explosive cyclogenesis at the surface. This process is depicted in Section 5.2.2.5.

5.2.2.1. Stage 0: The basic state

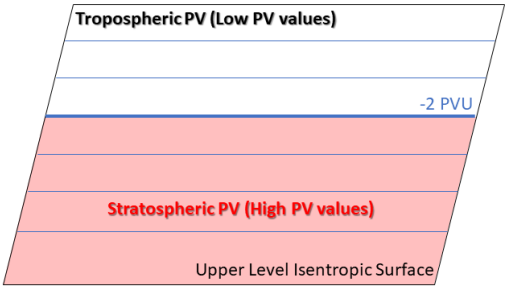

Figure 57: An upper level isentropic surface with the -2 PVU contour representing the dynamical tropopause

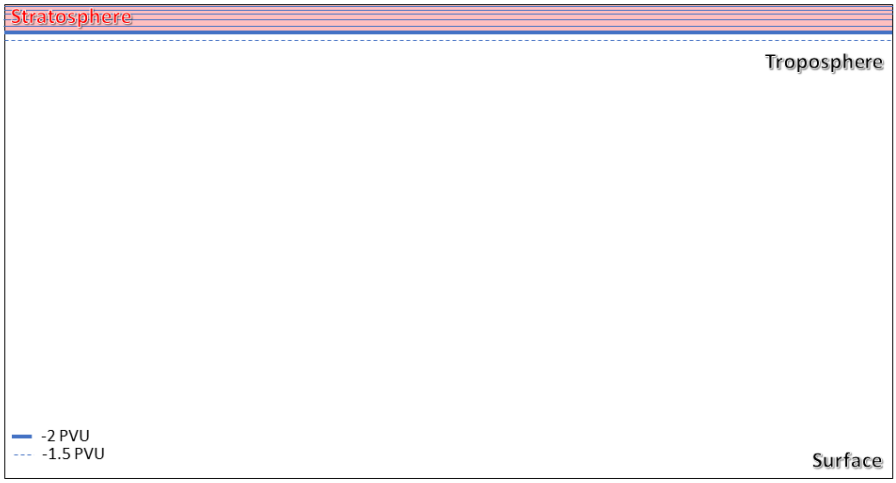

Figure 58: A longitudinal cross-section through the PV field

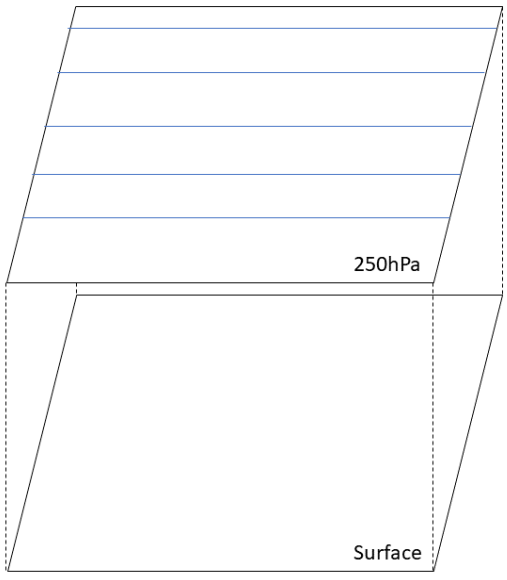

Figure 59: The surface and upper level (in this case 250hPa) pressure levels

5.2.2.2. Stage 1: Initial perturbation

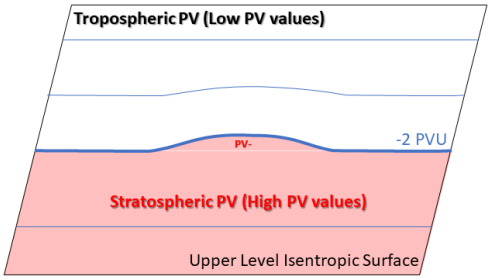

Figure 60: An upper level isentropic surface with the -2 PVU contour showing minimal equatorward amplification of the dynamical tropopause

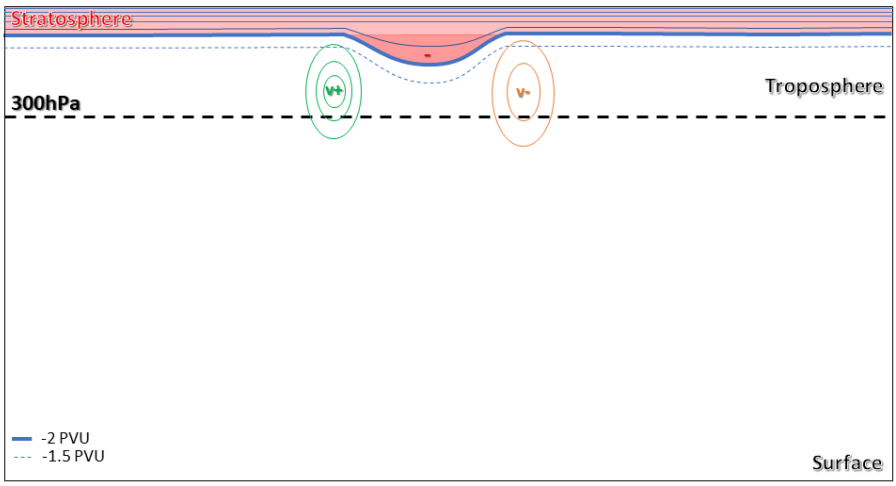

Figure 61: A cross section through the perturbation in the PV field reveals a slight surfaceward amplification of the dynamical tropopause. Cyclonic rotation in a small vicinity of the amplification results with no (or negligible) effect on the surface.

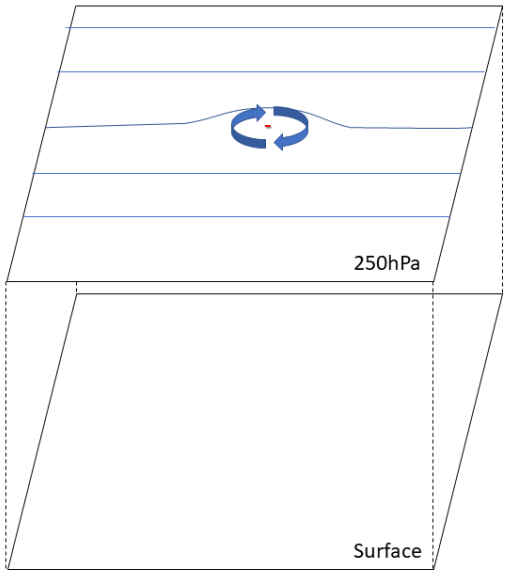

Figure 62: A small perturbation in the upper pressure levels results, with minimal cyclonic forcing onto the field.

5.2.2.3. Stage 2: Surface cyclonic development and Rossby wave amplification

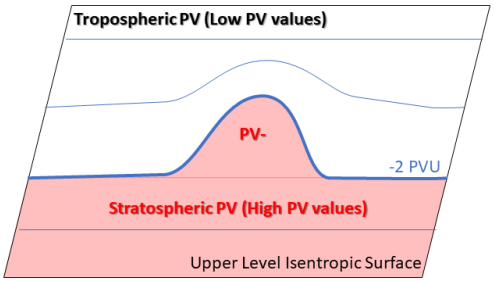

Figure 63: Further amplification of the dynamical tropopause on the upper level isentropic surface

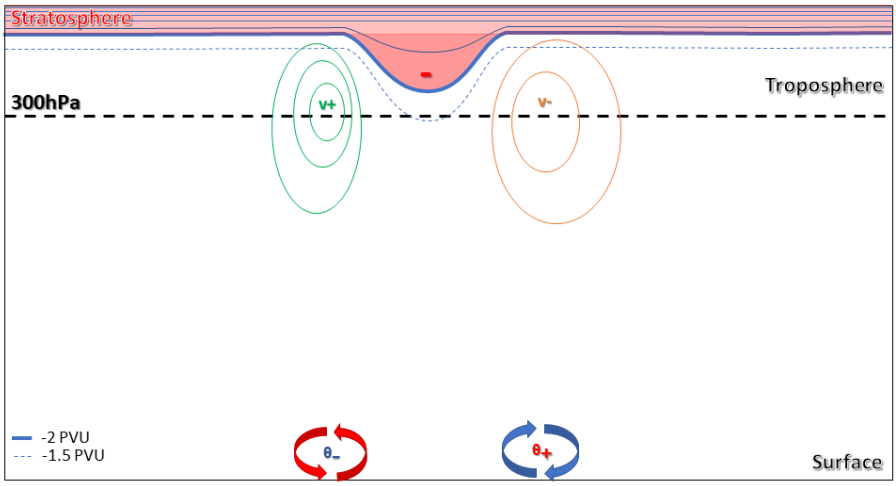

Figure 64: The stratospheric intrusion grows surfaceward. This results in an increase in cyclonic circulation in the upper levels. Some minimal warm air advection in the mirrored surface circulation results in the development of a warm surface potential temperature anomaly to the east of the anomaly axis which forces its own cyclonic circulation. A cold surface anomaly to the west forcing its own anticyclonic circulation is also present. This represents the process of surface high pressure cell ridging.

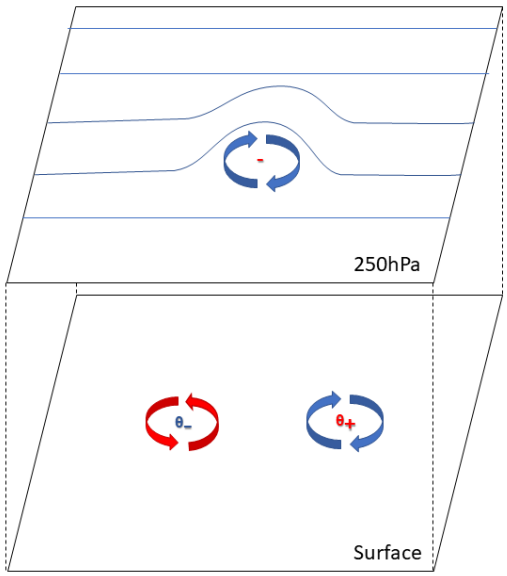

Figure 65: The upper level trough continues to amplify with minimal cyclonic circulation taking place on the surface

5.2.2.4. Stage 3: RWB, COL and surface cyclone development

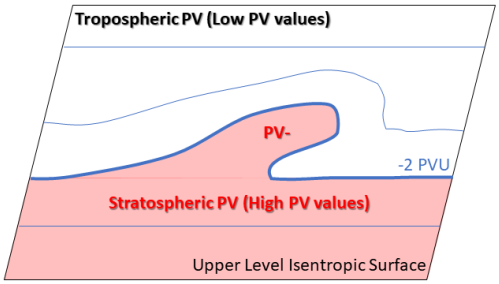

Figure 66: An overturned dynamical tropopause on the upper level isentropic surface, a sign of RWB in the upper troposphere.

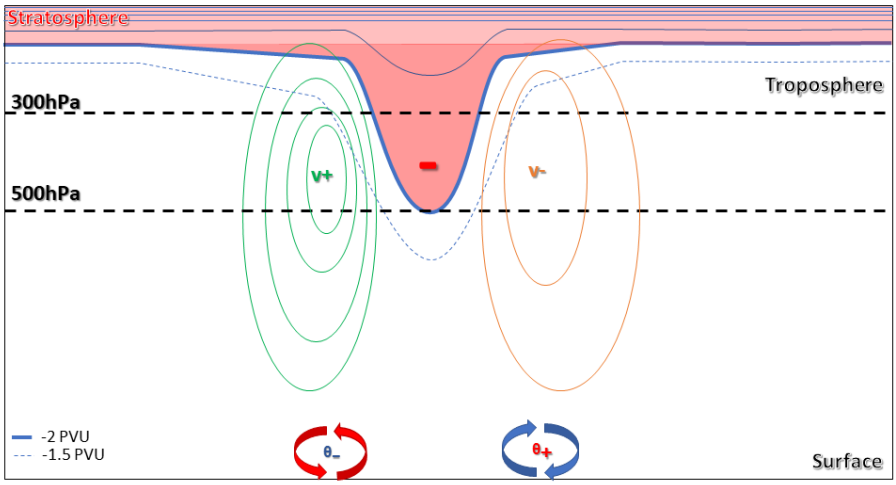

Figure 67: The stratospheric intrusion continues to grow towards the mid-levels. Cyclonic circulation is amplified throughout the troposphere. This enhances warm air advection the east of the anomaly axis which increases surface cyclonic circulation.

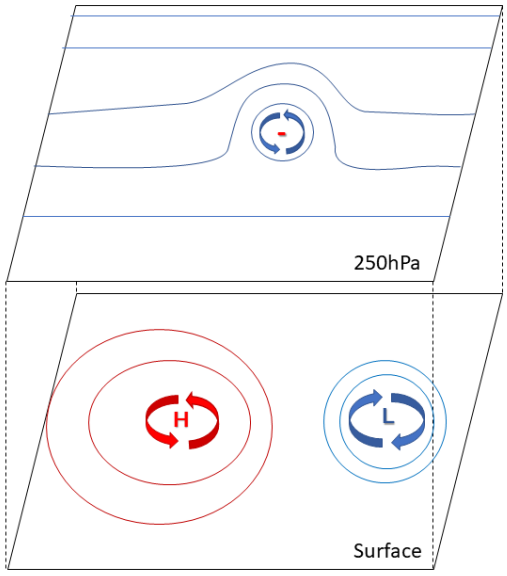

Figure 68: The continued amplification of the upper level trough and increased cyclonic circulation driven by the upper level stratospheric intrusion eventually results in clearly defined closed cyclonic circulations in the upper levels (COL) and surface.

5.2.2.5. Stage 4: Explosive surface cyclogenesis

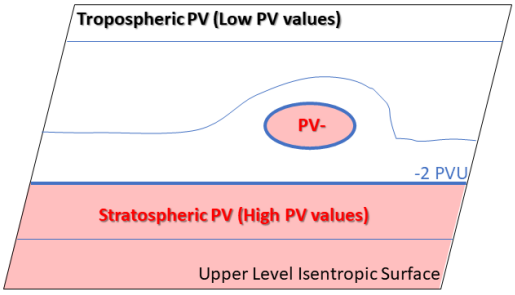

Figure 69: An overturning of the dynamical tropopause can lead to upper atmospheric isentropic PV cut-offs. This is not a requirement for explosive cyclogenesis but can be the final stage of a RWB event

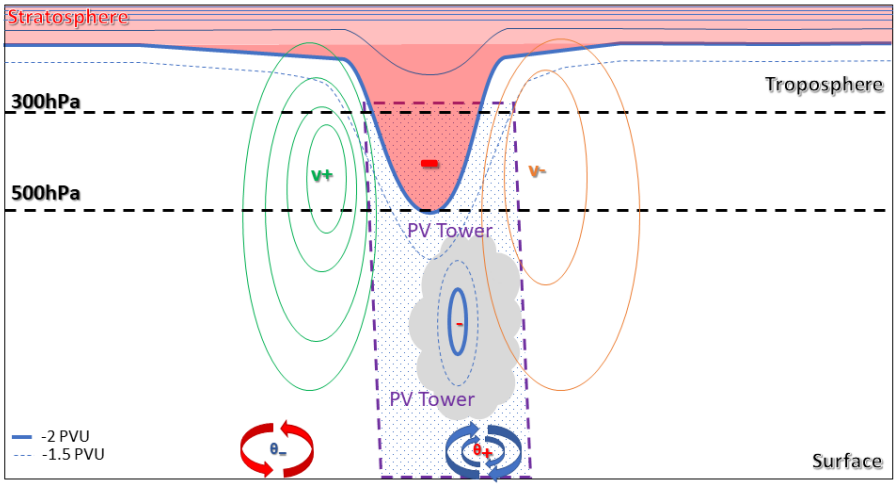

Figure 70: Diabatic heating associated with precipitation can resulting in the formation of a low-level PV anomaly. The alignment of the upper, lower and surface PV anomalies results in a so-called "PV Tower" which promotes explosive cyclogenesis of the surface low.

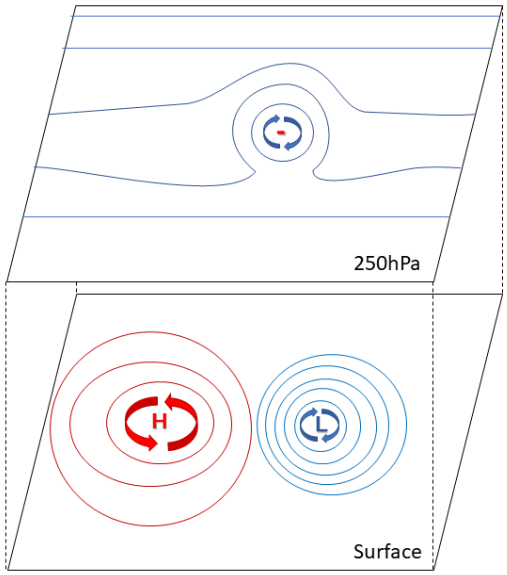

Figure 71: The PV tower stimulates explosive cyclogenesis at the surface resulting a rapid deepening of the surface low.

5.3. Dynamical postprocessing of NWP

5.3.1. Data and processing

Quality data is a key ingredient in the accuracy of operational forecasts. However, this data can be manipulated in many different ways. The manner in which data is presented and postprocessed is critical in assisting forecasters to interpret and analyse the mass of data that NWP provides. PV diagnostics is one tool which can assist forecasters in diagnosing weather systems. Dynamical PV theory in South Africa tends to largely remain a theoretical construct. University students learn about these processes but never really see how PV unfolds in weather systems they become very familiar with in the forecasting environment. Dynamical postprocessing scripts are created and ported to a webpage for immediate PV analysis. The postprocessed fields are created in such a way that the features shown the in the conceptual model above can be readily seen for "live" synoptic scale weather systems, such as COLs.

The PV postprocessing code was developed from potential vorticity python code published by Barlow (2017). The code uses freely available Global Forecast System (GFS) 0.25-degree NWP data. Potential vorticity is not an explicit variable of the GFS NWP suite. Therefore, the potential vorticity is calculated from the available variables such as wind velocity, pressure and temperature. PV is calculated by the potential vorticity equation (Hoskins *et al.*, 1985):

$$PV = -g\left(f\hat{k} + \nabla_p \times \hat{v}\right) \cdot \nabla_p \theta \tag{11}$$

where f is the Coriolis parameter, g is gravitational acceleration, $\hat{v}$ is the horizontal vorticity vector, p is pressure and θ is the potential temperature. It should be noted that equation (5) makes use of potential temperature which is not a variable available as part of the GFS suite. Potential temperature θ is calculated using temperature t using the equation $\theta = t\left(\frac{p_0}{p}\right)^{R/c_p}$ where R is the gas constant of air and c_p is the specific heat capacity for constant pressure.

In order to calculate PV at each point on the grid, we first deal with the curl of the horizontal vorticity vector with respect to pressure co-ordinates $\nabla_p \times \hat{v}$ where $\hat{v} = u\hat{\imath} + v\hat{\jmath} + 0\hat{k}$. From basic mathematical principles,

$$curl(\hat{v}) = \nabla_p \times \hat{v} = \left(\frac{\partial 0}{\partial y} - \frac{\partial v}{\partial p}\right)\hat{\imath} + \left(\frac{\partial u}{\partial p} - \frac{\partial 0}{\partial x}\right)\hat{\jmath} + \left(\frac{\partial v}{\partial x} - \frac{\partial u}{\partial y}\right)\hat{k}$$

$$= -\frac{\partial v}{\partial p}\hat{\imath} + \frac{\partial u}{\partial p}\hat{\jmath} + \left(\frac{\partial v}{\partial x} - \frac{\partial u}{\partial y}\right)\hat{k} \tag{12}$$

Reorganising equation (5) by substituting equation (12) into (5), yields,

$$PV = -g\left(f\hat{k} + \frac{\partial v}{\partial p}\hat{\imath} + \frac{\partial u}{\partial p}\hat{\jmath} + \left(\frac{\partial v}{\partial x} - \frac{\partial u}{\partial y}\right)\hat{k}\right) \cdot \nabla_p \theta$$

$$\therefore PV = \left[-g\left(\frac{\partial v}{\partial x} - \frac{\partial u}{\partial y} + f\right)\hat{k} - g\left(\frac{\partial v}{\partial p}\hat{\imath} + \frac{\partial u}{\partial p}\hat{\jmath}\right)\right] \cdot \nabla_p \theta \quad (13)$$

Noting that from basic mathematical principles $\hat{\imath} \cdot \hat{\imath} = \hat{\jmath} \cdot \hat{\jmath} = \hat{k} \cdot \hat{k} = 1$ and $\hat{\imath} \cdot \hat{k} = \hat{\jmath} \cdot \hat{k} = 0$ equation (13) yields,

$$PV = -g\left(\frac{\partial v}{\partial x} - \frac{\partial u}{\partial y} + f\right)\frac{\partial \theta}{\partial p} - g\left(\frac{\partial v}{\partial p}\frac{\partial \theta}{\partial x} + \frac{\partial u}{\partial p}\frac{\partial \theta}{\partial y}\right) \quad (14)$$

Barlow (2017) solves the derivatives of using gradient functions available as part of the scientific computing package (NumPy) within Python. Utilising the gradient functions and the u and v variables within the GFS suite together with the potential temperature θ calculated previously, PV is easily obtained.

5.3.2. Example case study

A case study is presented of an intense COL and associated surface low pressure system in order to showcase the dynamically postprocessed forecast products. A surface low pressure system approached the South African region on 12 July 2020. The system was associated with an upper level (300hPa) trough which developed into a COL during 13 July 2020. The deep surface low pressure cell with a central pressure of 976hPa was associated with strong surface winds of 25m.s^{-1} prevailing close to the core of the system, with 20-25m.s^{-1} winds along the south and south-western coastline during 13 July 2020. The weather system was extremely similar to that of Cape Storm as studied in Chapter 2. In fact, with the exception of the wildfires associated with Cape Storm, this system produced very similar meteorological and societal impacts within the Western Cape, especially along the coastline. Heavy rainfall and flooding were experienced along the Western Cape coastline and adjacent interior. Strong winds resulted in significant infrastructure damage and uprooted trees along the south-western Cape. The strong winds drove a wave climate with close to 12m significant wave height recorded at the Slangkop waverider buoy off of the Cape Peninsula. As shown, in Chapter 2, the strong winds, low pressure and wave setup drove significant surge around the Western Cape coastline. The wave climate together with the raised water levels caused extensive issues around the south and west coasts of the country including vessels running aground in Port Nolloth, a container vessel stuck in Table Bay nearly running aground, a container vessel in Algoa Bay losing cargo causing major

disruptions at the Port of Ngqura as well as infrastructure damage to coastal walkways and breakwaters. The synoptics of the case study are shown in Figure 72 using GFS 0.25-degree data for 12-13 July 2020 using the forecast initialised at 12 July 2020 00h00 UTC.

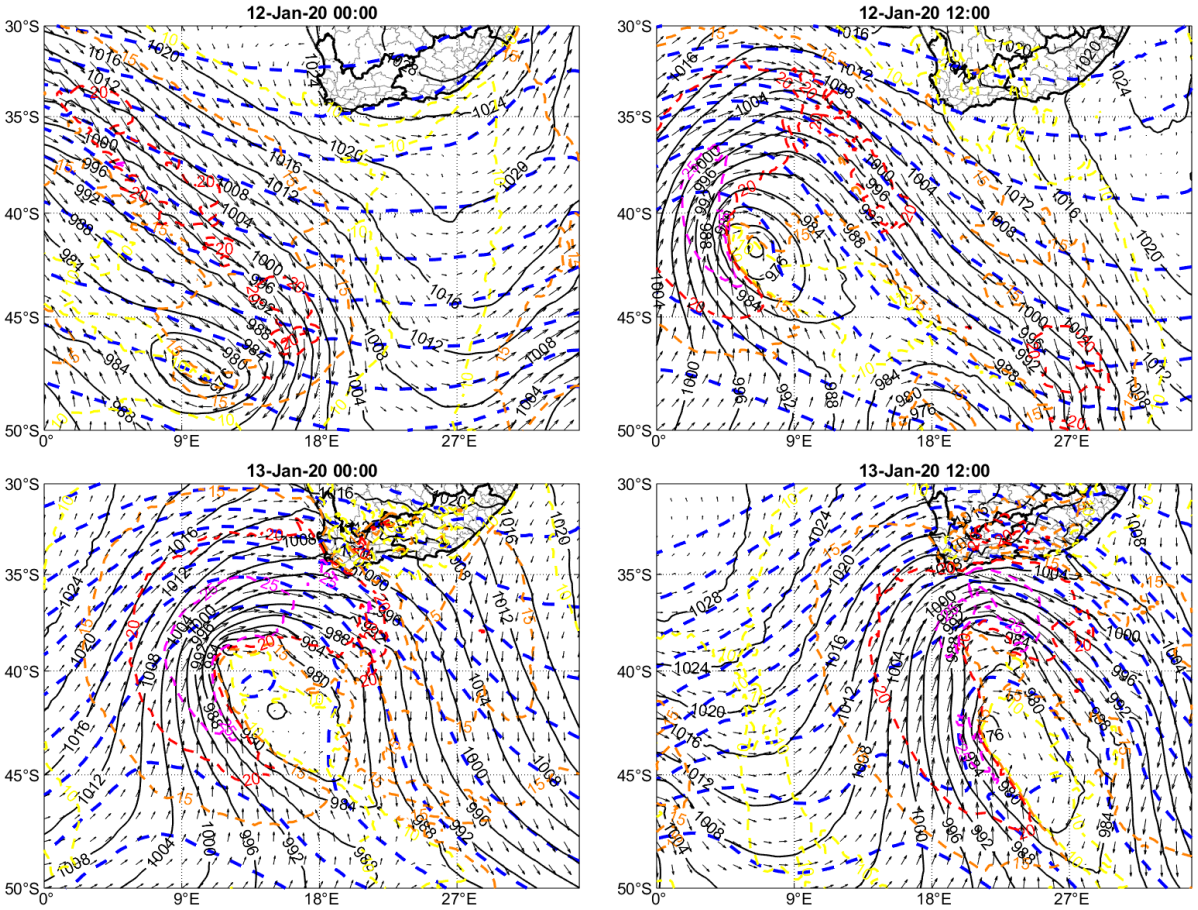

Figure 72: GFS 12 July 2020 00h00 UTC forecast data valid for 12-13 July 2020. Mean sea level pressure (black contours), 10m winds (black arrows) and 300hPa geopotential heights (blue dashed) are shown together with 10m wind speed contours at 10 (yellow), 15 (orange), 20 (red) and 25m.s^{-1} (magenta)

5.3.3. Postprocessed fields

The PV postprocessed NWP fields for the weather system in the above example are based on GFS 0.25-degree forecast data initialised on 10 July 2020 00h00 UTC. GFS data is processed in order to accentuate and reveal PV features for easy identification and analysis.

5.3.3.1. Isentropic PV for Rossby wave breaking analysis

Isentropic PV surfaces are not available within the GFS forecast suite. Therefore, PV on constant potential temperatures needs to be calculated. In order to achieve this, the code by Barlow (2017) first finds the pressure levels between which the isentropic level exists. PV on the specified isentropic surface is then calculated by:

$$PV_{\theta_{surf}} = \frac{(\theta_{surf} - \theta_{lower}) \times PV_{upper} + (\theta_{upper} - \theta_{surf}) \times PV_{lower}}{\theta_{upper} - \theta_{lower}} \quad (15)$$

where θ_{surf} is the potential temperature value for the isentropic surface required, θ_{lower} is the potential temperature at the pressure level below the isentropic level, θ_{upper} is the potential temperature at the pressure level above the isentropic level, PV_{lower} is the PV corresponding to θ_{lower} and PV_{upper} is the PV corresponding to θ_{upper}. The fields are plotted assuming the -2 PVU value is the tropopause, separating tropospheric air from stratospheric air. The colour scale emphasises this by plotting all PV values less than -2 PVU in blue colours whilst tropospheric air is shown with red colours. We also highlight the dynamical tropopause with a thick, blue dashed line in order to easily identify overturned contours for RWB identification. The operational postprocessing scripts calculated and plot isentropic PV on the 310-, 320-, 330-, 340- and 350K surfaces. An example of the layout of isentropic PV plots for both the 310K and 330K surfaces are shown in Figure 73. The dynamical tropopause (-2 PVU) on the 310K potential vorticity surface in Figure 73 shows clear signs of overturning to the south of South Africa. This is seen in the conceptual model for COL extension in Figure 66. Stratospheric air (in blue shades), wraps around the developing COL.

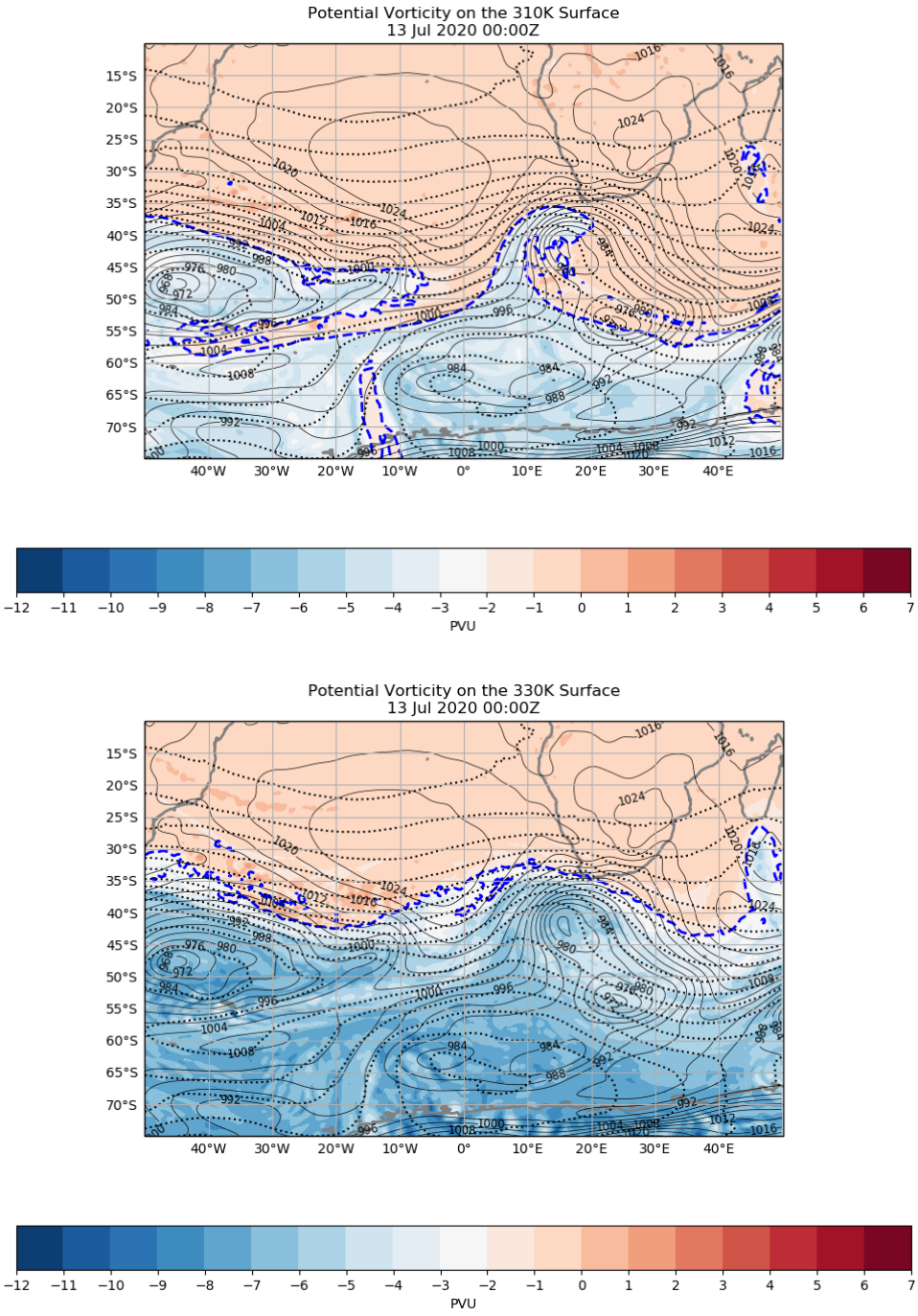

Figure 73: Isentropic PV on the 310K (top) and 330K (bottom) surfaces. Stratospheric air is denoted by shades of blue, whilst tropospheric air is denoted by red shades. The dynamical tropopause (at -2 PVU) is shown by a thick blue dashed line.

5.3.3.2. Dynamical tropopause products

Chapters 2-4 have shown that the height of the dynamical tropopause is critical in identifying where surface cyclogenesis is likely and where potential explosive cyclogenesis is possible. A simplistic version of stratospheric intrusion algorithm shown in Chapter 3 is employed. The stratosphere is initialized at 100hPa. The three-dimensional PV variable is used. For each horizontal grid-cell within the domain, the first value in the vertical column below the 100hPa level is identified and is defined

as the first tropospheric pressure level. The pressure level above this value is therefore deemed the tropopause and the level is recorded. The result of this procedure is a dynamical tropopause height or stratospheric intrusion depth variable in terms of pressure level. An example of the variable is shown in Figure 74. This field results in the user gaining a 2-dimensional sense of the tropospheric intrusion height (as depicted in Figure 64, Figure 67 etc.). It assists the user in identifying regions in which to investigate further by 2-dimensional cross-section. In the case of Figure 74 a large intrusion wrapping around the COL between 35˚S and 45˚S is depicted by the dark shades of magenta.

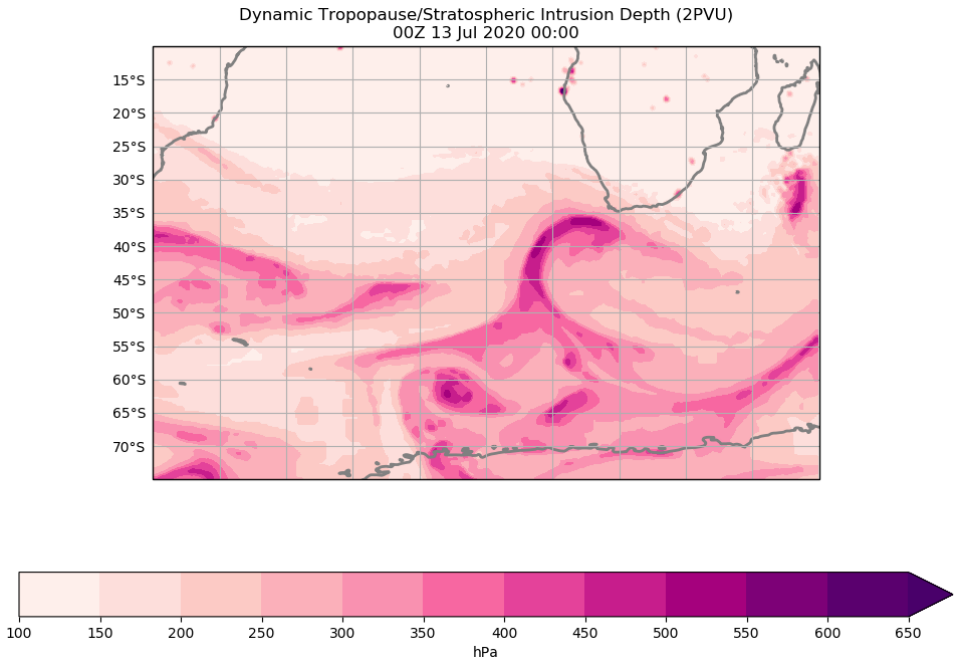

Figure 74: Dynamical tropopause height /stratospheric intrusion depth with respect to pressure level for 13 July 2020 00h00 UTC using GFS data initialised at 10 July 2020 00h00 UTC

The study of Cape Storm in Chapter 2 showed the importance of low-level PV features on surface cyclogenesis. This is also depicted in Figure 70. For a quick identification of low-level PV features, we provide a two-dimensional variable of low-level high-PV structures. The low-level high-PV field is obtained in a similar way to the dynamical tropopause height. However, for the low-level PV field, the lowest pressure level in which a PV value of -2 PVU or less is obtained and recorded for the entire domain. This methodology will not identify every PV structure within the column. i.e. If an anomaly exists on the surface (1000hPa) and another in the low-levels (700-800hPa), the low-level high-PV field will return a value of 1000hPa. An example of the low-level high-PV field is shown in Figure 75.

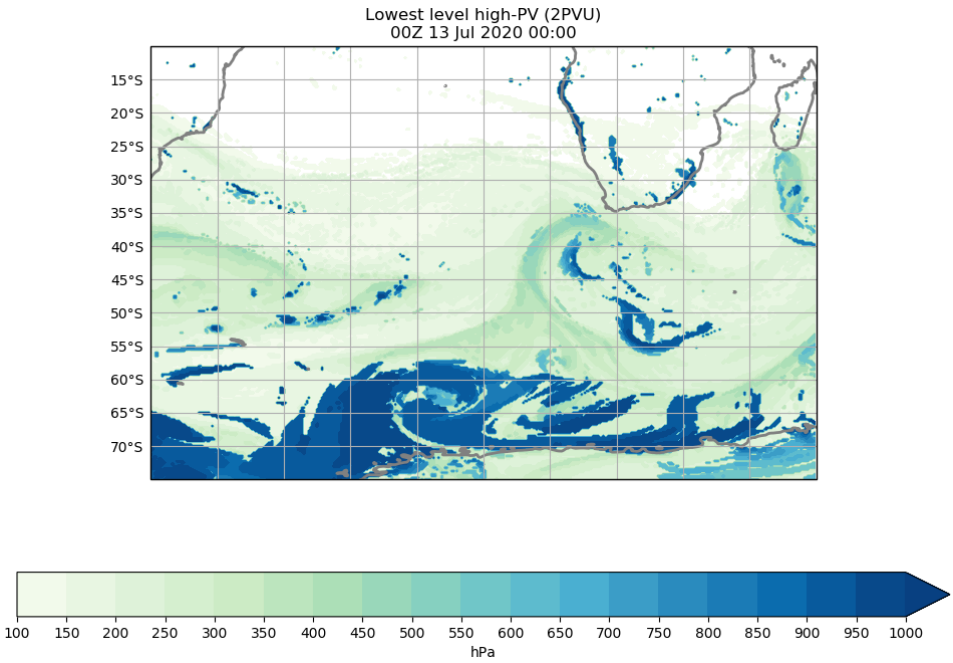

Figure 75: Low-level high-PV field for13 July 2020 00h00 UTC using GFS data initialised at 10 July 2020 00h00 UTC. In this field, the lowest level at which a PV values less than -2 PVU is shown.

5.3.3.3. PV longitudinal cross-sections

One of the most effective views of a stratospheric intrusion is a two-dimensional longitudinal cross-section as depicted in the Cape Storm case study in Chapter 2 as well as the conceptual model in Section 5.2.2. A simple PV longitudinal cross-section plot is created as shown in Figure 76. The cross-sectional view easily shows the stratospheric intrusion depth. Apart from the depth of the stratospheric intrusion, the width of the intrusion can also be determined easily. This was shown to be important to the degree of surface cyclogenesis. Cross-sectional PV fields also allow the detection of other anomalies within the field, in particular low-level PV anomalies. Low-level anomalies are a key ingredient in analysing whether explosive cyclogenesis may occur. Figure 76 shows the 2-dimensional stratospheric intrusion reaching down to the 500-600hPa level. This PV feature together with the low-level PV structure between 600hPa and 800hPa is very similar to the PV structures in the conceptual model for explosive cyclogenesis beneath a COL (Figure 70).

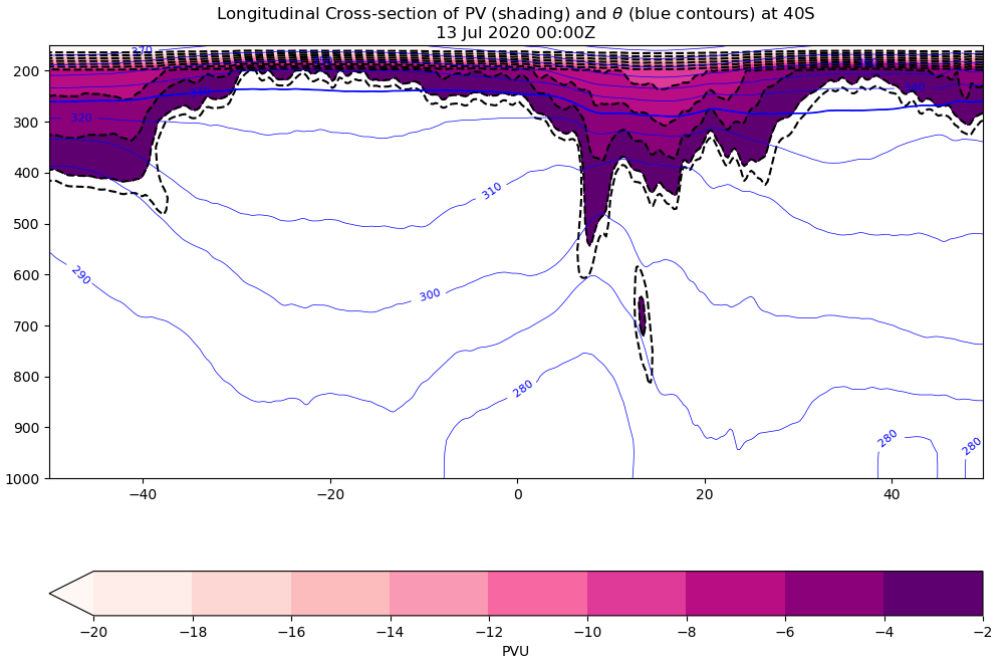

Figure 76: PV longitudinal cross-section depicting a deep stratospheric intrusion and a low- to mid-level PV anomaly below it. Stratospheric PV contours (values below -2 PVU) are shaded. The -1.5 PVU contour are also shown by a thick black dashed line. Potential temperature contours are also shown by the blue contours. The field is valid for 13 July 2020 00h00 UTC using GFS data initialised at 10 July 2020 00h00 UTC.

5.3.4. PV dynamical NWP website for the University of Pretoria

A web portal has been created to house the postprocessed fields. The portal is designed with a similar layout to the University of Pretoria webpage so that it can be easily integrated. The portal can be run operationally, producing the postprocessed fields for any of the four GFS updates on the day. At this stage, the scripts output the 00h00 UTC initialised GFS for the current day with a lead time of 5 days. Users can scroll through a variety of fields as listed in Section 5.3.3. Clicking on the images provided allows users to access and click through the fields for forecasts for the coming 5 days. PV cross-sections (Section 5.3.3.3) have been selected for latitudes between 25˚S and 55˚S at a 5˚S resolution. This can be easily amended based on the needs of that particular user. The portal can be found at: https://weathermanbarnes.github.io/UPDynamicalForecasts. The webpage currently houses the case study as shown in this Chapter with GFS data initialised at 10 July 2020 00h00 UTC. The layout of the website is shown in Figure 77 and the scrollable viewer is shown in Figure 78.

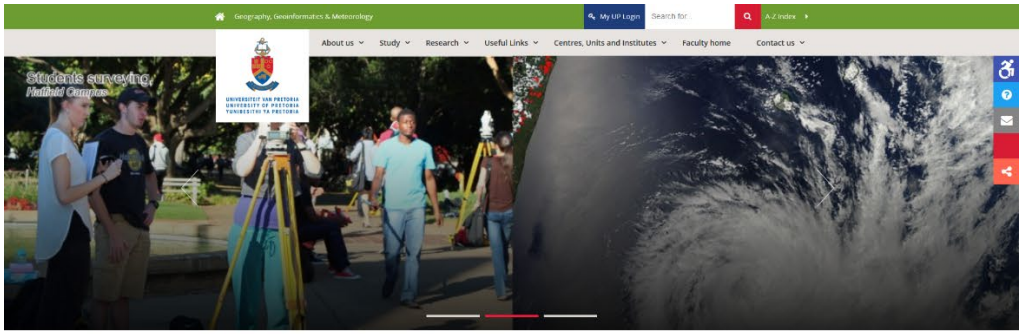

Dynamical Postprocessed Forecasts

Geography, Geoinformatics & Meteorology / Dynamical Postprocessed Forecasts

This page features dynamically post processed Numerical Weather Prediction products. The products are for use by students in order to help gain an understanding of how the dynamical properties taught throughout Dynamical Meteorology coursework affect weather systems. All fields are derived from the 00h00Z GFS 0.25 degree suite. The analysis is done from a Potential Vorticity (PV) thinking point of view as described in all basic dynamical theory texts (eg. Holton and Hakim, 2013). Presented are the depth of dynamical tropopause (with a definition of 2 PVU), isentropic PV for Rossby Wave Breaking (RWB) analysis and longitudinal cross-sections of PV.

These products are for research and educational purposes only. For official forecasts, please visit the South African Weather Service (SAWS) at www.weathersa.co.za or the SAWS

Dynamical Tropopause

Dynamical Tropopause

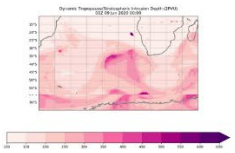

High PV Depth

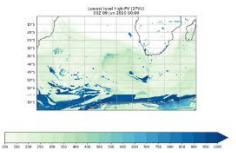

Rossby Wave Breaking

RWB on 310K

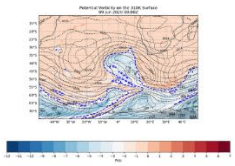

RWB on 320K

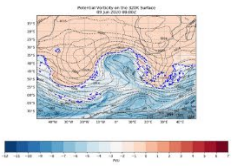

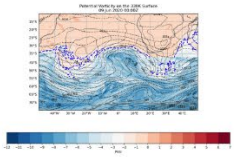

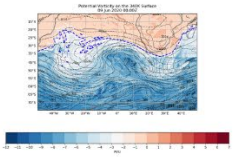

RWB on 250K

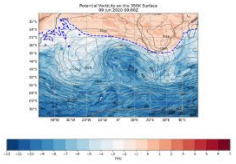

Cross-sections

25S

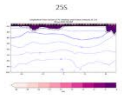

30S

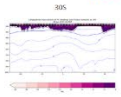

35S

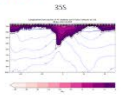

40S

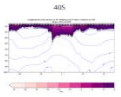

45S

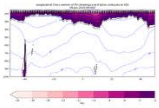

50S

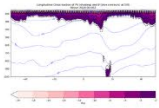

55S

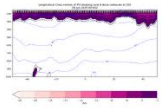

This webpage was created by Michael Barnes in support of an MSc(Meteorology) thesis submitted in 2020. For more information email u10313029@tuks.ac.za or contact either Dr. Thando Ndarana or Prof. Willem Landman.

Figure 77: University of Pretoria PV dynamical postprocessed forecasts webpage

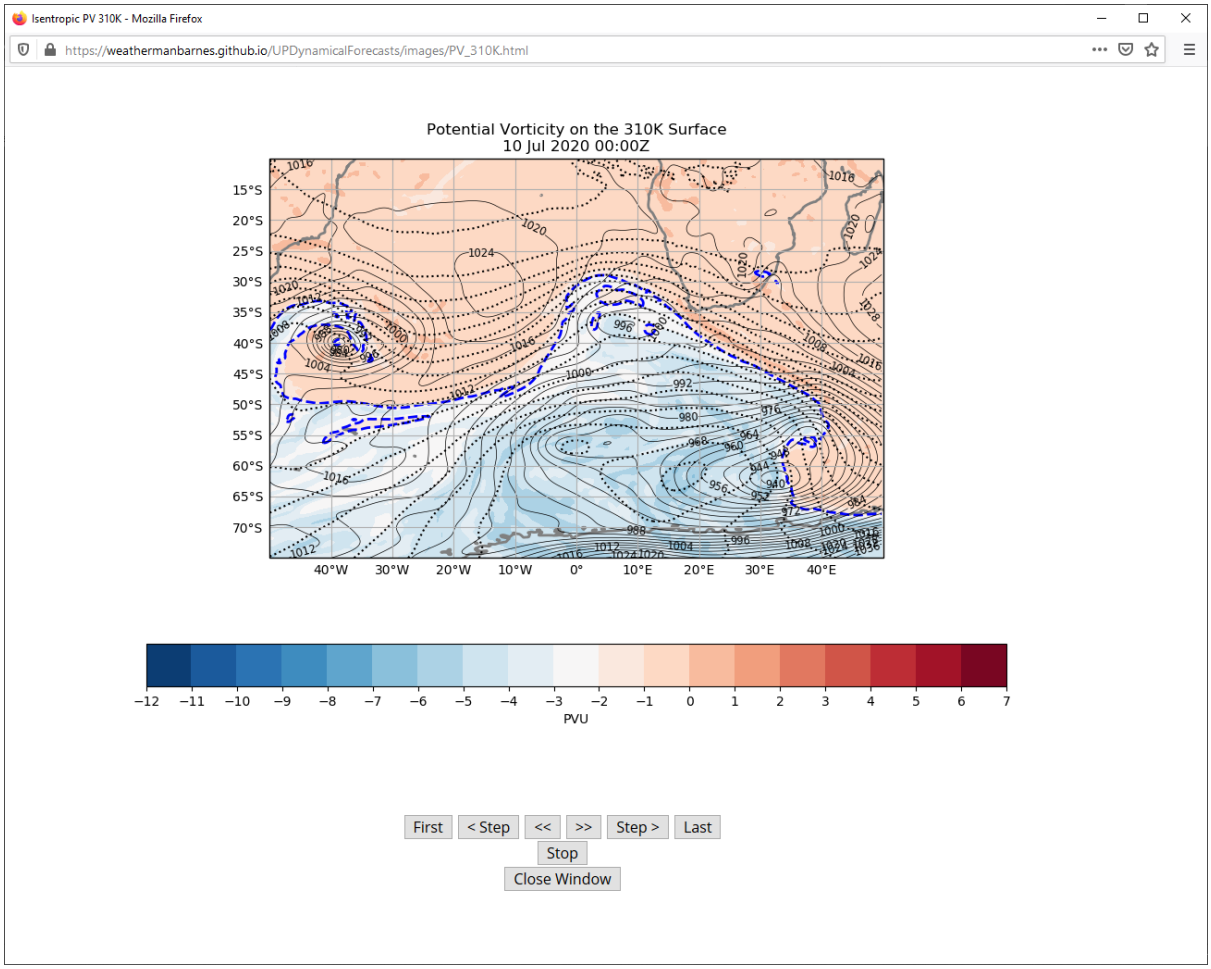

Figure 78: Popup window that allows users to scroll through a particular forecast field for coming 5 days.

5.4. References

Barlow M. 2017. potential-vorticity-v1.2. GitHub. https://doi.org/10.5281/zenodo.1069032.

Bauer P, Thorpe A, Brunet G. 2015. The quiet revolution of numerical weather prediction. *Nature*, 525(7567): 47–55. https://doi.org/10.1038/nature14956.

Benjamin SG, Brown JM, Brunet G, Lynch P, Saito K, Schlatter TW. 2019. 100 Years of Progress in Forecasting and NWP Applications. *Meteorological Monographs*, 59(Bjerknes 1911): 13.1-13.67. https://doi.org/10.1175/amsmonographs-d-18-0020.1.

Brennan MJ, Lackmann GM, Mahoney KM. 2008. Potential vorticity (PV) thinking in operations: The utility of nonconservation. *Weather and Forecasting*, 23(1): 168–182. https://doi.org/10.1175/2007WAF2006044.1.

Holton JR, Hakim GJ. 2013. *An Introduction to Dynamic Meteorology*. *Academic Press*. Elsevier.

Hoskins BJ. 1991. Towards a PV-theta view of the general circulation. *Tellus A*, 43(4): 27–35. https://doi.org/10.1034/j.1600-0870.1991.t01-3-00005.x.

Hoskins BJ, McIntyre ME, Robertson AW. 1985. On the use and significance of isentropic potential vorticity maps. *Quarterly Journal of the Royal Meteorological Society*, 111(470): 877–946. https://doi.org/10.1002/qj.49711147002.

Lackmann GM. 2011. *Midlatitude synoptic meteorology: Dynamics, analysis and forecasting*. American Meteorological Society: Boston, MA.

Mansfield DA. 1996. The use of potential vorticity as an operational forecast tool. *Meteorological Applications*, 3(3): 195–210. https://doi.org/10.1002/met.5060030301.

Stein THM, Keat W, Maidment RI, Landman S, Becker E, Boyd DFA, Bodas-Salcedo A, Pankiewicz G, Webster S. 2019. An evaluation of clouds and precipitation in convection-permitting forecasts for South Africa. *Weather and Forecasting*, 34(1): 233–254. https://doi.org/10.1175/WAF-D-18-0080.1.

World Meteorological Organization. 2012. *Manual on the Implementation of Education and Training Standards in Meteorology and Hydrology, Volume I*. .

Postface

As Neil Armstrong once wrote: *"Research is creating new knowledge"*. New knowledge gained is critical in order to improve our understanding of ourselves, our environment and the Earth on which we exist. This new knowledge is however pointless if the new knowledge generated is not fed into users who would benefit from it. In this chapter we have taken some of the critical concepts learned within this study about COL extensions and created products in which this knowledge can be transferred to the users – current and future operational meteorologists. The first of these tools in a conceptual model of COL extension. Conceptual models are frequently used in meteorology and are critical tools used to convey how complex processes work. The conceptual model can be used to feed the knowledge of COL extension to meteorology students and operational meteorologists alike. Secondly, a webpage has been created contained PV postprocessed NWP fields, which can be easily converted to be run operationally. These fields provide insight into the PV dynamical processes of weather systems, such as COLs, that may be currently affecting South Africa. These tools can not only enhance our understanding of the weather systems that will impact the country but can also assist students to gain an understanding of how PV dynamical processes influence weather systems that affect them on a day-to-day basis.

Chapter 6: Summary and conclusion

6.1. Summary and conclusion

This thesis begins with an extensive case study of Cape Storm, a cut-off low (COL) and associated surface low that affected the Western Cape of South Africa on 6 and 7 June 2017. A novel feature of this work is the dual analysis of both the dynamical processes at play during an extended COL and the resulting meteorological and societal impacts, which few dynamical studies do. An analysis of the meteorological and societal impacts associated with the system show the destructive nature of the storm. The deep surface low-pressure system was associated with strong and gusty winds that resulted in infrastructure damage throughout the province. These strong winds, associated with a large fetch of with 20m.s^{-1} wind offshore of the country, drove extremely high seas of up to 12m significant wave height along the coastal strip of the Western Cape and in combination with the low pressure drove a large storm surge event. These effects resulted in both damage to coastal infrastructure, particularly in the Cape Town metropole area. The strong winds in the eastern parts of the province resulted in berg winds, particularly along the cape south coast. The strong and gusty, warm and dry winds provided ideal meteorological conditions for the spreading of wildfires that were started during the afternoon of 6 June 2017. The wildfires in towns such as Knysna and Plettenberg Bay caused death and destruction in these areas. In contrast, heavy rainfall and localised flooding also resulted from Cape Storm in the south-western parts of the province. Although the totals were not unusual for the region, the rainfall brought some relief to the deep drought conditions the area had been experiencing for the preceding 3 years.

Various case studies of COLs and COL extensions have been done throughout the southern hemisphere (e.g. Funatsu *et al.* 2004; Iwabe and Da Rocha 2009) and over the southern African region (e.g. Baray *et al.* 2003; Singleton and Reason 2007). Few have however focussed on their dynamical characteristics from a potential vorticity (PV) perspective and its relation to its extension to the surface. A PV dynamical analysis of Cape Storm is also performed in Chapter 2. The weather system developed as a COL extension to a surface low pressure system to the west of South America. The system developed coincident with a Rossby wave breaking (RWB) event and a deep stratospheric intrusion. An intrusion of high-PV air into the troposphere drove both the development of the COL and surface low which developed within a few hours of one another. The weather system moved north-eastwards over the South American continent. A second and third RWB event and associated COL and stratospheric intrusions maintained and developed the surface low pressure further, with the

surface low and associated COLs moving across the south Atlantic Ocean. The first of these stratospheric intrusions was associated with a rapid, explosive deepening of the surface low pressure system beneath it. The explosive cyclogenesis event was associated with a tightly wrapped RWB event, a deep stratospheric intrusion together with a PV tower. The sustained development and maintenance of the surface low pressure by the upper level driven processes ultimately contributed to the affect that the surface low pressure system has on the South African region.

Since many COL case studies understandably focus on a single COL, this case study highlights various concepts with respect to the associated surface cyclone that eventually impacted South Africa, which have rarely been captured before. The initial COL that developed the surface circulation below it, developed far west of South Africa. This study highlights the importance of looking at weather systems from a hemispheric point of view in both research and operational mode. It also emphasises that weather systems can develop long before and far away from their eventual region of impact. An observation that was critical to the remainder of study is the timing between the development of the various COLs and the surface low pressure system beneath it. Conceptually, we think of COLs as upper-level weather systems that build towards the surface. The surface cyclone developed before the closed circulation developed in the upper troposphere, suggesting that slow, surfaceward extensions of COLs towards the surface may not always be the case. The two subsequent COLs and stratospheric intrusions that developed over the south Atlantic further intensified the surface cyclone. This observation highlights that COLs don't necessarily always develop their own circulations but can develop over pre-existing surface cyclones, intensifying them further.

From the observational case study analysis, Chapter 3 explores the concepts of stratospheric intrusions and COL extensions in a more generalised setting. Various COL climatologies have been performed, but none have provided a fully detailed analysis of the seasonal, temporal and regional variability of COL extensions and their potential links to stratospheric depth in the southern hemisphere. The COL depth climatology classifies COLs into deep COLs (dCOLs, COLs which extend to the 1000hPa level) and shallow COLs (sCOLs, COLs which only extend to the 500hPa level). Close to 60% of the COLs identified could be classified in the southern hemisphere, with up to 40% classified as sCOLs. dCOLs follow the spatial variability of COLs in this and other studies with the Australia-New Zealand sector being the most abundant region for dCOL development. sCOLs are however most prevalent in the African sector. There also seems to be a distinct latitudinal dependence with the majority of sCOLs with tracks in the subtropics and dCOLs tending to be prevalent closer to the extratropics. Similarly to COL temporal variability discussed in the open literature, both dCOLs and sCOLs are often short lived (up to 4 days). There is however a tendency for dCOLs to last longer than

sCOLs. Up to 50% of sCOLs identified lasting only between 1-2 days, compared to 40% of all dCOLs. Analysis of these two distinct types also reveal that sCOLs are more prevalent in the summer months, with a maximum of dCOLs during the later autumn months.

The variability of COL extensions provides important, cursory information as to the mechanisms that drive these surfaceward extensions. A further novel analysis of the COL extension climatology with respect to stratospheric intrusion depth is also performed to explore the dynamical drivers of COL extension. The stratospheric intrusion depth analysis reveals that dCOLs are more often associated with deeper intrusions compared to sCOLs. Deeper intrusions are driven by RWB events which were collocated with 98% of COLs in this study. dCOLs were found to be associated with “deeper” RWB events. This is emphasised by a composite analysis of RWB events with respect to both dCOLs and sCOLs. dCOLs are on average associated with a greater number of RWB signatures on more levels and contours compared to sCOLs. In terms of stratospheric intrusion depth, an analysis of the -1.5 PVU dynamical tropopause reveals that the majority of dCOLs are associated intrusions below 300hPa whilst sCOLs are associated with intrusions above 350hPa. Extended COLs are therefore more often associated with deeper intrusions of high-PV air. There however exists a “middle-world’ in the region of 300-350hPa that both sCOLs and dCOLs exist. An analysis of the low-level potential temperature anomalies shows that sCOLs are generally associated with a warm air surface anomaly that is out of phase with the upper level processes. dCOLs are however associated with warm and cold surface potential temperature anomalies to the east and west of the COL axis respectively. The relative phase of these surface processes associated with the upper level processes may result in COL extensions either being inhibited or enhanced at these “middle-word” levels.

Another important finding of Chapter 3 involves the evolution of COL extensions. Operational meteorologists conceptually think of COLs as upper-level systems that slowly extend towards the surface. This works finds that this is not necessarily the case. COLs can move over pre-existing surface cyclones and enhance their development. An example of this is also seen in the case study of Cape Storm in Chapter 2. COLs that do result in the development of their own surface cyclone are vertically coupled, developing troughs throughout the atmosphere. Surface cyclones that develop as a result of the COL tend to develop within 12 hours of the COLs development. This represents an important advancement in our understanding of how COL extensions develop.

Based on the findings of the COL extension climatology, an idealised experiment is performed in order to investigate the affect that upper level processes have on surface cyclogenesis in an idealised setting. The numerical experiment makes use of the concept of PV inversion which allows for the calculation of meteorological variables such as pressure, wind and temperature from the PV values. PV inversion

has been utilised extensively in reanalysis and case study settings but with little contribution in an idealised environment. A secondary novelty of the idealised experiment is that the experiment takes place in a southern hemisphere, with most studies taking place in the northern hemisphere (e.g. Fehlmann 1997; Sprenger 2007). The idealised experiment shows that deeper intrusions of stratospheric air are in-fact associated with enhanced surface cyclogenesis and surface pressure lowering compared to shallower intrusions. Very shallow intrusions found to be associated with sCOLs in the preceding chapter were shown to be associated with minimal surface cyclogenesis. The latitudinal dependence of sCOLs is also investigated using the numerical experiment by altering the height of the specified dynamical tropopause. With the same vertical intrusion depth, intrusions from higher tropopauses resulted in lesser surface cyclogenesis compared to lower tropopause. These numerical experiments together with intrusions extending to similar heights above the surface reveal that the height of stratospheric intrusions above the surface is more important to surface cyclogenesis than the vertical intensity of the intrusions. Horizontal size of the intrusion was however found to be an important factor with wide intrusions found to stimulate a greater degree of surface low pressure deepening.

This thesis finds that the hypothesis that deeper stratospheric intrusions of high-PV air are more often associated COL extensions is indeed correct. This knowledge is important to our understanding of the southern hemispheric and southern African climate system. It is however critical that this type of research finds its way into the hands of operational meteorologists and atmospheric science students. To this end, two separate tools have been developed. Firstly, a conceptual model has been designed in order to provide meteorologists with a graphical view of how stratospheric intrusions result in surface cyclogenesis. The five-step conceptual model comprising of 15 images provides the information required to know how COL extensions work and how PV dynamics are involved. Secondly, numerical weather prediction post-processing scripts are created to process Global Forecast System (GFS) data into PV dynamical fields. These fields can be operationalised and a webpage showing forecast data with a five-day lead time has been created. These dynamically postprocessed forecasts not only provide operational personnel with information as to how PV dynamics are affecting upcoming systems, but also can provide meteorology students with a live view of PV dynamics. Looking at how these PV fields are affecting weather system currently over the currently will increase their understanding of the dynamical processes at play.

This thesis has presented and documented aspects of the southern African climate system never before documented in the open literature. Firstly, our analysis of Cape Storm is one of the first of its kind in the region, meshing together societal and meteorological impacts together with a highly

academic PV dynamical analysis. Very few case study-type studies are presented in the open literature for South Africa, especially for non-tropically induced weather systems. More importantly, we provide a climatology of southern hemispheric COL extensions which has never been documented before this work, adding to our existing climatological knowledge of COLs. We also enhance our understanding of these extensions through PV dynamical analysis and idealised numerical experimentation.

6.2. Future research

This thesis has made significant contributions in improving our understanding of the dynamics of COLs and in particular COL extensions. PV dynamics is an understudied niche within the South African atmospheric science community. Very few case studies are available in the open literature within the South African sector with respect to atmospheric dynamics and PV dynamics in particular. In addition, the societal and meteorological impacts of extreme weather events is also lacking. More case studies of COLs and other extreme and significant events should be performed for the South African region. Our COL climatology is based on COLs identified at the 250hPa. An analysis of COL vertical depth-based COLs identified on different levels could be performed. Additionally, our COL extension climatology offers some degree of analysis of these extensions in terms of surface level processes. The effects of other processes at the surface and in the low- to mid-levels could hinder or help COL extensions. This study provides a good starting point for these aspects to be further investigated.

The current COL extension climatology analyses COL extensions over the full hemispheric domain, making no differentiation between extensions over land or ocean. Understanding COL extensions in these different environments is a crucial ingredient in our understanding of these important weather systems, but this was beyond the scope of the current work. Anecdotally, low pressure systems are often seen moving off the east coasts of Australia, South America and South Africa and these are often associated with PV intrusions and associated COLs or steep upper troughs. Understanding the role that terrain and land-ocean heating differences plays in a COL's extension is therefore crucial. Future work should include the role that terrain and the oceans of the southern hemisphere play in COL extensions.

An idealised numerical framework is used to provide detail on linking stratospheric depth to development at the surface. However, the idealised framework has the disadvantage that it represents instantaneous effects of high-PV intrusions into the troposphere. Future work in this area should include the use of a dynamical core to include a temporal aspect to the evolution of COL extensions. This would allow for the idealised investigation of some of the aspects of COL evolution seen in Chapter 3 whereby surface cyclones are shown to generally develop close to the time that the COL develops. Additionally, warm air temperature advection at the surface is a key part of the

evolution of surface cyclones. Investigating this factor in an idealised setting requires a temporal aspect to the dynamical framework. A dynamical would also allow for the analysis of surface cyclones because of PV intrusions in different temperature vertical profiles, for example where a low- or mid-level inversion is present.

This thesis applies a PV perspective with respect to COL extensions. It is important to enhance our understanding of the climate system with respect to differing types of cyclogenesis. OF particular interest, which has not been fully dealt with here, is rapid cyclogenesis. Rapid cyclogenesis has the potential to result in extreme weather, in particular for the western and southern parts of South Africa as was shown in Cape Storm in Chapter 2. Although southern hemispheric rapid cyclogenesis studies have been performed (e.g. Sinclair 1995; Allen *et al.* 2010), a regional climatology is necessary to our understanding of the development of these destructive events as the proximity and orientation of these events can have a significant impact on the how extreme the societal and meteorological impacts of these events can be. This is especially pertinent in the context of climate change.

Our knowledge about other weather systems at all spatial scales can be enhanced by studying PV dynamics. Of particular interest to South Africa is mesoscale thunderstorm dynamics associated with respect to severe thunderstorms and tornado development. Severe thunderstorms are prevalent through large parts of the country and especially when associated with tornadoes can be highly impactful to society. Some preliminary work has shown that tornadoes can be associated with upper level PV anomalies and lower level forcing such as surface fronts (Graf *et al.*, 2011). With operational high-resolution NWP relatively advanced in South Africa, these types of PV features could be useful in being able to forecast these high impact events.

This thesis also brings dynamical post-processing tools to the forefront. There is a dire need to improve the knowledge base of dynamical meteorology in South Africa and put dynamical processes back onto the table of meteorological professionals. The webpage created as a result of this work can be extended further to display other dynamical meteorological analyses. Outputs of student projects that deal with dynamical analyses including quasi-geostrophic issues such as Q-vectors, local energetics amongst others can add additional fields to the webpage. The webpage and associated processing scripts will be made available to the meteorology department within the University of Pretoria.

6.3. References

Allen JT, Pezza AB, Black MT. 2010. Explosive cyclogenesis: A global climatology comparing multiple reanalyses. *Journal of Climate*, 23(24): 6468–6484. https://doi.org/10.1175/2010JCLI3437.1.

Baray JL, Baldy S, Diab RD, Cammas JP. 2003. Dynamical study of a tropical cut-off low over South

Africa, and its impact on tropospheric ozone. *Atmospheric Environment*, 37(11): 1475–1488. https://doi.org/10.1016/S1352-2310(02)00999-8.

Fehlmann R. 1997. Dynamics of seminal PV elements. Swiss Federal Institute of Technology Zurich.

Funatsu BM, Gan MA, Caetano E. 2004. A case study of orographic cyclogenesis over South America. *Atmosfera*, 17(2): 91–113.

Graf MA, Sprenger M, Moore RW. 2011. Central European tornado environments as viewed from a potential vorticity and Lagrangian perspective. *Atmospheric Research*. Elsevier B.V., 101(1–2): 31–45. https://doi.org/10.1016/j.atmosres.2011.01.007.

Iwabe CMN, Da Rocha RP. 2009. An event of stratospheric air intrusion and its associated secondary surface cyclogenesis over the South Atlantic Ocean. *Journal of Geophysical Research Atmospheres*, 114(9): 1–15. https://doi.org/10.1029/2008JD011119.

Sinclair MR. 1995. A Climatology of Cyclogenesis for the Southern Hemisphere. *Monthly Weather Review*, 123(6): 1601–1619. https://doi.org/10.1175/1520-0493(1995)123<1601:ACOCFT>2.0.CO;2.

Singleton AT, Reason CJC. 2007. A Numerical Model Study of an Intense Cutoff Low Pressure System over South Africa. *Monthly Weather Review*, 135(3): 1128–1150. https://doi.org/10.1175/mwr3311.1.

Sprenger M. 2007. Numerical piecewise potential vorticity inversion: A user guide for real-case experiments. , 98.